Towards Sustainable Construction: Experimental Approach and Multi-Scale Simulation in High-Strength Self-Compacting Concrete Design

By

Abdullah Abdulrahman M Alshahrani

B.Sc., M.Sc.

A thesis submitted to Cardiff University for the degree of

Doctor of Philosophy

School of Engineering

Cardiff University

United Kingdom

May 2024

ACKNOWLEDGEMENTS

I extend my deepest gratitude to those who have supported me throughout my thesis. Firstly, I am deeply grateful to the Kingdom of Saudi Arabia, my beloved country, and Najran University for their significant support and funding of my PhD.

I thank the School of Engineering faculty and staff for their help. I am particularly indebted to my supervisor, Dr Kulasegaram, whose transformative guidance was pivotal to the success of my academic journey. His insights, advice, and continuous support were crucial in my journey.
In addition, I must acknowledge my co-supervisor, Dr Kundu, for his support and engaging discussions throughout the research process.

Gratitude is due to the administrative and technical staff in the concrete and structure laboratories at the School of Engineering.

My family have been my constant source of love and encouragement. I reserve heartfelt thanks for my parents and siblings who have given me unwavering support throughout this endeavour. To my wife and daughters, Tooq and Nadin, thank you for your patience and understanding.

Lastly, I appreciate the camaraderie and support received from my friends and colleagues, especially those in my office, during my PhD journey.

SYNOPSIS

Concrete production constitutes approximately 10% of the yearly global carbon dioxide emissions while consuming substantial non-renewable resource quantities. The urgent need to mitigate the significant negative economic and environmental impacts necessitates sustainable design approaches for concrete production. This thesis explores the development of sustainable High-Strength Self-Compacting Concrete (HSSCC), investigates sustainable mix designs, evaluates elastic properties through multi-scale simulation, and assesses the effects of steel fibre properties on fresh and mechanical characteristics of such concrete.

The research reported in this thesis is divided into three parts. The first part focuses on the development of an effective and robust mix-proportioning procedure for designing sustainable HSSCC based on targeted compressive strength and plastic viscosity, utilising 40% Supplementary Cementitious Materials (SCMs) as cement replacement and supported by design charts. Sixteen divergent HSSCC mixes were designed and produced using the proposed design method. The experimental test results for these mixes demonstrated that the proposed mix design method could produce HSSCC with excellent fresh and mechanical characteristics while being eco-efficient in terms of CO_2 emissions and cement consumption.

The second part of the thesis studies the elastic properties of HSSCC reinforced with steel fibre and varying proportions of coarse aggregate (CA). A two-step homogenisation method was developed to evaluate the elastic properties of HSSCC through mean-field homogenisation (MFH) and finite element modelling of the homogenised concrete. This method was used to determine the elastic modulus of HSSCC, considering variations in CA and steel fibre content, thereby facilitating mix design optimisation and constituent selection. Additionally, the effect of fibre content and orientation, CA content and particle shape, and porosity of the mix on the homogenised elastic modulus of HSSCC was evaluated.

The last section reviews the effect of steel fibre properties on the rheological and mechanical properties of eco-friendly HSSCC, together with the combined effect of CA content and steel fibre. The results demonstrated that using steel fibres with higher tensile strength and smaller

diameter significantly enhanced the splitting tensile strength, flexural strength, and fracture energy, compared to steel fibres with larger diameters and lower tensile strengths. It was thus concluded that CA content and fibre properties are two critical factors that impact the performance of HSSCC and should, therefore, be carefully considered in the mix design process.

Keywords: Sustainable Construction, High-Strength Self-Compacting Concrete, Mix Design, Multi-Scale Simulation, Steel Fibre Reinforcement

LIST OF PUBLICATIONS

Journal papers:

1. **Alshahrani, A.,** Cui, T. and Kulasegaram, S. 2022. Effect of sand to aggregate ratio on the properties of self-compacting high-performance concrete. *International Journal of Civil Infrastructure*, 5, pp. 37-42. Available at: https://doi.org/10.11159/ijci.2022.006.

2. **Alshahrani, A.**, Cui, T., Almutlaqah, A. and Kulasegaram, S. 2023. Designing sustainable high-strength self-compacting concrete with high content of supplementary cementitious materials. *European Journal of Environmental and Civil Engineering*, 28(8), pp. 1830-1849. Available at: https://doi.org/10.1080/19648189.2023.2279563.

3. **Alshahrani, A.**, Kulasegaram, S. and Kundu, A. 2023. Elastic modulus of self-compacting fibre reinforced concrete: Experimental approach and multi-scale simulation. *Case Studies in Construction Materials*, 18. Available at: https://doi.org/10.1016/j.cscm.2022.e01723.

4. **Alshahrani, A**. and Kulasegaram, S. 2023. Effect of fibre diameter and tensile strength on the mechanical, fracture, and fibre distribution properties of eco-friendly high-strength self-compacting concrete. *Construction and Building Materials*, 403. Available at: https://doi.org/10.1016/j.conbuildmat.2023.133161.

5. Cui, T., **Alshahrani, A.**, and Kulasegaram, S. 2024. Effects of mineral admixtures on the rheological properties of self-compacting concrete: A review. Proceedings of the ICE - Construction Materials. (Accepted)

Conference papers:

1. **Alshahrani, A**., Cui, T. and Kulasegaram, S. 2022. Influence of sand to aggregate ratio on the fresh and mechanical properties of self-compacting high-performance concrete. Presented at: *The 7th World Congress on Civil, Structural, and*

Environmental Engineering (CSEE'22), 10-12 April 2022. In: *Proceedings of the 7th World Congress on Civil, Structural, and Environmental Engineering (CSEE'22)*. ICSECT. Available at: https://doi.org/10.11159/icsect22.171

2. **Alshahrani, A**. and Kulasegaram, S., 2023, June. Effect of fibre tensile strength, aspect ratio and volume fraction on rheological and mechanical properties of high-strength self-compacting concrete. Presented at: *Building for the Future: Durable, Sustainable, Resilient Proceedings of the fib Symposium 2023*, Turkey, 5-7 June 2023. In: *Building for the Future: Durable, Sustainable, Resilient Proceedings of the fib Symposium 2023.*, vol. 349 Springer, pp. 588-598. Available at: https://doi.org/10.1007/978-3-031-32519-9_57

3. Almutlaqah, A., **Alshahrani, A**., Maddalena, R. and Kulasegaram, S. 2023. The effect of temperature and ageing on the behaviour of self-compacting concrete containing supplementary cementitious materials. Presented at: SynerCrete23, 14-16 June 2023. In: *International RILEM Conference on Synergising expertise towards sustainability and robustness of CBMs and concrete structures*, Springer Nature, pp. 942-953. Available at: https://doi.org/10.1007/978-3-031-33187-9_86

TABLE OF CONTENTS

LIST OF FIGURES

LIST OF TABLES

NOMENCLATURE

Acronym	Description
SCC	Self-compacting concrete
SP	Superplasticiser
w/cm	Water-to-cementitious material ratio, %
CA	Coarse aggregate
VMAs	Viscosity-modifying admixtures
OPC	Ordinary Portland Cement
CO_2	Carbon dioxide
HSC	High-strength concrete
SFR-SCC	Steel fibre-reinforced self-compacting concrete
RVE	Representative volume element
HSSCC	High-strength self-compacting concrete
SCMs	Supplementary cementitious materials
S/A	Sand-to-aggregate ratio, %
P/S	Paste-to-solid, %
M-T	Mori-Tanaka
MFH	Mean-field homogenisation
CT	Computed tomography
ITZ	Interfacial transition zone
HPC	High-performance concrete
NVC	Normal vibrated concrete
w/c	Water-to-cement ratio, %
GGBS	Ground granulated blast-furnace slag
w/p	Water-to-powder ratio, %
cm	Cementitious materials
F-A	Fine aggregate
RHA	Rice husk ash
F-A/TA	Fine aggregate to total aggregate
HRWRAs	High range water reducing admixtures
CRMs	Cement replacement materials

SFR-CC	Steel fibre-reinforced cementitious composites
UHPFRC	Ultra-high-performance fibre-reinforced concrete
WFM	Work of Fracture Method
SEM	Size Effect Method
SFRC	Steel fibre-reinforced concrete
BC	Boundary condition
CMOD	Crack mouth opening displacement
LVDT	Linear Variable Differential Transformer
RILEM	International Union of Laboratories and Experts in Construction Materials, Systems, and Structures
ACI	American Concrete Institute
ASTM	American Society for Testing and Materials
JSCE	Japan Society of Civil Engineers
BS EN	British Standards European Norm
AASHTO	American Association of State Highway and Transportation Officials

Symbol	**Definition**
t_{500}	The time taken to reach a spread diameter of 500 mm in the slump cone test (t)
t_{500j}	The time taken to reach a spread diameter of 500 mm in the J-ring test (t)
B_j	Blocking step, mm
t_{200}	The time taken for the mix to reach the 200 mm line in the L-box test (t)
t_{400}	The time taken for the mix to reach the 400 mm line in the L-box test (t)
l_f	Fibre length, mm
d_f	Fibre diameter, mm
l_f/d_f	Fibre aspect ratio
V_f	Volume fraction of fibres
G_f	Fracture energy, N/m
f_{cu}	Cube compressive strength at 28 days, MPa
η_i	Plastic viscosity of the i^{th}liquid–solid suspension, Pa·s
η_{i-1}	Plastic viscosity of the preceding $(1-i)^{th}$ phase, Pa·s
η_{paste}	Plastic viscosity of the paste, Pa·s
η_{mix}	Plastic viscosity of the concrete mix, Pa·s

ϕ_i	Volume fraction of solids
$f_i(\phi_i)$	Relative plastic viscosity function
ϕ_m	Maximum packing fraction
$\phi_{fineAgg}$	Volume fraction of the fine aggregate
$\phi_{coarseAgg}$	Volume fraction of coarse aggregate
E	Elastic modulus, GPa
mm	Millimetre
µm	Micrometre
$\langle f \rangle$	The mean of the stress/strain field
σ	Stress
ε	Strain
$\bar{x}$	Macro point
x	Meso point
ν_0	Volume of matrix
ν_1	Volume of inclusion
$\boldsymbol{I}$	Symmetric equivalent tensor
I	Single ellipsoidal inclusion
C_1	Uniform stiffness
C_0	Infinite matrix of uniform stiffness
e	Remote uniform strain
H^{ε}	Single inclusion strain concentration tensor
C	Macro stiffness
FE	Finite element
ROI	Region of interest
µ	Poisson's ratio
G	Shear modulus, GPa
f_{st}	Splitting tensile strength, MPa
b	Prismatic beam width, mm
a_0	Notch depth, mm
n_0	Notch width, mm
(δ)	Mid-span deflection, mm

W_0	The area under the load-deflection curve, kN.mm
g	Gravity, m/s^2
h	Prismatic beam depth, mm
L_{ch}	Characteristic length, mm
f_t	Tensile strength, MPa
N^T_f	Total number of fibres intersecting the plane
d_n	The number of fibres per unit area, fibres/cm^2
A_c	The area of cross-section, cm^2
d_{n3D}	The theoretical value of the density of fibres within a 3D space
v_f	Fibre volume fraction
A_f	The cross-sectional area of a single fibre
θ	Inclined angle of a single fibre
η_θ	The fibre orientation factor

Chapter 1 Introduction

1.1 Research background

In the construction sector, the rapid population growth and the complex evolution of urban landscapes have given impetus to the drive for innovative processes. This dynamic has led to a pressing need for unique structural design, significantly increasing the demands placed on reinforced concrete (RC) structures. Currently, these structures are characterised by intricate shapes and sections, accompanied by densely packed and clustered reinforcement. This high reinforcement density presents formidable challenges for concrete pouring and compaction.

Inadequate compaction significantly compromises the in-situ performance of hardened concrete and raises concerns regarding its durability. Ensuring the long-term durability of RC structures requires thorough compaction, which depends on the availability of skilled labour. In the 1980s, Japan experienced a pronounced shortage of skilled construction workers, adversely affecting the quality of construction (Okamura and Ouchi 2003). This scenario created the opportunity for a transformative development in 1986, when a Japanese researcher, Okamura, introduced 'self-compacting concrete' (SCC) as a solution to address quality assurance challenges and improve durability and working conditions in concrete construction.

SCC is designed to easily fill every corner of the formwork, flowing through complex geometries and densely reinforced areas that are traditionally challenging to access, thereby eliminating the need for any external compaction during the pouring process (Okamura and Ouchi 2003). This advanced concrete type offers numerous benefits for construction practices, notably enhancing on-site efficiency and effectiveness by reducing labour costs and shortening the overall construction time. SCC improves the quality of surface finishes, leading to fewer defects, and promotes a healthier and quieter construction environment by reducing noise pollution and health hazards associated with the use of vibration equipment.

However, SCC is a sophisticated mix blend that is highly sensitive to the specific characteristics and proportions of its components. Designing an SCC mix requires a delicate balance between fluidity for ease of deformability and resistance to segregation to ensure stability. Despite the introduction of multiple mix proportioning methods for SCC over the past three decades, based on various concepts and control parameters, none have fully met

all construction specifications and requirements. The challenge of assessing the viability of available design methods is further amplified by the absence of precise design specifications for SCC. Typically, SCC mixes are designed with a reduced coarse aggregate (CA) content with a small maximum particle size, a high superplasticiser (SP) volume, and an increased fine material content to achieve the required fresh properties, including standard flow, passing ability, and stability criteria. These challenges highlight the need for ongoing research to refine SCC mix design processes, which could significantly benefit construction practices by enhancing the efficiency, sustainability, and structural integrity of concrete applications.

1.2 Research motivation

One of the significant challenges associated with SCC is the substantial increase in material costs, attributed to the high volumes of ordinary Portland cement (OPC) and SP content required. This reliance on a high cement content raises material costs and results in increased hydration heat, significant autogenous shrinkage, and creep (Jalal et al. 2015; Hussien and Mohammed 2023; Aidjouli et al. 2024). Furthermore, the carbon footprint of concrete is predominantly due to the production of OPC, accounting for approximately 5-7% of the annual anthropogenic CO_2 emissions (Berndt 2015; Celik et al. 2015; de Grazia et al. 2019). This underscores environmental concerns about concrete production alongside the extensive use of natural resources (Kaish et al. 2018; Adesina and Awoyera 2019). These challenges highlight the need for conscientious design of SCC, given its economic and environmental implications. With the anticipated increase in concrete production, a considerable strain on natural resources and an upturn in environmental pollution is expected (Gupta et al. 2021). Therefore, meeting future concrete demand necessitates the development of sustainable and eco-friendly concrete production processes to reduce CO_2 emissions and conserve non-renewable natural resources.

In response, waste material offers a viable alternative to traditional construction materials in SCC production. Incorporating such alternative materials not only boosts the sustainability of SCC and offers numerous benefits, such as cost reductions, environmentally responsible use of by-products, conservation of natural resources, pollution mitigation, and decreased expenses associated with landfill use (Gupta et al. 2021). Consequently, there is an urgent need for further research to develop a sustainable version of SCC that optimises the use of

waste materials, with a specific focus on achieving the ideal SCC mix composition (Adesina and Awoyera 2019).

An effective strategy for reducing carbon emissions in the construction sector is to decrease the volume of concrete used in buildings by adopting High-strength Concrete (HSC). HSC provides performance comparable to traditional concrete but with significantly less material for the same application (de Matos et al. 2019; Campos et al. 2020). In addition to reducing concrete quantities, the adoption of HSC often leads to enhanced durability. Aïtcin (2019) proposed that increasing the compressive strength of concrete could diminish the quantity of concrete required to support structural loads, thereby lowering cement usage. Campos et al. (2020) concluded that HSC presents benefits from both an environmental and an economic standpoint due to its decreased reliance on cement.

However, increasing the compressive strength of concrete often leads to increased brittleness, posing a significant challenge to structural integrity (Deeb et al. 2014). This issue arises primarily from plain concrete's inherent poor tensile strength and pronounced brittleness. To mitigate this, steel fibres are incorporated into concrete mixes, significantly enhancing ductility, toughness, and both flexural and shear strengths by bridging micro- and macro-cracks. Despite these advantages, the incorporation of steel fibres has a substantial influence on the fresh properties of SCC, depending on the volume fraction of fibres, their properties, and the specific composition of the mix (Deeb et al. 2012).

Meeting the fresh state standards for SCC necessitates careful control over the fibre content, a judicious selection of steel fibre properties, and adjustments to CA's content and particle size. These compositional changes can affect the concrete's mechanical properties, including the elastic modulus and fracture behaviour. Identifying the optimal mix of materials and their effect on the mechanical performance of Steel Fibre-reinforced Self-compacting Concrete (SFR-SCC) is crucial, given the existing gaps in mix design procedures and recommendations for SFR-SCC (de la Rosa et al. 2018; Rajakarunakaran et al. 2022), highlighting a vital area of research and development within the construction industry.

Evaluating the elastic properties of composite materials, such as SCC and SFR-SCC, poses complex challenges due to the varied microstructures inherent in these composites, stemming from differences in fibre content and type, as well as the size, shape, content, and type of CA, coupled with adjustments to the water-to-cement (w/cm) ratios. Multiscale analysis stands out as a suitable method for simulating the elastic behaviour of SFR-SCC by linking its micro or meso-structures, interconnected through a Representative Volume Element (RVE). At the mesoscale, the RVE comprises heterogeneous materials, each characterised by unique mechanical and geometric properties (Yu et al. 2020) .

The theory of homogenisation focuses on deriving effective properties from smaller-scale structures and plays a crucial role in determining the overall properties of a heterogeneous material (Nguyen et al. 2011). This homogenisation process enables the substitution of the heterogeneous material with an equivalent homogeneous counterpart. Utilising multiscale simulation as an analysis tool offers a pathway to optimise the performance and cost-effectiveness of such composite materials and enhances the understanding of the impacts of fibre orientation and distribution, CA content and shape, and porosity on the mechanical properties of SFR-SCC.

1.3 Research aims and objectives

This study aims to advance the sustainability and performance of high-strength self-compacting concrete (HSSCC) by developing a mix design that optimises the use of Supplementary Cementitious Materials (SCMs) and refines constituent material characteristics, including steel fibres, through a combination of experimental investigations, theoretical and multiscale analyses. To achieve this aim, the research undertook the following objectives:

1. To develop an effective and simple mix design method for a sustainable HSSCC based on plastic viscosity and compressive strength, aimed at reducing cement content by incorporating a high content of SCMs.

2. To validate the viability of the proposed mix design method to produce HSSCC mixes that meet the self-compacting concrete criteria in their fresh state and achieve the target compressive strength in the hardened state.

3. To incorporate steel fibres into HSSCC and investigate the effect on the elastic modulus by considering variations in CA and steel fibre content through experimental studies while developing a multiscale homogenisation method to predict the elastic properties of such mixes.

4. To conduct a comprehensive parametric study and quantitative analysis of the effects of steel fibre content and orientation, CA content and shapes, and porosity on the elastic modulus of sustainable HSSCC using the proposed multiscale homogenisation method.

5. To investigate the influence of steel fibre properties, namely diameter, and tensile strength, on the fresh and mechanical properties of eco-friendly HSSCC designed with varying CA content.

1.4 Research methodology

The methodology adopted in this research includes a varied approach, integrating experimental investigations and a theoretical multiscale homogenisation method to address the research objectives outlined.

1. The proposed mix design method employed SCMs to substitute up to 40% of the cement content in the HSSCC. The target plastic viscosity for the HSSCC mixes was determined based on the rheology of the paste and the micro-mechanical constitutive models developed by Ghanbari and Karihaloo (2009). The mixes determined by this method were developed for target compressive strengths of 70 MPa, 80 MPa, 90 MPa, and 100 MPa by maintaining the required w/cm ratio and employing the procedure proposed by Abo Dhaheer et al. (2016). The proposed design approach was numerically programmed, and design charts were developed to offer clear and practical design guidance.

2. Various HSSCC mixes were designed to validate the proposed methodology, based on target compressive strength and plastic viscosity. Four series of HSSCC mixes were prepared, differentiated by compressive strengths (70–100 MPa) and plastic viscosities (1.6–12 Pa·s). Each series comprised four mixes with distinct plastic viscosity values and varied sand-to-aggregate (S/A) and paste-to-solid (P/S) ratios. To assess the self-compaction properties of the mixes, slump flow, J-ring, and L-box tests were conducted following EFNARC (2005) guidelines. Cube compressive strengths were tested at 7, 28, and 90 days. Sustainability assessments were conducted to determine the CO_2 emissions of each material, as per values reported in existing literature. These emissions and the cement consumption necessary to achieve 1 MPa of compressive strength were subsequently incorporated into the efficiency calculations.

3. The elastic modulus of HSSCC reinforced with short steel fibres, with varying CA and steel fibre contents, was investigated through experimental tests and numerical methods. Numerically, a two-step homogenisation method was developed to evaluate the macroscopic elastic properties of SFR-SCC. In the first step, the mortar, air voids, and CA were homogenised as plain SCC using the Mori-Tanaka (M-T) model within the framework of the Mean-Field Homogenisation (MFH) approach. X-ray computed tomography (CT) scanning was utilised to analyse and determine the volume fractions, shapes, and numbers of voids of each mix for validation purposes. In the second step, a finite element model of the RVE was generated with steel fibre inclusions and the homogenised SCC matrix, thereby determining the bulk elastic modulus of the HSSCC mixes through computational homogenisation.

4. Following the two-step homogenisation method, a quantitative analysis was conducted to examine the influence of steel fibre content and orientation, CA content and particle shape, the porosity of the mix, and the Interfacial Transition Zone (ITZ) on the homogenised elastic modulus. The proposed method was intended for use in preliminary mix optimisation and the selection of constituents for HSSCC, aiming to replace time-consuming laboratory tests and reduce the use of non-renewable resources.

5. The HSSCC in this study was designed primarily to reduce cement consumption and mitigate its environmental consequences. Accordingly, the influence of fibre diameter and tensile strength on the fresh, mechanical, and fracture properties was investigated for HSSCC designed with varying CA and fibre contents. The adherence to the primary performance criteria of HSSCC in the fresh state was assessed through tests, such as the slump flow and J-ring tests. The mechanical properties of hardened concrete were evaluated, including compressive strength, splitting tensile strength, elastic modulus, and four-point and three-point flexural strength on notched prismatic beams. In addition, the distribution and alignment of steel fibres in the HSSCC were assessed using image analysis techniques.

Through the above methodologies, this thesis seeks to contribute to the body of knowledge on sustainable concrete solutions, focusing on optimising the mix design and performance of HSSCC to meet future construction demands while providing a deeper understanding of factors affecting the performance of such composite materials.

1.5 Research contribution

This thesis aims to contribute to the development of sustainable HSSCC mix designs through the evaluation of elastic properties using multiscale simulation, and the assessment of the effects of steel fibre properties within various mix compositions on fresh and mechanical characteristics. The key contributions of this research are as follows:

1. Development of a sustainable HSSCC mix design: A novel mix design methodology is proposed and detailed, tailored specifically for HSSCC. This methodology significantly reduces the content of OPC by optimising the use of SCMs, thereby decreasing the environmental footprint of concrete production. Four design charts (70–100 MPa) were developed to determine the mix proportions for achieving targeted viscosities and compressive strengths.

2. Experimental validation of the new mix design: The research undertakes the rigorous design, production, and testing of various HSSCC mixes to validate the proposed mix design method. This empirical investigation confirms the viability of the proposed

mix design and contributes valuable data to enhance the understanding of mix proportioning and its effect on the fresh and hardened properties of HSSCC and the environmental impact of such mixes.

3. Development of a multiscale homogenisation method: This research makes a key methodological contribution by developing a two-step homogenisation approach for predicting the elastic properties of HSSCC. The agreement between the proposed homogenisation results and experimental data underscores the feasibility of employing this two-step homogenisation approach in the development of HSSCC mix designs.

4. Parametric analysis of the elastic modulus of HSSCC: A pivotal contribution of this research is the targeted parametric analysis that quantifies the impacts of several factors such as steel fibre content, steel fibre orientation, CA content, porosity, particle shape of CA, and the ITZ on the elastic modulus of HSSCC. This focused investigation into selected variables offers crucial insights, paving the way for the refinement of future mix designs and the advancement of HSSCC's structural applications.

5. Influence of steel fibre properties on HSSCC performance: This thesis provides a comprehensive analysis of the influence of variations in steel fibre properties such as diameter, and tensile strength on the fresh and mechanical properties of HSSCC formulated with different CA contents. The findings aim to provide guidelines for selecting the optimal fibre properties and content, facilitating the most effective combination with CA content. This strategy is expected to enhance the efficiency and cost-effectiveness of steel fibre usage in concrete, thus lowering production costs and enhancing sustainability and durability.

1.6 Outline of the thesis

This PhD thesis comprises six chapters, followed by bibliographical references and appendices, as outlined below:

Chapter 1 presents the research scope, aims, and objectives, along with the research methodology.

Chapter 2 presents a comprehensive literature review on SCC, detailing its evolution, advantages, challenges, and distinctive construction properties. It explores mix design methods, rheology, and the impact of constituent materials and steel fibre reinforcement and introduces homogenisation methods for evaluating the mechanical properties of composites.

Chapter 3 explores the development and validation of a sustainable mix design method for HSSCC, incorporating up to 40% SCMs as substitutes for cement. It outlines the process and steps for creating a sustainable HSSCC mix design based on cube compressive strength and plastic viscosity. Furthermore, it details the experimental validation of this methodology through the production and testing of various HSSCC mixes, categorised by their compressive strengths and plastic viscosities. Sustainability evaluations are presented for the CO_2 emissions and cement consumption of each mix, assessing the effectiveness of the proposed method.

Chapter 4 investigates the elastic modulus in HSSCC reinforced with steel fibres, considering various CA and steel fibre contents. It details an experimental and numerical study, emphasising a two-step homogenisation method to assess the macroscopic elastic properties of SFR-SCC. This chapter proposes relevant quantitative analyses which can be undertaken to determine the influence of varied factors on the homogenised elastic modulus.

Chapter 5 is devoted to the effect of steel fibre properties on sustainable HSSCC. This chapter explores how fibre properties and content influence HSSCC's fresh, mechanical, and fracture properties across varying CA contents. It evaluates the distribution and alignment of

such steel fibres within HSSCC using image analysis. The chapter aims to provide guidelines for selecting optimal fibre properties and content to enhance efficiency and cost-effectiveness in using steel fibres, contributing to sustainability in construction.

Chapter 6 summarises the conclusions drawn from this research and offers recommendations for future research.

Chapter 2 Literature Review

2.1 Introduction

Concrete is the most extensively used construction material globally and boasts an annual consumption of approximately 30 billion tonnes (Thomas et al. 2021). Its widespread usage stems from several factors, including the global availability of raw materials, cost-effective production, and resilience in harsh environments. Reinforced concrete structures have seen a surge in demand within the construction industry due to new development needs, innovative architectural designs, and a growing population, often leading to more densely packed and clustered reinforcement in such structures. This increase in reinforcement density presents significant challenges in the placing and compaction of concrete during construction. It is crucial for the concrete to flow smoothly around densely arranged reinforcing bars, avoiding blockages without segregation. The design of such concrete is a complex task; improper placement or inadequate vibratory compaction can result in honeycombing, undermining the long-term structural integrity and durability of the concrete. Consequently, addressing these challenges in reinforced concrete construction has been a critical area of focus for engineers for many years.

Over the past decades, the field of concrete technology has experienced significant advancements, most notably with the introduction of self-compacting concrete (SCC). This innovative form of high-performance concrete (HPC), also known as self-consolidating, self-levelling, and self-placing concrete, marks a new era in concrete technology with its remarkable deformability and uniformity in the fresh state. It uniquely fills every space around the reinforcement and navigates through densely packed steel bars, achieving compaction solely under its self-weight, eliminating the need for external vibration. SCC's superior attributes have revolutionised design and architectural possibilities. It enables the creation of lighter, more slender structural elements, the development of expansive bridges, and the construction of intricate underwater structures, positioning SCC as a ground-breaking material for both in-situ and pre-cast construction sectors. Initially adopted in Japan, SCC has gradually emerged as a viable alternative to conventionally normal vibrated concrete (NVC), especially in situations where such traditional methods prove challenging. While the application of SCC continues to expand, NVC remains the norm in construction. Nonetheless, as research and exploration into SCC continue to grow, it is poised to transition from a niche innovation to a preferred material in the construction industry.

This chapter outlines the fundamental aspects of SCC, beginning with its definition to establish a clear framework for discussion. The historical development of SCC is examined to evaluate its advantages and challenges and to summarise the key properties that distinguish it in the field of construction. The chapter presents an overview of current mix design methods for SCC, along with an exploration of SCC's rheology. Moreover, it reviews the constituent materials of SCC, emphasising their impact on its properties, and discusses the role of steel fibres in reinforcement. In addition, this chapter provides a concise overview of homogenisation, a technique used to determine the mechanical properties of composite materials, providing a background to a comprehensive exploration of the subject, aligning with the research objectives detailed in Chapter 1.

2.2 Definition of SCC

Self-compacting concrete (SCC) is defined by the British Standard, BS EN 206-9 (2010), as "*concrete that is able to flow and compact under its own weight, fill the formwork with its reinforcement, ducts, boxouts, etc., whilst maintaining homogeneity*" (BS EN 206-9 2010). SCC is also commonly referred to as 'super-workable concrete' and 'self-consolidating concrete'. The Australian Standard, AS 1012.3.5 (2015), further defines SCC as "*concrete that is able to flow and consolidate under its own weight, completely fill the formwork or borehole even in the presence of dense reinforcement, whilst maintaining homogeneity and without the need for additional compaction*". Additionally, the ACI 237 Committee's 2007 report describes self-consolidating concrete (SCC) as "*highly flowable, non-segregating concrete that can spread into place, fill the formwork, and encapsulate the reinforcement without any mechanical consolidation*" (ACI 237R 2007).

As extensively documented in key literature, the efficacy of SCC is founded on three primary requirements: (1) filling ability, referring to the capability of SCC to flow freely under its own weight, thus ensuring complete occupancy of all sections of formwork; (2) passing ability, indicating SCC's proficiency in navigating around obstructions, such as reinforcement, and through narrow spaces without causing blockages; and (3) segregation resistance, a crucial characteristic ensuring that SCC maintains its homogeneous composition both during and after transportation and placement (Khayat et al. 1999b; BS EN 206-9 2010).

2.3 Historical development of SCC

In early 1983, development efforts in Japan focused primarily on eliminating the issue of poor compaction in concrete, identified as a major factor affecting the durability of concrete structures (Okamura and Ozawa 1996). It was recognised that achieving uniform and complete compaction of concrete was challenging due to a shortage of skilled workers. Consequently, Okamura proposed the use of SCC, which was designed to self-compact through its own weight, thereby eliminating the need for vibration and enhancing the durability of concrete structures (Okamura and Ouchi 1999). In 1988, the prototype of SCC was developed at the University of Tokyo by Ozawa (Shi et al. 2015).

SCC technology was introduced in Europe in the late 1990s, initially in Sweden and thereafter in other Scandinavian countries (Al-Rubaye 2016). Development and research into SCC continued in countries such as France, the UK, the USA, and Germany. Presently, SCC technology has been widely adopted in numerous countries around the world, attributed to its numerous benefits such as improved durability of concrete, reduced construction time, and the reduced need for skilled labour in concrete placement and finishing (Goodier 2003). The superior performance of SCC compared to NVC is evident in many modern structural elements, such as thin-walled steel, closely spaced steel bars, and high-rise concrete placement.

2.4 Advantages and challenges of using SCC

Introducing an innovative technology such as SCC into established practice relies on its proven advantages over traditional methods. This section provides a concise summary of the key benefits and challenges associated with the use of SCC, offering a succinct evaluation of its practical implications.

2.4.1 Advantages of using SCC

SCC offers a multitude of advantages owing to its distinctive properties, including enhanced passing ability, superior filling capacity, and improved resistance to segregation. These qualities notably surpass those of traditional concrete. Table 2.1 summarises these

advantages under cost efficiency, quality enhancement, health and safety, and environmental impact.

Table 2.1 Advantages of SCC extracted from literature

Aspect	SCC Advantage	Summary
Economy and cost efficiency	Reduced labour and equipment	The self-compacting nature of SCC significantly lowers the dependency on manual labour and reduces the need for extensive equipment (ACI 237R 2007).
	Reduced construction cost	While the initial production cost of SCC exceeds that of NVC, the overall construction cost is reduced due to efficiencies gained during the construction process (Rasekh et al. 2020). These cost reductions can range between 5% and 21.4%, effectively mitigating the initial higher investment (Rich 2014).
	Reduced construction time	SCC facilitates faster construction due to its rapid concrete pumping capabilities and the reduced time required for casting (Moravvej and Rashidi 2020). Rich (2014) further suggests that the use of SCC can reduce the overall project duration by approximately 20%.
Quality enhancement	Vibration-free	Eliminating the need for vibration during consolidation reduces equipment use, operational costs, and construction time.
	Reduced screeding for flat surfaces	The self-levelling characteristic of SCC minimises the need for screeding operations to achieve flat surface finishes (ACI 237R 2007).
	Ideal for complex structures	The exceptional filling ability of SCC makes it suitable for complex architectural forms, nullifying the need for compaction in constrained spaces (Alyhya 2016).
	Enhanced durability	The lower permeability of SCC mitigates environmental degradation risks (Shi et al. 2015), thus extending the lifespan of concrete structures and reducing long-term maintenance.
	Improved interfacial transition zone (ITZ)	SCC enhances the bond between the cementitious paste, the coarse aggregate, and reinforcement (Stefaniuk et al. 2019; Zhu 2020)
Health and safety	Enhanced labour safety	The use of SCC minimises health risks associated with vibration equipment, such as vibration-induced white finger and hearing loss (Skarendahl 2000).

Table 2.1 (continued)

Environmental impact	Noise pollution reduction	SCC contributes to a quieter construction environment, effectively lowering noise pollution at job sites, precast factories, and in nearby residential areas (Alyhya 2016).
	Energy savings	The high fluidity of SCC conserves energy by eliminating the need for mechanical vibration (Alyhya 2016).

2.4.2 Challenges of using SCC

In recent years, SCC has been increasingly utilised in a variety of civil engineering projects, such as bridges, skyscrapers, tunnel linings, slabs, and precast concrete structures. Despite its many benefits, challenges associated with the use of SCC have been identified (Moruza and Ozyildirim 2017; Moravvej and Rashidi 2020). These challenges provide vital learning opportunities for professionals and researchers engaged in this advanced field, and their resolution is crucial for enhancing the future application and effectiveness of SCC in construction projects. These challenges can be categorised into five key areas as listed in Table 2.2, to facilitate further discussion and analysis.

Table 2.2 Challenges associated with SCC extracted from literature

Aspect	SCC Challenge	Summary
Economic factors	Higher raw material costs	Although SCC reduces overall construction costs, it often has higher raw material costs than NVC (Rich 2014) due to its high cement and chemical admixture content, posing budget challenges in some instances.
Sustainability and environmental impact	Increased cement consumption	The typical higher cement content in SCC enlarges its environmental footprint, mainly from increased CO_2 emissions during cement production (Rich et al. 2012; Adesina and Awoyera 2019).
Structural concerns	Reduced shear strength	Lower coarse aggregate content in SCC mixes weakens the aggregate interlock mechanism, affecting the concrete's shear strength (Griffin and Myers 2016; Moravvej and Rashidi 2020), which results in diminished shear load capacity, expedited deterioration, and reduced energy dissipation under cyclic loads compared to NVC.

Table 2.2 (continued)

Structural concerns (continued)	Reduced elastic modulus	The elastic modulus of SCC is approximately 20% lower than NVC for the same compressive strength (Schlumpf 2004; Bonen and Shah 2005; Jawahar et al. 2013), largely due to the coarse aggregate content and size and their elastic moduli.
	Heat of hydration concerns	The high powder content at low water-to-binder ratios in SCC can lead to heat-induced stress differences, increasing the risk of cracking during the hardening process (Grunewald 2004; Jalal et al. 2015).
	Higher sensitivity	SCC has a greater sensitivity to variations in mix components and proportions than NVC (Alyhya 2016; Van Der Vurst et al. 2017). Minor changes, particularly in water content, can considerably alter SCC's strength (Moruza and Ozyildirim 2017), while the use of local materials can result in a variety of mix compositions.
Construction methodology	Placement methodology adaptation	SCC implementation requires significant alterations to NVC placement methods, demanding more detailed planning and decision-making than with NVC (Rich 2014; Moruza and Ozyildirim 2017; Moravvej and Rashidi 2020).
Quality control	Critical for successful application	Effective quality management is crucial for SCC due to its varied mix designs and constituents. Precise testing and control are required throughout production and construction (Moravvej and Rashidi 2020), as lapses in quality control can lead to significant structural issues, potentially necessitating demolition to prevent later failures.

2.5 Functional requirements of SCC

For an effective SCC design, three critical criteria must be fulfilled: high filling ability, high passing ability, and robust "segregation resistance". These properties are interrelated and influence one another such that alterations in one property typically result in changes in the others. For example, a compromised filling ability and/or a heightened resistance to segregation can lead to inadequate passing ability and may cause blockages. Therefore, designing SCC is a delicate balance between its capacity to fill spaces efficiently and its ability to resist segregation (Alyhya 2016).

2.5.1 Filling ability

The filling ability of fresh SCC refers to its capability to flow into and completely fill all the spaces within the formwork, relying solely on its self-weight. These characteristic mirrors SCC's deformability attribute, defined as the concrete's capacity to change its shape, propelled by its own weight and the energy imparted during casting (Alyhya 2016). Deformability in SCC involves two key aspects: firstly, deformation capacity, which measures the extent to which the concrete can spread, and secondly, deformation velocity, which is a measure of the time taken for the concrete to stop flowing, essentially gauging the flow speed (Khayat 1999). The filling ability represents a synergy between the deformation capacity and velocity. For example, an SCC with substantial deformation capacity but reduced deformation velocity would typically be more viscous, leading to a prolonged duration in filling the formwork, but with the same end result.

To improve the filling ability of SCC, it is critical to provide a sufficient quantity of paste to not only envelop the surface area of each aggregate but also exist in excess to reduce the inter-aggregate friction significantly. An adequate paste layer is essential as its absence would lead to an undesirable increase in friction between the aggregates, considerably decreasing the workability of the concrete. This is schematically illustrated in Figure 2.1, depicting the formation of cement paste layers around the aggregates.

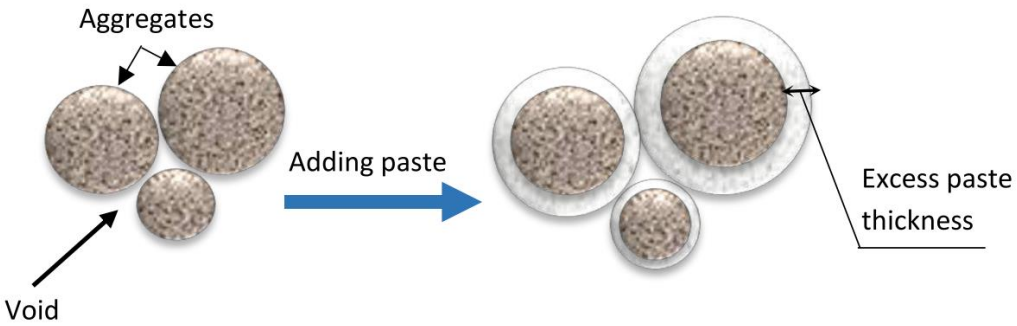

Figure 2.1 Enhanced workability in SCC due to excess paste thickness around aggregates (Deeb 2013)

2.5.2 Passing ability

Passing ability is the characteristic of SCC that reflects its ability to navigate through tightly packed reinforcement without blockage, while simultaneously ensuring a homogeneous

distribution of solid particles (aggregates and fibres). This homogeneity is critical in preventing the formation of arches or stoppages around obstacles; the J-ring and L-box tests are commonly utilised to assess this property.

The passing ability of SCC is significantly influenced by the shape, size, and volume of the coarse aggregate (CA) incorporated into the mix (Al-Rubaye 2016). The potential for the occurrence of blockages increases as larger-sized CA or higher fibre contents are included in the mix. In situations where the concrete flows through tight spaces, the CA may form bridges or arches at the restricted areas, leading to the obstruction of subsequent concrete flow, such as illustrated in Figure 2.2. Moreover, the addition of fibres, particularly those that are long and have hooked or crimped ends, can further impede the flow of SCC through the reinforcement mesh (Deeb 2013).

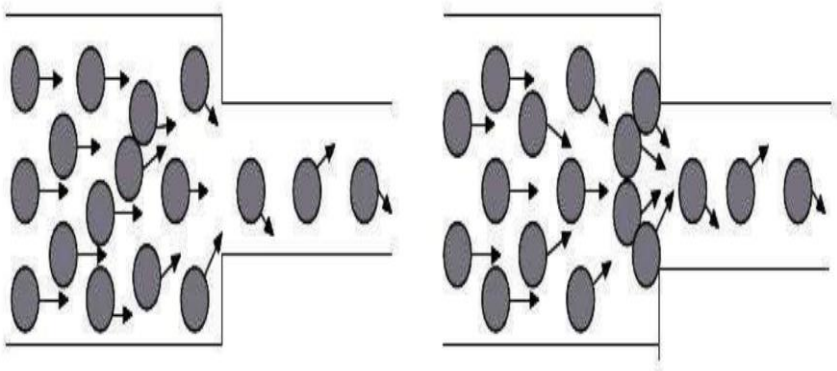

Figure 2.2 Aggregate blocking in SCC at constricted openings (Al-Rubaye 2016)

2.5.3 Segregation resistance

Segregation resistance, also known as stability in SCC, is the property of a concrete mix that ensures the even distribution of its CA and fibres, which is crucial for maintaining the uniformity of the mix. The stability of SCC is greatly influenced by its cohesiveness and viscosity, which are typically improved by reducing the water content not bound by cement and increasing the fines content (Tangtermsirkul and Khayat 2000). Bleeding, a specific type of segregation, is characterised by water rising and separating from the mix due to capillary action. While some bleeding is typical in concrete, excessive bleeding can compromise its strength, increase the porosity, and adversely affect the concrete's durability, especially at the surface (Deeb 2013).

Segregation resistance is characterised by two fundamental aspects. The first is static segregation, which is the separation of solid particles from the paste when the concrete is stationary. The second aspect, dynamic segregation, occurs during the transportation and placement of the concrete (Esmaeilkhanian et al. 2014). To ensure adequate concrete stability in both scenarios, two fundamental methods are utilised. The first follows the Japanese model and employs a superplasticiser (SP), a low water-to-cement (w/c) ratio, high powder content, admixtures, and a lower CA content. The second method involves the use of viscosity-modifying admixtures (VMAs) coupled with a low to moderate powder content and SP (Bonen 2005).

2.6 Proportioning of SCC mixes

Mix designs for SCC are specifically chosen to fulfil the required performance criteria in both fresh and hardened states, while being tailored for specific applications. This involves the selection of the powder material contents, the water-to-cementitious material ratio (w/cm) or water content, the sand-to-aggregate ratio (S/A), the CA content, and the air content to meet durability specifications (Sonebi and Yahia 2020). With the increasing availability of a variety of materials, the complexity of SCC mix design has grown. These materials include a range of cement and aggregate types (such as both rounded and crushed), supplementary cementitious materials (SCMs), and chemical admixtures, including VMAs and SP.

Consequently, the proportioning of SCC involves careful consideration of numerous variables and extensive testing to optimise its composition (Abo Dhaheer 2016). Currently, three primary approaches are used for SCC mix proportioning: (a) the powder approach, which increases the powder and fine material content using materials such as fly ash, ground granulated blast-furnace slag (GGBS), or limestone powder; (b) the viscosity agent approach, employing VMAs for enhanced stability; and (c) the combined approach, which merges elements of both the powder and viscosity agent approaches (Sonebi and Yahia 2020). The following sections examine the proportioning of SCC mixes in comparison to NVC, analyse the range of quantities for SCC components, and review the methodologies developed for SCC design.

2.6.1 Comparative analysis of mix proportions: SCC versus NVC

SCC comprises the same fundamental ingredients as NVC, namely cement, water, aggregates, and admixtures. However, SCC is distinct due to its increased use of fine particles, reduced CA content, lower w/cm, and the addition of SP, enabling its flowability and compaction characteristics. Figure 2.3 provides a visual representation of the typical volumetric percentages of the constituent materials in both SCC and NVC.

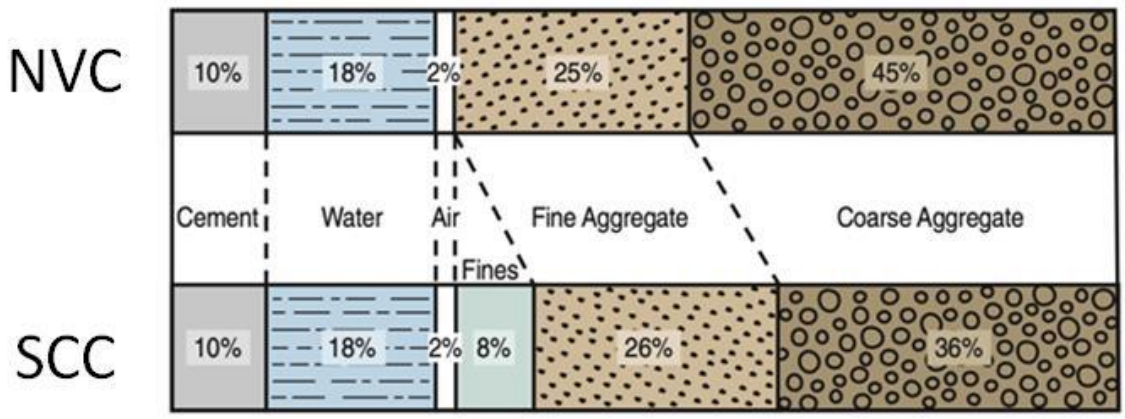

Figure 2.3 Materials used in NVC and SCC, expressed by absolute volume (Kerkhoff et al. 2002)

2.6.2 Quantitative ranges of constituent materials in SCC mixes

In the field of SCC mix design, determining the optimal percentages of constituent materials is crucial in attaining the intended properties. The literature offers varied research on the ideal ranges for these components. Although the composition of SCC involves specific ranges for each constituent, these can be adjusted based on the required strength and performance objectives of the concrete; typical ranges extracted from EFNARC (EFNARC 2005) are listed in Table 2.3.

Domone (2006) examined 56 SCC applications, highlighting the diversity and flexibility in SCC mix compositions. His analysis revealed that CA typically constitutes 28–38% of the concrete volume and fine aggregate 38–54% of the mortar volume. The study results also indicated that the water-to-powder (w/p) ratio ranges from 0.26 to 0.48 by weight, the paste content varies from 30% to 42% of the total concrete volume, and the powder content ranges from 445 kg/m³ to 605 kg/m³. These insights underscore the adaptable nature of SCC mix design, accommodating a broad range of structural and durability requirements.

Table 2.3 Typical range of SCC mix compositions according to EFNARC (2005)

Constituent	Typical range by mass (kg/m^3)	Typical range by volume (litres/m^3)
Cementitious material	380–600	––
Paste	––	300–380
Water	150–210	150–210
Coarse aggregate	750–1000	270–360
Fine aggregate	48–55% of total aggregate weight	
Water/cm ratio by Vol.	0.85–1.10	

2.6.3 Overview of mix design methods for SCC

Mix design is a crucial step that lays the groundwork for both research and practical concrete implementation. It is essential to start with an understanding of SCC applications in the construction industry as this determines the target properties for mix designs. The proportioning of constituent materials must be precisely designed to balance the fresh properties of SCC, such as segregation resistance versus deformability.

Segregation resistance can be achieved by controlling the mortar rheology by increasing the powder content and possibly adding VMAs, whereas deformability is achieved by managing the CA volume (Shi et al. 2015). Moreover, SCC's characteristics, such as strength, durability, shrinkage, and rheology, are influenced by the mix proportions. The incorporation of mineral and chemical admixtures, the characteristics of the raw materials, the aggregate packing density, and the w/cm all affect SCC's properties (Wang et al. 2014; Al-Rubaye 2016). Thus, mix proportioning for SCC should be broadly applicable, meet all technical criteria, and be both sustainable and cost-effective (Alyhya 2016).

Despite multiple proposals for mix proportioning methods for SCC over the past three decades, based on varying concepts and control parameters, none have fully satisfied all the specifications and requirements. The lack of precise design specifications for the SCC design process compounds the challenge of determining the viability of available designs. To achieve high-quality SCC with the necessary properties, the most effective method should be selected based on the specific circumstances and the desired characteristics for each

application. The various design methods can be categorised into six groups according to their design principles and parameters; this will be discussed in the subsequent sections.

2.6.3.1 Empirical design method

In the context of SCC mix design, this approach is grounded in empirical evidence and comprises the determination of the initial mix proportions based on key components like coarse and fine aggregate content, water, SP dose, and cementitious materials (cm). This process includes the production of a series of sample blends and modifications, which are crucial for determining the appropriate blend proportions to achieve the desired SCC properties (Shi et al. 2015). The design method proposed by Okamura and Ouchi (1999) is a notable example of this approach. This method stipulates a fixed fine aggregate (F-A) content of 40% of the mortar volume and a CA content of 50% of the solid volume. An integral part of this methodology is the careful adjustment of the SP dosage and the w/p ratio, recommended as between 0.9 and 1.0 by volume, to ensure the self-compacting ability of the concrete. The advantage of this empirical approach is its wide applicability in various SCC projects. Nonetheless, it presents certain limitations. Extensive laboratory research is required to determine the most effective mix proportions and to understand the interactions and compatibility of the different constituents. A further drawback is the absence of detailed criteria for aggregate properties, such as maximum aggregate size and grading, which are crucial in the mix design process.

2.6.3.2 Strength-based design method

The strength-based SCC design method focuses on determining the material quantities, such as mineral admixtures, cement content, water, and aggregate, based on the required compressive strength. Kheder and Al Jadiri (2010) proposed a SCC mix modelling approach that integrated and enhanced the ACI 211.1-91 (1991) method, which is traditionally used for proportioning NVC, along with the EFNARC (2005) guidelines specifically designed for SCC. This approach thus combines the foundation principles of both methods with specific improvements tailored for SCC. Notably, while the ACI 211.1-91 method prescribes a compressive strength range of 15 to 40 MPa for NVC, the range for SCC using this improved

method extends 75 MPa, while the determination of the CA content is influenced by the overall aggregate size and the fineness modulus of the fine aggregate.

A mix design method for SCC incorporating GGBS was developed based on the compressive strength requirements and the efficiency of GGBS, achieving strength ranges of 30–100 MPa, with GGBS replacements varying between 20% to 80% (Dinakar et al. 2013). In addition, Dinakar and Manu (2014) introduced an SCC mix design approach based on the efficiency principle for varying percentages of metakaolin, with the w/c ratios varying between 0.22 and 0.31. For a consistent powder content of approximately 550 kg/m^3 and metakaolin replacement levels of 7.5%, 15%, and 22.5%, the compressive strengths of SCC were found to be 80, 100, and 120 MPa, respectively. Compared to NVC, the SCC containing metakaolin exhibited a higher strength gain after 28 days of curing, with compressive strengths surpassing those of NVC.

The compressive strength-based approach has the advantage of providing a straightforward and clear procedure for obtaining variable quantities of constituents, reducing the need for trial mixes. This method also considers the contribution of pozzolanic materials and the grading of F-A and CA, which are integral to enhancing the properties of SCC. However, it necessitates modifications to all materials, including F-A, CA, water, and SP, to achieve the optimal mix proportion (Ashish and Verma 2019).

2.6.3.3 Close aggregate packing method

The close aggregate packing method for SCC mix design establishes mix proportions by initially identifying the smallest voids present between the aggregates using a packing model and using paste to fill the identified voids (Shi et al. 2015). This method emphasises the critical interaction between paste and aggregate blending processes in SCC. A significant advantage of this method is its simplicity, primarily attributed to the minimal use of binders and the focus on minimising paste volume. This reduced paste volume approach simplifies the process and economises the mix by using less of the typically more expensive component - the binder. However, a noteworthy disadvantage of this method is the increased tendency for the SCC to segregate during application in construction scenarios.

2.6.3.4 Statistical factorial method

The statistical factorial method in SCC mix design is centred around the evaluation of the impact of key parameters, including the volume of cement, CA, and fillers, w/cm, and SP dosage. These elements are critical in determining the workability and strength of SCC (Shi et al. 2015). In this method, the mix proportions are determined by assessing each parameter's contribution, akin to the process used in NVC mix design. Khayat et al. (1999a) introduced a notable protocol incorporating various mix parameters, such as VMA dosage, cm content, CA volume, SP dosage, and w/c ratio. In addition, F-A content is adjusted to satisfy the total volume requirements. The efficacy of these parameters is statistically correlated with each measured property, including slump flow, V-funnel flow time, filling ability, and compressive strength.

A primary advantage of this technique is its versatility, enabling application in a diverse array of scenarios. This adaptability is crucial in providing insights into how principal variables affect the properties of SCC. However, a significant limitation of this approach is the need to develop statistical correlations, necessitating extensive laboratory research with readily available raw materials.

2.6.3.5 Eco-SCC mix design method

The Eco-SCC method introduces a more sustainable model for SCC. Eco-SCC is defined by a maximum powder content of 315 kg/m³ and integrates materials such as clay, fly ash, silica fume, and limestone filler (Ashish and Verma 2019). To enhance stabilisation and mitigate segregation and bleeding, the use of VMAs is recommended (Ashish and Verma 2019). The robustness field is a crucial factor in Eco-SCC and is vital for determining its self-compacting status (Mueller et al. 2016). The low paste capacity of Eco-SCC poses challenges in achieving the necessary flow workability, increasing its susceptibility to blockage. To address this, it is essential for the granular skeleton to maintain a high packing density and to carefully control the CA volume to minimise the risk of blockage. Cement replacement in Eco-SCC requires careful consideration to ensure compliance with standards for both the fresh and hardened states of the concrete (Ashish and Verma 2019). Esmaeilkhanian et al. (2017) proposed a low carbon footprint design for Eco-SCC based on the optimisation of powder, sand, and CA

compositions. The chosen powder fractions aim to provide sufficient mechanical and durability properties while reducing water requirements. SCC mixes with powder contents ranging from 278 to 312 kg/m³ and compressive strength target ranges of 25–35 MPa have shown to possess adequate passing ability, high filling efficiency, and stability.

In addition, Long et al. (2015) explored the environmental impact of SCC in relation to its mix proportion parameters to develop a greener and more sustainable SCC mix design method. This method incorporates three indices: embodied energy consumption, CO_2 emission, and resource expenditure indices, all linked with the mix compressive strength. Notably, partially replacing the cement with mineral admixtures such as fly ash, GGBS, and limestone powder has been observed to reduce these indices significantly.

2.6.3.6 Paste rheology method

The paste rheology method in SCC design conceptualises SCC as a two-phase material consisting of solid aggregate particles suspended in a viscous paste. This framework underscores the significant influence of the paste's rheological properties on the workability of SCC, complemented by the physical properties and content of the solid aggregates (Ashish and Verma 2019). In this context, Saak et al. (2001) developed a design method for SCC, emphasising that the rheology and density of the cement paste matrix are key factors affecting segregation resistance and workability of fresh concrete. This method is particularly focused on managing segregation in SCC, yet it excludes a thorough exploration of the impact of aggregate properties and materials on the concrete's filling and passing abilities and omits specific guidelines for achieving high strength and durability.

Karihaloo and Ghanbari (2012) proposed a mix modelling approach that concentrates on plastic viscosity for proportioning both standard and high-strength self-compacting concrete (HSSCC) mixes. While this method does not directly incorporate compressive strength as a design parameter, it effectively uses the SCC mix's plastic viscosity characteristics. To address this gap, Abo Dhaheer et al. (2016) introduced a fundamental mix proportioning approach that integrated compressive strength into the existing method. This approach offers practical guidance through design charts that focus on rheological properties defined by the

concrete's plastic viscosity and compressive strength, aiming to achieve a plastic viscosity range of 3 to 15 Pa·s and a compressive strength range of 30–80 MPa.

A comprehensive overview of SCC mix design approaches is provided in the literature (Shi et al. 2015; Ashish and Verma 2019). These references offer an extensive analysis from 1995 to 2017, providing an empirical foundation for selecting appropriate SCC mix design methods and discussing in detail the processes, strengths, and weaknesses of the various approaches.

2.7 The rheology of SCC

The fresh properties of concrete are of great significance due to their impact on the formation process and the construction casting quality, as well as on the hardened properties of the concrete. The behaviour of fresh concrete is often described in terms of flowability, workability, consistency, mobility, compatibility, pumpability, and achievable surface finish. However, these terms are subjective, qualitative, and empirical and lack a quantitative basis. For example, in comparison with the standard workability tests, such as the slump test, rheological parameters allow for a precise phenomenological description of flow characteristics and significant investigation and can be used as input for numerical simulations (Feys et al. 2017). Applying fundamental physical quantities is crucial to accurately characterise the fresh properties of concrete, thereby minimising potential errors (Jiao et al. 2017).

The term *'Rheology'* was first proposed by Professor Bingham in 1920. Rheology is defined as *'the science of flow and deformation of matter'* (Barnes et al. 1989). This introduction sparked a significant interest in the field, leading to the establishment of the Society of Rheology and the Journal of Rheology. Rheology has become an indispensable tool for researchers and engineers across various industries, such as the printing, plastics, detergents, oils, and paint industries. In the domain of concrete and cementitious materials, rheology focuses on an understanding of the changes in plasticity, elasticity, and viscosity of cement-based materials under shear stress. The rheological properties of concrete are critically influential on the construction and casting processes (Jiao et al. 2017).

The study of the rheology of SCC is particularly vital for the construction industry since concrete is utilised in its plastic state (Ghanbari and Karihaloo 2009). Yen et al. (1999) noticed that the rheological approach provided more consistent results in describing the flowability of concrete, compared with single-point tests such as the slump flow test. Rheology is instrumental in characterising the workability of SCC, predicting its stability, flow behaviour, and even compatibility. Moreover, the fresh properties of concrete significantly impact its hardened properties and its suitability for various engineering applications (Jiao et al. 2017).

2.7.1 Rheological models of SCC

Numerically describing and predicting the flow and deformation of complex fluids such as fresh concrete presents a significant challenge. Fresh concrete comprises both organic and inorganic components, with particle solids varying in size from micrometres to millimetres. In addition, the rheological behaviour of concrete changes over time due to the intricate process of cement hydration (Jiao et al. 2017). Despite these complexities, numerous rheological models have been proposed in the literature to characterise the rheology of SCC in its fresh state. Among these models, the Bingham model and the Herschel-Bulkley model have garnered widespread recognition for their ability to describe the relationships between shear stress and shear rate in fresh concrete (Chidiac and Mahmoodzadeh 2009; Mahmoodzadeh and Chidiac 2013).

2.7.2 The rheology of SCC as a suspension

SCC is a composite material composed of cement, water, mineral additions, chemical admixtures, and aggregates. Numerous researchers have conceptualised fresh SCC as a two-phase suspension, where solid aggregate particles constitute the solid phase and are suspended in a viscous liquid phase (cement paste) (Ferraris 1999; Geiker et al. 2002; Fuglsang Nielsen 2003; Koehler and Fowler 2007; Ghanbari and Karihaloo 2009). The viscosity behaviour of this suspension is influenced by the solid phase volume fraction. At low solid phase concentrations (volume fractions < 0.1), the relationship between the plastic viscosity of the suspension and the shear rate remains relatively constant, making it feasible to consider the suspension as a Newtonian fluid. However, as the volume fraction of solids

approaches a critical value, approximately equal to the maximum packing fraction (ϕ_m), the suspension's behaviour transitions to that of a non-Newtonian fluid (Ghanbari and Karihaloo 2009).

Generally, three types of forces act on particles within flowing suspensions, each playing a significant role. Firstly, colloidal forces may lead to either attraction or repulsion between particles, influenced by factors such as electrostatic charges, London Dispersion forces, and Van der Waals forces. Secondly, Brownian forces cause random motion and are particularly influential for particles smaller than 1 µm due to their strong size-dependency. Thirdly, viscous forces play a crucial role, as these are proportional to the local velocity difference between the particles and the surrounding fluid (Barnes et al. 1989).

The rheology observed in such systems is heavily influenced by these microstructural considerations. For instance, the presence of isolated particles alters the fluid flow lines, leading to increased viscosity (Barnes et al. 1989). At low shear rates, colloidal and Brownian forces are capable of restoring the suspension's random structure. However, at higher shear rates, the restorative capability of these forces becomes inadequate, and the particles align along the flow direction. In the context of aggregate suspensions, viscous forces are the predominant factor. Nonetheless, for the smallest aggregate particles, the effects of colloidal and Brownian forces cannot be disregarded (Koehler and Fowler 2007).

2.7.3 Measurement of the rheological properties of cement paste

Measuring the rheological properties of cement paste is a complex task, necessitating careful attention before, during, and after the measurements (Feys et al. 2017). Several key issues must be considered when assessing the rheological properties of cement paste, two of which are key to this thesis:

1. The cement paste contains a considerable number of particles which are borderline non-colloidal and colloidal in size (Wallevik 2009). The behaviour of colloidal particles is significantly influenced by interparticle interactions, such as electrostatic repulsion forces and Van der Waals dispersion forces (Roussel et al. 2010).

2. The rheological properties of the paste are dynamic, changing due to chemical reactions that progress over time (Wallevik 2009).

The nature, size distribution, and morphology of the particles critically influence the plastic viscosity of the paste (de la Rosa et al. 2020). The plastic viscosity can be easily measured using viscometers to a reasonable degree of accuracy. These devices may not be suitable for field use or be available in every laboratory. In such instances, alternative cheap and simple instruments can be used to obtain good approximations of the actual rheological properties of the paste, such as the EN445 cone test, mini-cone slump test (Ferrara et al. 2012b), the Marsh funnel, and the Cannon-Fenske viscometer (see Figure 2.4) (de la Rosa et al. 2020).

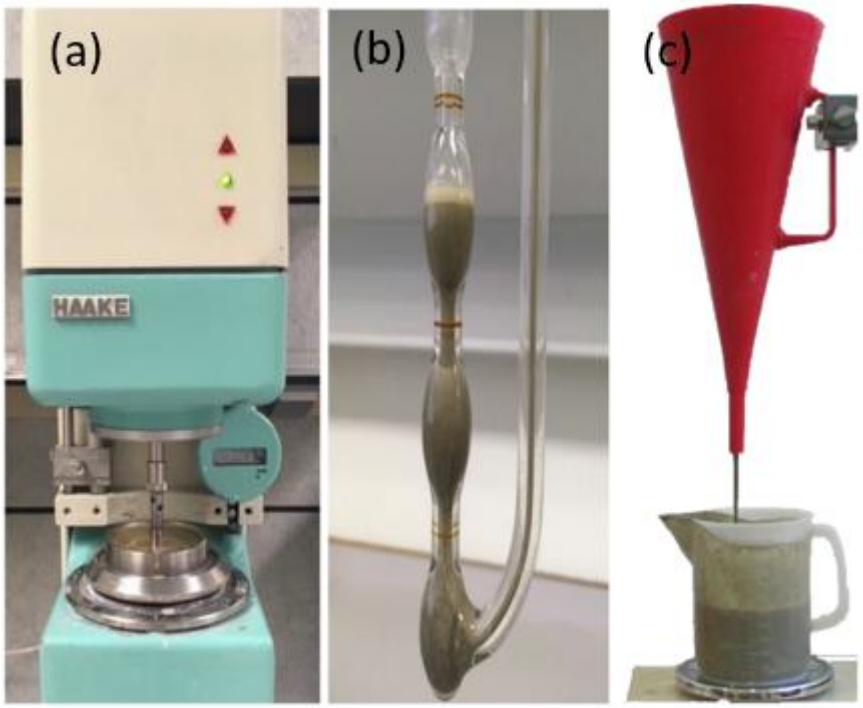

Figure 2.4 Measuring devices: (a) Haake RS50 rheometer, (b) Cannon–Fenske viscometer, and (c) Marsh funnel (de la Rosa et al. 2020)

It is important to note that the plastic viscosity of cement paste is primarily influenced by the w/cm ratio and the proportion of SP to cementitious materials and water (Ghanbari and Karihaloo 2009). However, several additional factors can impact the plastic viscosity of the paste. These include the dosage and type of SP (Lachemi et al. 2004; Mikanovic and Jolicoeur 2008), the type of cement additives used (Ferraris et al. 2001; Mikanovic and Jolicoeur 2008; Diamantonis et al. 2010), time and mixing sequence (David A. Williams et al.

1999; Aiad et al. 2002), as well as various environmental conditions such as temperature and pressure (de la Rosa et al. 2020).

2.7.4 Evaluation of the rheological properties of SCC

Over the past decade, numerous tests have been developed for measuring concrete flow. The primary objective of these tests is to evaluate the quality of concrete delivered on construction sites or to determine the optimal mix for specific applications. However, most of these tests are based on empirical methods rather than on the application of rheological properties. A comprehensive list and descriptions of these tests can be found in the RILEM reports TC 145-WSM (Bartos et al. 2002) and TC 266-MPR (Feys et al. 2023), and the American Concrete Institute report ACI 238 (2008).

Terms such as workability, flowability, mobility, consistency, and pump ability are commonly used to describe the rheological behaviour of concrete in its fresh state. However, these terminologies often reflect subjective interpretations rather than scientific precision (Wallevik and Wallevik 2011), as they rely on visual inspection and subjective assessment of the concrete. In response to this, studies have focused on transitioning from empirical testing to scientifically based approaches that yield results in fundamental units (Ferraris and Martys 2012). To facilitate this shift, the rheometer test apparatus has been developed and is increasingly used in the field of concrete rheology. Rheometers are widely utilised for measuring the rheological properties of fresh concrete. The first such apparatus, a two-point workability test designed by Tattersall, was developed to measure the plastic viscosity and yield stress of fresh concrete. Subsequently, various devices have been developed based on similar principles and concepts (Rasekh et al. 2020), such as the Tattersall MK III rheometer, coaxial rheometer BML, Vikomat rheometers, ICAR rheometer, and the BTRHEOM rheometer (Sonebi and Yahia 2020), as shown in Figure 2.5.

It is important to note that these rheometers often yield differing results for the yield stress and plastic viscosity of a single concrete mix (Feys et al. 2007; Feys et al. 2023), as illustrated in Figure 2.6, sometimes up to twice as high (Feys et al. 2017). Due to the complex behaviour of concrete and the varied rheometer setups, it has been reported that obtaining actual rheological parameters (yield stress and plastic viscosity) in fundamental units from

rheometer readings is nearly impossible (Vasilić 2015). Measuring the plastic viscosity of SCC presents several challenges and potential inaccuracies, largely due to the presence of large particles in the concrete, and this issue becomes particularly pronounced when steel fibres are included in such mixes. In contrast, the plastic viscosity of the paste component of SCC can be measured with a reasonable degree of certainty (Ghanbari and Karihaloo 2009). Given the significant discrepancies observed in rheological parameters obtained from varying rheometers, Ghanbari and Karihaloo proposed a micro-mechanical model designed to estimate the plastic viscosity of SCC mixes, both with and without fibre, based on the plastic viscosity of the paste (Ghanbari and Karihaloo 2009). This concept of the micro-mechanical model has been further utilised and developed by other researchers and has been applied to predict the plastic viscosity of SCC mixes containing steel fibres (Ghanbari and Karihaloo 2009; Karihaloo and Ghanbari 2012; Deeb and Karihaloo 2013; de la Rosa et al. 2018) and those without steel fibres (Karihaloo and Ghanbari 2012; Deeb and Karihaloo 2013; Abo Dhaheer et al. 2016a; Abo Dhaheer et al. 2016b; Alyhya et al. 2016). The principles and procedures of this micro-mechanical model will be discussed in detail in later sections of this thesis.

Figure 2.5 Rheometer types: (a) BML-rheometer, (b) Tattersall MK III rheometer, and (c) Vikomat XL rheometer (Sonebi and Yahia 2020)

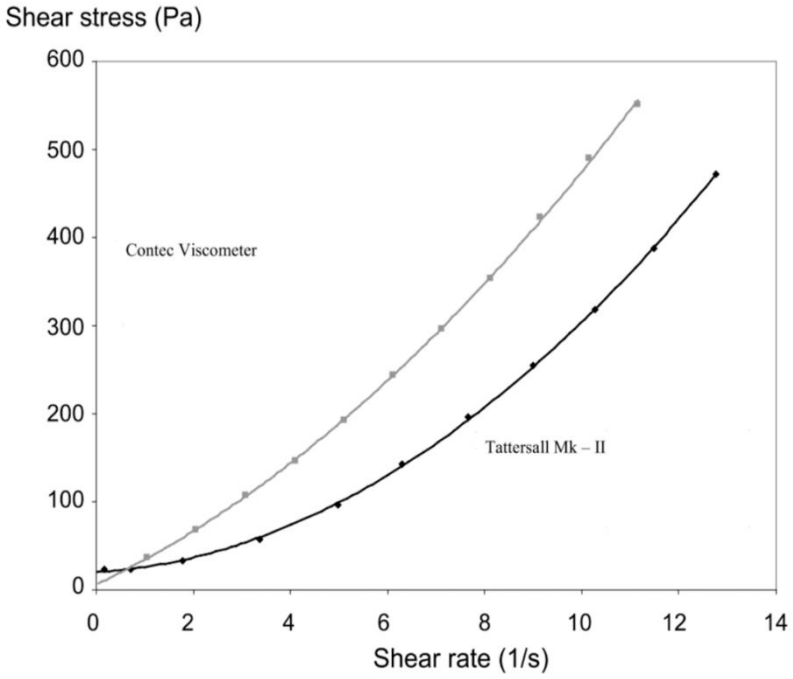

Figure 2.6 Varying shear stress results for a single SCC mix from two rheometers (Feys et al. 2007)

2.8 Constituent materials of SCC mix

SCC is composed of materials similar to those found in NVC but with specific criteria unique to SCC. These criteria often cannot be fulfilled using standard materials and design procedures. A detailed discussion of the materials involved in SCC, along with their effects on the properties of the concrete in both its fresh and hardened states, is discussed in the subsequent subsections.

2.8.1 Cement

Portland cement is the predominant cement type used in a wide array of concrete structures. Various Portland cement classes have been employed in the formulation of SCC, including CEM Type I, sulphate-resistant cement, and blast furnace slag cement. The selection of cement is generally guided by the specific demands of the given application, rather than by requirements unique to SCC. As per the European guidelines for SCC established by EFNARC (EFNARC 2005), any cement category adhering to the standards of EN 197-1 is deemed suitable for the production of SCC (British Standards Institute 2015).

Portland cement is predominantly composed of four major compounds: tricalcium silicate (C_3S), dicalcium silicate (C_2S), tetracalcium aluminoferrite (C_4AF), and tricalcium aluminate

(C_3A), along with an appropriate quantity of gypsum. The hydration process and subsequent setting characteristics are significantly influenced by the relative proportions of these mineral components and the w/c ratio. It is recognised that the rheological behaviour of cement paste may be affected by the cement's mineralogical makeup. During hydration, when cement interacts with water, ions such as hydroxide (OH^-), potassium (K^+), sodium (Na^+), and sulphate (SO_4^{2-}) are released. These ions can affect the adsorption of SP to the cement particles, thereby altering the rheological properties of the cement paste (Jiao et al. 2017). Furthermore, the fineness of cement significantly influences the rheological properties of cement paste, as the finer cement particles hydrate quicker than their coarser counterparts, and consequently require a greater quantity of water to achieve the same level of workability (Jiao et al. 2017).

2.8.2 Water

Water content plays a pivotal role in defining the characteristics of both NVC and SCC at both fresh and hardened stages. It has been observed that SCC has a greater sensitivity to water content variations than NVC. The appropriate amount of water is fundamental to the cement hydration process, leading to the formation of a cohesive paste that is key in binding the aggregates together. As recommended by EFNARC (2005), the ideal water content range for SCC lies between 150 and 210 litres per cubic meter of concrete.

2.8.3 Mineral additive

The prevailing method to formulate SCC involves reducing the CA content, adding SP, increasing the paste volume, and minimising the maximum CA particle size. This reduction in CA content leads to an increase in the mortar content within the mix; consequently, the powder content in SCC is substantially greater than that in NVC, owing to the augmented paste volume.

However, the high cement volume in SCC can induce issues in specific structural applications, such as elevated hydration heat, heightened autogenous shrinkage, and increased costs (Rasekh et al. 2020). In addition, the CO_2 emissions and the depletion of natural resources inherent in cement production pose severe environmental concerns (Jalal et al. 2015). Despite these challenges, enhancing the paste content is crucial for achieving superior

quality SCC (Mechtcherine et al. 2020; Rasekh et al. 2020). To address these concerns, mineral additives have been introduced to mitigate the adverse effects. The incorporation of mineral additives not only reduces the environmental footprint of concrete production but also enhances the sustainability of SCC, while concurrently diminishing production costs. Table 2.4 presents the advantages and disadvantages of typical mineral additives such as GGBS, Fly Ash, Rice Husk Ash (RHA), and Metakaolin.

Table 2.4 Benefits and limitations of mineral additives

Material	Advantages	Disadvantages
GGBS: By-product of the quenching of iron blast furnace slag in steam or water (Öner et al. 2003; Boukendakdji et al. 2012; Al-Oran et al. 2022)	• Enhances workability and prolongs the setting time of fresh concrete. • Reduces segregation and bleeding in fresh concrete due to the lower density of GGBS. • Demonstrates increased resistance to sulphate attacks, exhibits lower permeability, and has a reduced heat of hydration. • The water demand tends to be lower, due to the smoother surface texture of slag particles and the delay in the chemical reaction process.	• Reduces the initial rate of hardening and compressive strength gain. • Can be an irritant to the eyes and respiratory system in humans.
Fly ash: By-product of the combustion of powdered coal in thermal power plants (Nehdi and Rahman 2004; Grzeszczyk and Podkowa 2009; Duran-Herrera et al. 2019; Matos et al. 2019; Li et al. 2021).	• Enhances workability and fluidity of fresh concrete, reducing water demand in the batching process. • Improves the mechanical properties and durability of SCC, particularly at later stages. • Reduces the requirement for expensive SP and cement, thereby lowering SCC production costs. • Mitigates thermal cracking and reduces the heat of hydration at early ages. • Increases both compressive and tensile strength of SCC when used in controlled Portland cement replacement proportions (up to 20%). • Suitable for producing lightweight, non-structural concrete at high percentages.	• Workability reduces at GGBS proportions greater than 10%. • Quality varies depending on the manufacturer and production processes. • Effectiveness is limited to certain percentages of cement replacement; beyond this, compressive strength may decrease.

Table 2.4 (continued)

Fly ash (continued):	• Reduces porosity and water absorption in SCC, helping to suppress alkali aggregate reactions. • Improves resistance to sulphate attack and chloride penetration. • Slightly enhances resistance to freezing and thawing.	
Rice Husk Ash (RHA): By-product of burnt rice husks (Salas et al. 2009; Thomas 2018)	• Enhances the durability of SCC. • Increases both compressive and tensile strength of SCC when used in controlled Portland cement replacement proportions (up to 20%). • Suitable for producing lightweight, non-structural concrete at high percentages. • Reduces porosity and water absorption in SCC, helping to suppress alkali aggregate reactions. • Improves resistance to sulphate attack and chloride penetration. • Slightly enhances resistance to freezing and thawing.	• Workability reduces at RHA proportions greater than 10%. • Decreases the workability of SCC, leading to increased water demand in the production process. • Compressive and tensile strength significantly decrease when RHA is used in high proportions, necessitating controlled use.
Metakaolin (Al-Oran et al. 2022)	• Environmentally friendly material. • Increases the strength of concrete at early ages. • Can improve the viscosity of concrete, contributing to better workability.	• Increasing Metakaolin content may lead to an increase in water content and SP requirement, potentially affecting the workability of SCC

2.8.4 Aggregate

Aggregates account for approximately 60% of the total volume of SCC. The physical properties of these aggregates play a crucial role in determining the performance of SCC. It is essential to include particle size fractions smaller than 0.125 mm in the fines content of the paste, and to consider these fractions when calculating the w/p ratio. Although the high volume of paste in the SCC mix helps to reduce internal friction between aggregate particles, achieving a suitable grain size distribution remains a critical factor for optimal concrete performance (EFNARC 2005). The typical mix proportions in SCC feature a lower aggregate content compared to NVC. This variance in composition can influence the mechanical properties of SCC, including aspects such as compressive strength, unit weight, modulus of elasticity, and splitting tensile strength, which are pivotal in the design and overall performance of concrete structures (Jawahar et al. 2013).

Numerous studies suggest that the rheological properties of concrete, specifically plastic viscosity and yield stress, are significantly influenced by aggregate composition. The overall consensus is that an increased CA volume fraction elevates both plastic viscosity and yield stress, whereas a higher F-A volume tends to increase yield stress but decrease plastic viscosity (Hu 2005; Hu and Wang 2007; Yardimci et al. 2014; Jiao et al. 2017). This phenomenon has been attributed to the fact that a greater proportion of F-A reduces friction among CA particles, raises the mix water demand, and increases the surface area of solid particles, consequently lowering plastic viscosity and raising yield stress (Jiao et al. 2017).

The fine aggregate to total aggregate (FA/TA) ratio is a critical factor in determining concrete's rheological properties. A low FA/TA ratio adversely impacts flowability due to insufficient mortar to fill the voids between the CA particles. Conversely, a high FA/TA ratio can also diminish flowability, as the increased specific surface area of solid particles reduces the thickness of the cement layer, thereby decreasing aggregate friction (Jiao et al. 2017). The European Guidelines for Self-Compacting Concrete EFNARC (2005) suggest that the typical range of F-A is 48–55% of the total aggregate by weight (see Table 2.3).

2.8.5 Chemical Admixtures

Central to the production of SCC are SP, otherwise known as high-range water-reducing admixtures (HRWRAs). In certain situations, VMAs are also used to enhance the mix. Further admixtures have been used successfully in SCC, such as air-entraining agents and set-modifying agents. The specific functions and contributions of HRWRAs and VMAs in SCC will be briefly discussed in the subsequent subsections.

2.8.5.1 Superplasticisers

SPs are virtually indispensable in modern concrete, offering both technical and economic advantages, such as a significant reduction in the plastic viscosity and yield stress of cement-based materials. A diverse range of SP, such as polycarboxylate, melamine, and naphthalene-based types, has been extensively employed (Santos et al. 2015). SP plays a vital role in the formulation of SCC to attain the necessary workability (Okamura and Ouchi 2003), where the primary aim of incorporating SP is to enhance the flow properties of concrete while maintaining a low w/p ratio.

2.8.5.2 Viscosity-modifying admixtures

VMAs, often referred to as anti-washout admixtures, improve several critical properties of concrete mixes, including plastic viscosity, yield stress, thixotropy, and the extent of shear thinning. In the context of SCC applications, VMAs significantly contribute to enhancing segregation resistance, reducing bleeding, and improving cohesion. They also facilitate the use of a wider variety of materials, such as manufactured sands and gap-graded aggregates, and help to counteract variations in material composition and mix ratios (Koehler and Fowler 2007). Furthermore, VMA presents a viable alternative to reducing the water content or increasing the powder content in concrete mixes.

2.9 Test methods for fresh SCC

A comprehensive framework has been established for evaluating the workability of SCC mixes, pivotal for their effective application and optimisation (Alyhya 2016). This framework is categorised into three main areas:

- Qualitative assessment tests: These tests give a wide-ranging overview of the self-compacting features of SCC without quantifying specific attributes such as filling ability, passing ability, and segregation resistance (discussed in Section 2.5).

- Quantitative principal assessment tests: These tests focus on the determination of the rheological properties of SCC, such as plastic viscosity and yield stress (discussed briefly in Section 2.7.4).

- Quantitative assessment and empirical tests: These tests offer a direct assessment of SCC's behaviour, utilising testing methods such as the slump flow and L-box tests. These evaluations play a crucial role in understanding SCC's properties and will be elaborated upon in the subsequent section, in accordance with the guidelines provided in (BS EN 12350-9 2010)

The unique properties of SCC require specific testing methods, as the standard tests designed for NVC are not suitable for accurately assessing the fresh properties of SCC. Specific tests are employed to effectively evaluate SCC's self-compactibility; these are outlined briefly in the following subsections.

2.9.1 Slump flow test

The deformability, or filling ability, of SCC is characterised by its ability to flow easily into and completely fill every corner of the mould/formwork without the need for any external mechanical vibration. The slump flow test is used to evaluate the free flow of the SCC mix in the absence of obstacles. A cone is placed at the centre of a non-absorbing level plate and filled with a sample of freshly mixed concrete in one lift, without compaction. The cone is lifted vertically, allowing the concrete to flow freely downwards under its own weight. The resulting horizontal flow diameter is measured, as well as the time taken for the flow spread to reach a diameter of 500 mm (t_{500}), as a measure of the flow velocity. The time t_{500} is a critical parameter, as the viscosity of the mix is proportional to the flow time. There are two viscosity classifications, Viscosity Class 1 (VS1) and Viscosity Class 2 (VS2), dependent on the t_{500} value: the mix is classified as VS1 when t_{500} < 2 seconds and as VS2 when t_{500} ≥ 2 seconds, as defined in BS EN 12350-8 (BS EN 12350-8 2010).

The final flow spread diameter, or slump flow (SF), is calculated from the average flow diameter, illustrated in Figure 2.7 and using the following equation:

$$SF = \frac{D_1 + D_2}{2} \quad (2.1)$$

where D_1 and D_2 are the spread diameters measured in orthogonal directions.

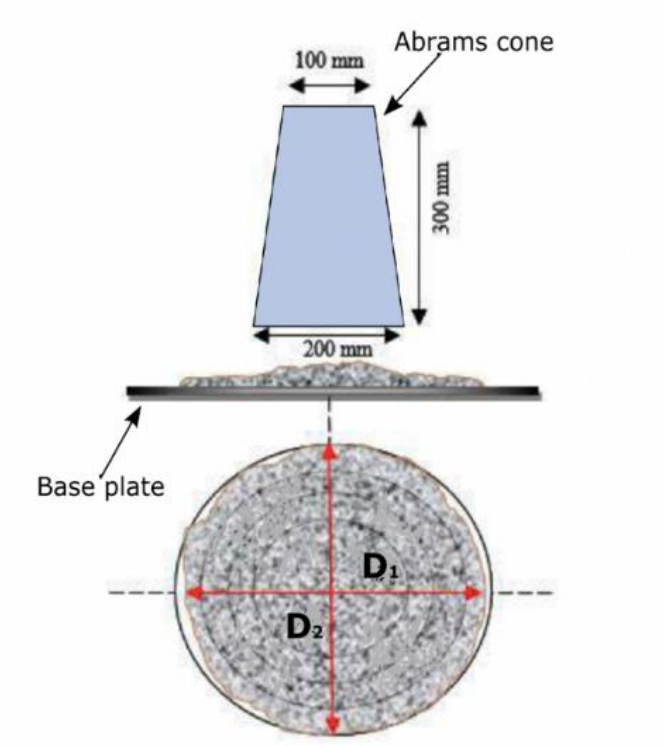

Figure 2.7 Apparatus for the slump flow test (Abo Dhaheer 2016)

The European Guidelines for Self-Compacting Concrete (EFNARC 2005) categorise slump flow (SF) into three classes based on the final spread, as detailed in Table 2.5. During the slump flow test, segregation resistance can also be assessed visually. Due to its straightforward procedure, the slump test is convenient for both laboratory and on-site execution.

Table 2.5 Slump flow classification for SCC based on European guidelines (EFNARC 2005)

Class	Slump flow in mm
SF 1	550 to 650
SF 2	660 to 750
SF 3	760 to 850

2.9.2 J-Ring test

Passing ability refers to the capability of freshly mixed concrete to flow through tightly spaced reinforcement without experiencing blockage or segregation. Enhancing the paste content and restricting the CA particle size can significantly improve this passing capability, thereby reducing the likelihood of blockage. The J-Ring test is an experimental procedure often used alongside the slump flow test and assesses the passing ability of concrete mixes through reinforcement gaps. The procedural details and test description are outlined in BS EN 12350-12 and ASTM C1621 (BS EN 12350-12 2010 and ASTM C1621 2014). This test primarily measures the restricted deformability of freshly mixed concrete, calculated from the following equation:

$$SF_j = \frac{D_1 + D_2}{2} \tag{2.2}$$

where SF_j is the final flow spread diameter measured in the J-Ring test.

During the test, the time taken for the flow to reach a diameter of 500 mm is recorded as t_{500j}. This test, in conjunction with the slump flow test, provides an assessment of potential blockage in the concrete mix, as detailed in Table 2.6 (ASTM C1621 2014).

Table 2.6 Assessment of blockage in SCC according to ASTM C1621 (2014)

Difference between Slump flow and J-Ring flow spread SF- SF_j (mm)	Blocking Assessment
0 to 25 mm	No visible blocking
From 25 to 50 mm	Minimal to noticeable blocking
More than 50 mm	Noticeable to extreme blocking

The passing ability of the concrete mix when using a J-ring can be quantified by the blocking step B_j, which is calculated from the following equation:

$$B_j = \frac{(\Delta \mathrm{hx}_1 + \Delta \mathrm{hx}_2 + \Delta \mathrm{hy}_1 + \Delta \mathrm{hy}_2)}{4} - \Delta \mathrm{h}_0 \tag{2.3}$$

where Δhx_1, Δhx_2, Δhy_1, Δhy_2, and Δh_0 represent the measurement heights, as indicated diagrammatically in Figure 2.8.

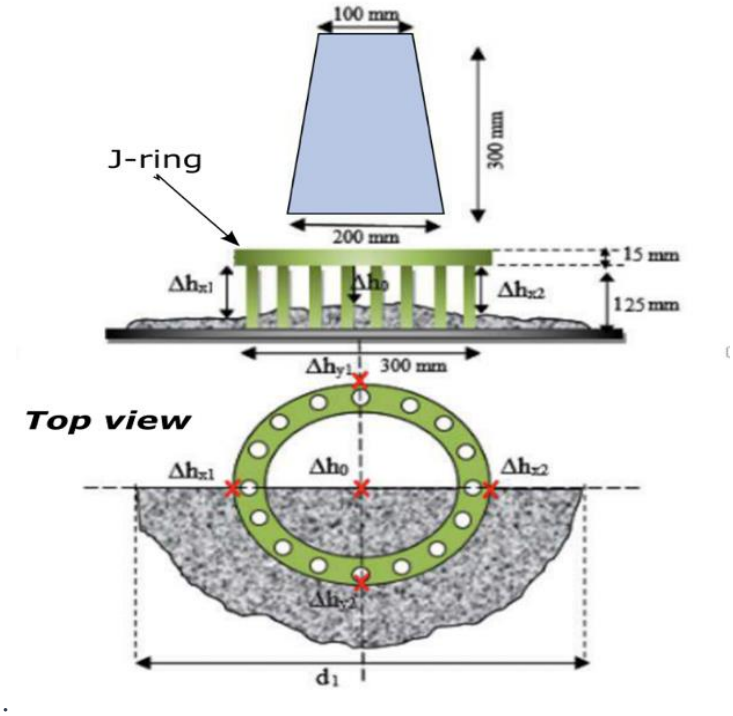

Figure 2.8 Apparatus for J-ring test (Abo Dhaheer 2016)

2.9.3 L-box test

The L-box test is designed to evaluate the passing ability of SCC, i.e., its ability to flow through narrow openings without experiencing blocking or segregation (EFNARC 2005). The methodology for determining the passing ability ratio of concrete using the L-box test is outlined in EN 12350-10 (EN 12350-10 2010). The apparatus for this test consists of a box with a rectangular section shaped like an 'L'; its shape and dimensions are depicted in Figure 2.9. Approximately 12.7 litres of fresh concrete are poured into the vertical section of the box with the gate lowered and left undisturbed for 60 seconds to observe any potential segregation (Sonebi and Yahia 2020). Subsequently, the gate is lifted, allowing the concrete to flow into the horizontal section through the vertical bars. Once the concrete ceases to flow, the height of the concrete at either end of the horizontal section of the L-box (H_1 and H_2) is measured, and the passing ability is calculated based on the ratio of H_2 to H_1.

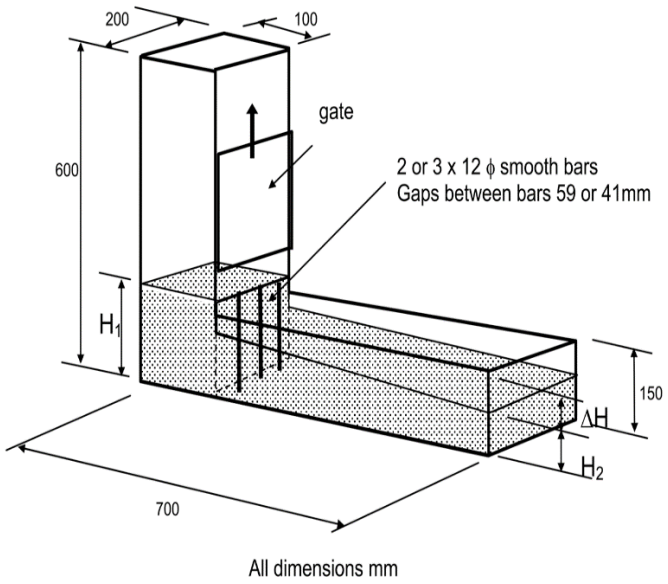

Figure 2.9 L-box test apparatus (EFNARC 2005)

The European Guidelines for Self-Compacting Concrete EFNARC (2005) classifies the passing ability in the L-box test into two distinct classes, as detailed in Table 2.7. In addition to evaluating the passing ability in the L-box, the flow time of the concrete is measured twice: (a) when the horizontal concrete flow measures 200 mm from the gate (t_{200}) and (b) when the horizontal concrete flow measures 400 mm from the gate (t_{400}). These values, t_{200} and t_{400}, serve as indicators of the filling ability of the concrete. Longer durations for t_{200} and t_{400} are indicative of higher concrete viscosity (Al-Rubaye 2016). This relationship between flow time and viscosity offers a useful metric for evaluating the workability of SCC in various construction scenarios.

Table 2.7 L-box test passing ability classification for SCC according to European guidelines (EFNARC 2005)

Class	Passing ability
PA1	≥ 0.8 with two rebars
PA2	≥ 0.8 with three rebars

2.10 Hardened properties of SCC

2.10.1 Compressive strength

Compressive strength serves as a key indicator of the overall quality and mechanical properties of hardened concrete (Neville and Aïtcin 1998; Abo Dhaheer 2016). The compressive strength of both NVC and SCC largely depends on the w/cm ratio, provided the curing conditions remain constant. In addition to the w/cm ratio, a wide range of studies have identified additional factors that affect the compressive strength of SCC (Domone 2006; Vilanova et al. 2011; Jawahar et al. 2013). These factors encompass the cement and the utilisation of pozzolanic materials, cement replacement materials (CRMs), the size and type of aggregates, and the specific types and quantities of admixtures.

Generally, SCC is expected to display a higher compressive strength compared to NVC when the w/cm is equivalent. This increase in strength is ascribed to the enhanced microstructure and homogeneity of SCC. The improved microstructure in SCC is notably linked to the interfacial transition zone (ITZ), which is considerably denser, and more uniform compared to that in NVC (refer to Table 2.1).

2.10.2 Tensile strength

The tensile behaviour of concrete is significantly influenced by factors that affect the microstructure of the cement matrix and the ITZ, which are crucial for determining the material's overall performance (Alyhya 2016). In this regard, SCC is noted for its superior tensile strength compared to NVC, an advantage that stems from SCC's higher paste content and the uniformity brought about by its vibration-free manufacturing process. These attributes contribute to a more homogenous and efficient ITZ and cement matrix microstructure, leading to enhanced mechanical properties (Domone 2006; Craeye et al. 2014; Abo Dhaheer 2016). The tensile strength of SCC is measured using tests such as splitting, flexural, and direct tensile tests. Many models have been developed to compare these tests or link them to the concrete's compressive strength (Parra et al. 2011; Craeye et al. 2014). These models fulfil two primary functions. First, they facilitate the conversion of test results from one test method to another, ensuring that results are comparable

regardless of the testing technique used. Second, they provide a mechanism to correlate the tensile strength measurements with the compressive strength of concrete.

2.10.3 Elastic modulus

Evaluating the elastic properties of concrete is of prime importance in civil and structural engineering, playing a critical role in ensuring the safety and service life of reinforced concrete structures (Parra et al. 2011). This is especially crucial when dealing with non-standard types of concrete such as SCC (Holschmacher and Klug 2002; Vilanova et al. 2011). In the design and assessment of concrete structures, the elastic modulus is a key mechanical parameter, essential for maintaining the serviceability of structures and preventing excessive deformation (Zhou et al. 1995). It also plays a vital role in calculating concrete elastic shortening and creep loss in prestressed concrete, as well as in seismic analysis for drift and deformation calculations (Aslani and Nejadi 2012).

The elastic modulus of concrete is influenced by several factors, including the CA content and type, compressive strength, and the concrete's unit weight (Jawahar et al. 2013). Typically, the elastic modulus is estimated from the concrete's compressive strength using empirical equations (Eurocode 2 2004; Aslani and Nejadi 2012). However, these equations often overlook the effects of concrete composition and the specific complexities of SCC on the elastic modulus. Research by Schlumpf (2004) indicates that for SCC with the same compressive strength as NVC, the elastic modulus of SCC is about 20% lower than that of NVC. Similarly, Bonen and Shah (2005) have reported that the elastic modulus of SCC is lower than that of NVC for comparable levels of compressive strength. Craeye et al. (2014) highlighted that CA plays a crucial role in the stiffness of concrete, suggesting that SCC generally exhibits a lower elastic modulus compared to NVC, due to its higher paste volume. This observation aligns with findings from previous research (Domone 2007; De Schutter et al. 2008), which have demonstrated that the elastic modulus for certain SCC mixes is lower than that of NVC mixes with a similar compressive strength.

2.11 Role of steel fibres in concrete reinforcement

The inherent limitations of plain concrete, particularly its susceptibility to fracture and sudden failure, are well-recognised challenges in structural engineering. This vulnerability

arises primarily from the low tensile strength and significant brittleness of plain concrete, which considerably restricts its suitability for civil infrastructure projects. An effective resolution for this issue is the addition of steel fibres to plain cementitious composites to enhance the concrete's toughness due to the ability of fibres to bridge cracks, effectively reducing crack propagation and increasing energy absorption (Trindade et al. 2020). This advancement has prompted the widespread use of steel fibre-reinforced cementitious composites (SFR-CC) among researchers and engineers. Steel fibres are now commonly employed as either the primary or secondary reinforcement in structural elements, conforming to established design codes and recommended guidelines (RILEM TC 162-TDF 2002; National Research Council 2006; ACI Committee 318. et al. 2007; FIB 2013; AS5100.5 2017).

Reinforcing cementitious materials with steel fibres can significantly improve their mechanical characteristics, including toughness, ductility, and flexural, shear, and tensile strengths, as well as their shrinkage behaviour and durability (Wu et al. 2019). The contribution of steel fibres to the structural integrity of reinforced concrete structures is not limited to merely augmenting SFR-CC's fundamental material properties. This enhancement is further evidenced by extensive research in key engineering areas, including seismic resilience in framed buildings, behaviour analysis under cyclic loading, and torsional response studies in beams (Chalioris and Karayannis 2009; Candido and Micelli 2018; Chalioris et al. 2019).

2.11.1 Properties of SFR-SCC in the fresh state

The use of HSSCC is often restricted due to its brittle behaviour, which can compromise structural integrity (Deeb et al. 2014). Although steel fibres may be added to form steel fibre-reinforced self-compacting concrete (SFR-SCC) and thereby improve the concrete's mechanical properties, the fresh properties of SFR-SCC are significantly impaired due to the large surface area and elongated shape of the steel fibres (Deeb et al. 2012). Therefore, the volume fraction of fibres that can be added to the SCC mix is limited and dependent on the specific mix composition and characteristics of the fibres themselves. The flow properties of SFR-SCC are significantly influenced by the fibre factor, which is defined as the product of the fibre volume (V_f) and the aspect ratio (l_f/d_f). When there is an increase in the volume of

fibres (V_f) and their aspect ratio (l_f/d_f), in conjunction with an increase in CA and a decrease in paste content, the fresh properties of SFR-SCC tend to worsen, leading to a reduction in slump flow (Kadhim 2020).

Furthermore, the passing ability and segregation resistance of the mix are influenced by the maximum size of the CA particles (De Figueiredo and Ceccato 2015; Weng et al. 2018; Wang et al. 2021). Khaleel et al. (2011) noted that increasing the maximum nominal size of CA diminishes the flowability of SCC. This effect is exacerbated as the fibre volume increases, with larger CA particles significantly compromising workability (De Figueiredo and Ceccato 2015). The presence of fibres can significantly alter the mix's flow characteristics, as their shapes may interfere with the flow of the mix, thereby increasing resistance. It is crucial to manage this resistance effectively; a uniform distribution of solid particles (CA and fibres) can help prevent segregation and avoid blockages in narrow areas. Reducing the length of fibres, along with the size and quantity of CA, can alleviate this resistance, thus improving the concrete workability (Khayat and Roussel 1999). As illustrated in Figure 2.10, reducing the maximum size of CA particles enables a greater dispersion of steel fibres within a unit volume, while larger CA particles restrict fibre movement, leading to clusters of fibres around the larger CA particles.

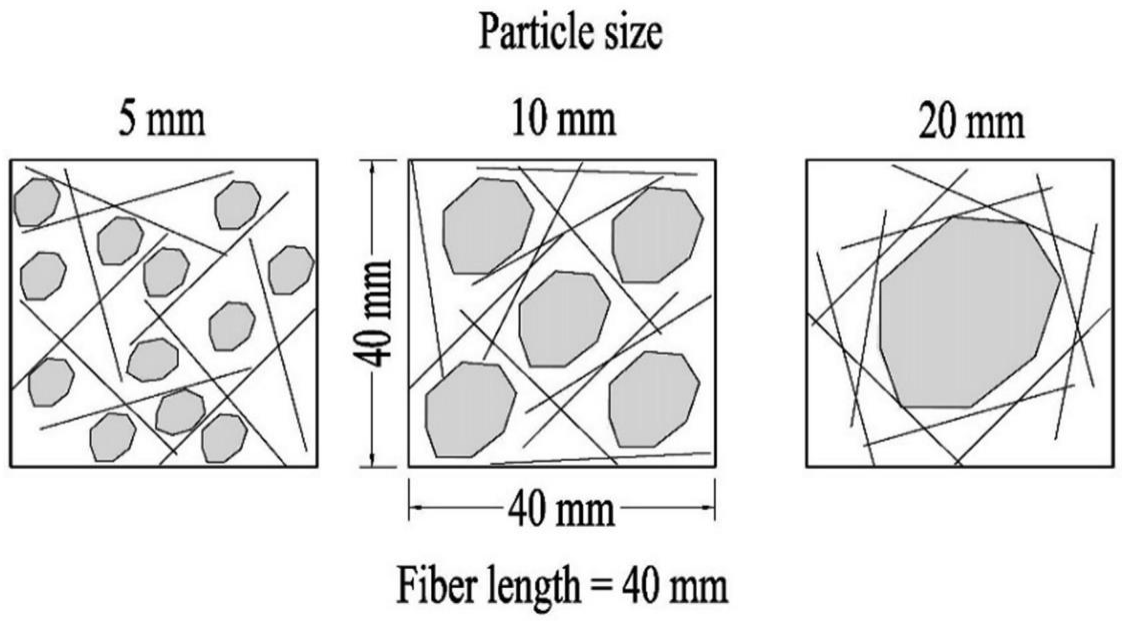

Figure 2.10 Comparison of fibre distribution with varying coarse aggregate sizes (Wang et al. 2021)

Yardimci et al. (2014) studied the effect of hooked-end steel fibre volume fractions, with fibre lengths of 30 mm and 60 mm, on the rheological and mechanical properties of SFR-SCC using varying fine-to-coarse aggregate ratios. The findings suggest that to enhance the flowability of SFR-SCC, a higher fine-to-coarse aggregate ratio (thereby reducing the overall CA content) should be employed, especially when the fibre volume fraction and length are comparatively high. Alrawashdeh and Eren (2022) investigated the effect of hooked-end steel fibres with aspect ratios of 60 and 80 and lengths of 30 mm and 50 mm, respectively, on the fresh, physical, and mechanical properties of SFR-SCC. The study noted the difficulties associated with mixing and placing the SCC with the longer fibres (50 mm)

2.11.2 Properties of SFR-SCC in the hardened state

Steel fibres are known to retain their stress-bearing capabilities even after the failure of the concrete matrix, significantly affecting the residual tensile and flexural strengths of concrete without substantially altering its compressive strength (Pająk and Ponikiewski 2013). This highlighted the importance of examining the post-peak behaviour of SFR-CC specimens, with methodologies recommended for this analysis including the RILEM TC 162-TDF (2002) recommendation, the Japan Society of Civil Engineers (JSCE) method (JSCE Concrete Committee 2007), (ASTM C1609 2007), and the BS EN 14651 (2007) standard. Comprehensive insights into the behaviour of SFR-SCC and the influence of fibre properties and composite composition can be found in (Naaman 2008).

Adding steel fibres to SCC offers primary benefits such as enhanced flexural strength, increased toughness, improved performance beyond peak loads, and greater fracture energy (Kadhim 2020). The extent of these improvements is influenced by the characteristics of the fibres (including their shape, length, diameter, and aspect ratio), their orientation within the composite, and the matrix's strength. Notably, enhancements in the properties of cementitious materials are achievable through increases in the volume fraction, aspect ratio, and length of the fibres (Al-Azzawi 2018). Experimental investigations were performed on the effect of the steel fibre shapes (straight and hooked-end) on the flexural behaviour of SCC (Pająk and Ponikiewski 2013). The results demonstrated that hooked-end steel fibres were more effective than straight fibres in enhancing post-peak characteristics, possibly due

to the improved bonding conditions provided by the deformed shape of the hooked-end fibres.

Şahin and Köksal demonstrated that the steel fibre tensile strength played a significant role in the flexural and splitting tensile strengths of HSC. Their research showed that using steel fibres with higher tensile strengths led to greater flexural and splitting tensile strength improvements compared to those with lower tensile strengths (Şahin and Köksal 2011). Moreover, a study investigated the effect of steel fibre length on the flexural behaviour of ultra-high-performance fibre-reinforced concrete (UHPFRC); the results indicated that longer steel fibres resulted in better flexural performance, but lower fibre orientation compared to shorter fibres (Yoo et al. 2016). The variation of the fracture parameters and brittleness of SFR-SCC with maximum aggregate size, w/c ratio, and fibre content was investigated; the findings indicated that using a larger maximum aggregate size (19 mm) in SFR-SCC reduced the fracture energy, as it provided less space for fibre rotation (Ghasemi et al. 2019).

2.11.2.1 Fracture energy of SFR-SCC

The fracture energy of concrete is a critical parameter for understanding concrete properties, performing fracture analyses, and determining design criteria for large concrete structures (Şahin and Köksal 2011; Pająk and Ponikiewski 2013; Kazemi et al. 2017; Zhang et al. 2023). Various methods have been proposed to measure fracture energy, such as the Work of Fracture Method (WFM), which is firmly grounded in the Fictitious Crack Model (FCM) developed by Hillerborg et al. (Hillerborg et al. 1976; Hillerborg 1985). As one of the most widely used fracture mechanics models for analysing concrete structures, WFM is distinguished by its simplicity and effectiveness, and is pivotal in assessing the fracture parameters of concrete (Şahin and Köksal 2011; Beygi et al. 2013; Beygi et al. 2014; Kazemi et al. 2017). This method calculates the fracture energy (G_f) by integrating the area under the load-deflection curve relative to the unit area of the fracture surface. Bazant and Kazemi (1990) introduced the Size Effect Method (SEM) to estimate fracture energy and fracture parameters that are consistent regardless of the specimen size. Both methods are endorsed by RILEM standards (RILEM FMC-50 1985; RILEM TC 89-FMT 1990). Importantly, Ghasemi et al. (2019) found that WFM yields superior results compared to SEM in SFR-SCC, particularly due to the fibres' significant influence on the post-peak response.

2.11.2.2 Fibre orientation and distribution

To improve strength and manage crack width in SFR-SCC, proper alignment and distribution of steel fibres relative to the crack plane are essential (Kadhim 2020). Fibres aligned in the direction of tensile stress are beneficial for structures subjected to unidirectional loads. The performance of these fibres in a cementitious composite declined from 100% effectiveness when parallel to the tensile stress to about 30% under random distribution (Martinie and Roussel 2011; Deeb et al. 2014; Marks et al. 2021). As illustrated in Figure 2.11, steel fibres oriented perpendicular to an emerging crack can immediately bridge the gap, effectively preventing further crack propagation. However, it should also be noted that the contribution of steel fibres to tensile strength is significantly diminished, or even rendered negligible, when their orientation is perpendicular to the direction of tension (Cunha et al. 2012; Yu et al. 2016; Zhang et al. 2020).

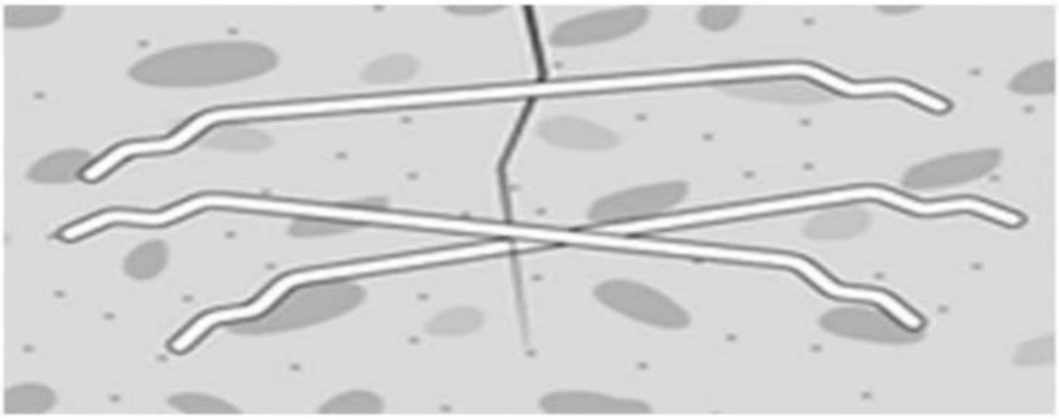

Figure 2.11 Steel fibre alignment in a cementitious matrix to inhibit crack propagation (Kadhim 2020)

Recent efforts to enhance the structural performance of Steel Fibre-reinforced Concrete (SFRC) specimens have utilised the high-flow properties of SCC to strategically align fibres in a beneficial direction to attain a more uniform distribution (Ferrara et al. 2012a; Alberti et al. 2018; Raju et al. 2020). Studies have shown that the fibre arrangement in SFR-SCC is not random but tends to align closely with the direction of flexural loads (Ponikiewski et al. 2015b; Zhao et al. 2021b). Furthermore, in SFR-SCC, fibre orientation is affected by various factors, such as the rheological properties of the mix, formwork geometry, fibre properties, the effect of walls, and the casting method (Jasiūnienė et al. 2018; Marks et al. 2021). These

elements thus significantly influence the mechanical properties and fracture behaviour of SFR-SCC.

2.11.2.3 Evaluation of fibre distribution and alignment

The assessment of fibre alignment and distribution within fibre-reinforced composites is crucial, significantly impacting the materials' mechanical properties and resistance to fracture. This importance has led to the adoption of a variety of advanced methodologies for analysis. These methodologies span a broad spectrum, from the use of expensive, sophisticated equipment to more manual, labour-intensive processes, and include both destructive and non-destructive post-test approaches (Alberti et al. 2018). A diverse array of techniques have been employed to evaluate the distribution and orientation of fibres in hardened concrete. Examples of these techniques include manual inspection through counting fibres in cross-sections (Gettu et al. 2005; Michels et al. 2012), image analysis (Abrishambaf et al. 2013; Yardimci et al. 2014; Huang et al. 2018; Zhao et al. 2021b; Zhao et al. 2021a), computed tomography (CT) scans (Abrishambaf et al. 2013; Ponikiewski et al. 2015a; Ponikiewski et al. 2015b; Ponikiewski and Katzer 2016; Qsymah et al. 2017; Zhou and Uchida 2017; Miletić et al. 2020), and analysis based on a magnetic approach (Faifer et al. 2011). Table 2.8 provides a comparative analysis of the commonest methods used in the assessment of fibre alignment and distribution within fibre-reinforced composites, detailing each method's type, advantages, and disadvantages.

Table 2.8 Comparative overview of techniques for assessing fibre alignment and distribution in concrete

Methods	Method type		Advantages	Limitations
Manual inspection	Destructive	Direct	Verifies number of fibres and detects fractures of fibre (Alberti et al. 2018)	Time-consuming and challenging to determine fibre alignment
Image analysis	Destructive	Direct	Efficient and reliable for shape and orientation analysis; simple and low-cost equipment (Kang et al. 2011; Abrishambaf et al. 2013).	Limited to 2D and prone to errors from cutting and image distortion (Yardimci et al. 2014; Huang et al. 2021; Wang et al. 2021)
CT scans	Non-destructive	Direct	Direct evaluation of fibre orientation in 2D or 3D (Huang et al. 2021); detailed insight into internal microstructures, such as pores (Qsymah et al. 2017).	Limited sample size, especially for industrial micro-X-ray CT (du Plessis et al. 2016; du Plessis and Boshoff 2019); requires costly advanced software for 3D analysis; 3D alignment challenges with fibres (Huang et al. 2021)
Magnetic approach	Non-destructive	Indirect	Simple, low-cost setup with a magnetic probe; assesses fibre density and orientation (Faifer et al. 2011)	Restricted to metal fibres; practical challenges include the need for complex analysis (Wang et al. 2021).

2.12 Homogenisation method

Homogenisation is a technique used to determine the overall properties of a heterogeneous material, thereby enabling the substitution of this material with an equivalent homogeneous counterpart (Nguyen et al. 2011), as depicted in Figure 2.12. A comprehensive overview of the various homogenisation methods is available in (Kanouté et al. 2009). Homogenisation techniques are extensively applied to forecast the mechanical characteristics of various composite materials; the following sections provide an overview of the mean-field homogenisation and computational methods, as applicable to this thesis.

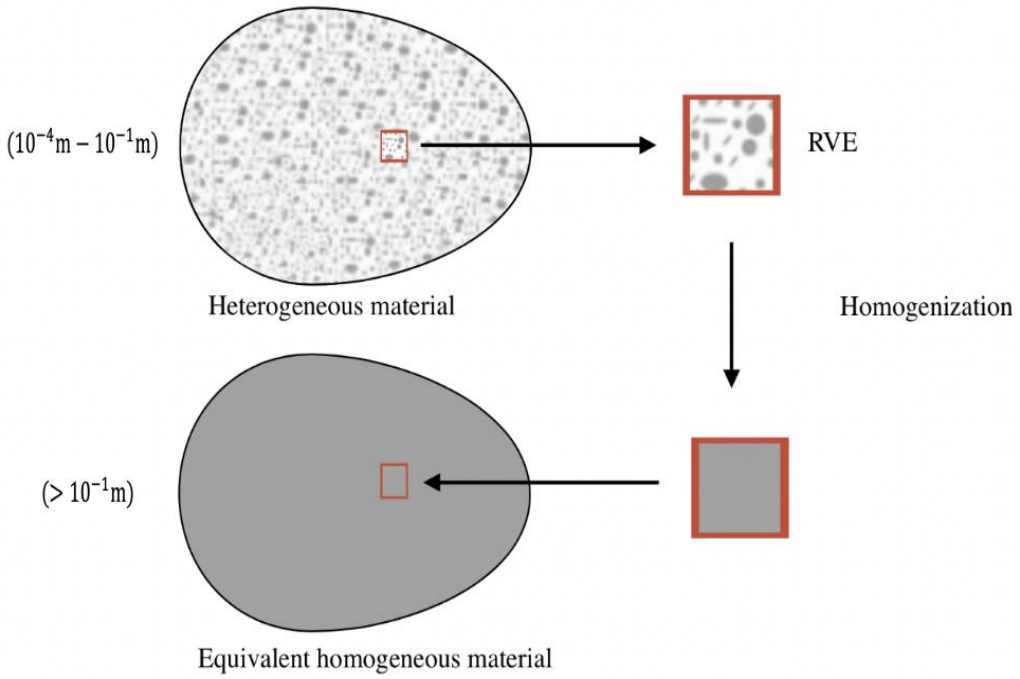

Figure 2.12 Diagram of the homogenisation process

2.12.1 Mean-field homogenisation.

Mean-field homogenisation (MFH) aims to generate approximate yet precise volume-averaged estimates for stress and strain fields both at the representative volume element (RVE) level (macro-level stresses and strains) and within each constituent phase. It is crucial to note that MFH ignores the detailed RVE problem and avoids the calculation of specific micro-level stress and strain distributions across the phases. Various models of MFH exist, each grounded in particular assumptions. These models are favoured for their simplicity,

rapid computation times (minimising CPU usage), and lower memory demands. However, these models are limited to the provision of estimated averages for stresses and strains, both on the macro scale and within individual phases.

A variety of homogenisation models have emerged, all premised on specific theoretical foundations, notably the single inclusion theory proposed by Eshelby (Eshelby 1957). These models include the Mori-Tanaka approximation model (Mori and Tanaka 1973), the generalised self-consistent model (Christensen and Lo 1979), and the double-inclusion model (Nemat-Nasser and Hori 1993).

2.12.1.1 Mori-Tanaka Model

The Mori-Tanaka (M-T) model (Mori and Tanaka 1973) is formulated through an approximation of Eshelby's solution. It demonstrates that the strain concentration tensor, linking the volume-averaged strain within all inclusions to the average strain in the matrix, aligns with the strain concentration tensor associated with a single inclusion problem. This observation prompted Benveniste (1987) to provide a clear interpretation of the M-T method. In this view, each inclusion within the actual RVE is considered as if it were isolated within the authentic matrix. The model assumes that the infinite body is subjected to the average matrix strains found in the actual RVE as the far-field (remote) strain, an idea illustrated in Figure 2.13. This semi-analytical model will be discussed further in Chapter 4.

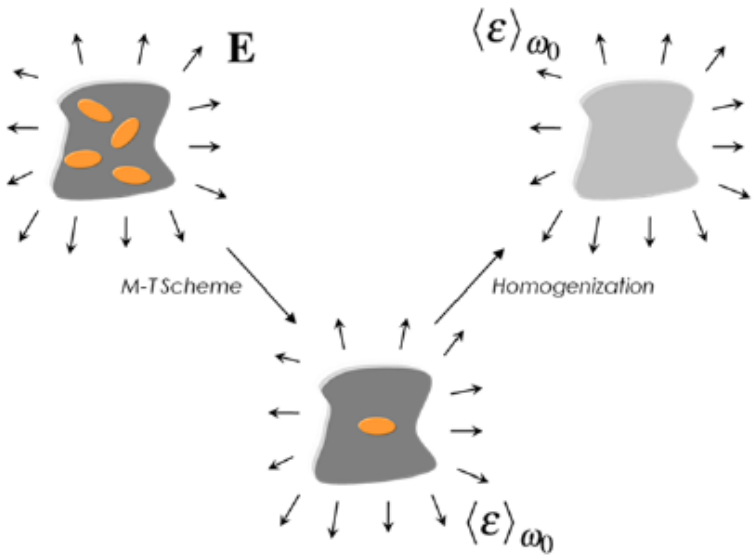

Figure 2.13 Depiction of the M-T Model (Digimat 2021)

2.12.2 Finite element method based numerical homogenisation.

The computational homogenisation method, predominantly utilising the finite element method, is notably efficient in simulating the complex structures of heterogeneous materials. This technique facilitates the calculation of the effective properties of a heterogeneous material by averaging its macroscopic properties over an RVE. The homogenised elastic properties of the material are then determined through the linear relationship between the volume-averaged stress and strain, in accordance with the generalised Hooke's law (Qsymah 2016).

2.12.2.1 Boundary condition

Various boundary conditions can be applied to the RVE. In principle, the RVE's response should remain unaffected by the choice of imposed boundary conditions. Yet, achieving this independence may necessitate the use of a significantly large RVE size (Kanit et al. 2003; Qsymah 2016). There are various methods for implementing these boundary conditions, including the Dirichlet boundary condition type, the Mixed BC type, and the Periodic BC type. Compared to Dirichlet and Mixed boundary condition types, periodic boundary conditions typically offer more accuracy (Digimat 2021). They exhibit a rapid convergence with increasing volume element size, although this results in an increased need for CPU time and memory for the finite element analysis. This reduction in efficiency is due to the considerable number of constraint equations required to be enforced.

Chapter 3 Designing Sustainable High-Strength Self-compacting Concrete

3.1 Summary

Sustainable and eco-friendly concrete design is crucial for the construction industry to reduce carbon dioxide (CO_2) emissions and conserve non-renewable natural resources. This chapter describes a novel mix design method for sustainable high-strength self-compacting concrete (HSSCC) based on rheological and mechanical properties, which aims to reduce the cement content in such mixes. Fly ash and ground granulated blast-furnace slag (GGBS) were used in the HSSCC mix designs to replace up to 40% of the cement content, and the compressive strength of the resulting mixes was tested with target strengths between 70 and 100 MPa. The design method was numerically programmed to produce design charts that could provide straightforward and realistic guidance for HSSCC mixes. This numerical method was verified by designing and testing sixteen HSSCC mixes with varying paste-to-solid (P/S) and sand-to-aggregate (S/A) ratios. All mixes satisfied the self-compacting concrete criteria and achieved the targeted viscosity in the fresh state and compressive strength values in the hardened state. The effects of the variance in P/S and S/A and ratios on the rheological properties were analysed. The results confirmed that this design method can produce HSSCC with superior fresh and mechanical properties while being environmentally friendly by reducing CO_2 emissions and cement usage.

The content of this chapter has been published in the journal *European Journal of Environmental and Civil Engineering* (Alshahrani, Cui, Almutlaqah, and Kulasegaram 2023); details are provided in the list of Publications.

3.2 Introduction

As mentioned in the earlier chapters, concrete is extensively utilised in construction, with an annual global consumption nearing 30 billion tonnes (Thomas et al. 2021). This large usage can be attributed to its multiple advantages, such as low-cost production, the worldwide availability of raw materials, and durability in aggressive environments. However, the global carbon dioxide (CO_2) emissions emitted during the production and transportation of concrete constitute approximately 10% of the total environmental anthropogenic CO_2 (Long et al. 2015; Guo et al. 2020). Concrete's carbon footprint is primarily caused by cement production of ordinary Portland cement (OPC), accounting for approximately 5% to 7% of

the annual CO_2 emissions (Berndt 2015; Celik et al. 2015; de Grazia et al. 2019). In addition, the production of concrete involves the significant use of non-renewable resources, including natural river sand (Sivakrishna et al. 2020). It has been predicted that the future increase in concrete production will result in a considerable depletion of natural resources and increased pollution of the environment (Gupta et al. 2021). Therefore, to meet the anticipated concrete demands without further environmental damage, it is essential to develop sustainable concrete production processes which limit CO_2 emissions and preserve finite natural resources.

As mentioned in previous chapters, self-compacting concrete (SCC) is one of the greatest innovations in concrete technology, valued for its superior properties and wide applications. SCC can flow through congested reinforcement under its own weight without external vibration (Okamura and Ouchi 1999). Despite its advantages in reduced construction time and improved quality compared with normal vibrated concrete (NVC), SCC often requires a greater quantity of cement, increasing construction costs and environmental concerns (Adesina and Awoyera 2019). Producing one tonne of OPC emits approximately one tonne of CO_2 (Kaish et al. 2018), prompting significant research into eco-friendly and sustainable SCC.

The concept of sustainable SCC production embraces the eco-friendly use of industrial by-products while providing feasible alternatives for the required raw materials. The replacement of traditional SCC constituents with alternative materials can make SCC more sustainable while imparting numerous advantages, such as eco-consumption of by-products, cost reduction, natural resource conservation, landfill cost-saving, and environmental protection from pollutants (Gupta et al. 2021). Industrial waste materials, such as silica fume, rice husk ash, slag, fly ash, sawdust ash, and limestone powder, have previously been used in SCC production. However, the majority of industrial waste materials are either discarded or used without fully exploiting their beneficial characteristics (Jalal et al. 2015). Further research is necessary to develop sustainable SCC utilising waste materials while focussing on optimal mix design (Adesina and Awoyera 2019). It is also important to assess the fresh properties as well as the long-term effect of these materials on the hardened properties of SCC. Fly ash and Ground granulated blast-furnace slag (GGBS) have been reported as industrial waste materials that can modify and improve the fresh and

mechanical properties of concrete, as well as its durability (Nehdi et al. 2004; Jalal et al. 2015; Adesina and Awoyera 2019). Despite these findings, only a small proportion of the global production of fly ash and GGBS is utilised in the construction industry. For example, Türkiye produces 13 million tonnes of fly ash annually, yet only 5% of this waste product is used in construction (Jalal et al. 2015). Similarly, although the annual production of GGBS is approximately 250 million tonnes, only 90 million tonnes are used in concrete manufacture each year (Al-Oran et al. 2022). Therefore, leveraging the potential of fly ash and GGBS in the production of SCC is a viable approach to enhance its sustainability performance.

An effective strategy to reduce the construction industry's CO_2 emissions is to decrease the quantity of concrete used in structures. This can be accomplished by using high-strength concrete (HSC), which offers similar performance to NVC but with significantly less material for the same strength (de Matos et al. 2019; Campos et al. 2020). In addition to reducing the overall concrete volume, HSC enhances durability and lowers raw material consumption. As noted by Aïtcin (2019), increasing the compressive strength of concrete reduces the quantity needed to support structural loads, thereby decreasing overall cement usage and increasing concrete efficiency. Concrete efficiency refers to the total amount of cement needed in a mix to achieve one unit of compressive strength (Campos et al. 2020). As compressive strength rises, cement consumption per cubic meter of concrete (kg/m³) per unit of compressive strength (MPa) decreases (Yousuf et al. 2019; Campos et al. 2020). In NVC, this ratio typically ranges from 9 to 14 (kg/m³)/MPa (de Grazia et al. 2019). In contrast, HSC has a ratio of approximately 5 (kg/m³)/MPa (Damineli et al. 2010), demonstrating higher efficiency than NVC. Additionally, as compressive strength increases, CO_2 emissions per unit of compressive strength decrease correspondingly (Campos et al. 2019). This highlights the environmental benefits of HSC, achieving greater strength with less material, leading to reduced carbon emissions. Campos et al. (2020) concluded that HSC is both environmentally and economically advantageous due to its lower cement consumption. In addition, HSC allows for thinner, more slender, and lightweight structural elements, leading to further savings in materials, costs, and construction time. The reduced weight and volume of concrete can also lower transportation costs and overall CO_2 emissions of construction projects. The enhanced durability of HSC results in longer-lasting structures, potentially reducing the need for maintenance and repairs over the building's design life.

This chapter describes the development of sustainable high-strength self-compacting concrete (HSSCC) mixes through optimisation of supplementary cementitious material (SCM) replacement ratios while maintaining or exceeding the fresh and mechanical properties of an unmodified HSC mix. A novel design method was developed based on rheological characteristics and mechanical properties, wherein CO_2 emissions and cement consumption could be reduced in comparison to the standard HSSCC mix proportions. To experimentally validate this method, four sets of HSSCC mixes, each set having four composition variations, were designed, produced, and assessed in both fresh and hardened states to address the extensive range of variables within the constrained timeframe. The sustainability of the test mixes was estimated and compared to that reported in the literature for HSSCC and conventional HSC conventional mixes.

3.3 Novel mix design method for sustainable HSSCC

The invention of SCC in 1988 has been attributed to Okamura in 1988 despite ongoing research on SCC since the early 1970s (Okamura and Ozawa 1996). Since then, various mix design methods have emerged, such as the empirical, aggregate packing, statistical factorial, compressive strength, and paste rheology methods (Shi et al. 2015). Karihaloo, Ghanbari, and Deeb (Deeb et al. 2012; Karihaloo and Ghanbari 2012; Deeb and Karihaloo 2013) proposed a mix design method based on the mix's plastic viscosity for proportioning conventional and HSSCC mixes but did not explicitly consider compressive strength as a design parameter. Their method used the plastic viscosity expression for SCC mixes to propose a mix design procedure for HSSCC. This approach could potentially reduce laboratory work and resource utilisation while establishing a basis for quality management. Abo Dhaheer et al. (2016a) subsequently introduced compressive strength as a design parameter for SCC and created a mix proportioning method for compressive strengths up to 80 MPa.

The current research considers a mix-proportioning approach for HSSCC, combining the above-mentioned approaches, using both the target plastic viscosity and compressive strength as design parameters while reducing cement consumption. This methodology is predicted to be suitable for a range of HSSCC compressive strengths (70, 80, 90, and

100 MPa) while offering practical guidelines to corroborate the effectiveness and simplicity of the approach.

3.3.1 Compressive strength target

It is widely accepted that the compressive strength of SCC is primarily determined by its water-to-cementitious material ratio (w/cm) and the composition of the cementitious materials included in the mix (Domone 2006). However, research indicates that the compressive strength of SCC is dominantly influenced by the w/cm as opposed to the total paste volume (Jawahar et al. 2013). Various empirical formulas have been proposed to estimate compressive strength from the w/cm ratio, following the well-known Abrams rule (Abo Dhaheer et al. 2016a; Aggarwal and Aggarwal 2020). Abo Dhaheer et al. (2016a) adopted the following equation to determine the 28-day compressive strength (f_{cu}) of SCC mixes:

$$f_{cu} = \frac{195}{12.65^{w/cm}} \tag{3.1}$$

This equation was validated through extensive testing of SCC mixes with compressive strengths ranging from 30 to 80 MPa. Based on the results, reducing the w/cm by 14% for 30 MPa SCC mixes and by 8% for 40 MPa SCC mixes was recommended. This equation was adopted and further validated in the present research for SCC mixes with compressive strengths up to 100 MPa.

3.3.2 Plastic viscosity target

The plastic viscosity of a homogeneous viscous fluid, such as cement paste consisting of cement, SCMs, superplasticiser (SP), and water, can be accurately measured using a conventional viscometer. However, this method is unsuitable for a non-homogeneous viscous fluid such as an SCC mix. Research has established that samples drawn from one SCC mix and measured with different rheometers show dissimilar plastic viscosity measurements (Feys et al. 2007; Wallevik and Wallevik 2011; Feys and Khayat 2013; Feys et al. 2023). To address these discrepancies, Karihaloo and Ghanbari proposed a micro-mechanical model to estimate the plastic viscosity of SCC mixes based on the plastic viscosity of the paste

(Ghanbari and Karihaloo 2009). Although their research compared the viscosity of SCC mixes with and without fibres, other researchers have used this model to predict the plastic viscosity of standard SCC mixes without fibres (Deeb et al. 2012; Deeb and Karihaloo 2013; Abo Dhaheer et al. 2016a; Abo Dhaheer et al. 2016b).

To utilise this method, the plastic viscosity of the homogeneous paste must first be determined. The micro-mechanical approach conceptualises the SCC mix as a two-phase suspension: the solid phase (comprising aggregates and other solids) is suspended within the liquid phase (the cement paste). This model estimates the increase in plastic viscosity of the liquid phase due to the incorporation of the solid phase. Initially, the finest solid particles, such as sand, are treated as a viscous liquid. The coarse aggregate (CA) is then considered the solid phase and is incrementally added to the liquid phase established in the initial step. This procedure is repeated, with each resulting two-phase suspension used as the liquid phase for the next addition of solid constituents, continuing until all solids are integrated.

The plastic viscosity of an i^{th} liquid-solid suspension can be predicted from the plastic viscosity of the previous $(i-1)^{th}$ phase using Equation (3.2):

$$\eta_i = \eta_{i-1} * f_i(\phi_i) \tag{3.2}$$

where

η_i plastic viscosity of the i^{th} liquid-solid suspension

η_{i-1} plastic viscosity of the preceding $(i-1)^{th}$ phase

$f_i(\phi_i)$ factor greater than one, predicting the increase in the plastic viscosity attributed to a solid phase having a volume fraction of ϕ_i.

Figure 3.1 depicts the schematical hierarchical structure of the two-phase suspensions to illustrate the progression of the liquid-solid phases used to estimate the plastic viscosity of the mixes formulated in this study.

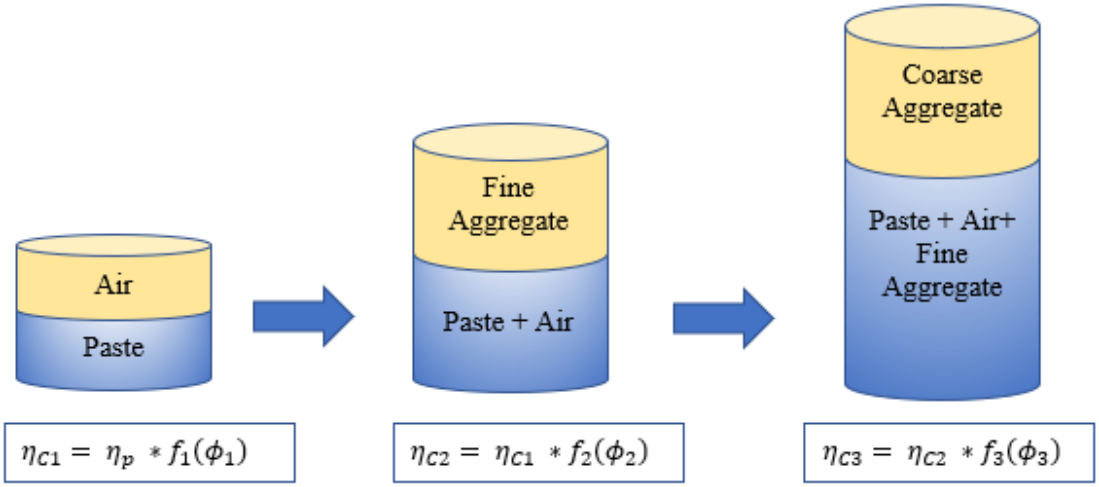

Figure 3.1 Hierarchy of two-phase liquid-solid suspensions for SCC mixes

For the initial step, $i = 1$, implying that η_0 is the plastic viscosity of the paste. Based on Equation (3.2), the plastic viscosity of SCC can thus be estimated as shown in Equation (3.3):

$$\eta_{mix} = \eta_{paste} * f_1(\phi_1) * f_2(\phi_2) * f_3(\phi_3) * \cdots * f_n(\phi_n) \tag{3.3}$$

where *n* represents the total number of solid phases in the mixture.

As illustrated in Figure 3.1, air voids are considered as a second (solid) phase in a viscous suspension, in addition to the fine aggregate (F-A) and CA. Einstein derived a fundamental equation for the viscosity of a dilute suspension, where a dilute suspension was defined as having a second phase volume fraction of less than 10%, consisting of rigid or hollow spheres with no hydrodynamic interactions (Struble and Sun 1995). He developed an expression $f_i(\phi_i)$ for suspensions with simple geometries, such as spheroids and spheres, in Newtonian fluids, where the expression $f_i(\phi_i)$ depended solely on the solid volume fraction ϕ_i, where the fraction was less than 10% (Koehler and Fowler 2007). Einstein's approximation for $f_i(\phi_i)$ is reproduced in Equation (3.4):

$$f_i(\phi_i) = 1 + [\eta]\phi_i \tag{3.4}$$

where η intrinsic viscosity of the suspension

The numerical factor η for air bubbles in suspension and rigid spherical particles with random hexagonal packing arrangements is 1 and 2.5, respectively. Further studies determined that a numerical factor of 2.5 was suitable for rigid ellipsoidal particles with aspect ratios less than 3 (Struble and Sun 1995; Koehler and Fowler 2007). At higher volume fractions (i.e. > 10%), the hydrodynamic interactions and random motion of suspended particles become significant, nullifying the applicability of Equation (3.4). In such cases, the Krieger-Dougherty formula can be used to calculate $f_i(\phi_i)$ as indicated in Equation (3.5) (Krieger and Dougherty 1959); this approach was considered appropriate for calculating viscosity in concentrated cementitious suspensions.

$$f_i(\phi_i) = \left(1 - \frac{\phi_i}{\phi_m}\right)^{-[\eta]\phi_m} \tag{3.5}$$

where

ϕ_i is the volume fraction of the dispersed solid phase in the suspension

ϕ_m is the maximum packing fraction of particles in the dispersed solid phase

η is the intrinsic viscosity of the suspension

The Krieger-Dougherty equation illustrates the dependence of $f_i(\phi_i)$ on the dynamic viscosity of the suspension and the maximum packing fraction. The maximum packing fraction, ϕ_m, represents the highest concentration of solid particles that can be incorporated into a viscous phase while still allowing it to flow. The dynamic viscosity of the suspension, η, reflects the impact of individual particles on the overall viscosity. Both ϕ_m and η are influenced by the rate of shear applied to the system. Specifically, the maximum packing fraction, ϕ_m, increases proportionally with the shear rate, whereas the dynamic viscosity, η, is inversely related, decreasing as the shear rate rises. Consequently, the final product of ϕ_m and η remains approximately constant, around 1.9 for rigid spherical particles (de Kruif et al. 1985).

As the proportion of F-A and CA in HSSCC mixes exceeds 10%, the Krieger-Dougherty equation was used to determine their effect on the known plastic viscosity of the paste. Trapped air bubbles account for around 2% of the volume fraction and, thus, Einstein's approximation for $f_i(\phi_i)$ (Equation 3.4) with a numerical factor equal to 1 can be used to

account for the trapped air bubbles. Essentially, the 2% increase in volume fraction resulting from trapped air is factored into the plastic viscosity of the paste. Substituting Equations (3.4) and (3.5) into Equation (3.3) and assuming a 2% increase in plastic viscosity due to trapped air, the plastic viscosity of a mix can be calculated using Equation (3.6):

$$\eta_{mix} = \eta_{paste} * \left(1 - \frac{\phi_{\ fine\ agg}}{\phi_{\ m}}\right)^{-1.9} * \left(1 - \frac{\phi_{coarse\ agg}}{\phi_{\ m}}\right)^{-1.9} \quad (3.6)$$

where

$\phi_{\text{fine agg}}$ is the volume fraction of the fine aggregate in the suspension

$\phi_{\text{coarse agg}}$ is the volume fraction of the coarse aggregate in the suspension

This equation provides a method to estimate the plastic viscosity of the mix by considering the contributions of both fine and coarse aggregates.

The packing density (maximum packing fraction, ϕ_m) increases as additional solid phases are added to the mixture. According to Abo Dhaheer et al. (2016a), when F-A is added to the cement paste, it can be viewed as forming a random hexagonal packing pattern, resulting in a maximum packing fraction ϕ_m of 0.63. When the CA is subsequently added as the final solid phase, the packing density further increases, leading to a close hexagonal packing pattern with ϕ_m reaching 0.74 (Abo Dhaheer et al. 2016a).

3.3.3 Method steps

The HSSCC design mix methodology was programmed in MATLAB to provide design charts to estimate the plastic viscosity (see Appendix A), as illustrated in Figure 3.2, with the procedural steps outlined in Figure 3.3. Water content and mix proportions were determined based on the mass and volume ranges of typical SCC compositions in accordance with the specifications given in EFNARC (2005) (detailed in Table 2.3 in Chapter 2). Four HSSCC mix series were designed for varying compressive strengths (70, 80, 90, and 100 MPa) based on their plastic viscosity. The protocol for mixing the cementitious paste was formulated following the guidelines provided by (ASTM C305 2004) and (AASHTO T162-04 2004). The plastic viscosity of the pastes was obtained from viscometer tests; the test results are indicated in Table 3.1 (Alshahrani et al. 2023).

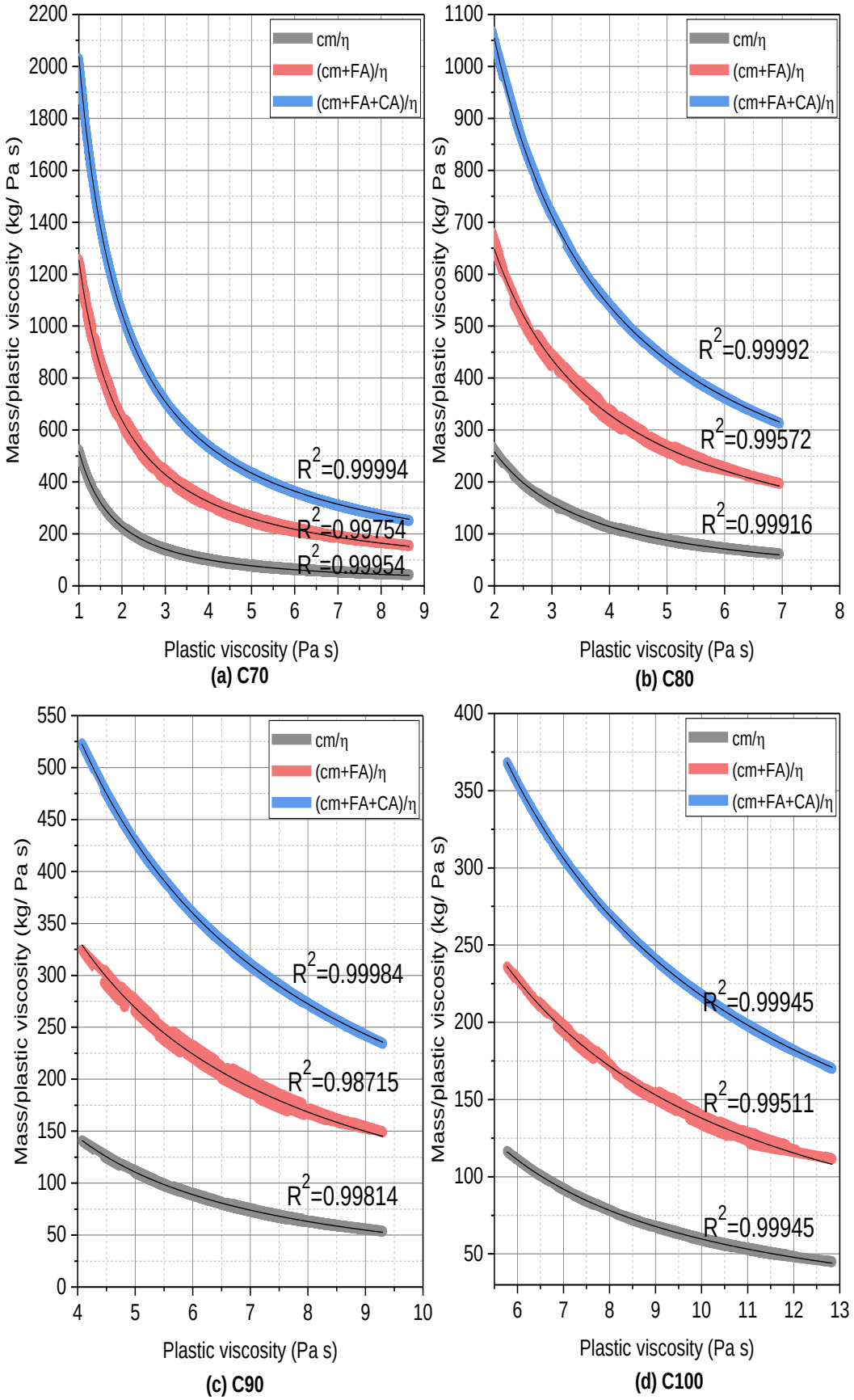

Figure 3.2 Design charts of concrete grades based on plastic viscosity: a) C70, b) C80, c) C90, and d) C100 (Alshahrani et al. 2023)

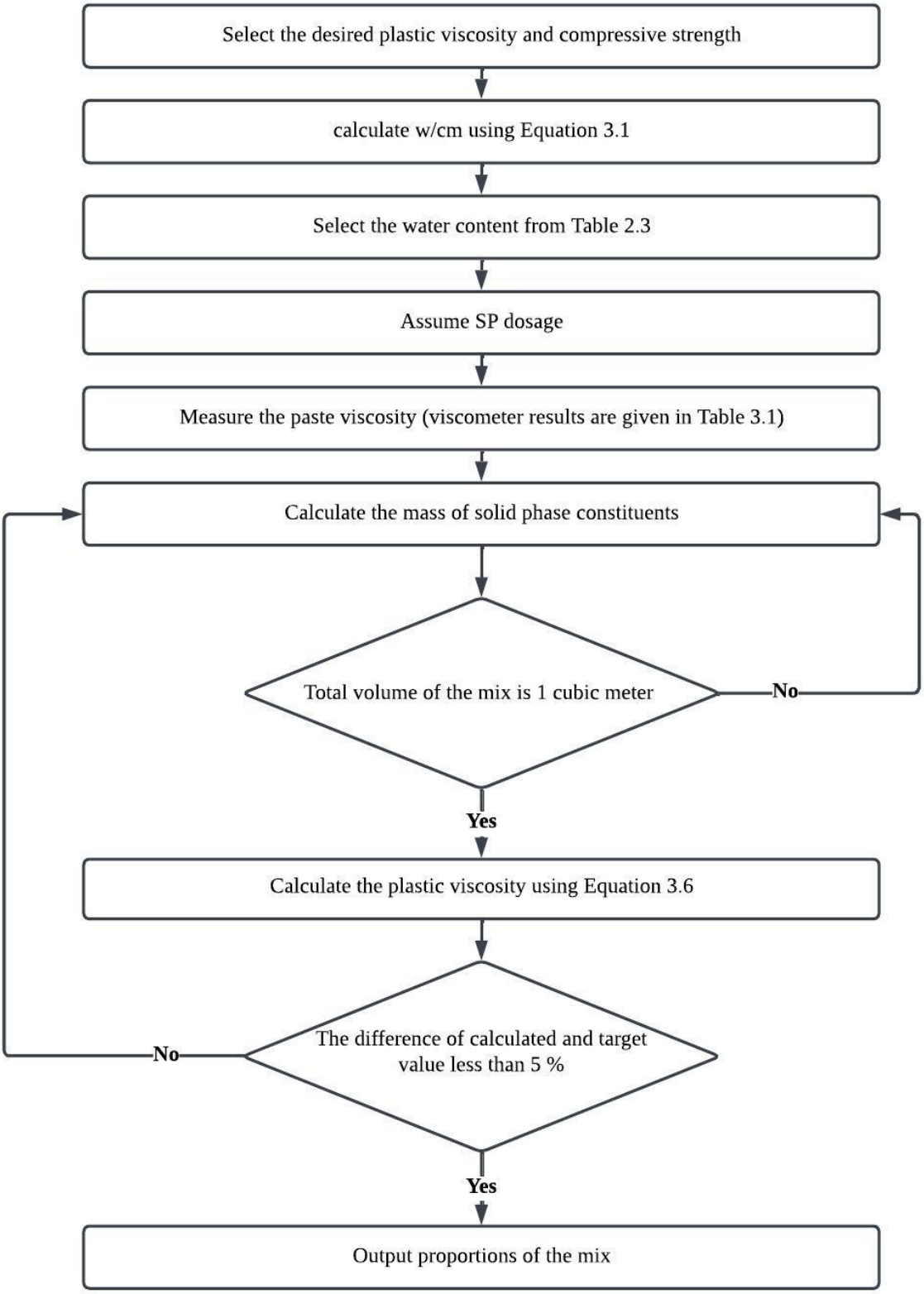

Figure 3.3 Methodology procedure for the HSSCC mix proportions

Table 3.1 Plastic viscosity of HSSCC cement paste (60% CEM I, 20% GGBS, 20% fly ash, SP, and water)

Mix code	w/cm	η_{paste} (Pa·s)	$\eta_{paste+air}$ (Pa·s)
C70	0.40	0.053	0.054
C80	0.35	0.073	0.075
C90	0.30	0.177	0.180
C100	0.26	0.381	0.390

3.3.4 HSSCC mix proportioning example calculations

Following the procedural steps indicated Figure 3.3, the target compressive strength and plastic viscosity were selected, and the w/cm ratio was calculated. Based on these, the cementitious material, fine aggregate, and coarse aggregate quantities were determined. An example of the mix proportioning procedure is given below for a mix with a target plastic viscosity of 3 Pa·s and compressive strength of 70 MPa. The applicable design chart is shown in Figure 3.4.

(a) W/cm ratio calculation:

For a 70 MPa target compressive strength, the (w/cm) ratio can be calculated using Equation (3.1).
As f_{cu} = 70 MPa, then *w/cm* = 0.40.

(b) Cementitious materials (cm) calculation for plastic viscosity η_{mix} = 3 Pa·s:

From Figure 3.4, $cm/\eta = 140.237$ kg/Pa·s (indicated by the grey curve)
For η = 3 Pa·s, *cm* = 420.71 kg/m^3
The cement is replaced by 20% each of fly ash and GGBS; therefore,
Cement = 252.43 kg/m^3, fly ash = 84.14 kg/m^3 and GGBS = 84.14 kg/m^3

(c) Water content calculation:

As *w/cm* = 0.40, then *w* = 0.4 * 420.71 = 168.28 kg/m^3.

(d) SP content:

Assume SP content to be according to the manufacturer's recommendation.

As a trial SP dosage, m_{sp}/m_{cm} was assumed to be 0.7%.

As *cm* = 420.71 kg/m^3, then SP = 2.95 kg/m^3.

(e) Solid phase component calculation, F-A and CA:

From Figure 3.4, (*cm* + *F-A*)/η = 425.72 kg/m^3 (indicated by the red curve)

As η_{mix} = 3 Pa·s and *cm* = 420.71 kg/m^3,

then *F-A* = 856.45 kg/m^3

From Figure 3.4, (*cm* + *F-A* + *CA*)/η = 711.21 kg/m^3 (indicated by the blue curve)

As η = 3 Pa·s; *cm* = 420.71 kg/m^3; *F-A* = 856.45 kg/m^3, then *CA* = 856.47 kg/m^3

(f) Concrete mix total volume (T_V) verification:

Verify that the total volume (T_V) of the concrete mix = 1 m^3

The densities of the materials are as follows: cement (3150 kg/m³), GGBS (2400 kg/m³), fly ash (2400 kg/m³), water (1000 kg/m³), superplasticiser (1070 kg/m³), fine aggregate (2550 kg/m³), and coarse aggregate (2650 kg/m³).

$$T_V = \frac{252.43}{3150} + \frac{84.14}{2400} + \frac{84.14}{2400} + \frac{168.28}{1000} + \frac{2.95}{1070} + \frac{856.45}{2550} + \frac{856.47}{2650} + 0.02 = 1 \text{ m}^3$$

(g) Plastic viscosity of the mix (η_{mix}):

Determine the plastic viscosity of the mix (η_{mix}) by using Equation (3.6).

$$\phi_{FA} = \frac{\frac{FA}{\rho_{FA}}}{\frac{c}{\rho_c} + \frac{GGBS}{\rho_{GGBS}} + \frac{fly\ ash}{\rho_{fly\ ash}} + \frac{w}{\rho_w} + \frac{SP}{\rho_{SP}} + \frac{FA}{\rho_{FA}} + 0.02} = 0.4960$$

$$\phi_{CA} = \frac{\frac{CA}{\rho_{CA}}}{\frac{c}{\rho_c} + \frac{GGBS}{\rho_{GGBS}} + \frac{fly\ ash}{\rho_{fly\ ash}} + \frac{w}{\rho_w} + \frac{SP}{\rho_{SP}} + \frac{FA}{\rho_{FA}} + \frac{CA}{\rho_{CA}} + 0.02} = 0.3231$$

$$\eta_{mix} = \eta_{paste} * \left(1 - \frac{\phi_{fine\ agg}}{\phi_m}\right)^{-1.9} * \left(1 - \frac{\phi_{coarse\ agg}}{\phi_m}\right)^{-1.9}$$

$$= 0.054 * \left(1 - \frac{0.4960}{0.63}\right)^{-1.9} * \left(1 - \frac{0.3231}{0.74}\right)^{-1.9} = 3.042\ \text{Pa·s}$$

where η_{paste} obtained by viscometer = 0.054

(h) Variation in viscosity:

The difference between the desired viscosity and the calculated viscosity is therefore:

D = (3.056 - 3)/3 = 1.4% < 5%, which is within the acceptable range.

The final mix proportions are shown in Table 3.2.

Table 3.2 Mix ingredients of C70 HSSCC mix with plastic viscosity of 3 Pa s (Alshahrani et al. 2023)

Materials	Water	Cement	GGBS	Fly ash	SP	FA	CA
Mass (kg/m^3)	168.28	252.43	84.14	84.14	2.95	856.45	856.47

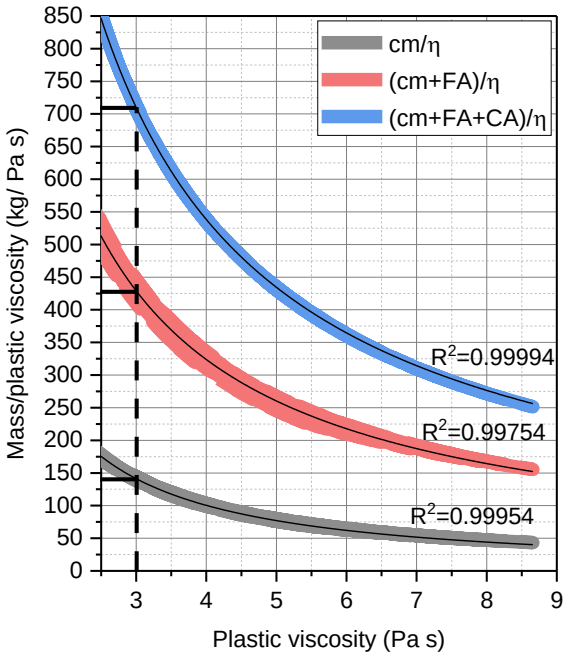

Figure 3.4 Design chart for 70 MPa HSSCC (Alshahrani et al. 2023)

3.4 Experimental method validation

3.4.1 Materials

The materials for the experimental mixes consisted of Portland Cement, GGBS, fly ash, and superplasticiser (SP). The Portland Cement, supplied by Tarmac Cement Ltd, had a compressive strength grade of 52.5 MPa, a specific gravity of 3.15, and a fineness of 384 m²/kg. The GGBS, sourced from Hanson Heidelberg Cement Group, and the fly ash from Tarmac Cement Ltd, served as cementitious binder materials, each with a specific gravity of 2.4. The SP utilised was MasterGlenium ACE 499, a polycarboxylate ether polymer with a specific gravity of 1.07. The chemical composition of these cementitious materials, as obtained from Hanson and Tarmac, is detailed in Table 3.3.

Table 3.3 Chemical composition of cementitious binder materials

Composition	SiO_2	Fe_2O_3	CaO	Al_2O_3	K_2O	Na_2O	MgO	So_3
OPC	19.69	2.85	63.04	4.32	0.74	0.16	2.17	3.12
Fly ash	53.10	8.93	6.12	20.64	2.17	1.68	1.79	1.93
GGBS	34.34	0.32	39.90	12.25	0.45	0.41	7.70	0.23

The aggregates used in the experimental mixes comprised crushed limestone coarse aggregate (CA) with a specific gravity of 2.65 and a maximum particle size of 20 mm, and natural river sand as fine aggregate (F-A) with a specific gravity of 2.55 and a maximum particle size of 2 mm. To enhance the mix, approximately 30% of the F-A was replaced with a coarser fraction of limestone dust (crushed rock sand) with a specific gravity of 2.6 and particle sizes between 0.125 mm and 2 mm. The particle size distribution curves for both fine and coarse aggregates are illustrated in Figure 3.5.

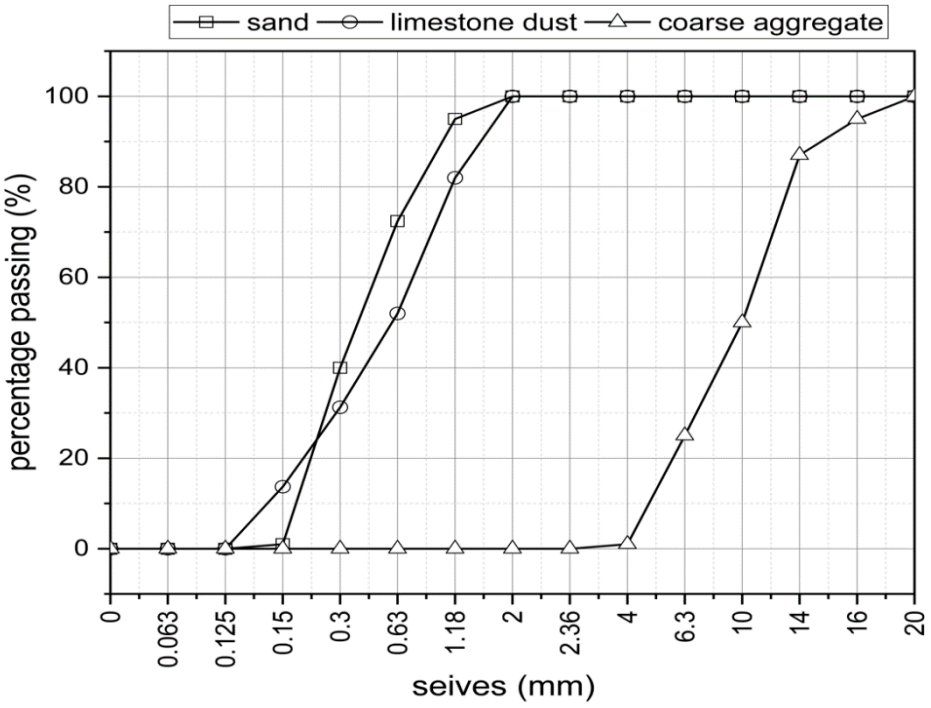

Figure 3.5 Particle grading curves for fine and coarse aggregate (Alshahrani et al. 2023)

3.4.2 Method validation

To validate the proposed methodology, various HSSCC mixes were designed based on target compressive strength and rheological properties. Four HSSCC mix sets were designed for compressive strengths of 70, 80, 90 and 100 MPa, with plastic viscosities ranging from 1.3 to 12 Pa s. Each set consisted of four mixes (A, B, C, and D) with varying plastic viscosity values and sand-to-aggregate (S/A) and paste-to-solid (P/S) ratios. The relative proportions and details of the mixes are given in Table 3.4 and Table 3.5, respectively. In partnership with a fellow PhD student (Tianyi Cui), the mixes were prepared during the COVID-19 pandemic, with Tianyi specifically preparing Mixes C and D, addressing the extensive range of variables within the constrained timeframe. Mixes A and C were designed with 48% sand to the total weight of aggregate (S/A), while B and D were designed for higher S/A ratios. Mixes A and B were designed with lower P/S ratios than Mixes C and D. The maximum cement replacement (indicated in Table 3.4) was limited to 40%, based on trial-and-error procedures to determine the maximum limit that would not compromise the target compressive strength.

To evaluate the self-compaction properties of the mixes, slump flow, J-ring, and L-box tests were performed following EFNARC (2005) guidelines. All tests were video-recorded in the

fresh state, and from a thorough visual review of the recordings, it was observed that none of the mixes revealed signs of segregation or bleeding. For each of the sixteen mixes, fifteen cubes (100 × 100 × 100 mm) were cast. After 24 hours, the specimens were de-moulded and subsequently cured in water at 20(±1)°C for the remaining test period. Compressive strength tests were conducted on the cubes at 7, 28, and 90 days, in accordance with BS EN 12350-3 (2019).

Table 3.4 Mix proportions of experimental HSSCC mixes, *kg/m³* (Alshahrani et al. 2023)

Mix code[1]	w/cm	Water	Cementitious material			SP	Aggregates		
			Cement	GGBS	Fly ash		F-A[2]		CA
							F-A*	F-A**	
70A	0.40	188.4	282.5	94.2	94.2	2.8	542.6	237.1	839.7
70B		188.4	282.5	94.2	94.2	2.8	593.6	259.4	763.9
70C		197.2	295.8	98.6	98.6	3.0	527.8	230.6	816.8
70D		197.2	295.8	98.6	98.6	3.0	561.4	245.3	766.9
80A	0.35	174.2	298.6	99.5	99.5	3.5	546.0	238.6	845.1
80B		174.2	298.6	99.5	99.5	3.5	604.0	263.9	750.6
80C		181.9	311.8	103.9	103.9	3.6	532.3	232.6	823.8
80D		181.9	311.8	103.9	103.9	3.6	574.1	250.9	761.7
90A	0.30	164.4	328.8	109.6	109.6	4.4	538.2	235.2	832.9
90B		164.4	328.8	109.6	109.6	4.4	590.0	257.8	756.0
90C		170.2	340.3	113.5	113.5	4.5	527.0	230.3	815.6
90D		170.2	340.3	113.5	113.5	4.5	566.4	247.5	750.0
100A	0.26	151.7	350.0	116.7	116.7	5.8	537.1	234.7	831.3
100B		151.7	350.0	116.7	116.7	5.8	590.6	258.1	751.1
100C		156.0	360.0	120.0	120.0	6.0	528.0	230.7	817.2
100D		156.0	360.0	120.0	120.0	6.0	563.2	246.1	762.8

Note 1: The mix code number indicates the target compressive strength.

Note 2: F-A* refers to natural river sand; F-A** refers to the coarser fraction of limestone dust.

Table 3.5 Design details of experimental HSSCC mixes (Alshahrani et al. 2023)

Mix code	Plastic viscosity (Pa·s)			Sand/total aggregate by weight (%)	Paste/solid by volume
	Paste	Target	Actual		
70A	0.054	1.6	1.60	48.15	0.61
70B		1.8	1.81	52.76	0.61
70C		1.3	1.30	48.15	0.66
70D		1.4	1.39	51.26	0.66
80A	0.075	2.3	2.34	48.14	0.60
80B		2.7	2.68	53.62	0.60
80C		1.9	1.92	48.15	0.64
80D		2	2.10	51.99	0.64
90A	0.18	5	5.00	48.15	0.62
90B		5.5	5.62	52.86	0.62
90C		4.2	4.28	48.15	0.66
90D		4.6	4.59	52.04	0.66
100A	0.39	10	10.68	48.14	0.63
100B		12	12.02	53.05	0.63
100C		9.5	9.40	48.14	0.66
100D		10	10.06	51.48	0.66

3.5 Results and discussion

3.5.1 Fresh state

Slump flow, J-ring, and L-box tests were utilised to assess the rheological properties of the HSSCC mixes in this study. Photographic records of the HSSCC Mix 70C test results are shown in Figure 3.6, Figure 3.7, and Figure 3.8.

The slump flow test measured the flow spread time, t_{500} (s), and flow spread diameter (mm) of the mixes in their fresh state. As shown in Figure 3.9, the spread time ranged from 1 to 4.3 seconds with a flow spread range of 750±100 mm. As the yield stress is closely correlated with the slump flow spread (Koehler and Fowler 2007; Abo Dhaheer 2016), the target flow spread for all the mixes was set within the range of 750±100 mm. Using a similar flow range implies that the mixes would have similar yield stresses, thereby making plastic viscosity the controlling parameter. The correlation between plastic viscosity and t_{500} is illustrated in Figure 3.9. This assumption is reinforced by findings from Koehler and Fowler

(2007), who highlighted that plastic viscosity is frequently the primary factor distinguishing the workability of different mixes. They noted that variations in plastic viscosity directly indicated changes in materials or mixture proportions, thus making the t_{500} measurement particularly useful for quality control. In addition, it was observed that as the plastic viscosity of the mixes increased, the t_{500} also increased, despite the higher SP content. This finding is consistent with previous research indicating that the mix flow time is determined by its plastic viscosity rather than the SP content (Abo Dhaheer et al. 2016a).

The J-ring test was conducted to evaluate the ability of the mixes to pass through congested reinforcement bars, simulating the passing ability of HSSCC in real-world reinforced construction scenarios. This study used a 300 mm diameter J-ring and twelve steel reinforcement bars (each 16 mm in diameter and 100 mm in height). Following a procedure similar to the slump flow test, the J-ring was placed at the centre of a horizontal base plate, sharing the same core circle as the slump cone. The expansion measured by the J-ring was calculated as the average of two diameters of the expanded surface, taken perpendicular to each other. As shown in Figure 3.10, the flow time t_{500j} demonstrated a strong correlation with the plastic viscosity of the respective HSSCC mixes.

Figure 3.6 Final slump flow diameter of Mix 70C (Alshahrani et al. 2023)

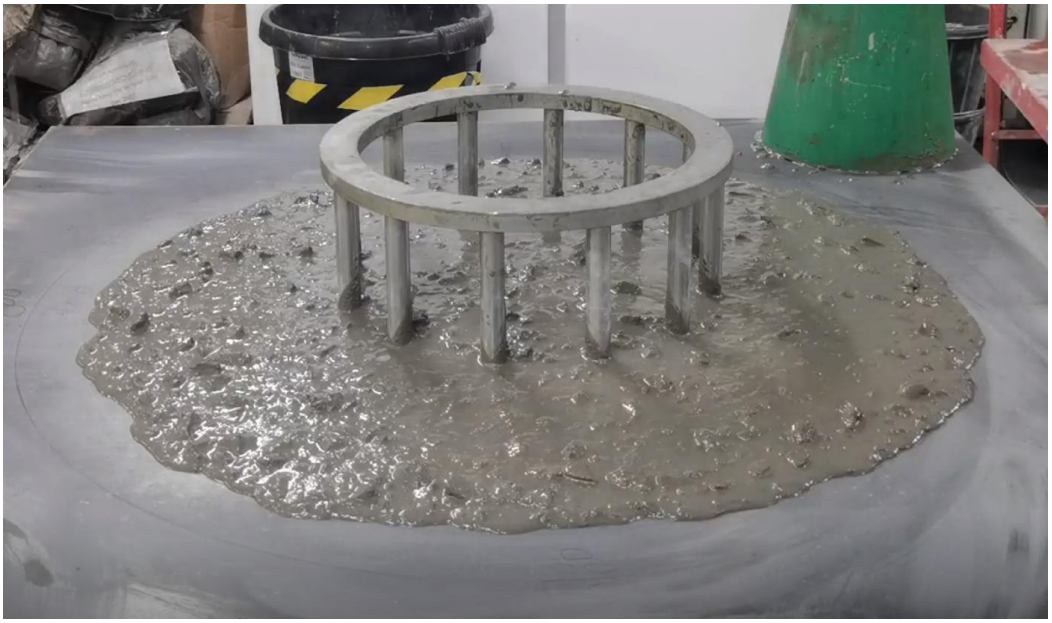

Figure 3.7 J-ring flow test of Mix 70C (Alshahrani et al. 2023)

Figure 3.8 L-box test of Mix 70C (Alshahrani et al. 2023)

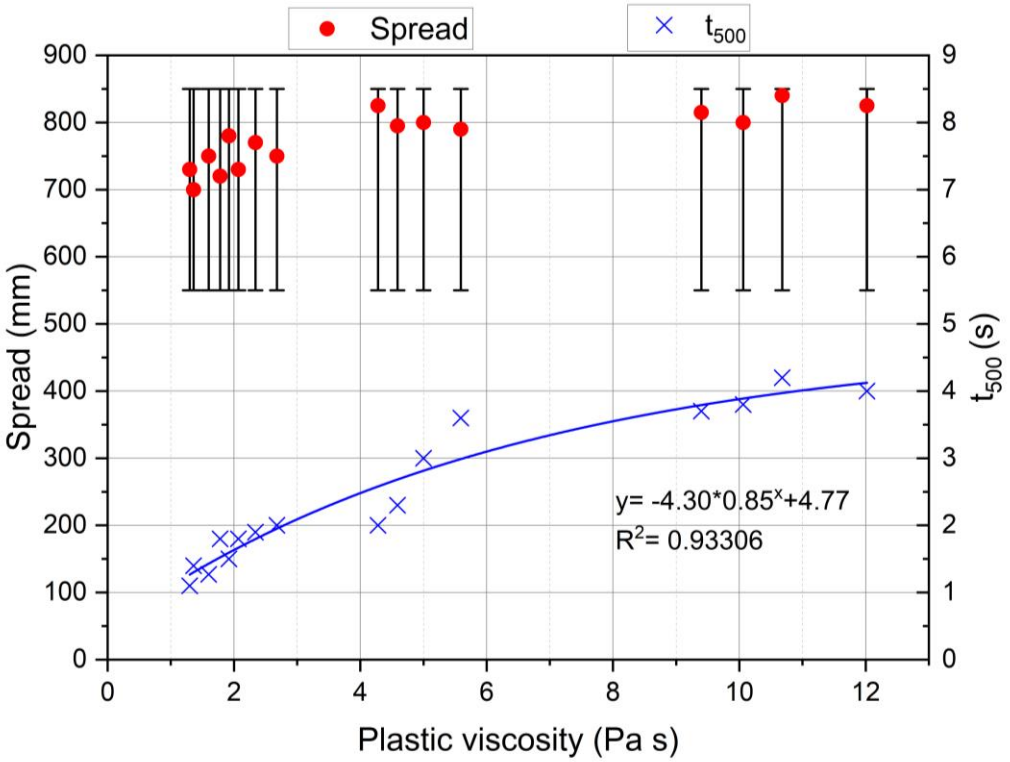

Figure 3.9 Slump flow diameters and t_{500} relative to plastic viscosity (modified from Alshahrani et al. 2023)

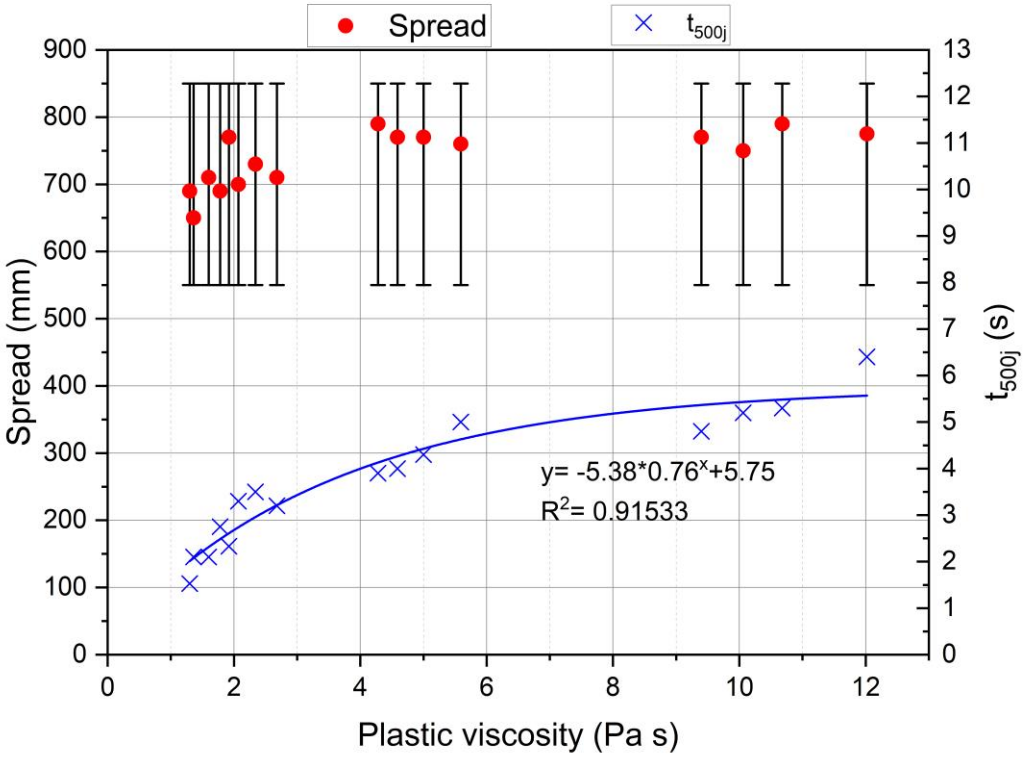

Figure 3.10 J-ring flow diameters and t_{500j} relative to plastic viscosity (modified from Alshahrani et al. 2023)

When the flow times for the slump (t_{500}) and J-ring (t_{500j}) tests were compared, it was noted that the variance in flow time between these tests increased as the plastic viscosity increased. This phenomenon was due to the properties of the viscous fluid; as the concrete mix became more viscous, HSSCC mixes took longer to pass through the reinforcement bars. In addition to the flow time, these tests also measured spread diameters; the results are presented in Table 3.6. According to (ASTM, 2014), the blocking characteristics of a mix can be determined by evaluating the difference in the flow spread diameters of the slump and J-ring tests. Specifically, differences of less than 25 mm suggest no visible blocking, differences between 25 and 50 mm indicate minimal to noticeable blocking, and differences greater than 50 mm suggest noticeable to extreme blocking. The data in Table 3.6 shows that the flow spread differences were less than 50 mm, indicating that no extreme blocking occurred during the tests.

Table 3.6 Flow spread diameters and variance in slump and J-ring tests (Alshahrani et al. 2023)

Mix code	D_{slump} (mm)	D_{J-ring} (mm)	$D_{slump} - D_{J-ring}$ (mm)
70A	750	710	40
70B	720	690	30
70C	730	690	40
70D	700	650	50
80A	770	730	40
80B	750	710	40
80C	780	770	10
80D	730	700	30
90A	800	770	30
90B	790	760	30
90C	825	790	35
90D	795	770	25
100A	840	790	50
100B	825	775	50
100C	815	770	45
100D	800	750	50

L-box tests were conducted to evaluate the ability of HSSCC mixes to flow through reinforced bars and into a frame using only their self-weight. A two-bar system (two 12 mm diameter vertical bars) was selected, similar to the gap between bars in the J-ring test. The time taken for each HSSCC mix to reach 200 mm (t_{200}) and 400 mm (t_{400}) horizontally after opening the gate was recorded. The passing ability ratio of a mix can be expressed as the ratio of the depth of concrete at either end of the horizontal leg of the L-box at the time of measurement (H1/H2). As indicated in Figure 3.11, all mixes achieved a Class PA1 passing ability ratio according to the European Guidelines for Self-Compacting Concrete (EFNARC 2005), thus indicating a good filling ability. Furthermore, an exponential correlation between flow time and plastic viscosity was observed in all HSSCC mixes.

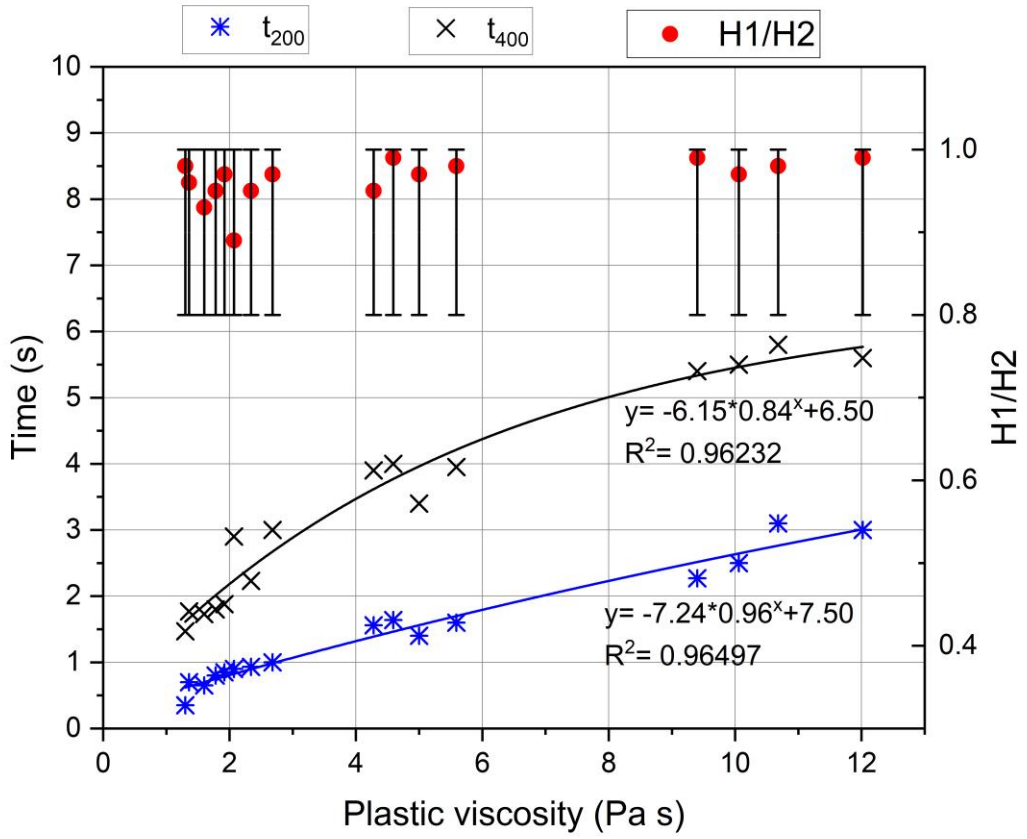

Figure 3.11 Passing ability ratios and t_{200} and t_{400} times in the L-box test relative to plastic viscosity (modified from Alshahrani et al. 2023)

Figure 3.12 shows the three-dimensional relationship between the S/A ratio and slump flow diameter. It can be observed that the slump flow diameters decreased as the S/A ratios increased in most of the test samples, while the P/S ratios and SP quantities remained

constant. This observation aligns with the results of experimental investigations reported in previous research (Jovein and Shen 2016). However, Yardimci et al. (2014) reported an increase in slump flow diameter as the S/A ratio increased from 0.48 to 0.71; these findings could be attributed to the increased quantity of SP used with the higher S/A ratios in their mixes.

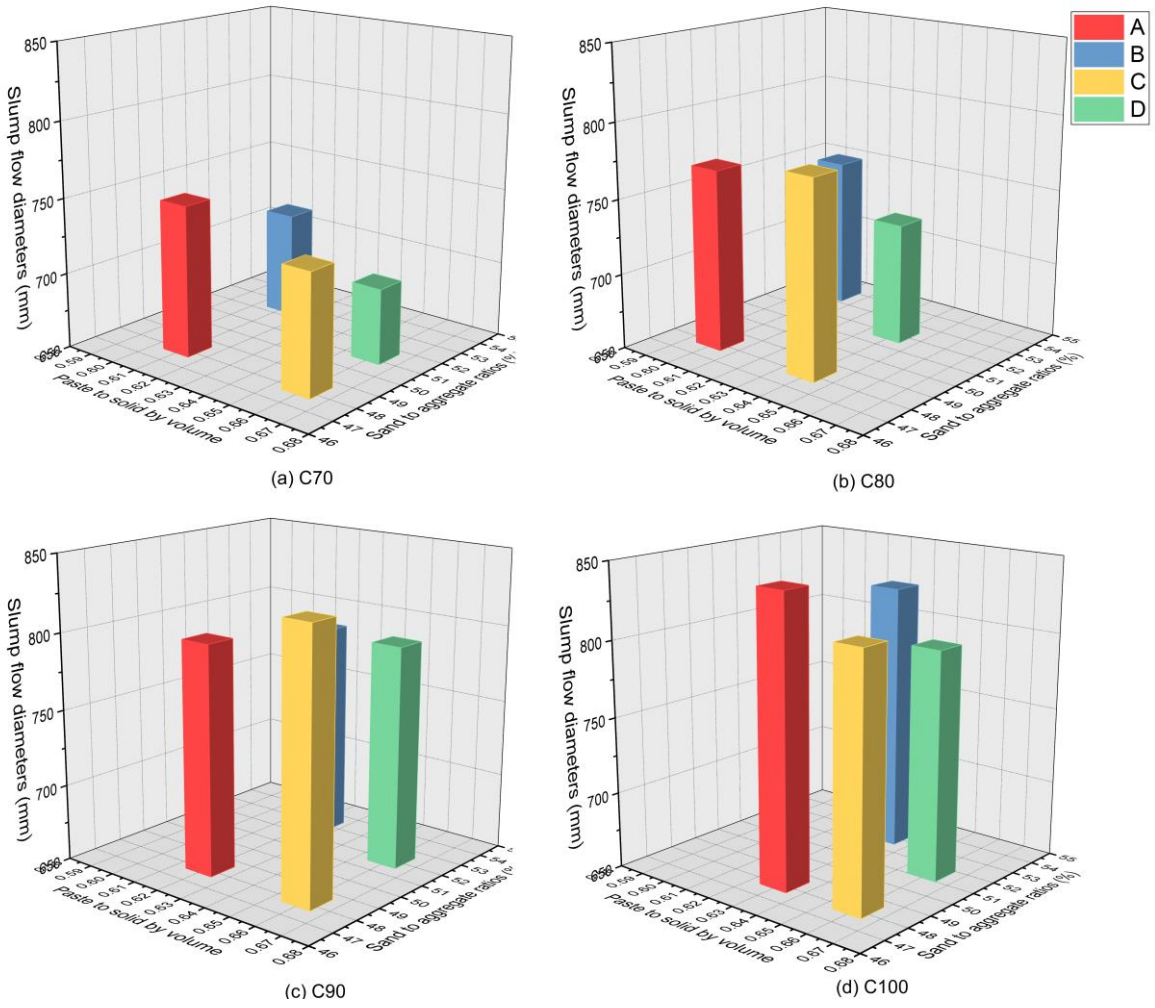

Figure 3.12 Relationship of sand-to-aggregate ratios and slump flow diameters for mix cases A, B, C, and D (Alshahrani et al. 2023)

3.5.2 Compressive strength

The compressive strength test results at 7, 28, and 90 days are detailed in Table 3.7. As previously mentioned, it is widely accepted that the compressive strength of concrete is primarily influenced by the w/cm ratio. Although the mixes with lower S/A ratios exhibited slightly higher compressive strengths compared to those with higher S/A ratios, the differences were minimal and deemed insignificant. The substitution of natural river sand

with a coarser fraction of limestone dust is both cost-effective and environmentally beneficial, and the results indicated that this substitution had a minimal impact on both the fresh and hardened states of the concrete. In addition, all mixes achieved compressive strengths close to the target strength at 28 days. Therefore, it can be concluded that the novel mix design method is effective and reliable for creating sustainable HSSCC.

Table 3.7 Compressive strengths of the HSSCC investigated (Alshahrani et al. 2023)

Target compressive strength (MPa)	Mix code	Compressive strength (MPa)		
		7 days	28 days	90 days
70	70A	48.3	74.9	79.5
	70B	45.3	70.4	75.6
	70C	47.3	70.1	78.8
	70D	48.6	68.6	76.5
80	80A	63.5	80.3	88.3
	80B	62.8	78.4	86.7
	80C	60.6	82.2	92.9
	80D	60.3	81.1	90.1
90	90A	72.3	91.1	101.9
	90B	69.4	88.4	96.4
	90C	71.6	93.2	103.2
	90D	70.4	91.3	98.6
100	100A	80.4	100.2	108.8
	100B	74.5	98.1	106.7
	100C	77.8	100.4	105.4
	100D	76.8	98.3	102.7

3.5.3 Evaluation of the sustainability performance

The concrete efficiency ((kg/m^3)/MPa) of the four mix sets of this chapter is illustrated in Figure 3.13. It can be noted that as the compressive strength increased, the quantity of cement needed to achieve 1 MPa decreased, with Mix 100A achieving the lowest cement quantity per MPa (3.48 (kg/m^3)/MPa). Additionally, the data presented in Figure 3.13 indicates a significantly reduced cement requirement per MPa than the quantity of 5 (kg/m^3)/MPa as documented in the literature for HSC and HSSCC (Damineli et al. 2010;

Deeb et al. 2012; Deeb and Karihaloo 2013). It can thus be concluded that this method is effective in reducing cement consumption per MPa of compressive strength.

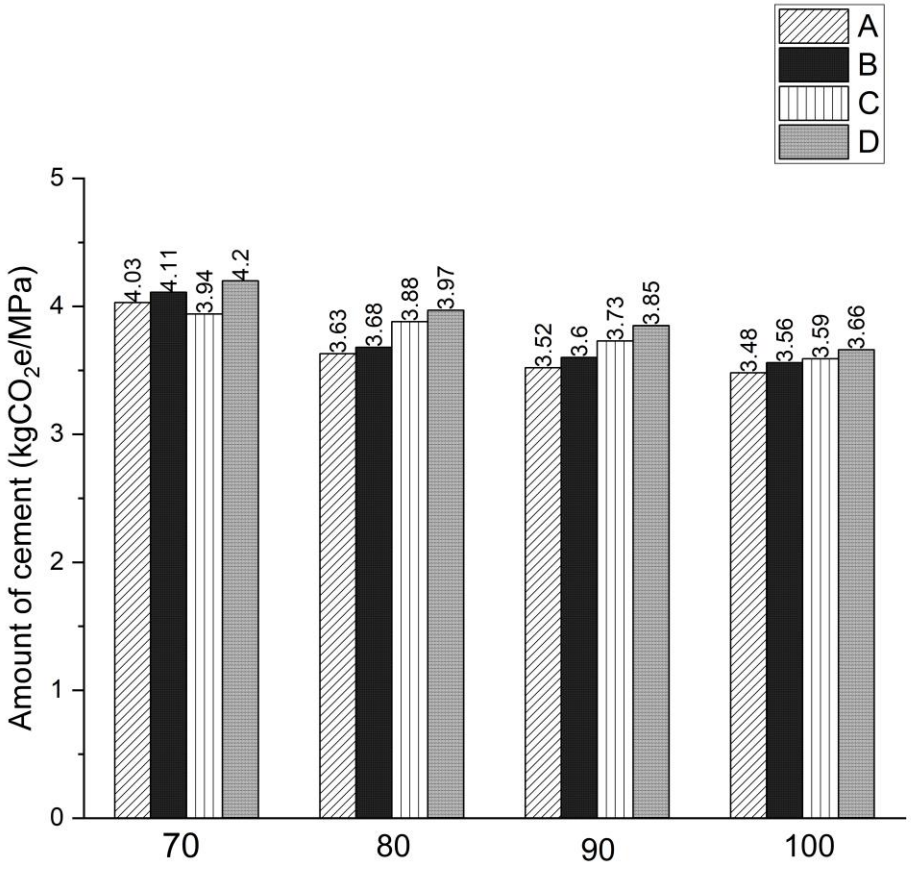

Figure 3.13 Concrete efficiency at 28 days for the HSSCC mixes (modified from Alshahrani et al. 2023)

A desktop study was conducted to determine the CO_2 emissions for each material used in the study (Table 3.8). These CO_2 emissions and the test data results for cement consumption required to achieve 1 MPa of compressive strength were subsequently factored into the efficiency calculations.

Figure 3.14 shows the calculated quantities of CO_2 emission per cubic metre ($kgCO_2e/m^3$) for the study mixes; the results indicate that CO_2 emissions per cubic metre increased with higher concrete strengths. This trend is attributed to the increased cement content required to achieve higher strengths. It has been proposed that the CO_2 emissions of concrete could be reduced by using industrial by-products with lower CO_2 emission values. In this study, this

was implemented by substituting 40% of the cement with pozzolanic materials (GGBS and fly ash) by weight and replacing 30% of the sand with limestone dust by volume.

Table 3.8 CO_2 emission factors of fine materials, aggregates, and SP collated from literature

Materials	CO_2 emissions (kgCO_2/kg)	Reference
Cement	0.931	(Hanif et al. 2017)
Fly ash	0.0001	(Mineral Products Association 2015)
GGBS	0.0796	(Mineral Products Association 2015)
SP	0.250	(Hanif et al. 2017)
Natural river F-A	0.003	(Hanif et al. 2017)
Limestone (stone powder)	0.0016	(Campos et al. 2020)
Natural CA	0.007	(Hanif et al. 2017)

The reduction in CO_2 emissions was primarily influenced by the cement replacement, correlating with findings from the literature (Celik et al. 2015). Conversely, the replacement of sand had a minimal impact on emissions. For example, partially replacing the cement in Mix 100A resulted in a 37.80% reduction in CO_2 emissions, while sand replacement only reduced emissions by 0.72%. Despite this, the replacement of natural river sand with coarser limestone dust is both economically viable and environmentally beneficial, and can enhance the durability of concrete (Kirthika et al. 2020).

It is evident from the data that mixes labelled C and D for each strength category exhibited higher CO_2 emissions compared to Mixes A and B, due to the higher cement content in Mixes C and D. For example, Mixes 70C and 70D, with design target strengths of 70 MPa and containing a greater quantity of cement, had higher CO_2 emissions than Mixes 70A and 70B. Similarly, Mixes 100C and 100D, with design target strengths of 100 MPa and containing an increased cement content, showed greater CO_2 emissions than Mixes 100A and 100B. This pattern is consistent across all strength categories, highlighting the direct relationship between cement content and CO_2 emissions.

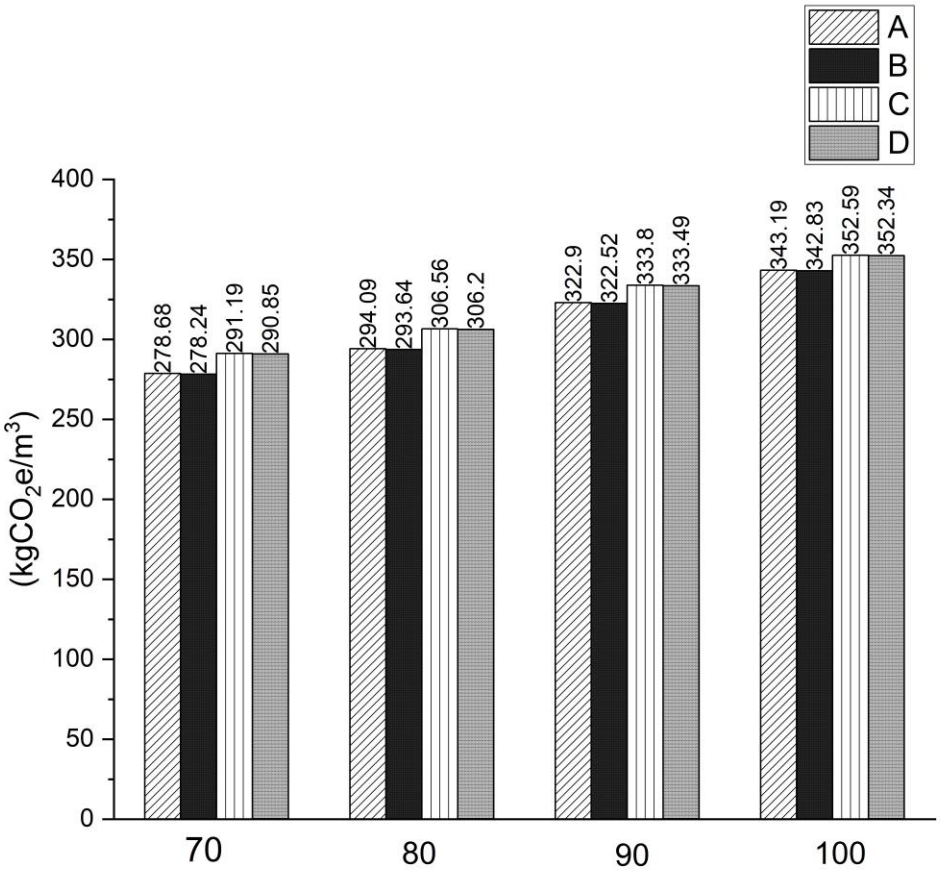

Figure 3.14 CO_2 per cubic metre of the experimental mixes (modified from Alshahrani et al. 2023)

Another strategy to reduce cement consumption and CO_2 emissions in concrete production is to use less concrete. This can be achieved by enhancing concrete efficiency, thereby reducing the amount of concrete required to support the same load. Efficiency can also be assessed by measuring the CO_2 emissions resulting from the achievement of 1 MPa of concrete compressive strength (Campos et al. 2020). Figure 3.15 illustrates the CO_2 emissions of the studied mixes relative to 1 MPa of compressive strength (kgCO_2 e/MPa) at 28 days, with Mix 100A exhibiting the lowest CO_2 emissions per MPa (3.4 kgCO_2 e/MPa). Comparing the amount of cement used in each mix with the corresponding CO_2 emissions per MPa revealed a proportional relationship (Figure 3.13 and Figure 3.15).

The analysis conducted by Rahla et al. (2019) indicated that incorporating fly ash or GGBS into concrete mixes led to lower environmental impacts and reduced costs, thereby enhancing overall sustainability. Similarly, Wang et al. (2017) carried out a comprehensive sustainability assessment that integrated the environmental, economic, and social performance of concrete into a single metric. Their findings showed that increasing the fly

ash content in concrete significantly improved the concrete's sustainability across all three variables.

To further advance the development of greener and sustainable HSSCC, future research could explore the use of alternative waste materials, such as rice husk ash, in mix designs, providing additional insights and guidance on creating more sustainable and eco-friendly concrete formulations.

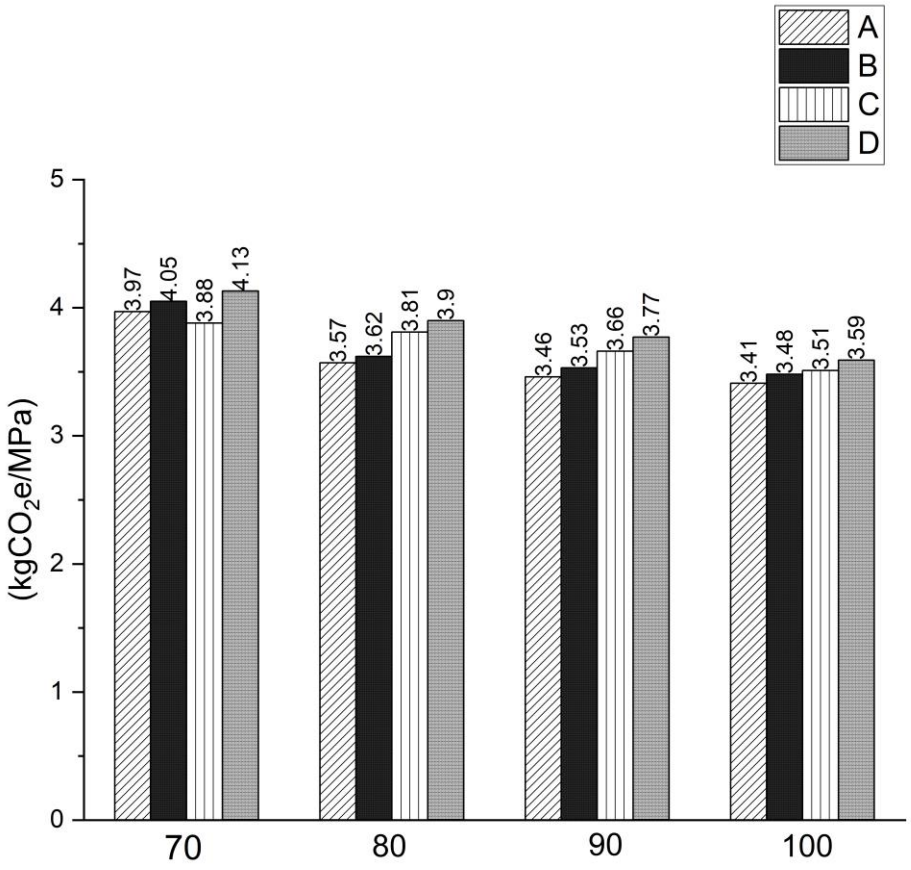

Figure 3.15 CO_2 emissions of the experimental mixes relative to 1 MPa of compressive strength at 28 days (modified from Alshahrani et al. 2023)

These fundamental results from previous research, combined with the analysis from the current study, demonstrate that HSSCC can enhance the properties of concrete while improving its sustainability. It can be concluded that the mix design employed in this study effectively optimises HSSCC performance and reduces the consumption of non-renewable resources, along with their associated CO_2 emissions. By increasing the compressive strength of the concrete, it is possible to achieve lower cement consumption, reduced CO_2 emissions,

and decreased costs. Consequently, this design method for HSSCC mixes could significantly improve both the economic and environmental aspects of concrete production.

3.6 Concluding remarks

This chapter described an effective mix-proportioning procedure for designing sustainable HSSCC by incorporating fly ash and GGBS as replacements for cement, guided by target plastic viscosity and compressive strength. The desired plastic viscosity of the HSSCC mixes was determined using the plastic viscosity of the paste and micro-mechanical constitutive models. This approach also facilitated the prediction of compressive strengths for the concrete mixes, targeting values of 70 MPa, 80 MPa, 90 MPa, and 100 MPa, by controlling the w/cm ratio. Design charts were developed to enable the straightforward application of the proposed methodology. Several strategies can enhance the sustainability performance of HSSCC, such as reducing the use of cement and non-renewable resources. Therefore, pozzolanic materials (fly ash and GGBS) and limestone dust were used in this study to partially replace cement and natural river sand, without compromising the concrete's fresh and hardened mechanical properties. Furthermore, increasing the compressive strength of the concrete can further enhance sustainability by allowing for the use of less concrete overall. The CO_2 emissions and cement consumption per unit of compressive strength (MPa) were lower for the study mixes than those reported in the literature. The method described in this study was validated through extensive experimental investigations, with all mixes achieving the design target strengths and meeting the required SCC criteria. Therefore, it can be concluded that this novel mix-proportioning method is highly effective in producing HSSCC with the desired fresh and hardened properties while being environmentally sustainable.

Chapter 4 Multiscale Homogenisation: Predicting Elastic Modulus in High-strength Self-compacting Concrete

4.1 Summary

Evaluating the elastic properties of concrete is of significant importance in civil and structural engineering, playing a critical role in ensuring the safety, durability, and service life of concrete structures (Parra et al. 2011). This is especially crucial for non-standard concrete such as self-compacting concrete (SCC) (Holschmacher and Klug 2002; Vilanova et al. 2011). This chapter reviews the elastic properties of steel fibre-reinforced self-compacting concrete (SFR-SCC), considering the effects of variations in coarse aggregate (CA) and steel fibre content. The elastic properties of concrete are traditionally measured through physical test methods, involving significant cost and time. However, the advent of multiscale homogenised simulations has revolutionised this testing approach by broadening the design space, allowing for the exploration of various mix configurations without the necessity for extensive physical experimentation. Therefore, a two-step homogenisation approach was proposed to predict the elastic properties of SFR-SCC. The first step comprised the homogenisation of the mortar, air voids, and aggregates based on mean-field homogenisation (MFH) using the Mori-Tanaka (M-T) model. X-ray computed tomography (CT) scanning techniques were used to determine and analyse the volume fractions, shapes, and number of air voids for validation purposes. The second step comprised the generation of a finite element (FE) model of a representative volume element (RVE) with steel fibre inclusions and homogenised concrete to determine the overall macroscale elastic modulus of the SFR-SCC mix. The results indicated that the content of CA and steel fibres, the porosity, and the fibre orientation in the mix substantially affect the elastic modulus. The impact of CA particle shape and the interfacial transition zone (ITZ) on the elastic modulus of SCC were also evaluated. The results obtained from the homogenisation method were compared with those obtained from a laboratory test study; it was found that the maximum error in the elastic modulus prediction using the proposed two-step homogenisation approach was less than 4%. This high level of agreement between the theoretical multiscale homogenisation and practical laboratory results indicates the feasibility of using the two-step homogenisation approach in the development of SFR-SCC and for preliminary mix optimisation and the selection of constituents for SFR-SCC. The results of this study verify that the proposed homogenisation method can replace time-consuming laboratory tests, saving both resources and time.

The content of this chapter has been published in the journal *Case Studies in Construction Materials* (Alshahrani, Kulasegaram, and Kundu 2023); details are provided in the List of Publications.

4.2 Introduction

Self-compacting concrete (SCC) as discussed in previous chapters, offers numerous advantages over Normal Vibrated Concrete (NVC), including reduced construction time, lower costs, and enhanced safety and durability due to its unique properties (Dinakar and Manu 2014). Unlike NVC, SCC is formulated with a high content of binder, a low coarse aggregate (CA) content, and other specific adjustment to achieve the desired flow and passing criteria of SCC. While these modifications improve the rheological properties, they may also influence key mechanical properties such as compressive strength, unit weight, elastic modulus, which are crucial for determining the design efficacy and structural performance of concrete (Jawahar et al. 2013)

Despite the favourable characteristics of SCC, the application of SCC in high-strength self-compacting concrete (HSSCC) may be limited owing to HSSCC's brittle nature, which could potentially cause structural integrity issues (Deeb et al. 2014). The enhancement of SCC's mechanical properties by the addition of fibres has been reported by numerous studies (Deeb et al. 2014; Madandoust et al. 2015; Haido et al. 2021; Majeed et al. 2021). *S*teel fibre-reinforced self-compacting concrete *(*SFR-SCC) combines the advantages of SCC technology with the benefits derived from the addition of fibres to a brittle cementitious composite. However, the rheological properties of SFR-SCC can be significantly impaired due to the large surface area and elongated shape of the steel fibres (Deeb et al. 2012). The fibre content in an SFR-SCC mix is thus limited and dependent on the fibre characteristics and the composition of the SCC mix. The sand-to-aggregate (S/A) ratio is a crucial factor in the design of SFR-SCC, playing an essential role in governing the fresh and hardened properties of SFR-SCC. Yardimci et al. (2014) investigated the effect of fibre content and S/A aspect ratios on the fresh and mechanical properties of SFR-SCC by using varying S/A ratios. The results indicated that to enhance the flowability and fracture energy of SFR-SCC, a higher S/A ratio should be used with relatively high fibre volume fractions and aspect ratios, thus decreasing the CA content. However, the effect of these variations in the mix composition on the

mechanical behaviour of SFR-SCC is a concern. An understanding of the optimal mix of constituents and their effect on the mechanical performance of SFR-SCC is a vital area of research and development for the construction industry, due to the lack of competent mix design procedures (Rajakarunakaran et al. 2022).

The elastic modulus is a crucial mechanical property in the design and assessment of concrete structures, ensuring serviceability while limiting excessive deformation (Zhou et al. 1995). As highlighted in Chapter 2, it is a fundamental variable in the calculation of elastic shrinkage and creep in prestressed concrete, as well as seismic analysis calculations concerning drift and deformation (Aslani and Nejadi 2012). The elastic modulus of concrete is traditionally estimated from the concrete's compressive strength using empirical formulae. However, such formulae neglect the influence of the specific composition and complexities of SCC and SFR-SCC. Studies have shown that SCC, despite having a comparable compressive strength to NVC, tends to exhibit an elastic modulus approximately 20% lower than NVC (Schlumpf 2004; Bonen and Shah 2005). This reduction can be partly attributed to SCC's higher paste volume and the significant contribution of CA to the concrete's stiffness (Domone 2007; De Schutter et al. 2008; Craeye et al. 2014). Therefore, research is required to attain a deeper understanding of the factors affecting the elastic modulus in SCC and SFR-SCC, with an emphasis on the importance of concrete composition, such as CA, mortar, pores, and fibre content.

Several homogenisation techniques have been developed for evaluating the effective elastic characteristics of composite materials, using a homogeneous continuum as a substitution of a heterogeneous substance. Analytical homogenisation methods involve an estimation of the upper and lower bounds of the continuum, such as the Hashin and Shtrikman bounds (Hashin and Shtrikman 1963) and the Voigt and Ruess bounds (Hill 1952). Eshelby's equivalent technique (Eshelby 1957) has been used as the basis for sophisticated analytical homogenisation techniques, such as the Mori-Tanaka approximation model (Mori and Tanaka 1973), the double-inclusion model (Nemat-Nasser and Hori 1993), the generalised self-consistent model (Christensen and Lo 1979), and the self-consistent approximation model (Hill 1965). Although these models are effective and simple to employ, they are unable to address realistic particle geometries or size gradations (Stefaniuk et al. 2019).

Where an analytical homogenisation technique is considered insufficient for the analysis of complicated microstructures, such as found in ultra-high-performance fibre-reinforced concrete (UHPFRC) (Qsymah et al. 2017), computational homogenisation can be applied. The direct finite element (FE) analysis of a representative volume element (RVE) is a common approach used in estimating the effective characteristics of composites (Pierard et al. 2007; Ogierman and Kokot 2017). Although the FE approach is able to overcome the limitations of analytical techniques, it is computationally expensive. Homogenisation techniques should ideally be simple and effective; hence, where the analytical homogenisation techniques are sufficient, the numerical and computational approaches should be avoided, not only to reduce the computational effort but also to reduce errors resulting from the selection of the RVE size or boundary conditions (Stefaniuk et al. 2019). For concrete, it is recommended that an RVE should be roughly 3–5 times the size of the largest aggregate's diameter to be statistically representative of the bulk material (Dunant et al. 2013). However, the exact size of RVE is strongly dependent on the volume fraction of the inclusions. Thus, the RVE size should be large enough in relation to individual grain size to represent general qualities such as stress and strain, but also be small enough to avoid masking the macroscopic heterogeneity (Gitman et al. 2007). Gal and Kryvoruk (2011) proposed a two-step homogenisation approach for fibre-reinforced concrete (FRC) comprising the initial analytical homogenisation of a spherical aggregate and its interfacial transition zone (ITZ) layer (Garboczi and Berryman 2001), followed by numerical homogenisation of the mortar, the homogenised aggregate, and the fibres to estimate the effective elastic properties of the FRC. However, the effect of the pores inherent in cementitious composites on the hardened properties have not been considered in detail (Nadeau 2003) and thus require further research.

X-ray computed tomography *(*CT) imaging has attracted considerable attention in recent years as it is a highly effective, non-destructive technique that produces high-resolution images which can be used to characterise and visualise the internal micro and mesoscale structures of various materials, enabling the visualisation of the internal details of materials. X-ray CT imaging has been used in several studies to evaluate the engineering characteristics of cement-based materials such as pore spaces (Kim et al. 2012) and the spatial distribution of air voids (Wong and Chau 2005). SCC composites are exposed to high air volumes in the

fresh state, directly affecting the porosity in the hardened state. Ponikiewski et al. (2014) used this technique for the determination of the 3D porosity of SFR-SCC.

At present, SFR-SCC is widely used in structural and civil engineering applications such as bridges, skyscrapers, tunnel linings, slabs, and various precast concrete structures (Bao et al. 2020). However, the use of SFR-SCC is accompanied by numerous empirical tests in the fresh and hardened states to ensure that the design standards and code specifications are met. The variations in SFR-SCC composition raise uncertainties concerning its elastic properties due to a lack of competent mix proportioning methods. A new strategy is needed for the design and testing of SFR-SCC to reduce laboratory work and costs and to improve the design of mix compositions and selection of their components.

This chapter details the study of the elastic modulus of SFR-SCC designed with varying contents of CA and steel fibres. Empirical tests and numerical methods were used to verify the accuracy of mesoscale finite element analysis in predicting the macroscopic elastic properties of SFR-SCC. A two-step homogenisation method was employed, incorporating the mean-field homogenisation (MFH) technique alongside FE model-based computational homogenisation. This hybrid approach significantly reduced the computational efforts required compared to numerical homogenisation alone, thereby validating the stated efficiency of this analysis process. Initially, the mortar, air voids, and CA were homogenised as plain SCC (i.e., without fibres) using MFH, leveraging X-ray CT imaging to assess the air void content and shapes within the SCC. Subsequently, a finite element model of an RVE with steel fibre inclusions was generated within the homogenised SCC matrix, using computational homogenisation to ascertain the bulk elastic modulus of the SFR-SCC.

4.3 Experimental methodology

4.3.1 Raw materials and mix design

The raw materials used in the concrete mixes were Portland cement (OPC) (supplied by Tarmac Cement Ltd), ground granulated blast-furnace slag (GGBS) (provided by Hanson Heidelberg Cement group), and a superplasticiser (SP) (MasterGlenium ACE 499) with specific gravities of 3.15, 2.4, 3.15, and 1.07, respectively. The crushed limestone CA had a specific gravity of 2.65 and a maximum gravel size of 10 mm, while the fine aggregate (F-A)

was natural river sand with a specific gravity of 2.55 and a maximum particle size of 2 mm. A portion of the natural river sand was replaced with an equivalent volume (30%) of the coarser fraction of limestone powder, which had a particle size range of 0.125–2 mm and a specific gravity of 2.6. The particle grading curves of the fine and coarse aggregates are shown in Figure 4.1.

The steel fibres used in the SFR-SCC mix were Dramix 3D 55/30 BG fibres, 30 mm long with hooked ends and 0.55 mm in diameter. The steel fibres' density, aspect ratio, and tensile strength were 7800 kg/m^3, 55 and 1345 N/mm^2, respectively.

Four HSSCC mix series were designed; the details and relative proportions are presented in Table 4.1 and Table 4.2. All the mixes were formulated with a water/cement (w/cm) ratio of 0.4 and 40% replacement of Portland cement with GGBS. Slight modifications were made to the F-A content to compensate for the addition of fibres, ensuring that the w/cm ratio and CA content remained consistent. Consequently, the HSSCC mixes varied in their volume proportions of CA and steel fibre volume fractions. The mixtures were identified by their CA content, fibre diameters, and steel fibre content. A control mix, referred to as plain HSSCC, was identified by its CA content alone. Mixes containing hooked-end steel fibres with diameters of 0.55 mm were labelled as SF55, with fibre diameters noted in hundredths of a millimetre. The mix designations were abbreviated to identify the percentages of CA and steel fibre in each mix. Thus, the mix labelled SF55-30-0.5 denotes an HSSCC mix with a 30% CA content and 0.55 mm diameter steel fibres, while CA-20 denotes an HSSCC mix with 20% CA content alone.

Table 4.1 Mix proportions of SCC mixes (kg/m^3)

Mix designation	Water	Cement	GGBS	SP	F-A	CA	Fibre
CA-20	205.6	308.4	205.6	2.6	997.5	530	-
SF55-20-1	205.6	308.4	205.6	3.6	972	530	78
CA-30	205.6	308.4	205.6	2.3	739	796	-
SF55-30-0.5	205.6	308.4	205.6	3	726	796	39

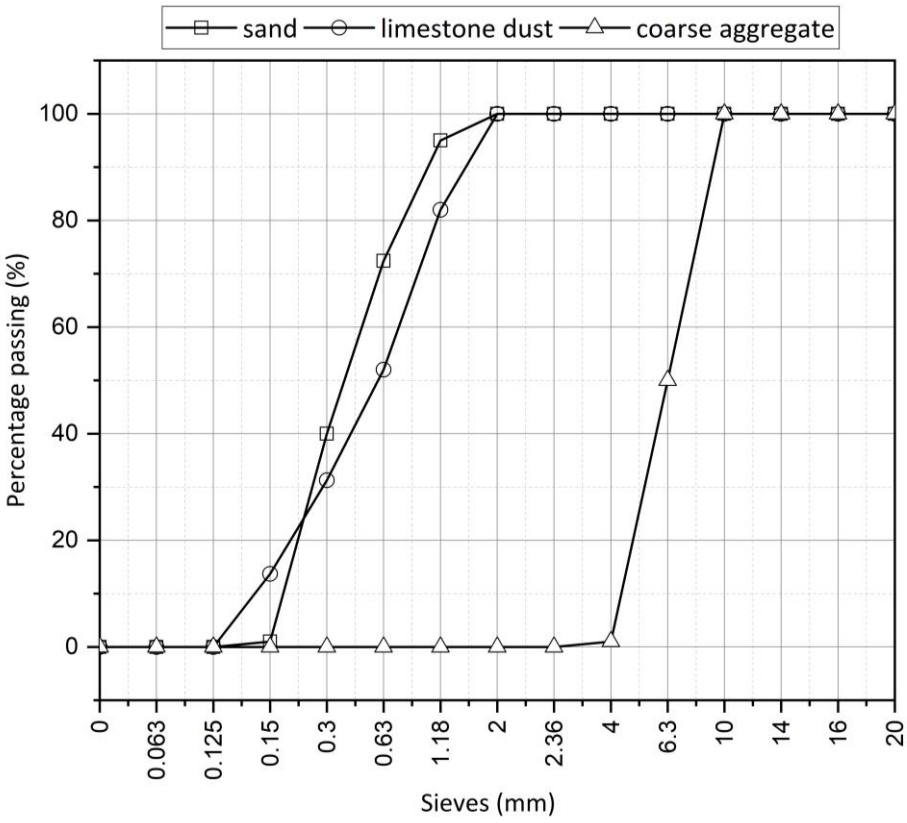

Figure 4.1 Particle grading curves of fine and coarse aggregates

Table 4.2 Percentage and relative proportions of mixes

Cementitious material = OPC + 40% GGBS		Water to cement ratio (w/cm) = 0.40	
Mix designation	CA content	Mortar content	steel fibre
	Percentage by volume		
CA-20	20	80	0
SF55-20-1	20	79	1
CA-30	30	70	0
SF55-30-0.5	30	69.5	0.5

4.3.2 Specimen preparation and test procedure

Slump flow and J-ring tests were conducted on each mix according to EFNARC (2005) to ensure that all mixes satisfied the required flow and passing ability criteria without segregation. Three cubes (100 × 100 × 100 mm) and three cylinders (ø100 × 200 mm) were cast for each HSSCC mix series. A beam of 150 × 150 × 600 mm was cast, and two cubes (100 × 100 × 100 mm and 50 × 50 × 50 mm) were extracted from the central portion of the beam. SFR-SCC composites do not undergo vibration during placement and tend to contain a

significant number of air voids in their fresh state compared to NVC. The extracted cubes were therefore used to assess the porosity of the mixes using X-ray CT imaging and micro-CT scanning. The specimens were de-moulded after one day and cured in water at a temperature of 20(±2) °C for 28 days. The compressive strength of the specimens was tested according to BS EN 12390-3 (BS EN 12390-3 2009), and the elastic modulus (E) was measured under static loading according to BS EN 12390-13 (BS EN 12390-13 2019). This entailed applying a load to a cylindrical specimen until the applied load was approximately one-third of the specimen's failure load and measuring the resulting strain using a 30 mm strain gauge; the test setup and dimensions are shown in Figure 4.2. Three loading cycles were carried out on each specimen, with a starting load of 0.5 MPa and a loading rate of 0.5 MPa/s (Figure 4.3).

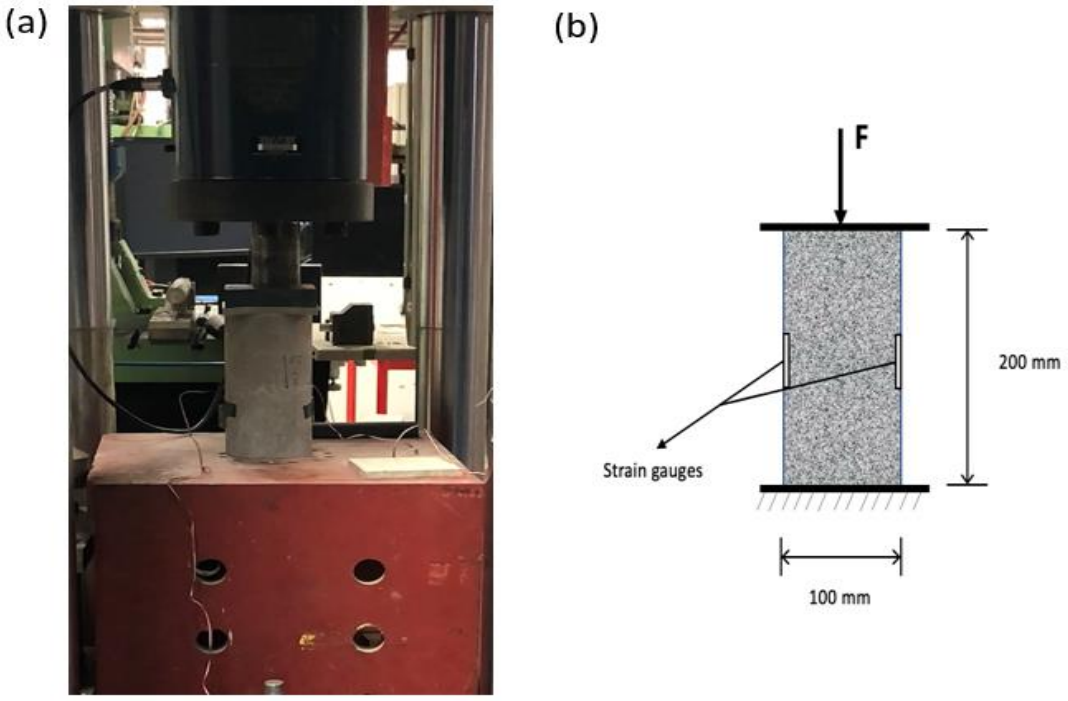

Figure 4.2 Elastic modulus test: (a) Experimental set-up, and (b) specimen dimensions

The elastic modulus (E) was calculated using Equation (4.1):

$$E = \frac{\Delta\sigma}{\Delta\varepsilon_s} \tag{4.1}$$

where E is the elastic modulus (MPa), $\Delta\sigma$ is the change in stress from preloading (0.5 MPa) to upper loading (one-third of the compressive strength), and $\Delta\varepsilon_s$ is the strain variation

during the third loading cycle. An example of a stress-strain curve under compressive loading is shown in Figure 4.4.

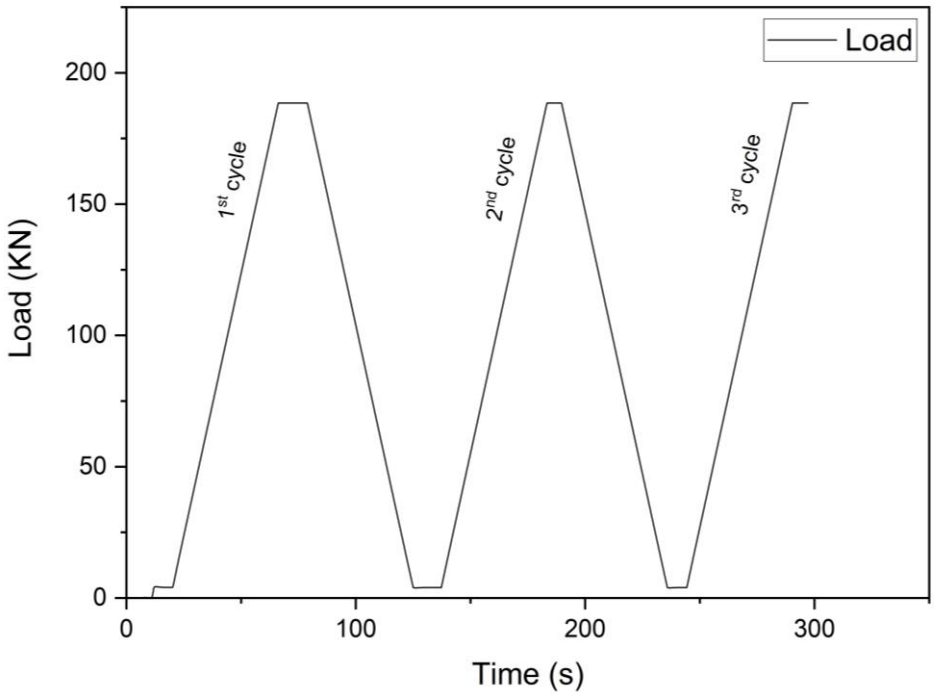

Figure 4.3 Loading cycles for the determination of elastic modulus

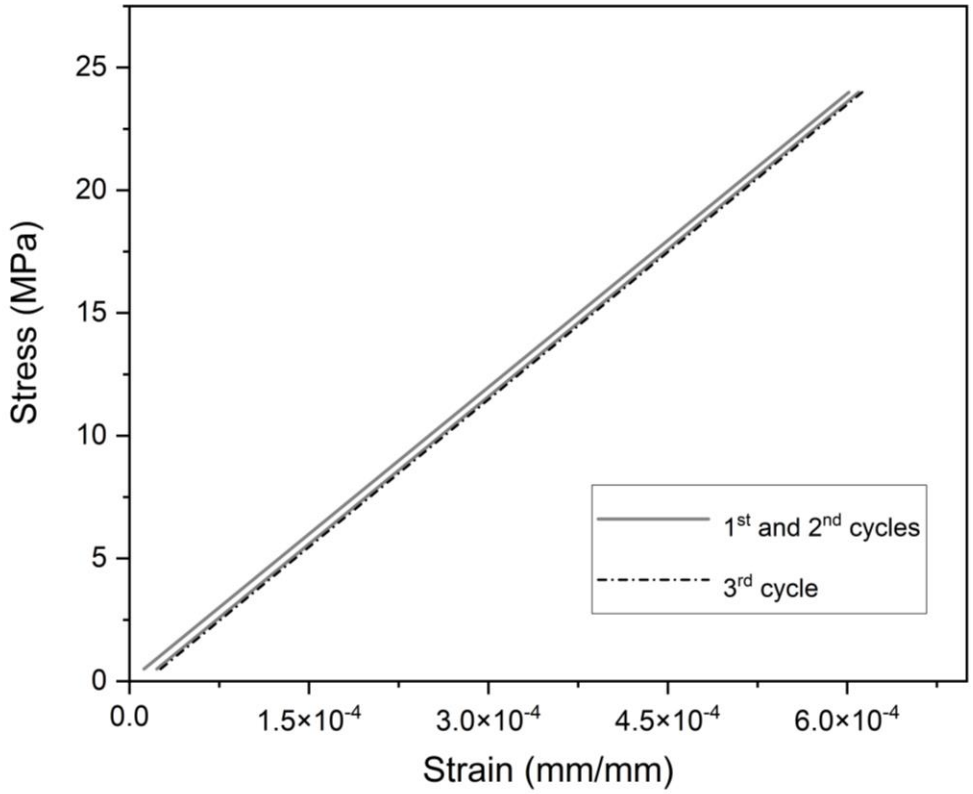

Figure 4.4 Stress-strain curve illustration in the elastic range

4.3.3 X-ray computed tomography (CT) scanning.

X-ray CT scanning is a non-destructive technique for capturing a large number of successive 2D slice images to reveal the internal microstructure of samples. In this study, a medical CT scanner was employed to analyse the volume, distribution, shape, and number of large pores within the SFR-SCC cube specimen (100 × 100 × 100 mm). The CT equipment used was a General Electric GE CT scanner at Najran University Hospital (Figure 4.5). The total number of CT slice images obtained was 882, with slice thicknesses of 0.27 mm. The X-ray tube scan settings for voltage and current were adjusted to 140 kV and 180 µA, respectively.

A micro-CT scan was conducted on the smaller 50 mm cube specimen at NeoScan in Belgium using a NeoScan N80 scanner. The voltage and current settings for this scan were 110 kV and 146 µA intensity, resulting in 1801 radiographs (2D images) with image pixel sizes of 30 µm. The scanning process took approximately 211 minutes.

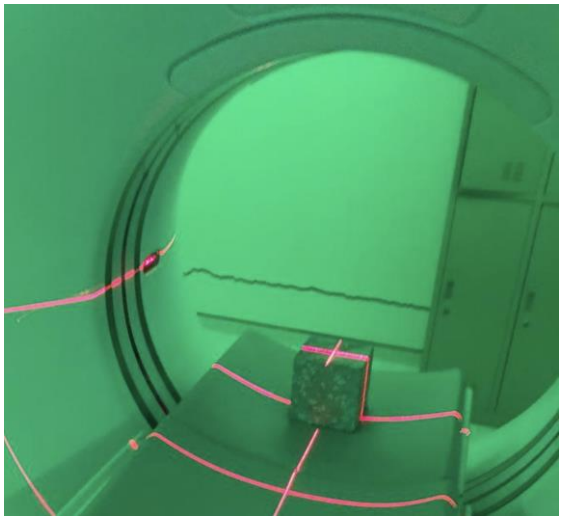

Figure 4.5 Cube positioned for medical CT scan to assess porosity.

4.4 Homogenisation methodology

The multiscale method commonly utilises the local homogenisation of macroscopic solids to address mechanical characteristics at the meso-scale (Gal and Kryvoruk 2011; Sun et al. 2019; Yu et al. 2020). The link between macroscale and mesoscale is created through a statistically representative model RVE of the microstructure, where the RVE comprises inhomogeneous materials consisting of a wide range of geometric and mechanical

properties at the mesoscale level. The constitutive behaviour of each phase is used to predict the macroscopic mechanical behaviour of the RVE via continuum mechanics to determine the macroscopic constitutive response of the composite. At the macroscale, each material point is assumed to be the centre of the RVE; thus, the RVE needs to be adequately large to accurately describe the underlying inhomogeneous microstructure, while simultaneously being small enough in comparison to the size of the solid body to avoid masking.

A novel two-step homogenisation method was used to investigate the elastic properties of SFR-SCC from a mesoscale perspective. The first step comprised MFH using the M-T model. At this stage, the mortar was equivalent to the homogeneous body and was considered as the matrix, while the CA and pores were treated as inclusions. In the second step, computational homogenisation was performed for the homogenised concrete (which included CA and pores) from step 1 (as matrix) and steel fibres (as inclusions). The developed approach hence combined the efficient semi-analytical method with a numerical simulation procedure. This method can predict the elastic modulus of SFR-SCC based on its compositions, wherein the effect of both fibre orientation and pore distribution are simultaneously considered.

A schematic diagram of the two-step homogenisation process is shown in Figure 4.6.

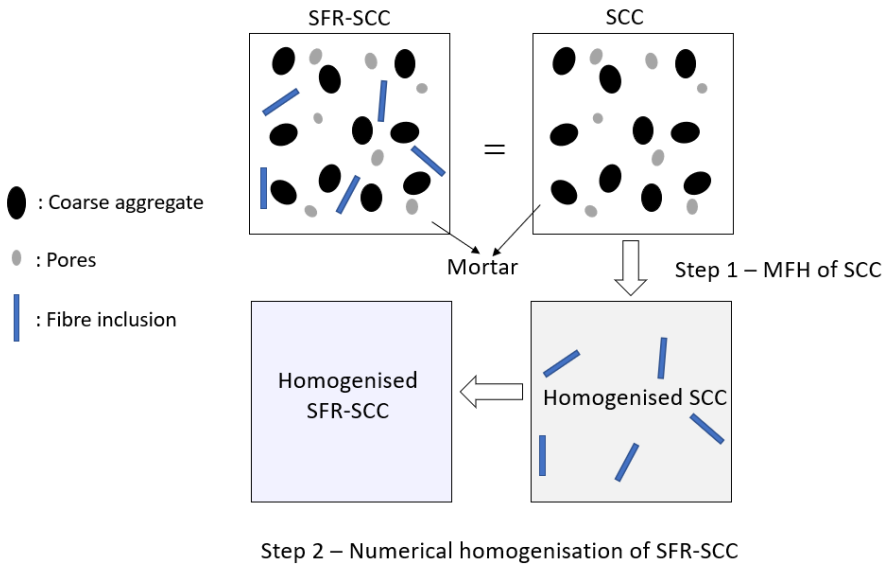

Figure 4.6 Schematic of the two-step homogenisation process

4.4.1 Step-1: Mean-field homogenisation

Based on a set of assumptions, several homogenisation models have been developed by adopting the Eshelby single inclusion theory (Eshelby 1957), such as the generalised self-consistent model (Christensen and Lo 1979), the M–T approximation model (Mori and Tanaka 1973), and the double inclusion model (Nemat-Nasser and Hori 1993). In these models, the macroscopic properties of composite materials are deduced based on the volume proportion and shape of the inclusions and the properties of the constituent materials, with the M–T model (Mori and Tanaka 1973) being widely used for the prediction of effective characteristics of composite materials. The original Mori-Tanaka (M-T) model for composites with a single inclusion type was extended by Benveniste (1987) by generalising the model for RVEs with several inclusions of similar shapes. The details of the Mori-Tanaka model (Mori and Tanaka 1973; Benveniste 1987) were described by Doghri and Ouaar (2003). The MFH model relates the mean stress and strain in the RVE; the mean of the stress/strain field, f, over the RVE of domain ω with a volume v is given as follows:

$$\langle f \rangle = \frac{1}{v} \int_{\omega} f(x, \overline{x})\, dv, \tag{4.2}$$

where f is the internal stress/strain field, $\overline{x}$ is the macro point, x is the meso point, and the integration is performed with respect to meso-coordinates x in the RVEω.

The mean of the stress/strain field over a single phase can be expressed as:

$$\langle f \rangle_{\omega_i} = \frac{1}{v_i} \int_{\omega_i} f(x, \overline{x})\, dv_i, \mathrm{i} = 0,1 \tag{4.3}$$

where '0' represents the matrix and '1' represents the inclusion.

The relationship between the average strains of RVE, the matrix, and the inclusion is given by Equation (4.4), while Equation (4.5), shows the average stress relationship:

$$\langle \varepsilon \rangle_{\omega} = v_o \langle \varepsilon \rangle_{\omega_0} + v_1 \langle \varepsilon \rangle_{\omega_1} \tag{4.4}$$

$$\langle \sigma \rangle_{\omega} = v_o \langle \sigma \rangle_{\omega_0} + v_1 \langle \sigma \rangle_{\omega_1} \tag{4.5}$$

where v_0 and v_1 are the volume of the matrix and inclusion, respectively, and $v_0 + v_1 = 1$.

The strain fields within different phases and the whole RVE are related to each other through the so-called strain concentration tensors (A and B) such that:

$$\langle \varepsilon \rangle_{\omega 1} = B^{\varepsilon} : \langle \varepsilon \rangle_{\omega_0} \; ; \; \langle \varepsilon \rangle_{\omega 1} = A^{\varepsilon} : \langle \varepsilon \rangle_{\omega} \tag{4.6}$$

The volume average of strain over all inclusions is connected to the volume average of strain over the matrix phase through the first tensor (*B*). Furthermore, the second tensor (A) relates the average volume strain over the entire RVE (macro strain) to the average volume strain over all inclusions. The two strain concentration tensors are dependent, as the latter can be determined from the former, as shown in Equation (4.7):

$$A^{\varepsilon} = B^{\varepsilon} : [\nu_1 B^{\varepsilon} + (1 - \nu_1)\boldsymbol{I}]^{-1} \tag{4.7}$$

where $\boldsymbol{I}$ represents the symmetric equivalent tensor, changing with B^{ε}.

Sophisticated MFH models are based on the fundamental solution derived by Eshelby (1957). The problem of a single ellipsoidal inclusion (I) of uniform stiffness C_1, embedded in an infinite matrix of uniform stiffness C_0, can be solved through Eshelby's solution. The uniform strain inside the inclusion can be related to the remote strain under a remote uniform strain (e) by:

$$\varepsilon(x) = H^{\varepsilon}(I, C_1, C_0) : e \, , \forall \in (I) \tag{4.8}$$

where H^{ε} is the single inclusion strain concentration tensor.

The macro stiffness for any homogenisation model specified by a strain concentration tensor can be expressed as:

$$C = [\nu_1 C_1 : B^{\varepsilon} + (1 - \nu_1) C_0] : [\nu_1 B^{\varepsilon} + (1 - \nu_1)\boldsymbol{I}]^{-1} \tag{4.9}$$

where the subscript '0' represents the matrix and '1' represents the inclusions.

In the macroscale, the relationship between stress and strain is given by:

$$\bar{\sigma} = \overline{C} : \bar{\varepsilon} \tag{4.10}$$

The first step in the homogenisation process of SFR-SCC comprised the homogenisation of CA and the pores. The elastic properties of SCC were predicted using MFH through the M-T model. Li et al. (2019) suggested a method based on image processing to evaluate the aspect ratio of CA and reported that the median aspect ratio value was 1.33. Using this method in the current study, the volume fraction of the air voids in the specimens was taken as 0.1% and the shape of the pores was assumed to be spherical; this was in agreement with the experimental observations of the CT scan results (refer to Figure 4.8 and Figure 4.10).

Table 4.3 shows the mechanical property parameters of each phase of SFR-SCC. The elastic modulus and Poisson's ratio of the aggregate were derived from Stock et al. (Stock et al. 1980), while the densities of the aggregate and mortar, and the elastic modulus of the mortar, were measured in the laboratory following the method described in Section 4.3.2. Prior to the elasticity tests, the density was measured after the specimens had cured for 28 days. The mass of cylindrical specimens was determined before the testing, and the density was computed from the volumetric measurements relative to their mass.

For the homogenised concrete properties, the elastic modulus and Poisson's ratio for each mix was calculated by integrating the properties of the mortar and aggregate using the Mori-Tanaka model. For example, after integration, Mix CA-20 had an elastic modulus of 36.60 GPa and a density of 2330 kg/m^3, while Mix CA-30 had an elastic modulus of 39.77 GPa and a density of 2370 kg/m^3. Moreover, the steel fibre used in the mix had an elastic modulus of 200 GPa and a density of 7800 kg/m^3, as given in the data sheet provided by the steel fibre manufacturer. The prediction of the elastic properties of SCC was implemented in Digimat-MF, a powerful software tool for calculating material characteristics through the incorporation of Mori-Tanaka homogenisation. As noted previously, the Mori-Tanaka model facilitates the rapid calculation of heterogeneous material characteristics and is extremely computationally efficient.

Table 4.3 Mechanical properties of high-strength SCC components

	Phase	Elastic modulus (GPa)	Poisson's ratio μ	Density (kg/m^3)
Step 1	Mortar	31.1	0.2	2250
	Aggregate	74.5 (Stock et al. 1980)	0.2 (Stock et al. 1980)	2650
	Porosity	-	-	-
Step 2	Homogenised concrete			
	1. CA-20	36.60	0.2	2330
	2. CA-30	39.77	0.2	2370
	Steel fibre	200	0.3	7800

4.4.2 Step-2: Finite element method-based numerical homogenisation.

Numerical homogenisation typically uses the FE method to represent sophisticated heterogeneous material structures at varying length scales and is an alternative to analytical methods. The computational homogenisation technique (Sharma et al. 2013; Qsymah et al. 2017) was used in this study to predict the effective elastic characteristics of SFR-SCC. After determining the homogenised properties of SCC using the MFH process (Step 1), the homogenised plain SCC with embedded steel fibres was simulated using finite element models based on RVEs of the composite, assuming the homogenised SCC as the matrix and the steel fibres as inclusions. The fundamental constitutive relationship of a heterogeneous material can be defined in terms of computational homogenisation as follows:

$$\langle \sigma \rangle = \overline{C} : \langle \varepsilon \rangle \tag{4.11}$$

To extract the equivalent orthotropic properties of SFR-SCC, six independent loadings with periodic boundary conditions were performed on RVEs and denoted as "automatic property evaluation" in Digimat-FE. The loadings were tensile load in 11 direction, tensile load in 22 direction, tensile load in 33 direction, shear load in 12 direction, shear load in 23 direction and shear load in 13 direction. The RVE generation algorithms available in Digimat-FE were used to generate random 3D geometric models of the meso-structural features based on the geometric shape and volume fraction of the steel fibres. The mechanical properties of the steel fibres and all phases are indicated in Table 4.3.

4.5 Results and analysis

4.5.1 Empirical results

The results of the slump flow and J-ring tests are presented in Table 4.4. No signs of bleeding or segregation were observed in the mixes, as confirmed by thorough visual inspections. The specimens were tested for compressive strength, unit weight, and elastic modulus, as described in Section 4.3.2; the test results are detailed in Table 4.5. It is widely recognised that the w/cm ratio primarily influences the compressive strength of SCC and SFR-SCC. Nonetheless, the test data indicated that the elastic modulus of SCC notably increased with the addition of CA for the same level of compressive strength. As indicated in Table 4.5, the mix containing 30% CA by volume (i.e., CA-30) had an elastic modulus (E_{exp}) of 41.06 GPa, while CA-20 (containing 20% CA by volume) had an elastic modulus of 37.02 GPa, despite both mixes achieving similar target compressive strengths of approximately 72 MPa. This finding demonstrates the limitations of empirical equations that predict the elastic modulus based solely on compressive strength, overlooking the impact of the mix composition of SCC and SFR-SCC on the elastic modulus evaluation. Additionally, it has been observed that incorporating steel fibres further increases the elastic modulus of SFR-SCC.

Table 4.4 Slump flow and J-ring flow test results of SCC mixes

Mix designation	Slump flow test		J-ring* flow test	
	Spread (mm)	t_{500} (s)	Spread (mm)	t_{500j} (s)
CA-20	690	1.8	670	2.3
SF55-20-1	680	2.9	670	3.8
CA-30	740	1.7	680	2
SF55-30-0.5	740	1.7	690	2.3

Table 4.5 Results of compressive strength and elastic modulus for all mixes at 28 days

Mix designation	Compressive strength (MPa)	Unit weight (kg/m^3)	Elastic Modulus (E_{exp})(GPa)
CA-20	71.9	2311	37.02
SF55-20-1	73.7	2361	38.55
CA-30	71.7	2398	41.06
SF55-30-0.5	69.2	2403	41.87

Several relationships have been suggested for the prediction of the elastic modulus of concrete, based mainly on the compressive strength of concrete, but these models tend to predict the elastic modulus of SCC inaccurately due to the lower aggregate content (Aslani and Nejadi 2012). The elastic modulus of concrete depends on the proportion of the individual constituents and their elastic moduli. Hence, the elastic modulus of concrete improves with increasing volume fractions of CA and reduces with increasing mortar content and porosity (Holschmacher and Klug 2002). The assessment of the elastic properties of SFR-SCC is often conducted through empirical tests, whereas the use of computational modelling is limited. Therefore, this study used a multiscale numerical simulation of SFR-SCC for the prediction of effective elastic properties.

4.5.2 X-ray CT results

The main objective of using the medical X-ray CT was to determine the volume fraction and number of large pores inside the concrete specimens. From the CT images, the identification of different materials can be derived from the density of each material; the greyscale of CT scans increases as the density of a material increases. Steel fibres have the highest density of the constituent materials in SFR-SCC; hence, steel fibres exhibited the maximum greyscale and the brightest colours in the CT images. Figure 4.7 shows one of the medical CT images in which the steel fibres, CA, voids, and mortar can be clearly seen and distinguished from one another.

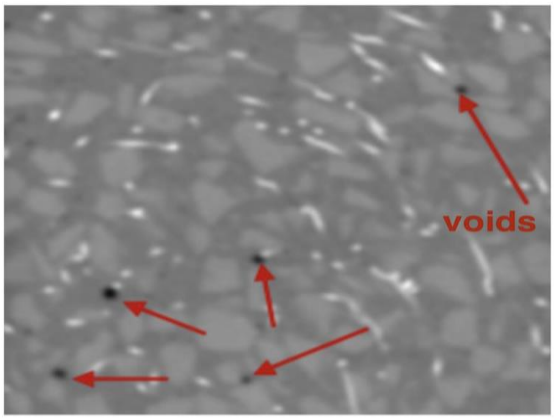

Figure 4.7 Typical 2D slice image from CT scan

The digital images produced by the CT scanner were analysed using the MIMICS image-processing software, which is considered a powerful tool in the reconstruction of CT image data (Shuguang and Qingbin 2015). Image segmentation, the process of detecting objects or the region of interest (ROI) from an input image, is an important stage in the transition from image processing to image reconstruction and analysis. Of the several image segmentation methods available, thresholding is a simple and efficient approach for image segmentation in digital image processing (Liu et al. 2013). MIMICS image-processing software was used to segment the 3D images into multiple phases based on the greyscale thresholds (-1024 to 3071). By filtering out image elements with predefined greyscale threshold values, the images of the voids can be acquired. After image thresholding segmentation, some defects may still appear in the images, requiring further elimination. The limitations of greyscale thresholds should thus be selected carefully. To identify the air voids, thresholds in the range of -1024 to -70 were adopted, which is consistent with the values reported by Qin and Xu (Qin and Xu 2016).

A 3D configuration of the air voids is presented in Figure 4.8, where the air void volume fraction was approximately 0.1%. The total number of air voids counted was 298; the frequency histogram of the air voids is shown in Figure 4.9. The results of this study showed that the majority of air voids in the SFR-SCC, as identified by medical CT scanning, were characterised by a small volume (less than 1 mm^3), aligning with findings from previous studies (Ponikiewski et al. 2014).

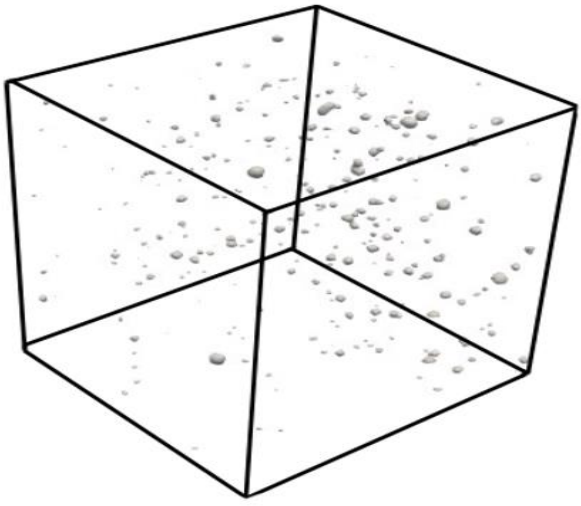

Figure 4.8 Typical 3D reconstruction of pore structure using medical CT scanning

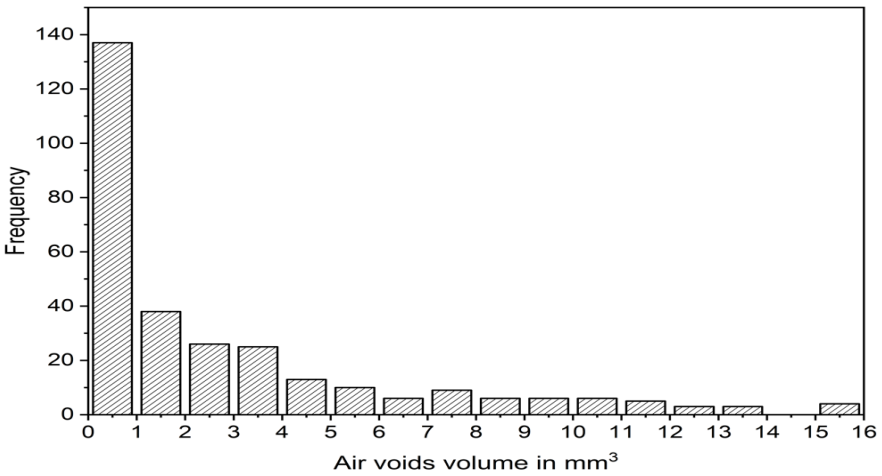

Figure 4.9 Frequency distribution of air voids volume in mm^3

For the micro-CT scan performed on the 50 mm cube, the 3D construction of the pore structure was carried out by NeoScan. The analysis showed that the pore volume fraction was 2.76%, with a total of 11,654 inclusions detected. A three-dimensional reconstruction of a micro-CT scan is shown in Figure 4.10, illustrating the distribution of pores in the small cube. This method offers higher accuracy in detecting pores with sizes larger than 30 µm. Furthermore, when the pore volume fraction was calculated for pores at a detection threshold of 150 µm, the results showed a volume fraction of 1.287%, with a count of 245 pores.

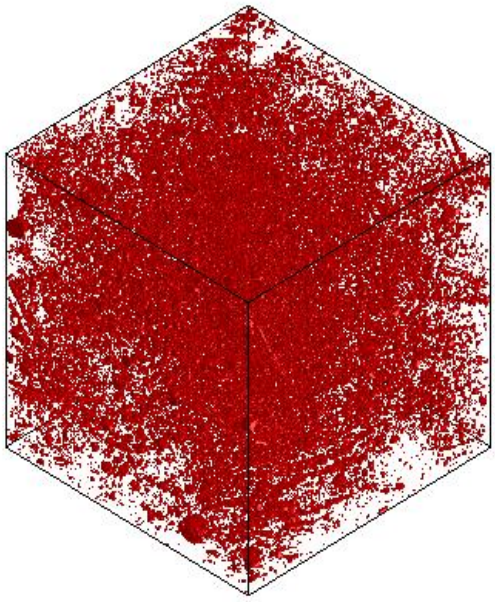

Figure 4.10 Typical 3D micro-CT Scan reconstruction of pore distribution

4.5.3 Numerical simulation results

4.5.3.1 Step 1: Mean-field homogenisation for self-compacting concrete

The prediction of the effective elastic modulus of SCC was based on MFH using the Mori-Tanaka homogenisation technique (Mori and Tanaka 1973; Benveniste 1987). Though the M-T model can provide excellent predictions for the effective properties of materials, it is inappropriate for high volume fractions of inclusions (i.e., greater than 30%) (Dunant et al. 2013). In the case of SCC, the volume fraction of inclusions (i.e., CA) is typically less than 30% and thus, this model is suitable for successfully predicting the macroscopic properties of SCC. The main advantage of using the MFH method is low computational cost.

The results of the elastic properties obtained for the SCC mixes are given in Table 4.6.

Table 4.6 Mechanical properties of SCC obtained by mean-field homogenisation method.

Mix designation	Mori Tanaka model		Density (kg/m^3)
	E_H (GPa)	μ_H	
CA-20	36.60	0.2	2330
CA-30	39.77	0.2	2370

4.5.3.2 Step 2: Numerical homogenisation

Research has shown that introducing fibres into SCC increases the achievement of uniform dispersion of fibres within structural components due to the rheological stability of the SCC matrix (Ferrara et al. 2012; Alberti et al. 2018; Raju et al. 2020). The properties of SFR-SCC are significantly dependent on the fibre content, orientation, aspect ratio, and the properties of the SCC matrix (Deeb et al. 2014). The fibre orientation in SCC is influenced by several factors, such as rheological properties, formwork geometry, fibre geometry, casting parameters into the formwork, and wall effects (Jasiūnienė et al. 2018; Marks et al. 2021). In general, steel fibre-reinforced concrete is regarded as an isotropic material with a random distribution of steel fibres (Zhang et al. 2018).

In the second step of the homogenisation process, the inclusions, i.e., fibres, were modelled as 30 mm long cylinders with diameters of 0.55 mm, giving them an aspect ratio of 55. The inclusions were randomly distributed in the matrix (see Figure 4.11 and Figure 4.12). It is

essential in any RVE-based numerical homogenisation to ensure that the homogenised properties are independent of the RVE size. Since the RVEs are computationally generated with the inclusions placed randomly within the matrix material, the homogenised properties can vary with each random realisation of the RVE, producing slightly different properties each time. To account for this, RVEs of varying sizes were produced (see Figure 4.11), with each size represented by a single RVE model; the homogenisation results are shown in Table 4.7. The RVE size was defined by the length of one edge, while the number of inclusions was determined using a volume fraction set to 1%.

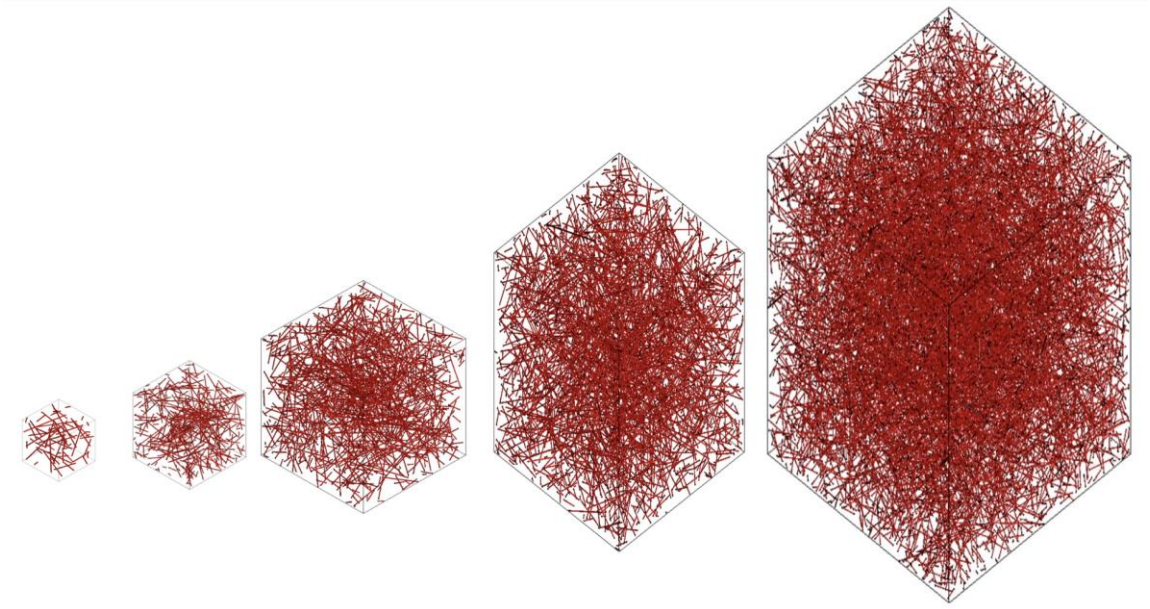

Figure 4.11 Variation in RVE size with a random orientation of fibres, from left 25 mm, 50 mm, 75 mm, 100 mm, and 150 mm

It is important to select appropriate RVE sizes to achieving stable and representative homogenised properties, to ensure the accuracy and reliability of the material behaviour predictions. As discussed in Section 4.2, choosing a suitable RVE size is crucial when predicting the elastic properties of SFR-SCC due to the impact that RVE size variations can have on the results. The detailed methodology used for this analysis is covered in Section 4.2.2.

The results of this analysis indicated that there is no significant dependence of homogenised properties on the size of the RVE when used for the prediction of elastic properties of SFR-

SCC. The variation in the homogenised RVE properties stabilised as a function of RVE sizes within the range investigated in this study.

Table 4.7 Engineering constants for RVEs of varying sizes

RVE size (mm)	25	50	75	100	150
Number of fibres	22	175	592	1403	4735
E_{11} (GPa)	37.38	37.39	37.38	37.37	37.39
E_{22} (GPa)	37.40	37.39	37.37	37.37	37.39
E_{33} (GPa)	37.37	37.39	37.37	37.38	37.39
μ_{12}	0.20040	0.20022	0.20024	0.20019	0.20019
μ_{21}	0.20053	0.20033	0.20019	0.20020	0.20022
μ_{13}	0.20070	0.20020	0.20024	0.20019	0.20021
μ_{31}	0.20047	0.20026	0.20024	0.20020	0.20022
μ_{23}	0.20068	0.20026	0.20020	0.20021	0.20020
μ_{32}	0.20033	0.20020	0.20025	0.20022	0.20019
G_{12} (GPa)	15.54	15.54	15.53	15.53	15.53
G_{23} (GPa)	15.53	15.54	15.53	15.53	15.53
G_{13} (GPa)	15.53	15.53	15.53	15.53	15.53
Density (kg/m^3)	2384.7	2384.7	2384.7	2384.7	2384.7

The RVE size selected for the subsequent analysis was 50 × 50 × 50 mm. In accordance with the experimental setup, two volume fraction inclusions were considered, namely 0.5% and 1% (refer to Figure 4.12). This resulted in 88 inclusions for Mix SF55-30-0.5 and 175 for Mix SF55-20-1. Voxel meshes were employed to generate the meshes for the FE model, resulting in 125,000 elements and 132,651 nodes. The average elastic moduli obtained for SF55-30-0.5 were E_{11} = 40.19 GPa, E_{22} = 40.18 GPa, and E_{33} = 40.19 GPa, while the average elastic moduli for SF55-20-1 were determined to be 37.39 GPa across E_{11}, E_{22}, and E_{33}. Consequently, the mesoscale analysis using the two-step homogenisation method yielded an average elastic modulus of 40.19 GPa for SF55-30-0.5 and 37.39 GPa for SF55-20-1.

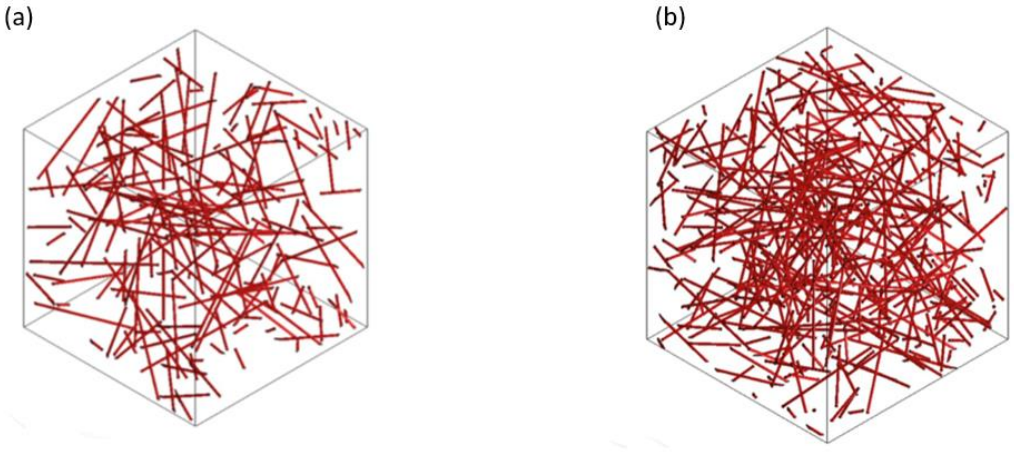

Figure 4.12 Final RVEs with steel fibre volume fractions: (a) 0.5%, and (b) 1%

4.6 Validation of proposed homogenisation method

To validate the two-step homogenisation methodology for determining the elastic modulus of SFR-SCC, the results of the homogenisation method (obtained from a single sample) were compared with the empirical results (obtained from the average of three samples). The comparison shown in Table 4.8 demonstrates that the elastic modulus predicted through multiscale numerical simulation using the MFH method and FE simulation for SFR-SCC is in excellent agreement with the empirical results. The consistency between the obtained numerical findings and the test data demonstrates the viability of using computer simulation in the design of multiphase materials. The coupling of MFH and FE homogenisation for the prediction of the effective properties of SFR-SCC resulted in substantial saving of computational effort compared to using numerical homogenisation alone. The ability to predict the mechanical properties of SFR-SCC could be very appealing to the concrete industry, as this would make it possible to deliver more predictable SFR-SCC products. The method used in this chapter can also be used for preliminary mix optimisation and the selection of constituents for SFR-SCC.

It can be concluded that the proposed two-step homogenisation method can effectively replace time-consuming laboratory tests, saving time and raw materials. This method combines efficient MFH techniques with numerical simulation to predict the elastic properties of SFR-SCC based on its composition while incorporating the effect of the pores which inherently exist in cement-based composites.

Table 4.8 Comparison of empirical (E_{exp}) and homogenised (E_H) elastic modulus

Mix designation	(E_H) (GPa)	(E_{exp})(GPa)	Discrepancy %
CA-20	36.60	37.02	1.13
SF55-20-1	37.39	38.55	3.01
CA-30	39.77	41.06	3.14
SF55-30-0.5	40.19	41.62	3.44

4.7 Effect of CA and fibre volume fraction on homogenised elastic modulus

The two-step homogenisation method was used to study the effect of CA and fibre volume fractions on the homogenised elastic modulus of SFR-SCC. The results shown in Figure 4.13 indicate that the homogenisation model can correctly capture the increase in the elastic modulus with increasing volume fractions of CA and fibres. The results also highlight the linear effect of the fibres and CA on the increase in elastic modulus. When the CA volume fraction was increased from 0% to 30%, the elastic modulus increased by approximately 9 GPa, irrespective of the fibre volume fraction. Similarly, increasing the fibre volume fraction from 0% to 2% resulted in an increase in the elastic modulus by approximately 1.6 GPa, irrespective of the CA volume fraction.

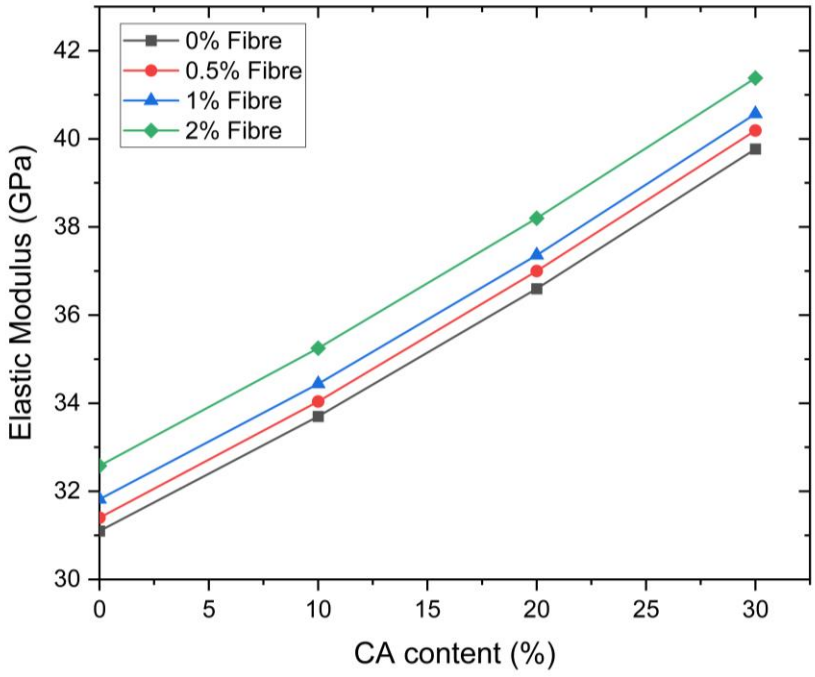

Figure 4.13 Effect of CA and fibre volume fraction on homogenised elastic modulus

4.8 Effect of porosity on the homogenised elastic modulus

SCC is susceptible to excessive air volumes in the fresh mix, which affects the porosity of the concrete structure. To understand the impact of porosity volume fraction on the elastic modulus of SCC, the elastic modulus was predicted for various pore contents, assuming the pores were spherical, as supported by CT scan data. Figure 4.14 illustrates the resulting effect of porosity of 0%, 0.5%, 1% and 2% on the elastic modulus of SCC. The results indicate that the porosity has a significant effect on the elastic modulus. The results indicate that SCC mixes with 0% porosity exhibit the highest elastic modulus, and as porosity levels increase to 0.5%, 1%, and 2%, there is a marked and substantial decrease in the elastic modulus of SCC, irrespective of the CA content.

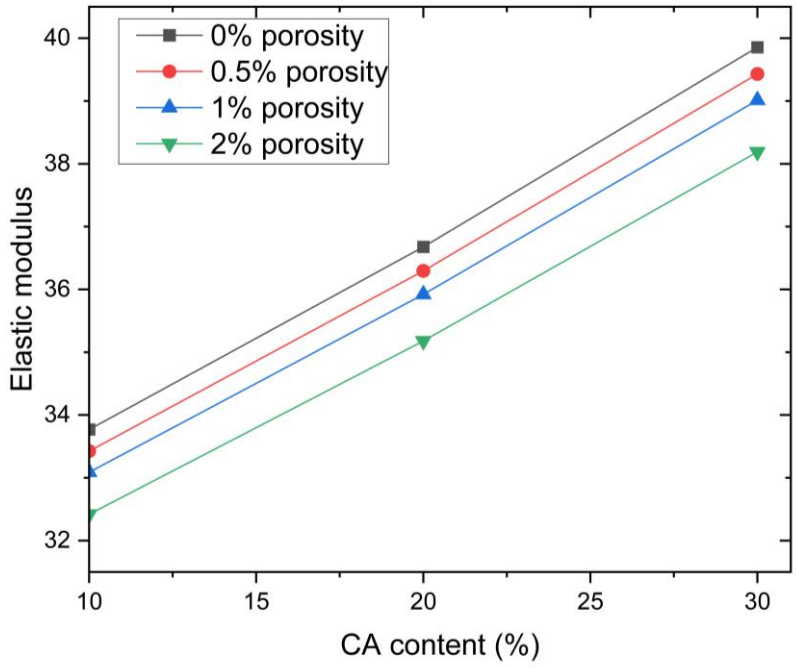

Figure 4.14 Effect of the porosity on the homogenised elastic modulus

4.9 Effect of fibre orientation on the homogenised elastic modulus

To assess the impact of steel fibre orientation on the elastic modulus of SFR-SCC, an RVE corresponding to SF55-20-1 was simulated. In this simulation, all steel fibres were randomly distributed but aligned along the x-axis (refer to Figure 4.15a). The resultant elastic moduli were E_{11} = 38.12 GPa, E_{22} = 37.16 GPa, and E_{33} = 37.16 GPa. As anticipated, the elastic modulus in the x-direction (E_{11}) exhibited the highest value. The difference between E_{11} and E_{22} (or E_{33}) was approximately 0.96 GPa, while for randomly oriented fibres (refer to Figure

4.14b), the variation between E_{11} and E_{22} (or E_{33}) was virtually nil, as indicated in Table 4.7. Subsequent analyses replicated this procedure for RVE models with higher fibre volume fractions (e.g., 2%), comparing the elastic moduli of RVEs with randomly oriented fibres to those with fibres aligned along the x-axis (refer to Figure 4.15). In the scenarios where the fibres were aligned along the x-axis, the average elastic modulus values were E_{11} = 39.67 GPa, E_{22} = 37.75 GPa, and E_{33} = 37.75 GPa. Notably, E_{11} was approximately 5% higher than E_{22} and E_{33}, representing a difference of around 1.92 GPa. Conversely, when fibres were randomly oriented, the average elastic modulus was E_{11} = 38.20 GPa, E_{22} = 38.19 GPa, and E_{33} = 38.19 GPa, showing a negligible 0.01 GPa discrepancy between E_{11}, E_{22}, and E_{33}. These findings underscore the hypothesis that fibre orientation exerts a more pronounced effect on the elastic modulus of SFR-SCC with increasing fibre volume fractions.

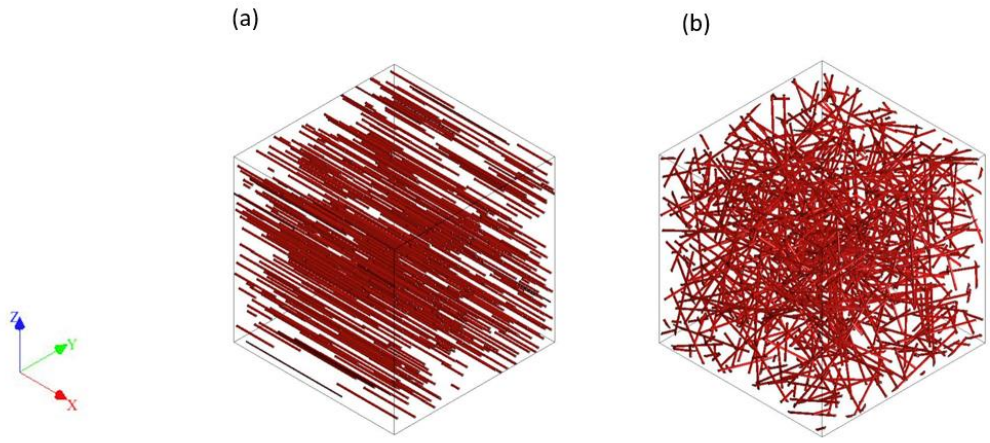

Figure 4.15 RVEs with varying fibre orientations: (a) Aligned along x-axis, and (b) random orientation

4.10 Effect of the interfacial transition zone on the homogenised elastic modulus

In concrete composites, the interfacial transition zone (ITZ) plays a pivotal role in affecting the mechanical properties. However, the ITZ in SCC becomes less flexible due to various factors, such as low w/cm ratios, smaller maximum aggregate sizes, lower CA content, and the use of SCMs. In the homogenisation technique of SCC, the ITZ between the CA and the mortar was neglected due to the increased ITZ strength when SCC is designed with a low w/cm. This low w/cm results in concrete with a high compressive strength and a low CA content, leading to a substantially lower volume fraction of the ITZ.

However, the reality is that factors such as w/cm ratios, curing age, cementitious binder type, aggregate content, and compaction during the concrete casting process can affect both the porosity and the ITZ thickness (Leemann et al. 2006; Gao et al. 2014). The impact of porosity and varying ITZ thickness on the homogenised elastic modulus of SCC can be assessed using the M-T homogenisation technique within the framework of the MFH. To explore the influence of the ITZ and its thickness on SCC's elastic properties, CA coated with ITZ was simulated within the matrix. The elastic properties of the ITZ, as detailed in Table 4.9, were sourced from Liang et al. (2022), with the ITZ density assumed to be equal to that of the mortar. Figure 4.16 illustrates the change in equivalent elastic modulus of SCC with varying ITZ thicknesses of 0, 0.002, 0.005 and 0.01 (relative to the aggregate particle size), showing a slight decrease in the homogenised elastic modulus with increasing ITZ thickness and CA content. Nonetheless, the impact of ITZ remained minor, regardless of thickness.

The influence of ITZ between the matrix and fibres on the homogenised elastic modulus was also examined. Numerical homogenisations were applied to RVEs where the inclusions, specifically steel fibres, were surrounded by an ITZ with a thickness of 50 μm within the concrete matrix (refer to Figure 4.17). The selection of a 50 μm thickness for the ITZ is justified as it falls within the generally accepted range of 40-70 microns for the thickness of steel fibre in concrete (Zhang et al. 2015). The average elastic modulus of SFR-SCC, including the effect of the ITZ, was found to be 40.19 GPa for Mix SF55-30-0.5 and 37.39 GPa for Mix SF55-20-1. These findings suggest that the ITZ between fibres and the concrete matrix has an insignificant, nearly negligible effect and could, therefore, be excluded from the homogenisation method. This conclusion is based on the low total volume fraction of ITZ and the analysis remaining within the elastic regime.

Table 4.9 Mechanical properties of ITZ

Phase	Elastic modulus (GPa)	Poisson's ratio μ	Density (kg/m^3)
ITZ	22.06	0.2	2250

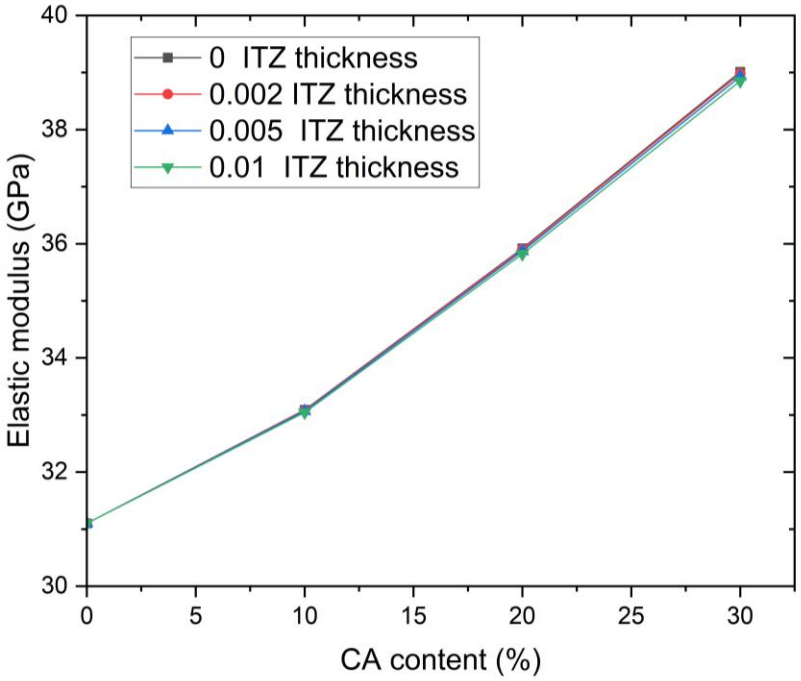

Figure 4.16 Effect of ITZ thickness on homogenised elastic modulus

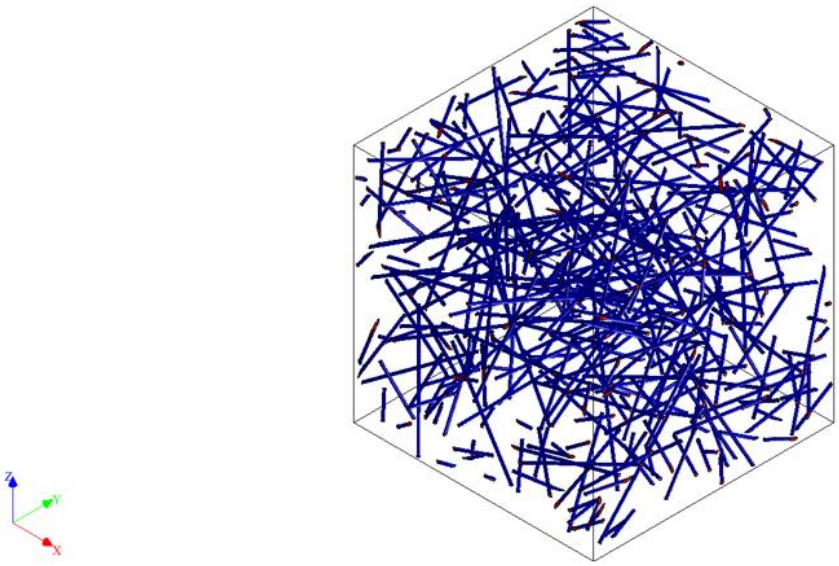

Figure 4.17 RVEs with steel fibres encased in ITZ of 50 µm thickness

The ITZ between the matrix and the inclusions in SCC and UHPFRC are dissimilar to that in ordinary concrete designed with a higher w/cm ratio (Leemann et al. 2006; Sorelli et al. 2008; Qsymah et al. 2017; Stefaniuk et al. 2019). Stefaniuk et al. (2019) investigated the ITZ in SCC using X-ray micro-CT and line indentation. Their results showed that the ITZ in SCC was as rigid as the bulk matrix and had no significant effect on the SCC composites. Thus, the

effect of the ITZ was neglected in the SCC homogenisation techniques in the present work. This strength in the ITZ in SCC can be related to factors such as low w/cm ratios, smaller maximum CA sizes, lower CA content, and the use of SCMs (Koehler and Fowler 2007). Furthermore, the incorporation of GGBS is known to improve mechanical and durability properties by substantially minimising the size and quantity of $Ca(OH)_2$ crystals at the aggregate-paste interface. This action results in a dense and strong microstructure in the transition zone between the aggregate and the cement paste (Pavía and Condren 2008; Limbachiya et al. 2016). Moreover, as discussed in Chapter 2, one of the advantages of SCC is the enhancement of the bond between the cementitious paste and CA or reinforcement (Zhu 2020).

4.11 Effect of CA shape on the homogenised elastic modulus

To investigate the influence of the geometric properties of CA on the homogenised elastic modulus of SCC, effective elastic moduli values of SCC were predicted for CAs with varying aspect ratios and contents; the results are depicted in Figure 4.18.

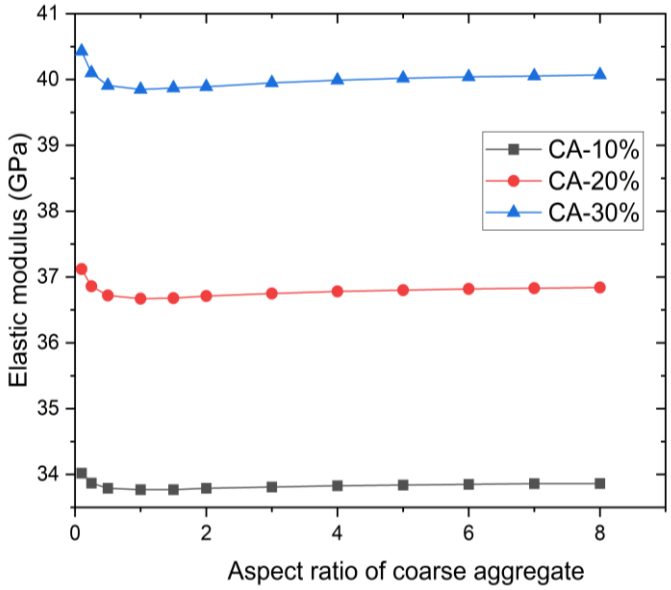

Figure 4.18 The effect of CA particle shape on the homogenised elastic modulus

As shown in Figure 4.18, the homogenised elastic modulus decreased sharply with an increase in the aspect ratio for oblate spheroids, while it increased slightly as the aspect ratio increased for prolate (elongated) spheroids, given a constant volume of CA. The lowest

effective elastic modulus value occurred when anisotropic spheroids transformed into spheres (i.e. when the aspect ratio equalled 1.0), indicating that the spherical shape of CA had the least impact on the effective elastic modulus of the cementitious composites. This observation aligns with the findings presented in (Chen et al. 2018).

4.12 Concluding remarks

In this chapter, the elastic modulus of SFR-SCC was determined empirically and using a theoretical two-step homogenisation method. Four different concrete mix compositions with the same w/cm ratio were prepared and tested. Although all mixes achieved approximately 70 MPa in compressive strength, the elastic moduli of the mixes were influenced by the mix compositions of SFR-SCC. The investigation into the porosity employed both medical and industrial micro-CT scans, allowing for a comprehensive analysis, comparison, and discussion of the results. In summary, while micro-CT offers greater precision, the accessibility and speed of medical CT scans make them preferable for studies needing rapid evaluation of large sample sizes. As du Plessis and Boshoff (2019) note, medical CT scanners can efficiently deliver acceptable results, particularly when moderate resolution suffices (du Plessis et al. 2016). Thus, depending on the research requirements and object size, the choice between these scanning technologies significantly impacts data acquisition efficiency and quality. The elastic modulus of SFR-SCC was also predicted using the two-step homogenisation method by coupling MFH and FE model-based computational homogenisation. The mortar, air voids, and CA were homogenised as SCC using MFH as the first step. Numerical homogenisation was performed for the homogenised SCC and steel fibres as the second step. A comparison of the estimated elastic modulus with empirically determined values showed that the results of the two-step method concurred with the empirical findings with a maximum error of 3.44% in the estimated elastic modulus. Furthermore, the effect of fibre orientation and porosity on the elastic modulus SFR-SCC was evaluated. The study explored the effects of CA particle shape and the ITZ on the homogenised elastic modulus of HSSCC. It showed that the content of CA significantly influenced the homogenised elastic modulus of HSSCC and that the geometric properties of CA had the least impact when the particles were spherical. This research showed that the two-step homogenisation method could quickly and effectively replace time-consuming laboratory testing, saving time and resources on raw materials. It could also be used for the

initial mix optimisation and the selection of constituents of SFR-SCC. The investigations and results presented in this chapter primarily focus on predictions for the elastic properties of SFR-SCC. For a comprehensive analysis of the hardened state of the concrete, it is essential to introduce a nonlinear constitutive damage model in mesoscale to predict the strength and fracture properties of SFR-SCC.

Chapter 5 Effect of Steel Fiber Properties and Coarse Aggregate Content on Performance of High-strength Self-compacting Concrete

5.1. Summary

The development of steel fibre-reinforced self-compacting concrete (SFR-SCC) has significant practical implications for the construction industry. However, this development is limited by the absence of established design guidelines and recommendations and the limited availability of design methodologies. Minimising production costs while simultaneously achieving the necessary rheological and mechanical properties requires a comprehensive understanding of the optimal blend of fibre and coarse aggregate (CA) content. This chapter addresses the impact of steel fibre properties on the rheological and mechanical properties of eco-friendly high-strength self-compacting concrete (HSSCC), with 40% ground granulated blast furnace slag (GGBS) as a cement replacement. This research focused on hooked-end steel fibres, 30 mm in length, with diameters of 0.55 mm and 0.38 mm and tensile strengths of 1345 MPa and 3070 MPa, respectively. The study investigated the combined effect of CA content and steel fibre characteristics on the performance of eco-friendly HSSCC. The fresh properties of the HSSCC mixes were assessed using slump flow and J-ring tests. Mechanical and fracture properties of the hardened specimens were evaluated, including axial strength (compression and tension), flexural strength, and elastic moduli. The distribution and alignment of steel fibres in the HSSCC specimens were assessed using image analysis techniques, leading to the conclusion that the steel fibre diameters had a significant effect on the fibre dispersion. The test results showed that steel fibres with higher tensile strengths and smaller diameters significantly enhanced the concrete's splitting tensile strength, flexural strength, and fracture energy, compared to steel fibres with larger diameters (lower aspect ratio) and lower tensile strengths. The study results also indicated that the CA content in eco-friendly fibre-reinforced HSSCC had a marked effect on the elastic modulus and fracture energy. This study highlighted the importance of CA proportion and steel fibre characteristics on the rheological and mechanical properties of HSSCC, emphasising that this must be considered during the mix design to optimise the desired properties while simultaneously minimising production costs.

The content of this chapter has been published in the journal *Construction and Building Materials* (Alshahrani and Kulasegaram 2023); details are provided in the List of Publications.

5.2 Introduction

The use of high-strength self-compacting concrete (HSSCC) is often restricted due to its brittle behaviour and resulting compromised structural integrity (Deeb et al. 2014). Steel fibres may be added to self-compacting concrete (SCC) to improve ductility, toughness, and flexural, shear, and tensile strengths. However, the large surface area and elongated shape of the steel fibres significantly impair the rheological properties of steel fibre-reinforced self-compacting concrete *(*SFR-SCC) (Deeb et al. 2012). Therefore, there is a limit to the volume fraction of fibres that can be added to an SCC mix, depending on the specific mix composition and the fibre characteristics. Research by Pająk and Ponikiewski (2013) highlighted that hooked-end fibres outperformed straight fibres in enhancing the flexural behaviour of SCC, attributed to the superior bonding conditions offered by the hooked-end fibres. Yardimci et al. (2014) studied the effect of hooked-end steel fibre volume fractions with varying fibre lengths (30 mm and 60 mm) on the rheological and mechanical properties of SFR-SCC using variable fine-to-coarse aggregate ratios. Their results indicated that a higher fine-to-coarse aggregate ratio should be used to improve the flowability and fracture energy of SFR-SCC when the fibre volume fraction and length are relatively high. The role of fibre tensile strength in improving flexural and splitting tensile strengths of high-strength concrete (HSC) was convincingly reported by Şahin and Köksal (2011), while Yoo et al. (2016) found that in ultra-high-performance fibre-reinforced concrete (UHPFRC), longer steel fibres enhanced the flexural performance despite having a lower fibre orientation factor than shorter fibres. Alrawashdeh and Eren (2022) investigated the effect of hooked-end steel fibres with aspect ratios of 60 and 80 and lengths of 30 mm and 50 mm, respectively, on the fresh, physical, and mechanical properties of SFR-SCC. The study noted the difficulties associated with mixing and placing the SFR-SCC with the longer fibres (50 mm). Ghasemi et al. (2019) explored the influence of variables, such as maximum coarse aggregate (CA) size, w/c ratio, and fibre content, on the fracture parameters and brittleness in SFR-SCC. Their research indicated that incorporating larger CA (up to 19 mm) in SFR-SCC formulations tended to decrease the fracture energy and attributed this to the reduced space available for fibre orientation. (Ghasemi et al. 2018) further suggested that the optimal maximum CA size to enhance the properties of SFR-SCC was 12.5 mm, a recommendation derived from fracture energy test results.

Numerous studies have been conducted on the mechanical characteristics of fibre-reinforced concrete (FRC) (Şahin and Köksal 2011; Kazemi et al. 2017). However, only a few studies of these studies have assessed the mechanical characteristics of SFR-SCC containing high mineral admixture content (Athiyamaan and Mohan Ganesh 2020). Minimal research has been conducted on the effects of fibre alignment on the mechanical characteristics of SFR-SCC. This requires further research to analyse fibre alignment in conjunction with the CA content (Huang et al. 2021), and the effect of fibre diameter and tensile strength on the structural performance of SFR-SCC. An extensive experimental study was conducted to investigate the effect of fibre diameter and tensile strength on the fresh and mechanical properties of eco-friendly HSSCC. The HSSCC in this research had a large ground granulated blast furnace slag (GGBS) content and considered two CA volume fractions together with fibre orientation and distribution in each mix composition. As SCC with steel fibres longer than 30 mm has been shown to exhibit a decrease in the rheological characteristics, hooked-end steel fibres with lengths of 30 mm, diameters of 0.55 mm and 0.38 mm, and tensile strengths of 1345 and 3070 MPa, respectively, were used in this study.

5.3 Experimental programme

5.3.1 Raw materials

The HSSCC mixes discussed in this chapter comprised the same base materials described in Chapter 4, consisting of Portland cement (Type 1) and ground granulated blast furnace slag (GGBS). The specific characteristics and compositions of these cementitious materials are detailed in Table 5.1. As with the earlier mix designs, a superplasticiser (polycarboxylate ether polymer, MasterGlenium ACE 499) was incorporated to increase the workability of the mixes.

The aggregate selection, namely crushed limestone coarse aggregate (CA) and natural river sand, had the same specifications outlined previously, including the gravel size and specific gravity values. The particle size distribution curves for fine aggregate (F-A) and CA are as detailed in Chapter 4. These grading curves have a significant impact on the fresh and hardened properties of the mixes.

The properties of the Dramix hooked-end steel fibres, designated as Dramix 55/30 and Dramix 80/30, used in this study are detailed in Table 5.2.

Table 5.1 Physical properties and chemical composition of cement and GGBS

Composition	Cement	GGBS
SiO_2 (%)	19.69	34.34
Fe_2O_3 (%)	2.85	0.32
Al_2O_3 (%)	4.32	12.25
MgO (%)	2.17	7.70
CaO (%)	63.04	39.90
SO_3 (%)	3.12	0.23
Fineness (m^2/kg)	384	426
Specific gravity	3.15	2.40
Initial Setting Time (mins)	158	-
Loss on ignition (%)	3.03	0.34

Table 5.2 Properties of steel fibres

Steel fibre code	Length, l_f (mm)	Diameter, d_f (mm)	Aspect ratio (l_f/d_f)	Density (kg/m^3)	Tensile strength (MPa)	Elastic modulus (GPa)
Dramix 3D 55/30 BG	30	0.55	55	7800	1345	200
Dramix 3D 80/30 BGP	30	0.38	80	7800	3070	200

5.3.2 Mix proportion

To assess the mechanical properties and ductility of SFR-SCC and the effect of steel fibre diameter and tensile strength, ten mixes were prepared with hooked-end steel fibres with varying diameters and tensile strengths (see Table 5.3). All the mixes were designed with a water-cement (w/cm) ratio of 0.4 and 40% replacement of cement by GGBS. Minor adjustments were made to the F-A content to account for the addition of the fibres while maintaining the w/cm ratio and CA content. The HSSCC mixes contained varying volume proportions of CA, sand-to-aggregate (S/A) ratio, and steel fibre volume fractions. CA contents of 20% and 30% were considered to assess the influence of CA on the properties of SFR-SCC and the fibre alignment. To assess the effects of steel fibres on the fresh and mechanical properties of eco-friendly HSSCC, steel fibre volume fractions of 0.25, 0.5, and 1% were considered. The naming convention adopted for the mixes was based on the CA

content, fibre diameters, and the proportion of steel fibres. The control mix was plain HSSCC (i.e., no fibres) and named solely according to its CA content. The mixes with hooked-end steel fibres were named according to their fibre diameters, 0.55 mm and 0.38 mm, namely SF55 and SF38, respectively, with the steel fibre diameters expressed in hundredths of a millimetre. Lastly, the mixes were named according to the CA and steel fibre percentages. For instance, the mix label SF38-20-0.5 indicated an HSSCC mix containing 0.38 mm diameter fibres, 20% CA and 0.5% steel fibres.

Table 5.3 Mix proportions of HSSCC (kg/m^3)

Mix ID	Water	Cementitious material		SP	Aggregates			Steel fibre	S/A by weight	CA	steel fibre
					F-A[1]		CA				
		Cement	GGBS		F-A*	F-A**				By volume %	
CA-20	205.6	308.4	205.6	2.6	698.3	299.3	530	-	0.65	20	-
CA-30	205.6	308.4	205.6	2.3	517.3	221.7	796	-	0.48	30	-
SF55-20-0.25	205.6	308.4	205.6	3.0	693.8	297.3	530	19.5	0.65	20	0.25
SF55-20-0.5	205.6	308.4	205.6	3.1	689.3	295.4	530	39.0	0.65	20	0.50
SF55-20-1	205.6	308.4	205.6	3.2	680.3	291.6	530	78.0	0.65	20	1.00
SF55-30-0.5	205.6	308.4	205.6	3.0	506.3	217.0	796	39.0	0.48	30	0.50
SF38-20-0.25	205.6	308.4	205.6	3.1	693.8	297.3	530	19.5	0.65	20	0.25
SF38-20-0.5	205.6	308.4	205.6	3.4	689.3	295.4	530	39.0	0.65	20	0.50
SF38-20-1	205.6	308.4	205.6	3.6	680.3	291.6	530	78.0	0.65	20	1.00
SF38-30-0.5	205.6	308.4	205.6	3.1	506.3	217.0	796	39.0	0.48	30	0.50

Note 1: F-A* refers to natural river sand; F-A** refers to the coarser fraction of limestone dust.

5.3.3 Specimen preparation

The mixing process was critical to achieving a good dispersion of the steel fibres. The ten mixes (detailed in Table 5.3) were prepared in a forced action pan mixer by first blending the coarsest (CA) and the finest (cement) materials, and then adding each material based on their fineness, alternating between coarse and fine materials. The materials were mixed for approximately two minutes before each addition. Two-thirds of the superplasticiser (SP) was mixed with water to fluidise the dry mix; the water-SP mixture was slowly added to the dry components and mixed for approximately four minutes. The last third of the SP was added

to the mix and blended for two minutes. Thereafter, the steel fibres were slowly added and mixed for a further 4 minutes.

It is stated in BS EN 14651 (2007) and Rilem TC 162-TDF (2002) that concrete pouring should start in the centre of the mould. However, some studies suggest that pouring concrete from one end of the mould is preferred in the case of SFR-SCC (Grunewald 2004; Ghasemi et al. 2019). Furthermore, Alberti et al. (2016) stated that pouring from the centre of the mould could reduce the fibre dispersion in self-compacting concrete. Therefore, in this study, the mixes were poured from one end. Eight prismatic beams (100 mm × 100 mm × 500 mm length), eight cubes (100 mm × 100 mm × 100 mm), and six cylinders (100 mm diameter × 200 mm length) were cast from each design mix. The specimens were kept under laboratory conditions for one day, de-moulded, and immersed in a water tank at 20(±1) °C for a further 28 days.

5.3.4 Test setup and procedure

In the fresh state, the ten mixes were tested for slump flow (flowability) and passing ability according to the recommendations in BS EN 12350-8 (2010) and BS EN 12350-12 (2010), respectively, to ensure that all mixes satisfied the minimum self-compaction criteria for SCC. The cube compressive strength of each mix was determined in accordance with BS EN 12390-3 (2009), while the elastic modulus (E) and the splitting tensile strength (f_{st}) were tested using the cylinder specimens as per BS EN 12390-13 (2019) and BS EN 12390-6 BS EN 12390-6 (2000), respectively.

The experimental setup for the elastic modulus test was identical to that described in Chapter 4. The flexural strength of the specimens was evaluated using the four-point bending test on the prismatic beams in accordance with BS EN 12390-5 (2009); the experimental setup for the test is shown in Figure 5.1. To ensure the consistency and reliability of the results, all samples underwent close monitoring. Any sample deviating significantly from the expected parameters was excluded from the analysis, while ensuring a minimum of three valid samples for each test.

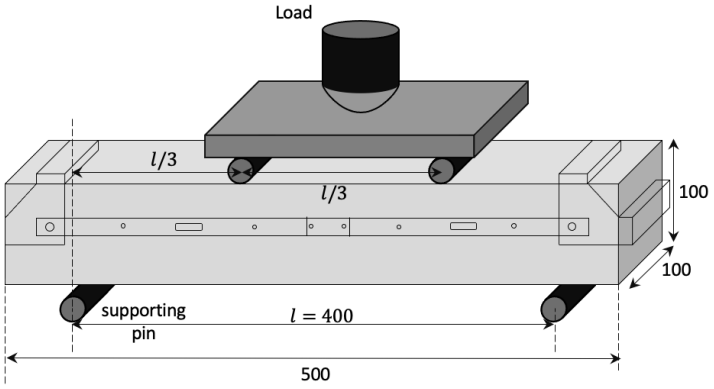

Figure 5.1 Experimental setup of the four-point bending test

The HSSCC fracture properties were measured using the three-point bending test on the notched beams, following the procedure outlined by RILEM in RILEM FMC-50 (1985), depicted in Figure 5.2. The mould width was designed to meet the recommendations outlined in ASTM C1609 (2007), which suggest that the width (b) should be at least three times the length of the fibres being used. However, the guidelines provided in JCI-S-002-2003 (2003) specify that the side length of the beam cross-section should be at least 100 mm when the fibre length used in the mix is 40 mm or less. As per the JCI standard, the notch depth (a_0) should be 0.3 times the beam depth with the notch width (n_0) not exceeding 5 mm. Therefore, the mould dimensions for this study were selected as 100 mm long, with a notch depth of 30 mm and a notch width of 5 mm, as indicated in Figure 5.2. For this test setup, the mid-span deflection (δ) and crack mouth opening displacement (CMOD) of the test specimens were measured using a Linear Variable Differential Transformer (LVDT) and a clip gauge attached to the knife edges on the specimens. These devices recorded the load-deflection and load-CMOD curves for all the test specimens.

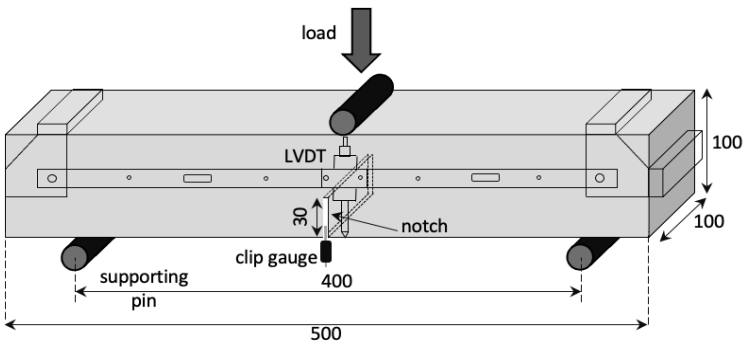

Figure 5.2 Experimental setup of the three-point bending test

5.3.5 Determination of fracture parameter

Fracture energy is a crucial factor in understanding concrete characteristics and establishing the design criteria for large concrete structures (Şahin and Köksal 2011; Pająk and Ponikiewski 2013). The HSSCC fracture parameters were determined through the three-point bending test as described in the previous section, according to the RILEM FMC-50 (1985) recommendations. The fracture energy of the specimens, G_F, was determined using the equation provided by RILEM:

$$G_F = \frac{W_0 + mg\delta}{b(h - a_0)} \tag{5.1}$$

where W_0 is the area under the load-deflection curve, m is the specimen mass (kg), g is gravitational acceleration (9.81 m/s²), δ is the deflection at final fracture, b is the beam width (m), h is the beam depth (m), and a_0 is the notch depth (m).

In this study, W_0 for the fibre-reinforced concrete mixes was measured to the limit of ℓ/150, equating to a deflection of 2.667 mm, according to ASTM C1609 (2007). For the plain concrete mixes, W_0 was measured over the full extent of the curve. The area under the curve was measured using Origin 2023b software; the load-deflection curves for all specimens are provided in Appendix B. The energy provided by the self-weight of the beam was represented by ($mg\delta$) in Equation (5.1). By utilising this method, the fracture energy G_F for each specimen can be accurately determined, allowing for a comprehensive understanding of the material's fracture properties. Hillerborg et al. (1976) believed that the fracture energy of concrete alone did not provide sufficient understanding of the concrete's brittleness or ductility and, therefore, proposed a characteristic length parameter (L_{ch}) as follows:

$$L_{ch} = \frac{E \cdot G_F}{f_t^2} \tag{5.2}$$

where E and f_t are the elastic modulus and the tensile strength, respectively (the splitting tensile strength, f_{st}, was used instead of f_t in this study).

The characteristic length, which is proportional to the fracture energy, G_F, and inversely proportional to the tensile strength, f_{st}, was used to assess the ductility of the concrete

specimens. To produce concrete that possesses both strength and ductility, it is essential to have an appropriate balance between high fracture energy and high strength of concrete. High fracture energy contributes to the toughness of the concrete, while high strength can lead to brittleness. Ensuring that the concrete possesses both strength and ductility is thus crucial for its overall performance.

5.3.6 Evaluation of fibre distribution

Following the three-point bending test, the alignment and distribution of fibres within the beam cross-sections were evaluated using a combination of visual inspection and image analysis. The locations of the cross-sectional cuts in the specimens are depicted in Figure 5.3. Once the cross-sections were cut, the surfaces were polished and cleaned to improve the clarity of the steel fibre sections in the cross-sections. A high-resolution camera that could capture colour (RGB) images was used to obtain clear and detailed images of the surfaces. During the image capture process, site lights were employed to enhance the visibility of the metal fibres within the cement matrix. The metal fibres had a high reflectivity level, allowing them to be easily distinguished from the cement matrix using this technique. The images were processed using Fiji ImageJ software to identify and distinguish the steel fibres within the RGB image, based on a methodology employed by other researchers in the field (Yardimci et al. 2014; Huang et al. 2018; Zhao et al. 2021b; Zhao et al. 2021a). Figure 5.4 (a)-(f) depicts the sequential analysis process of the cross-sectional images; Figure 5.4 illustrates a small portion of the cross-section image.

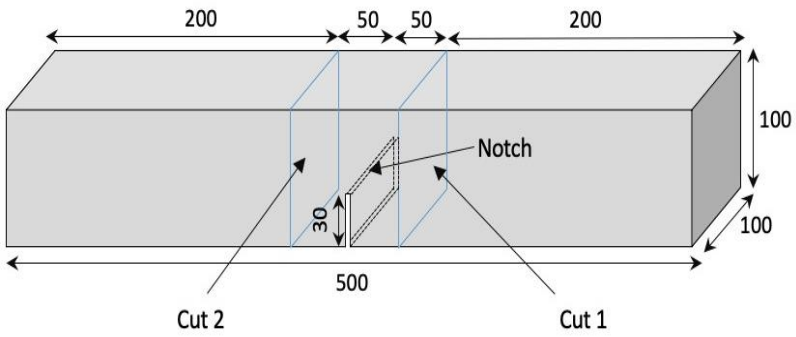

Figure 5.3 Cutting locations on the beam used in the three-point bending test

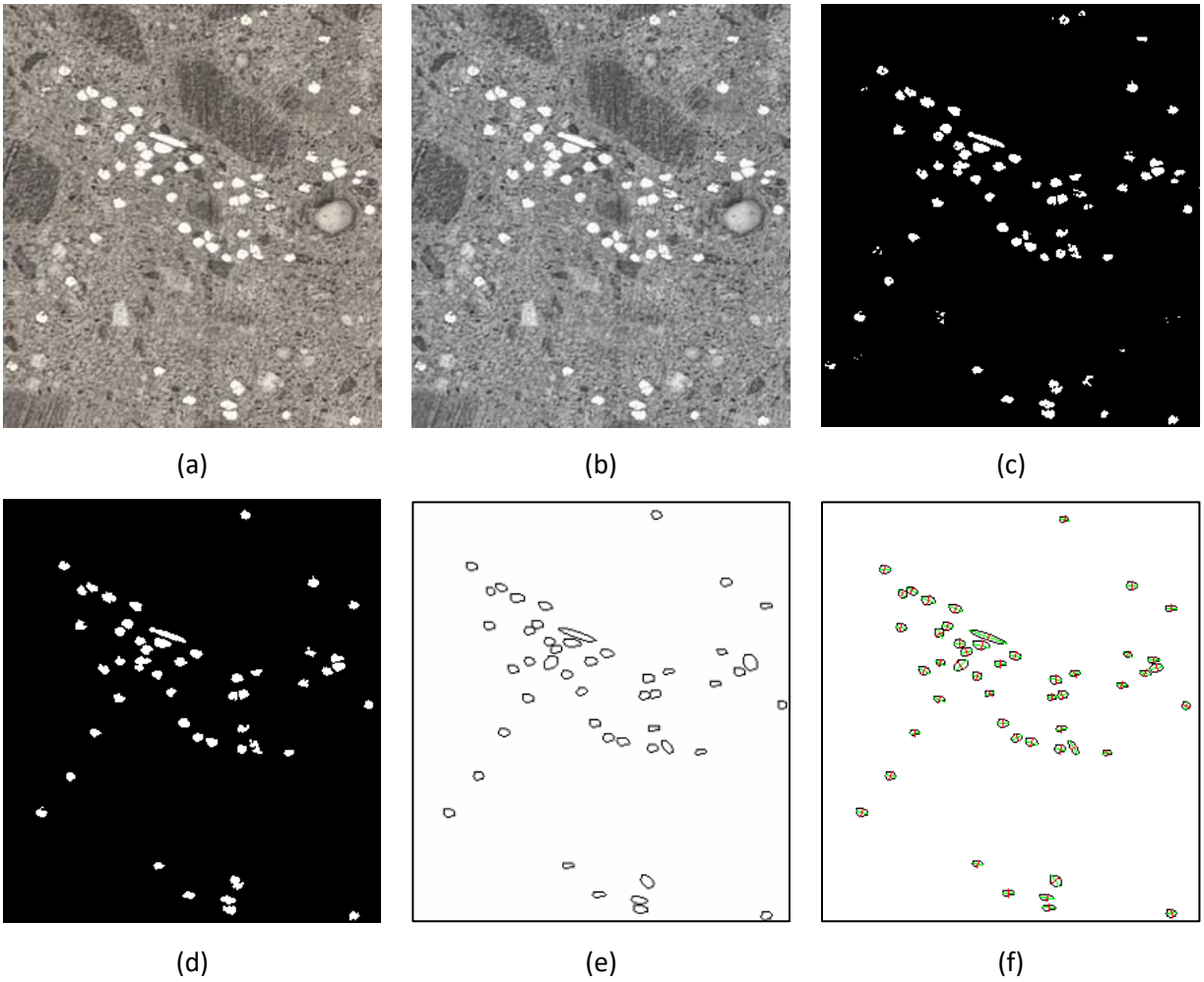

Figure 5.4 Image analysis procedure: (a) RGB image, (b) grayscale image, (c) binary image using a threshold, (d) fibre identification, (e) detection of fibre borders using morphological operations, (f) calculation of ϑ_i based on major axes of ellipses

From the image analyses, the total number of fibres intersecting the plane (N^T_f), the fibre density (d_n), the inclined angle (θ) of each fibre, and the fibre orientation factor (η_θ) could be determined.

The fibre density (d_n), defined as the number of fibres per unit area, can be calculated as follows:

$$d_n = \frac{N_T^f}{A_c} \tag{5.3}$$

where N_T^f represents the total number of fibres in the cross-section and A_c represents the area of that cross-section.

When the fibres are randomly and evenly distributed throughout a three-dimensional space, the theoretical value of the density of fibres within the space, denoted as d_{n3D}, can be calculated as given in Equation (5.4) (Zhao et al. 2021a):

$$d_{n3D} = 0.5\,\frac{v_f}{A_f} \tag{5.4}$$

where v_f and A_f stand for the fibre volume fraction in concrete and the cross-sectional area of a single fibre, respectively.

The inclined angle of a single fibre (θ) to a cross-section plane can be determined as:

$$\theta = cos^{-1}\frac{d_f}{l} \tag{5.5}$$

where l and d_f are the length of the major axis of an elliptical fibre cross-section and the fibre diameter, respectively.

The fibre orientation factor (η_θ) can be computed based on the total number of fibres at the cross-section (N_T^f) and the inclined angle as follows (Abrishambaf et al. 2013):

$$\eta_\theta = \frac{1}{N_T^f}\sum_{i=1}^{N_T^f} cos\theta_i \tag{5.6}$$

5.4 Results and discussion

5.4.1 Fresh tests

The slump flow test, which assesses the flowability of HSSCC in the absence of obstacles or hindrances, was used to evaluate the rheological properties of the HSSCC mixes. The slump flow test measured the t_{500} (the time required for the concrete to spread by 500 mm) and the slump flow diameter of the fresh HSSCC mixes; the test results for the HSSCC mixes are presented in Table 5.4. The average flow spread range was measured as 700 ± 50 mm, with all mixes satisfying the flowability criterion without signs of segregation or bleeding. It is generally accepted that the incorporation of fibres into HSSCC mixes can reduce the flowability and increase the plastic viscosity of such mixes. In addition, it is often observed

that the viscosity of the mix increases correspondingly with an increase in the fibre aspect ratio (Deeb et al. 2012). As mentioned previously, the addition of steel fibres to the study mixes required increased SP volume fractions to achieve the desired flowability; this effect was more pronounced for the fibres with smaller diameters (higher aspect ratio). Figure 5.5 shows the HSSCC slump flow and J-ring test results.

Table 5.4 Results of slump flow and J-ring flow test of HSSCC mixes

Mix designation	Slump flow test		J-ring flow test			$D_{slump} - D_{J-ring}$
	Spread (mm)	T_{500} (s)	Spread (mm)	Blocking step (mm)	T_{500j} (s)	
CA-20	690	1.8	670	2	2.3	20
CA-30	740	1.7	720	3	2.0	20
SF55-20-0.25	700	2.1	670	3	2.7	30
SF55-20-0.5	750	2.5	700	3	3.1	50
SF55-20-1	680	2.9	620	11	3.8	60
SF55-30-0.5	740	1.7	690	9	2.0	50
SF38-20-0.25	670	2.8	670	6	3.0	0
SF38-20-0.5	710	2.3	660	9	3.3	50
SF38-20-1	700	3.1	610	26	4.2	90
SF38-30-0.5	730	2.0	690	10	2.9	40

The J-ring test evaluates the ability of the HSSCC mixes to pass through a configuration of reinforced bars, simulating the flow behaviour of HSSCC in practical reinforced concrete structural scenarios. The test setup in this study consisted of a 300 mm diameter J-ring equipped with 16 steel rods, each with a diameter of 16 mm. The J-ring was placed at the centre of the horizontal bottom plate, with the same circular core as the slump cone used in the slump flow test. The passing ability of a mix can be evaluated by the blocking step in the J-ring test, i.e., a measure of the height difference between the centre and the edge of the concrete sample being tested, and the variation between flow diameter in the slump flow and the J-ring tests. A higher blocking step suggests that the mix is more resistant to flow and has a lower passing ability, while a lower blocking step indicates that the mix is more fluid and has a better passing ability. Therefore, a mix with a higher blocking step will experience greater difficulty in passing through a small opening, while a mix with a lower blocking step can flow more easily through a confined space. The J-ring test can be

combined with the slump flow test to determine passing ability based on (ASTM C1621 (2014). If the difference in final spread diameter between the slump flow and J-ring flow tests is less than 25 mm, there is no visible blocking, while a difference between 25 mm and 50 mm indicates partial blockage.

As indicated in Table 5.4, the incorporation of steel fibres into HSSCC mixes was overall found to negatively affect the mix passing ability, particularly for the mixes with smaller diameter fibres. For example, the passing ability of Mix SF38-20-1 was significantly lower than that of Mix SF55-20-1. This decrease in passing ability can likely be ascribed to the higher surface area and aspect ratio of these steel fibres (SF38) at a constant fibre volume content and length compared to the thicker fibres (SF55). It can, therefore, be deduced that the surface area and shape of the fibres may be more effective at obstructing the flow of the HSSCC mix, leading to a decrease in its passing ability. Research has indicated that the use of steel fibres with an increased length and aspect ratio can significantly reduce the flowability and passing ability of mixes as compared to fibres with a lower length and aspect ratio (Deeb et al. 2012; Yardimci et al. 2014; Alrawashdeh and Eren 2022). Furthermore, it is widely understood that increasing the steel fibre volume fractions in SCC can increase the risk of the SCC not meeting the required passing ability criteria. Yardimci et al. (2014) suggested that increasing the ratio of fine to coarse aggregate, thereby decreasing the CA content, could improve the passing ability of SCC with high steel fibre volume fractions. However, the mechanical and fracture properties of SCC can be influenced by such variations in the CA volume fraction. Therefore, when adjusting the CA content to enhance the passing ability of SCC, it is important to note the potential effect on the mechanical and ductility properties of HSSCC.

(a)

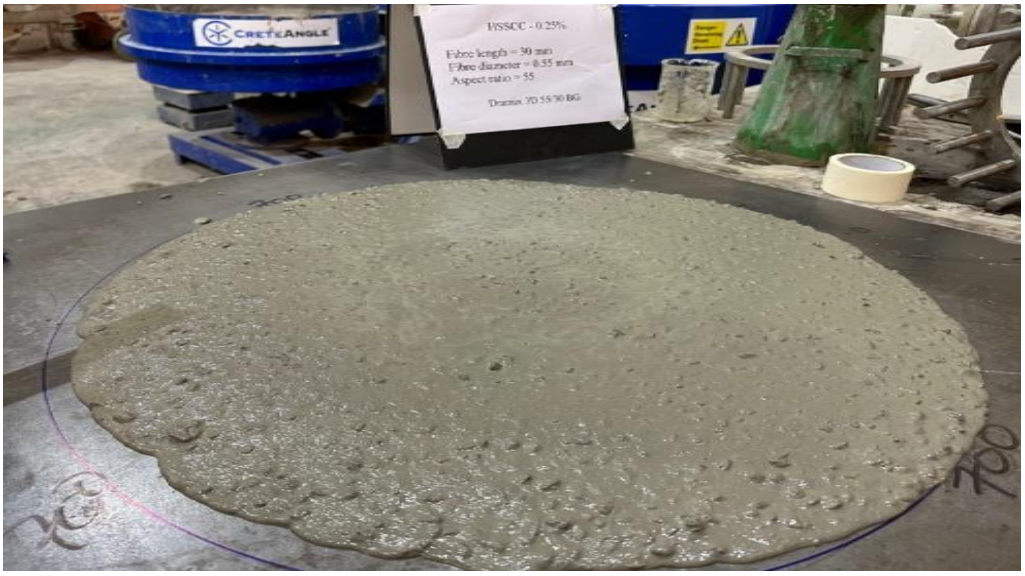

(b)

Figure 5.5 Fresh test: (a) Slump flow test, (b) J-ring test

5.4.2 Mechanical performance

5.4.2.1 Compressive strength

It is well established that the compressive strength of HSSCC is influenced by the w/cm ratio and the powder composition, as discussed in earlier chapters. It has been widely recognised that the addition of steel fibres to HSSCC has an overall limited effect on the compressive strength of the composite material but can significantly enhance its tensile, flexural, and splitting strengths and HSSCC post-peak behaviour. The test results in Table 5.5 show that the addition of steel fibres in the HSSCC led to a slight decrease in compressive strength in all the specimens (±1-8% reduction). The results also indicate that the variation in the CA

volume fractions, and steel fibre had an insignificant effect on the compressive strength of HSSCC.

There are conflicting reports regarding the effect of steel fibres on the compressive strength of SCC. Some studies (Khaloo et al. 2014; Yardimci et al. 2014) have shown that an increase in the percentage of hooked-end steel fibres leads to a decrease in compressive strength, while others (Pająk and Ponikiewski 2013; Sivanantham et al. 2022) have found that the inclusion of hooked-end steel fibres increases compressive strength. Alrawashdeh and Eren (2022) reported that the addition of fibres in an SCC mix resulted in the entrapment of additional air voids around the fibres, which had an inverse effect on the compressive strength. It can thus be seen that the effect of steel fibres on the compressive strength of HSSCC is complex and multi-faceted. It has been shown that the manner in which steel fibres affect the rheological properties of SCC can significantly affect the compressive strength of such mixes. These findings suggest that the inclusion of steel fibres in SCC may alter the mix properties and workability of the concrete, in turn affecting its compressive strength.

Table 5.5 Results of unit weight and compressive strength of all mixes

Mix designation	Unit weight (kg/m^3)	Compressive strength (MPa)	
		7 days	28 days
CA-20	2322	48.4	69.5
CA-30	2398	48.2	70.4
SF55-20-0.25	2317	47.6	65.6
SF55-20-0.5	2333	46.7	66.4
SF55-20-1	2361	49.7	66.1
SF55-30-0.5	2403	47.7	69.3
SF38-20-0.25	2342	46.0	64.4
SF38-20-0.5	2344	46.1	68.2
SF38-20-1	2346	52.4	67.6
SF38-30-0.5	2418	51.6	66.7

5.4.2.2 Elastic modulus

The elastic modulus test results are shown in Figure 5.6. The findings showed that the elastic modulus of HSSCC significantly increased with the addition of CA. Mix CA-30 (30% CA by

volume) exhibited an elastic modulus of 41.06 GPa, while Mix CA-20 (20% CA by volume) produced an elastic modulus of 37.02 GPa, despite both mixes achieving approximately 70 MPa compressive strength. Furthermore, incorporating a 1% volume fraction of steel fibres enhanced the elastic modulus of HSSCC by 4.13% and 3.81% for fibres with diameters of 0.55 and 0.38 mm, respectively. In contrast, the addition of 0.25% steel fibres had a negligible impact on the elastic modulus of HSSCC, regardless of fibre diameter. These results suggest that using steel fibres in HSSCC at a 1% volume fraction can improve the material's elastic modulus, while lower levels of fibre incorporation may have an insignificant effect. As discussed in Chapter 4, the elastic modulus of concrete is influenced by the proportions of its individual constituents and their respective elastic moduli. As such, increasing the CA and steel fibre volume fractions in concrete can improve the concrete's elastic modulus, while an increase in the mortar content and porosity can decrease the elastic modulus. This correlation emphasises the importance of meticulously selecting and proportioning the various components of HSSCC to achieve the desired elastic modulus.

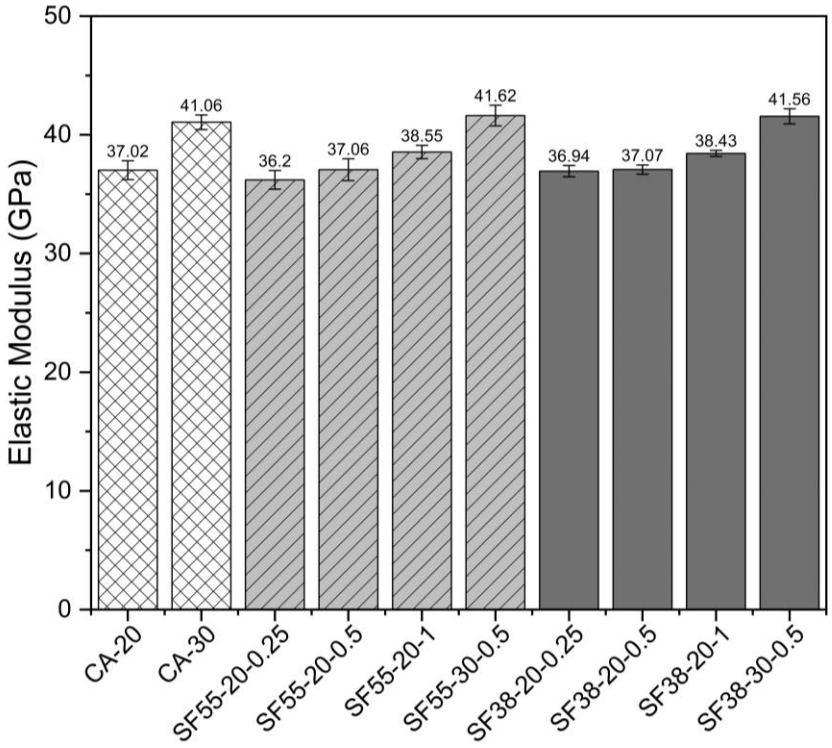

Figure 5.6 Result of elastic modulus of HSSCC

5.4.2.3 Splitting tensile strength

It was observed that the splitting tensile strength of HSSCC was significantly enhanced with increased CA volume fractions and the incorporation of the steel fibres. As shown in Figure 5.7, the addition of a 1% volume fraction of 0.55 mm diameter steel fibres (lower tensile strength) to the HSSCC resulted in a 21.32% increase in splitting tensile strength, while the inclusion of 0.38 mm diameter fibres (higher tensile strength) led to a 57.97% increase in splitting tensile strength. For plain HSSCC, the difference in splitting tensile strength between mixes with varying CA content (CA-20 and CA-30) was approximately 2.79%. However, when the steel fibre volume fraction was maintained at 0.5%, while the CA content was increased from 20% to 30%, the tensile splitting strength increased by 9.17% and 8.3% for steel fibres with diameters of 0.55 mm and 0.38 mm, respectively. This suggests that optimising the content of aggregate and fibres could improve the tensile performance of HSSCC.

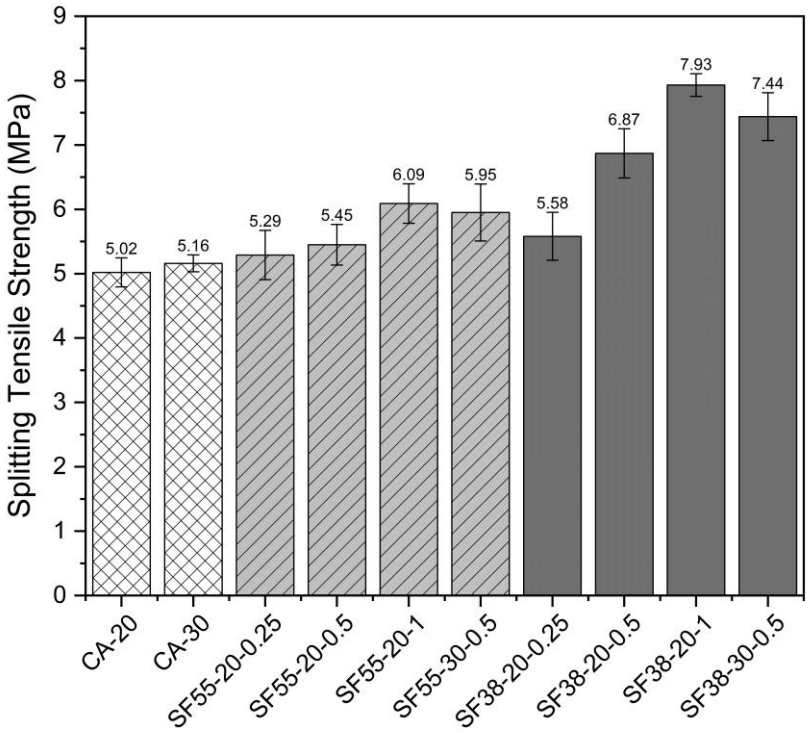

Figure 5.7 Results of splitting tensile strength of HSSCC

5.4.2.4 Flexural strength

The four-point bending test results for the HSSCC mixes are presented in Figure 5.8, showing that the flexural strength increased with increased CA volume fraction and incorporation of steel fibres. Notably, the addition of lower diameter, high tensile strength steel fibres

significantly improved the HSSCC flexural strength. At a volume fraction of 20% coarse aggregate and the incorporation of 0.25%, 5%, and 1% of 0.55 mm diameter steel fibres, the flexural strength increased by 9.79%, 11.92%, and 53.03%, respectively. Similarly, at the same volume fraction of coarse aggregate (i.e., 20%) but incorporating 0.38 mm diameter steel fibres, the improvement was 12.10%, 43.77%, and 86.3%. When the CA volume fraction was increased from 20% to 30% with a constant steel fibre volume fraction of 0.5%, the flexural strength increased by 2.07% and 7.43% for steel fibres with diameters of 0.55 mm and 0.38 mm, respectively. These results suggest that the performance of HSSCC can be improved by optimising the content of both aggregate and fibre types. As shown in Figure 5.8, Mix SF38-30-0.5 (0.5% volume fraction of 0.38 mm diameter steel fibres and 30% coarse aggregate) demonstrated better mechanical properties, including compressive strength, elastic modulus, splitting, and flexural strength, as compared to Mix SF55-30-1 (1% volume fraction of 0.55 mm diameter steel fibres and 30% coarse aggregate). This indicates that steel fibres with a lower diameter and higher tensile strength, combined with 30% coarse aggregate, can enhance the mechanical performance of HSSCC mixes and be used more efficiently and cost-effectively, reducing the cost of fibre-reinforced structures and rendering them more attractive for practical applications.

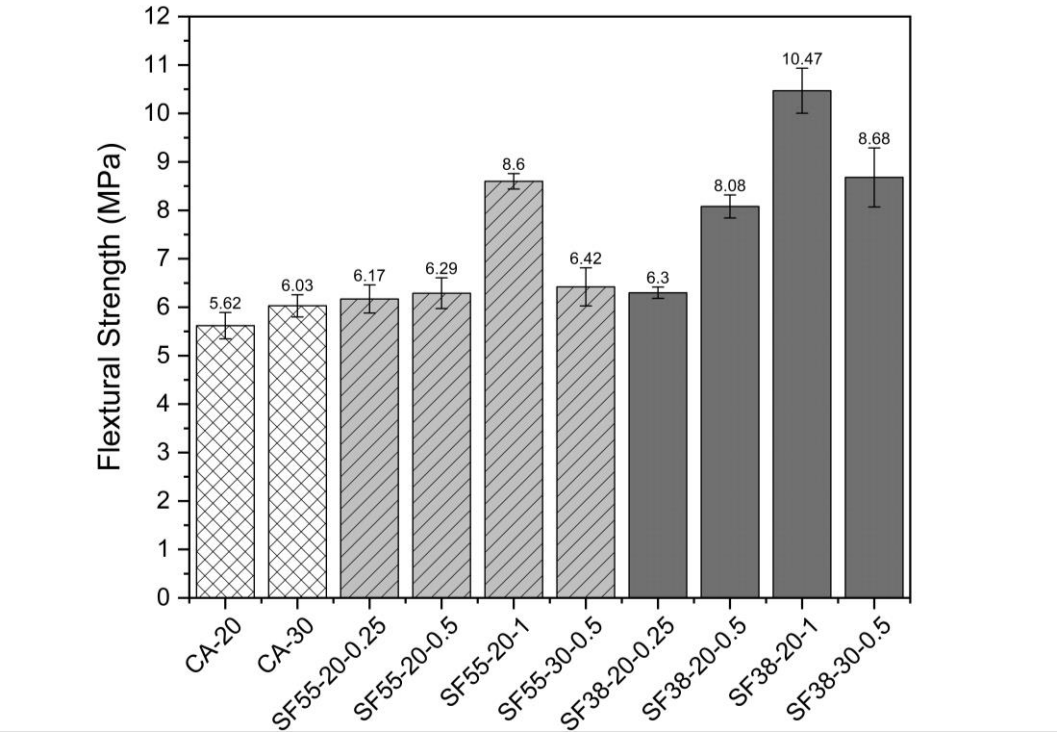

Figure 5.8 Results of flexural strength obtained from four-point bending test

5.4.2.5 Fracture parameter

The results of the fracture energy tests and characteristic length calculations of HSSCC, determined from Equations (5.1) and (5.2) respectively, are presented in Figure 5.9 and Figure 5.10. The results showed that increasing the CA content from 20% to 30% led to a 10.13% increase in fracture energy and a 14.37% increase in characteristic lengths for plain HSSCC. The load-deflection and load-CMOD curves of the plain HSSCC were determined from the averaged results of the three-point bending tests of the notched beams of each mix; these curves are shown in Figure 5.11. The individual curves for load-deflection and load-CMOD for each specimen are included in Appendices B and C, respectively. The results obtained in this study regarding the influence of CA content on the HSSCC fracture parameters are consistent with those reported by previous studies (Yardimci et al. 2014; Alyhya et al. 2016).

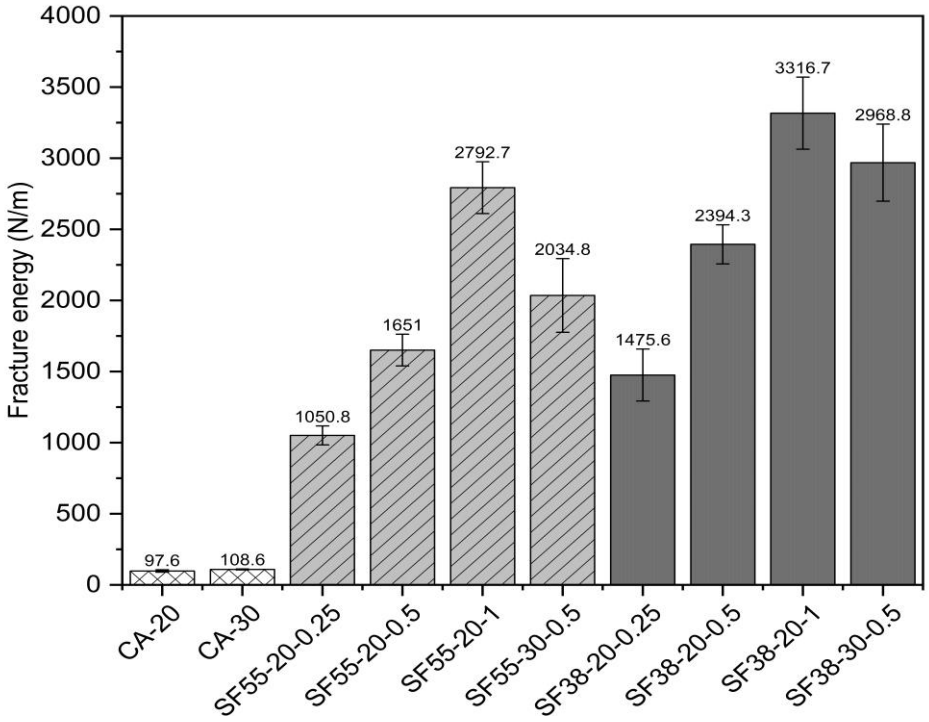

Figure 5.9 Measured fracture energy from the HSSCC three-point bending tests

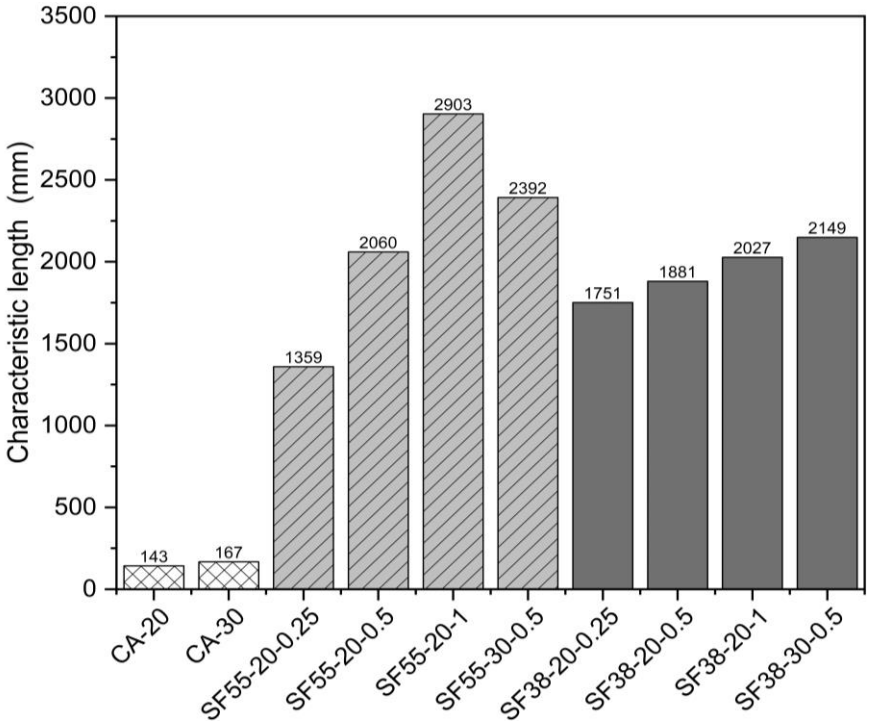

Figure 5.10 Characteristic lengths of HSSCC

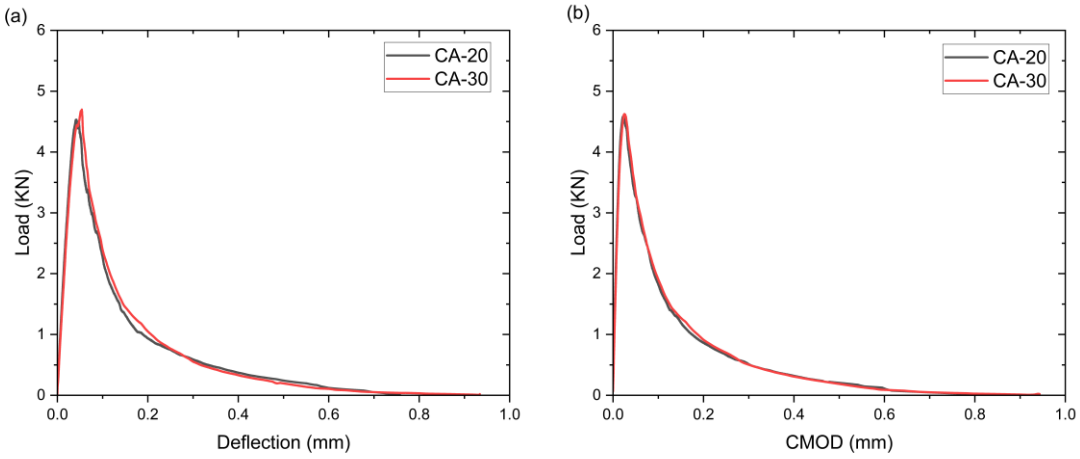

Figure 5.11 The average load-deflection and Load-CMOD curves of the plain HSSCC varying by CA content

The addition of steel fibres to the concrete mixes was found to significantly increase the fracture energy, influenced by the tensile strength and diameter of the fibres as well as the fibre volume content. The addition of 0.25%, 0.5%, and 1% volume fractions of steel fibres with high tensile strength and small diameters (0.38 mm) to a concrete mix containing 20% of CA resulted in significant increases of 15.12, 24.53, and 33.98 times the fracture energy of plain concrete with 20% CA, respectively. In contrast, the inclusion of fibres with lower

tensile strength and large diameter (0.55 mm) for the same mix composition resulted in smaller increases in fracture energy at 10.76, 16.92, and 28.61 times, respectively. The load-deflection and load-CMOD curves obtained from the three-point bending tests on the notched beams are plotted in Figure 5.12 and Figure 5.13 as a function of the steel fibre volume fraction. As can be observed, the load-deflection and load-CMOD curves of HSSCC depend on the volume fraction and properties of the fibres. The steel fibres with high tensile strength and small diameter had a greater effect on the post-peak behaviour of HSSCC than those with lower tensile strength and larger diameter.

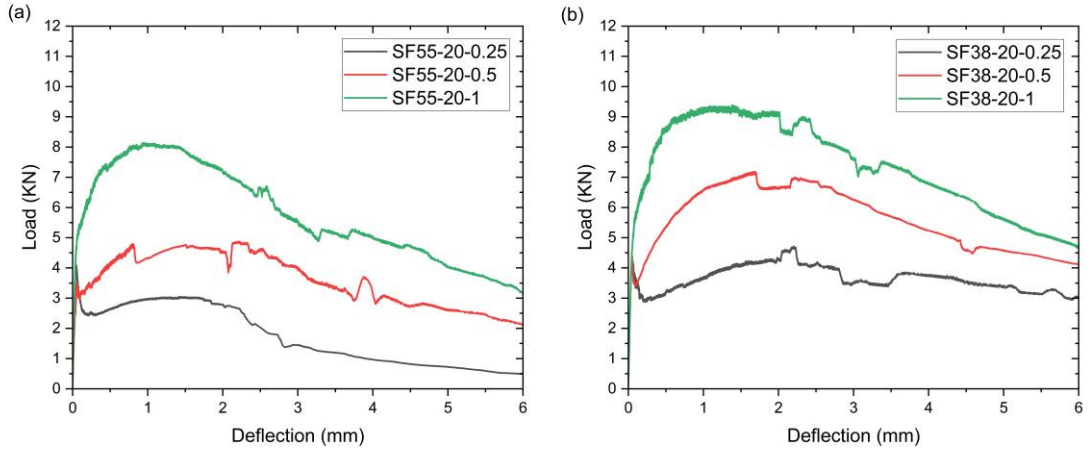

Figure 5.12 Load-deflection curves of reinforced HSSCC: (a) Dramix 55/30, (b) Dramix 80/30

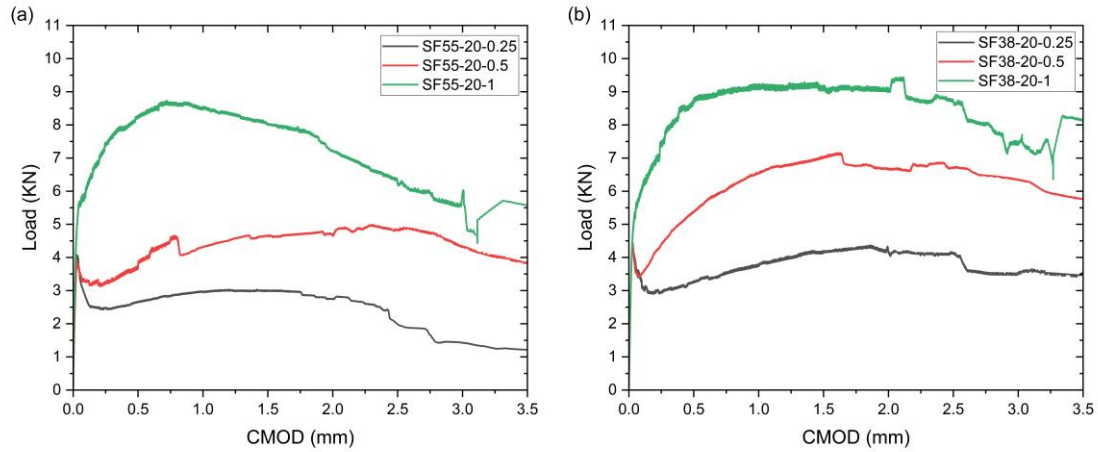

Figure 5.13 Load-CMOD curves of reinforced HSSCC: (a) Dramix 55/30, (b) Dramix 80/30

To clarify the combined effects of the CA content and the steel fibre characteristics on the fracture energy of HSSCC, the CA volume fraction was increased from 20% to 30% while maintaining a constant steel fibre volume fraction (0.5%). The fracture energy subsequently increased by 23.25% and 23.99% for steel fibres with diameters of 0.55 mm and 0.38 mm, respectively. The load-deflection and load-CMOD curves for these combined effects are shown in Figure 5.14 and Figure 5.15. It can be seen that the steel fibres with high tensile strength and smaller diameters had a significant impact on the HSSCC post-peak behaviour, regardless of the CA content. In addition, increasing the CA content while maintaining a constant steel fibre volume fraction and type significantly enhanced the HSSCC fracture properties. This observation differs from the findings of Yardimci et al. (2014), who found that using a higher fine-to-coarse aggregate ratio (i.e., reducing the CA content) could improve the fracture energy of SFR-SCC when the fibre content and aspect ratio were relatively high. This discrepancy in the findings may be attributed to the steel fibre lengths (60 mm) and the maximum CA size (15 mm) used in Yardimci's study. Ghasemi et al. (2019) studied the effect of the maximum size of the CA on different steel fibre volume fractions in SFR-SCC and found that an aggregate with a maximum size of 12.5 mm was most suitable for SFR-SCC, while using an aggregate with a maximum size of 19 mm in SFR-SCC reduced the fracture energy due to reduced space for fibre rotation. Xu et al. (2019) investigated the effect of the CA content (0%, 16%, 28%, and 38%) combined with steel fibres on the mechanical properties of high-performance concrete and found that the optimal level of coarse aggregate in HPC was approximately 28%.

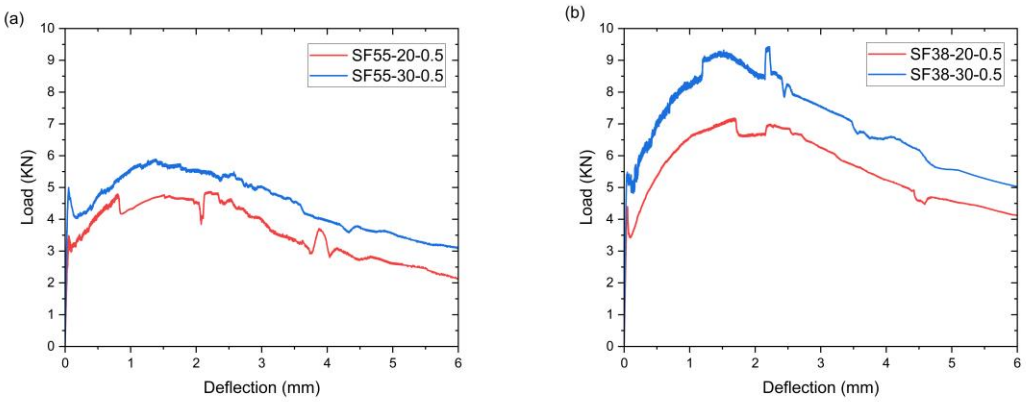

Figure 5.14 Load-deflection curves of reinforced HSSCC: (a) Dramix 55/30, (b) Dramix 80/30

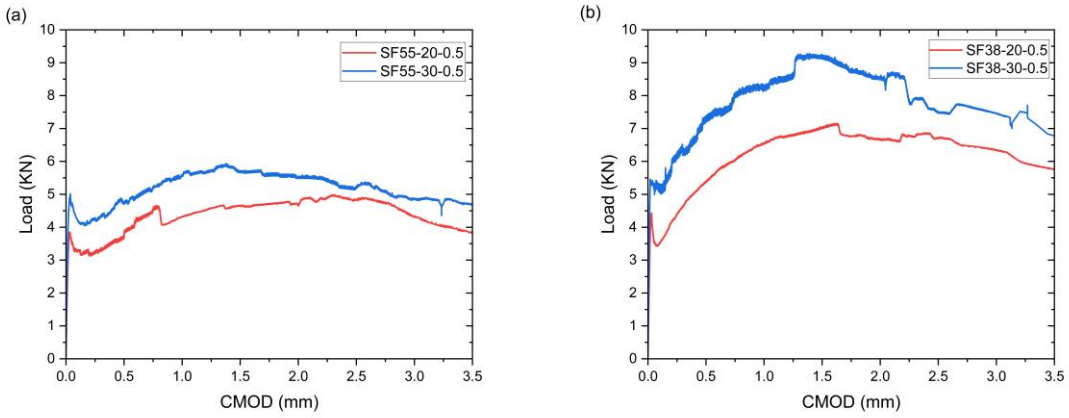

Figure 5.15 Load-CMOD curves of reinforced HSSCC: (a) Dramix 55/30, (b) Dramix 80/30

The design of mix compositions for SFR-SCC is a challenging area of research and development in the construction industry. It requires a thorough understanding of the optimal combinations of steel fibre type and content as well as CA content to achieve the desired rheological and mechanical concrete properties while maintaining economical production costs. The experimental investigation described in this chapter has shown that a mix composition with 0.5% steel fibres of 0.38 mm diameter and 30% of CA (SF38-30-0.5) has superior fracture energy than a mix with 1% steel fibres of 0.55 mm diameter and 20% aggregate (SF55-20-1). This indicates that steel fibres with a lower diameter and higher tensile strength, in combination with a higher aggregate content (30%), are more effective at increasing fracture energy and can be used more efficiently and cost-effectively. The CA content and the fibre properties are two important factors contributing to the performance of SFR-SCC and should be considered carefully in the mix design process.

5.5 Fibre distribution and orientation

The use of steel fibres in concrete can significantly improve its post-peak load-bearing capacity, with the extent of improvement depending on the type, volume fraction, and orientation of the included fibres. There is a strong relationship between the number of fibres on the fracture surfaces and the composite's post-peak behaviour (Zerbino et al. 2012). The analysis results of the fibre density, theoretical fibre density, and the fibre orientation factors of each mix are presented in Table 5.6. The results demonstrate that the increase in the fibre volume fraction, regardless of the type of steel fibres used, led to a corresponding increase in fibre density. However, it was observed that the fibre density was

significantly higher with smaller diameter fibres (0.38 mm) compared to larger diameter fibres (0.55 mm) at the same volume fraction. The fibre density of Mix SF55-20-0.25 was 0.64 fibres/cm^2, while in Mix SF38-20-0.25, the density was almost double at 1.34 fibres/cm^2. Yoo et al. (2016) reported that fibre density was not significantly affected by the fibre length for fibres with different aspect ratios but the same diameters. Therefore, the current study results suggest that fibre diameter plays a significant role in the number of fibres on the fracture surfaces of HSSCC.

Table 5.6 Results of fibre density, theoretical density, and fibre orientation factor

	SF55-20-0.25	SF55-20-0.5	SF55-20-1	SF55-30-0.5	SF38-20-0.25	SF38-20-0.5	SF38-20-1	SF38-30-0.5
Fibre density d_n	0.64	1.41	2.56	1.44	1.34	2.71	5.22	2.40
Theoretical fibre density d_{n3D}	0.53	1.05	2.10	1.05	1.10	2.20	4.41	2.20
Fibre orientation factor η_θ	0.68	0.74	0.74	0.78	0.67	0.74	0.77	0.74

As shown in Table 5.6, the measured fibre density (d_n) was higher than the theoretical fibre density (d_{n3D}) across all HSSCC mixes. This difference in density can be attributed to the high flowability of the HSSCC and the influence of the wall effect (Raju et al. 2020; Zhao et al. 2021a). The fibre orientation factor generally increased with the increased content of both steel fibre types, with fibre orientation factors of 0.68-0.78 and 0.67-0.77 for fibres with diameters of 0.55 mm and 0.38 mm, respectively. When the CA content in the mixes with steel fibres was increased from 20% to 30%, the fibre orientation factor increased from 0.74 to 0.78 for the 0.55 mm diameter fibres. However, for the 0.38 mm diameter fibres, there was no significant change in the fibre orientation factor with increased aggregate content. Further research is necessary to analyse the influence of varying sizes and proportions of CA and steel fibre dimensions on the three-dimensional distribution of steel fibres in HSSCC. Such research will facilitate the advancement of knowledge regarding the influence of CA and the geometry of steel fibres on the efficacy of short steel fibre reinforcement in HSSCC and will have implications for the optimisation of reinforcement strategies in HSSCC.

5.6 Concluding remarks

Developing a mix design for SFR-SCC in the construction sector is an intricate process, necessitating a comprehensive understanding of the optimal blend of fibre type and content, corresponding with the optimal CA content, to achieve the required rheological and mechanical properties while maintaining low production costs. This chapter focused on the performance of environmentally friendly HSSCC comprising cement and GGBS, reinforced with hooked-end steel fibres of various diameters and tensile strengths. The results showed that the addition of steel fibres considerably enhanced the flexural and splitting tensile strength and post-peak behaviour of the HSSCC, with a negligible decrease in compressive strength. However, steel fibres with higher tensile strengths and smaller diameters demonstrated superior performance in splitting tensile strength, flexural strength, and fracture energy compared to those with larger diameters and lower tensile strengths. The study also highlighted that the diameter of steel fibres is a crucial factor affecting their dispersion within HSSCC. These insights indicate that using steel fibres with smaller diameters and higher tensile strengths, combined with increased CA content, is more effective in boosting the mechanical and fracture properties of HSSCC. This method can potentially lower the costs of fibre-reinforced structures and enhance their practical applicability. It was also noted that changes in CA content significantly affected the elastic modulus and post-peak behaviour of HSSCC reinforced with both types of steel fibres. Therefore, CA content and fibre properties are essential factors that should be considered in the mix design process of SFR-SCC.

Chapter 6 Conclusions and Recommendations for Future Research

6.1 Conclusions

This thesis aimed to further the sustainability and performance of high-strength self-compacting concrete (HSSCC) through the development of a mix design that reduces cement consumption while optimising mix properties through the combination of experimental investigations, theoretical analyses, and multiscale simulations. The key research findings are summarised as follows:

- **Sustainable HSSCC mix design**: The novel mix design method for HSSCC effectively reduced cement content through the inclusion of Supplementary Cementitious Materials (SCMs) while maintaining the target plastic viscosity and compressive strengths ranging (70-100 MPa). Through experimental investigations and theoretical analyses, it was validated that this method could provide clear and practical guidance for mix proportioning through the use of design charts, the details of which are given in Chapter 3.

- **Validation of mix design**: The HSSCC mixes were designed with the proposed mix design. The test results showed that these mixes fulfilled the required self-compacting concrete (SCC) criteria and achieved the targeted compressive strengths, thus validating the viability of this method to enhance sustainability by reducing reliance on cement while maintaining the desired strength properties. The proposed mix design was also shown to minimise environmental impact, evidenced by lower calculated CO_2 emissions per unit of compressive strength compared to designs based on existing methods.

- **Multiscale homogenisation:** A novel two-step homogenisation method was developed to determine the effective elastic properties of HSSCC reinforced with steel fibre. This method proved accurate, with a maximum error of 4% compared to experimental data, validating its potential to replace time-consuming laboratory tests and optimising efficient mix designs for HSSCC.

- **Impact of mix constituents on elastic properties**: The research studied the influence of mix constituents on the elastic modulus of HSSCC, namely steel fibre content and

orientation, coarse aggregate (CA) shape and content, and mix porosity. The results indicated that porosity and CA content and steel fibre content had the most significant influence on the elastic properties, while the geometric properties of CA had the least impact when the particles were spherical.

- **Enhanced design and HSSCC performance through steel fibre integration**: The influence of steel fibre properties on HSSCC performance was studied. The results showed that integrating steel fibres of varying diameters and tensile strengths significantly enhanced the flexural and splitting strengths of eco-friendly HSSCC mixes while minimally affecting their compressive strength. Notably, fibres with higher tensile strength and smaller diameters led to marked improvements in the splitting tensile strength, flexural strength, and fracture energy. These findings demonstrate that smaller diameter, higher tensile strength fibres, when combined with a higher content of coarse aggregate (CA), effectively enhance the mechanical and fracture properties of HSSCC. This combination allows for efficient and cost-effective steel fibre use in concrete, potentially reducing the costs associated with fibre-reinforced structures. Moreover, the variations in CA content combined with the included fibres significantly affected the mechanical properties and post-peak behaviour of the reinforced HSSCC, indicating a robust relationship between mix composition and structural performance.

6.2 Recommendations for future research

The following strategies are recommended for future research on this topic:

- The effects of alternative cementitious and waste materials, such as Limestone Calcined Clay Cement (LC3) and rice husk ash (RHA), on the rheology of SCC should be investigated. Subsequently, mix proportioning methods could be developed to offer guidance towards improving the sustainability of SCC.

- To reduce the CO_2 emissions currently reported for the construction industry, a proposed strategy is to decrease the volume of concrete used in structures through the use of high-strength concrete (HSC). This concrete type performs comparably to

conventional concrete but requires substantially less concrete for the same strength. However, structural standards and codes typically recommend minimum sizes for each structural element based on conventional concrete and exclude guidelines for sizes based on HSC. Further research focused on these parameters could significantly enhance the understanding of HSC's contribution to the sustainability performance of concrete structures.

- Research into the elastic properties of SCC containing recycled steel fibre and recycled coarse aggregate through the homogenisation method proposed in this thesis would contribute to a deeper understanding of the impact of such constituents and potentially replace time-consuming laboratory tests, thereby saving resources and time.

- The research in this thesis primarily focused on the prediction of the elastic properties of SFR-SCC using the developed homogenisation method. For a more comprehensive analysis of such concrete in its hardened state, the introduction of a nonlinear constitutive damage model at the mesoscale is crucial to predict the strength and fracture properties of SFR-SCC. Pursuing further research in this field could significantly advance the capability to predict mechanical properties such as compressive and tensile strength. In addition, investigating the fracture performance of SFR-SCC through three-point bending tests, considering varying spatial distributions and fibre orientations, would contribute to the ongoing research in this area.

- Further studies are essential to analyse the effect of varying CA sizes and proportions, and steel fibre properties on the fibres' three-dimensional (3D) orientation within HSSCC. It is also suggested that the influence of the method used to pour HSSCC into moulds on fibre orientation be investigated. Advancements in this area of research would highlight the influence of CA and the geometry of steel fibres on the efficacy of short steel fibre reinforcement in HSSCC and would be instrumental in optimising reinforcement strategies for HSSCC.

References

AASHTO T162-04. 2004. *Standard method of test for mechanical mixing of hydraulic cement pastes and mortars of plastic consistency*. Available at: https://www.astm.org.

Abo Dhaheer, M. 2016. *Design and properties of self-compacting concrete mixes and their simulation in the J-Ring test*.

Abo Dhaheer, M.S., Al-Rubaye, M.M., Alyhya, W.S., Karihaloo, B.L. and Kulasegaram, S. 2016a. Proportioning of self–compacting concrete mixes based on target plastic viscosity and compressive strength: Part I - mix design procedure. *Journal of Sustainable Cement-Based Materials* 5(4), pp. 199–216. Available at: http://dx.doi.org/10.1080/21650373.2015.1039625.

Abo Dhaheer, M.S., Al-Rubaye, M.M., Alyhya, W.S., Karihaloo, B.L. and Kulasegaram, S. 2016b. Proportioning of self-compacting concrete mixes based on target plastic viscosity and compressive strength: Part II - experimental validation. *Journal of Sustainable Cement-Based Materials* 5(4), pp. 217–232. Available at: http://dx.doi.org/10.1080/21650373.2015.1036952.

Abrishambaf, A., Barros, J.A.O. and Cunha, V.M.C.F. 2013. Relation between fibre distribution and post-cracking behaviour in steel fibre reinforced self-compacting concrete panels. *Cement and Concrete Research* 51, pp. 57–66. Available at: https://doi.org/10.1016/j.cemconres.2013.04.009.

ACI 211.1-91. 1991. *Standard Practice for Selecting Proportions for Normal, Heavyweight, and Mass Concrete (ACI 211.1-91)*.

ACI 237R. 2007. *ACI 237 R Self-Consolidating Concrete*.

ACI Committee 238. 2008. *238.1R-08: Report on Measurements of Workability and Rheology of Fresh Concrete*.

ACI Committee 318., American Concrete Institute. and International Organization for Standardization. 2007. *Building code requirements for structural concrete (ACI 318-08) and commentary*. American Concrete Institute.

Adadja, C.E., Labintan, C.A., Gibigaye, M. and Zahrouni, H. 2019. Prediction of the Elastic Properties of the Clay-Rice Straw Composite by Numerical Homogenization Technique using Digimat. *International Journal of Recent Technology and Engineering* 8(4), pp. 9906–9910.

Adesina, A. and Awoyera, P. 2019. Overview of trends in the application of waste materials in self-compacting concrete production. *SN Applied Sciences* 1(9), pp. 1–18. Available at: https://doi.org/10.1007/s42452-019-1012-4.

Aggarwal, P. and Aggarwal, Y. 2020. Strength properties of SCC. In: Siddique, R. ed. *Self-Compacting Concrete: Materials, Properties and Applications*. Woodhead Publishing, pp. 83–115. Available at: http://dx.doi.org/10.1016/B978-0-12-817369-5.00004-0.

Aiad, I., Abd El-Aleem, S. and El-Didamony, H. 2002. Effect of delaying addition of some concrete admixtures on the rheological properties of cement pastes. *Cement and Concrete Research* 32(11), pp. 1839–1843.

Aidjouli, Y., Belebchouche, C., Hammoudi, A., Kadri, E.H., Zaouai, S. and Czarnecki, S. 2024. Modeling the Properties of Sustainable Self-Compacting Concrete Containing Marble and Glass Powder Wastes Using Response Surface Methodology. *Sustainability* 16(5). https://doi.org/10.3390/su16051972.

Aïtcin, P.C. 2019. The influence of the water/cement ratio on the sustainability of concrete. In: Peter C. Hewlett and Martin Liska ed. *Lea's Chemistry of Cement and Concrete*. Fifth Edit. Butterworth-Heinemann, pp. 807–826.

Al-Azzawi, B.S. 2018. *Fatigue of Reinforced Concrete Beams Retrofitted with UHPFRC*.

Alberti, M.G., Enfedaque, A. and Gálvez, J.C. 2016. Fracture mechanics of polyolefin fibre reinforced concrete: Study of the influence of the concrete properties, casting procedures, the fibre length and specimen size. *Engineering Fracture Mechanics* 154, pp. 225–244. Available at: http://dx.doi.org/10.1016/j.engfracmech.2015.12.032.

Alberti, M.G., Enfedaque, A. and Gálvez, J.C. 2018. A review on the assessment and prediction of the orientation and distribution of fibres for concrete. *Composites Part B: Engineering* 151(May), pp. 274–290. Available at: https://doi.org/10.1016/j.compositesb.2018.05.040.

Al-Oran, A.A.A., Safiee, N.A. and Nasir, N.A.M. 2022. Fresh and hardened properties of self-compacting concrete using metakaolin and GGBS as cement replacement. *European Journal of Environmental and Civil Engineering*, pp. 1–14. Available at: https://doi.org/10.1080/19648189.2019.1663268.

Alrawashdeh, A. and Eren, O. 2022. Mechanical and physical characterisation of steel fibre reinforced self-compacting concrete: Different aspect ratios and volume fractions of fibres. *Results in Engineering*. Available at: https://doi.org/10.1016/j.rineng.2022.100335.

Al-Rubaye, M.M. 2016. *Self-compacting concrete: Design, properties and simulation of the flow characteristics in the L-box*.

Alyhya, W.S. 2016. *Self-Compacting Concrete : Mix Proportioning , Properties and Its Flow Simulation in the V-Funnel*.

Alyhya, W.S., Abo Dhaheer, M.S., Al-Rubaye, M.M. and Karihaloo, B.L. 2016. Influence of mix composition and strength on the fracture properties of self-compacting concrete. *Construction and Building Materials* 110, pp. 312–322. Available at: http://dx.doi.org/10.1016/j.conbuildmat.2016.02.037.

AS 1012.3. 5. 2015. *Methods of testing concrete—Determination of properties related to the consistency of concrete—Slump flow, T500 and J-ring test*.

AS5100.5:2017. 2017. Bridge design Part 5: Concrete. *Australian Standards*.

Ashish, D.K. and Verma, S.K. 2019. An overview on mixture design of self-compacting concrete. *Structural Concrete* 20(1), pp. 371–395. Available at: https://doi.org/10.1002/suco.201700279.

Aslani, F. and Nejadi, S. 2012. Mechanical properties of conventional and self-compacting concrete: An analytical study. *Construction and Building Materials* 36, pp. 330–347. Available at: http://dx.doi.org/10.1016/j.conbuildmat.2012.04.034.

ASTM C305. 2004. *Standard method of test for mechanical mixing of hydraulic cement pastes and mortars of plastic consistency*.

ASTM C1609. 2007. Standard Test Method for Flexural Performance of Fiber Reinforced Concrete (Using Beam with Third-point Loading). pp. 1–8.

ASTM C1621. 2014. Standard test method for passing ability of self-consolidating concrete by J-Ring.

Athiyamaan, V. and Mohan Ganesh, G. 2020. Experimental, statistical and simulation analysis on impact of micro steel – Fibres in reinforced SCC containing admixtures. *Construction and Building Materials* 246, p. 118450. Available at: https://doi.org/10.1016/j.conbuildmat.2020.118450.

Bao, C., Bi, J.H., Xu, D., Guan, J. and Cheng, W.X. 2020. Numerical simulation of the distribution and orientation of steel fibres in SCC. *Magazine of Concrete Research* 72(21), pp. 1102–1111. Available at: https://doi.org/10.1680/jmacr.18.00432

Barnes, H.A., Hutton, J.F. and Walters, K., 1989. *An introduction to rheology* (Vol. 3). Elsevier.

Bartos, P.J.M., Sonebi, M. and Tamimi, A.K. 2002. *Workability and Rheology of Fresh Concrete: Compendium of Test*.

Bazant, Z.P. and Kazemi, M.T. 1990. Determination of fracture energy, process zone length and brittleness number from size effect, with application to rock and concrete. *International Journal of Fracture* 44, pp. 111–131.

Benveniste, Y. 1987. A new approach to the application of Mori-Tanaka's theory in composite materials. *Mechanics of Materials*, pp. 147–157.

Berndt, M.L. 2015. Influence of concrete mix design on CO2 emissions for large wind turbine foundations. *Renewable Energy* 83, pp. 608–614. Available at: http://dx.doi.org/10.1016/j.renene.2015.05.002.

Beygi, M.H.A., Kazemi, M.T., Nikbin, I.M. and Amiri, J.V. 2013. The effect of water to cement ratio on fracture parameters and brittleness of self-compacting concrete. *Materials and Design* 50, pp. 267–276. Available at: http://dx.doi.org/10.1016/j.matdes.2013.02.018.

Beygi, M.H.A., Kazemi, M.T., Vaseghi Amiri, J., Nikbin, I.M., Rabbanifar, S. and Rahmani, E. 2014. Evaluation of the effect of maximum aggregate size on fracture behavior of self compacting concrete. *Construction and Building Materials* 55, pp. 202–211. Available at: http://dx.doi.org/10.1016/j.conbuildmat.2014.01.065.

Bonen, D. and Shah, S.P. 2005. The effects of formulation on the properties of self-consolidating concrete. pp. 43–56.

Boukendakdji, O., Kadri, E.H. and Kenai, S. 2012. Effects of granulated blast furnace slag and superplasticizer type on the fresh properties and compressive strength of self-compacting concrete. *Cement and Concrete Composites* 34(4), pp. 583–590. Available at: http://dx.doi.org/10.1016/j.cemconcomp.2011.08.013.

BS EN 12350-8. 2010. Testing fresh concrete. Self-compacting concrete. Slump-flow test.

BS EN 12350-10. 2010. Testing fresh concrete. Self-compacting concrete. L-Box.

BS EN 12350-12. 2010. Testing fresh concrete. Self-compacting concrete. J-ring test

BS EN 12390-3. 2009. Testing hardened concrete: compressive strength of test specimens.

BS EN 12390-5. 2009. Testing hardened concrete : Flexural strength of test specimens.

BS EN 12390-6. 2000. Testing hardened concrete — Part 6: Tensile splitting strength of test specimens.

BS EN 12390-13. 2019. Determination of secant modulus of elasticity in compression.

BS EN 14651. 2007. Test Method for Metallic Fibre Concrete. Measuring the Flexural Tensile Strength (Limit of Proportionality (LOP), Residual).

BS EN 206-9 2010. Additional rules for self-compacting concrete (SCC)

Campos, H.F., Klein, N.S. and Marques Filho, J. 2020. Proposed mix design method for sustainable high-strength concrete using particle packing optimization. *Journal of Cleaner Production* 265, p. 121907. Available at: https://doi.org/10.1016/j.jclepro.2020.121907.

Campos, H.F., Richa, T.M.S., Reus, G.C., Klein, N.S. and Marques filho, J. 2019. Determination of the optimal replacement content of Portland cement by stone powder using particle packing methods and analysis of the influence of the excess water on the consistency of pastes. *Revista IBRACON de Estruturas e Materiais* 12(2), pp. 210–232. Available at: https://doi.org/10.1590/S1983-41952019000200002

Candido, L. and Micelli, F. 2018. Seismic behaviour of regular reinforced concrete plane frames with fiber reinforced concrete in joints. *Bulletin of Earthquake Engineering* 16(9), pp. 4107–4132. Available at: https://doi.org/10.1007/s10518-018-0325-9.

Celik, K., Meral, C., Petek Gursel, A., Mehta, P.K., Horvath, A., and Monteiro, P.J.M. 2015. Mechanical properties, durability, and life-cycle assessment of self-consolidating concrete mixtures made with blended portland cements containing fly ash and limestone powder. *Cement and Concrete Composites* 56, pp. 59–72. Available at: http://dx.doi.org/10.1016/j.cemconcomp.2014.11.003.

Chalioris, C.E. and Karayannis, C.G. 2009. Effectiveness of the use of steel fibres on the torsional behaviour of flanged concrete beams. *Cement and Concrete Composites* 31(5), pp. 331–341. Available at: http://dx.doi.org/10.1016/j.cemconcomp.2009.02.007.

Chalioris, C.E., Kosmidou, P.M.K. and Karayannis, C.G. 2019. Cyclic response of steel fiber reinforced concrete slender beams: An experimental study. *Materials* 12(9). Available at: https://doi.org/10.3390/ma12091398

Chen, H., Zhu, Z., Lin, J., Xu, W. and Liu, L. 2018. Numerical modeling on the influence of particle shape on ITZ's microstructure and macro-properties of cementitious composites: a critical review. *Journal of Sustainable Cement-Based Materials* 7(4), pp. 248–269. Available at: https://doi.org/10.1080/21650373.2018.1473818.

Chidiac, S.E. and Mahmoodzadeh, F. 2009. Plastic viscosity of fresh concrete - A critical review of predictions methods. *Cement and Concrete Composites* 31(8), pp. 535–544. Available at: https://doi.org/10.1016/j.cemconcomp.2009.02.004.

Christensen, R.M. and Lo, K.N. 1979. Solutions for Effective Shear Properties in. *Journal of the Mechanics and Physics of Solids* 27(4), pp. 315–330.

Craeye, B., Van Itterbeeck, P., Desnerck, P., Boel, V. and De Schutter, G. 2014. Modulus of elasticity and tensile strength of self-compacting concrete: Survey of experimental data and structural design codes. *Cement and Concrete Composites* 54, pp. 53–61. Available at: http://dx.doi.org/10.1016/j.cemconcomp.2014.03.011.

Cunha, V.M.C.F., Barros, J.A.O. and Sena-Cruz, J.M. 2012. A finite element model with discrete embedded elements for fibre reinforced composites. *Computers and Structures* 94–95, pp. 22–33. Available at: https://doi.org/10.1016/j.compstruc.2011.12.005

Damineli, B.L., Kemeid, F.M., Aguiar, P.S. and John, V.M. 2010. Measuring the eco-efficiency of cement use. *Cement and Concrete Composites* 32(8), pp. 555–562. Available at: http://dx.doi.org/10.1016/j.cemconcomp.2010.07.009.

David A. Williams, Aaron W. Saaka and Hamlin M. Jennings. 1999. The influence of mixing on the rheology of fresh cement. *Cement and Concrete Research* 29, pp. 1491–1496.

Deeb, R. 2013. Flow of Self-Compacting Flow of Self-Compacting.

Deeb, R., Ghanbari, A. and Karihaloo, B.L. 2012. Development of self-compacting high and ultra high performance concretes with and without steel fibres. *Cement and Concrete Composites* 34(2), pp. 185–190. Available at: http://dx.doi.org/10.1016/j.cemconcomp.2011.11.001.

Deeb, R. and Karihaloo, B.L. 2013. Mix proportioning of self-compacting normal and high-strength concretes. *Magazine of Concrete Research* 65(9), pp. 546–556. Available at: http://dx.doi.org/10.1680/macr.12.00164

Deeb, R., Karihaloo, B.L. and Kulasegaram, S. 2014. Reorientation of short steel fibres during the flow of self-compacting concrete mix and determination of the fibre orientation factor. *Cement and Concrete Research* 56, pp. 112–120. Available at: http://dx.doi.org/10.1016/j.cemconres.2013.10.002.

Diamantonis, N., Marinos, I., Katsiotis, M.S., Sakellariou, A., Papathanasiou, A., Kaloidas, V. and Katsioti, M. 2010. Investigations about the influence of fine additives on the viscosity of cement paste for self-compacting concrete. *Construction and Building Materials* 24(8), pp. 1518–1522. doi: 10.1016/j.conbuildmat.2010.02.005.

Digimat. 2021. *Digimat 2021 FE User's Guide*. Available at: https://nexus.hexagon.com/documentationcenter/ja-JP/bundle/Digimat_2021.4_FE_User_Guide/resource/Digimat_2021.4_FE_User_Guide.pdf.

Dinakar, P. and Manu, S.N. 2014. Concrete mix design for high strength self-compacting concrete using metakaolin. *Materials and Design* 60, pp. 661–668. Available at: http://dx.doi.org/10.1016/j.matdes.2014.03.053.

Dinakar, P., Sethy, K.P. and Sahoo, U.C. 2013. Design of self-compacting concrete with ground granulated blast furnace slag. *Materials and Design* 43, pp. 161–169. Available at: http://dx.doi.org/10.1016/j.matdes.2012.06.049.

Doghri, I. and Ouaar, A. 2003. Homogenization of two-phase elasto-plastic composite materials and structures study of tangent operators, cyclic plasticity and numerical algorithms. *International Journal of Solids and Structures* 40(7), pp. 1681–1712. Available at: http://dx.doi.org/10.1016/S0020-7683(03)00013-1.

Domone, P.L. 2006. Self-compacting concrete: An analysis of 11 years of case studies. *Cement and Concrete Composites* 28(2), pp. 197–208. Available at: http://dx.doi.org/10.1016/j.cemconcomp.2005.10.003.

Domone, P.L. 2007. A review of the hardened mechanical properties of self-compacting concrete. *Cement and Concrete Composites* 29(1), pp. 1–12. Available at: http://dx.doi.org/10.1016/j.cemconcomp.2006.07.010.

Dunant, C.F. et al. 2013. A critical comparison of several numerical methods for computing effective properties of highly heterogeneous materials. *Advances in Engineering Software* 58, pp. 1–12. Available at: http://dx.doi.org/10.1016/j.advengsoft.2012.12.002.

Duran-Herrera, A., De-León-Esquivel, J., Bentz, D.P. and Valdez-Tamez, P. 2019. Self-compacting concretes using fly ash and fine limestone powder: Shrinkage and surface electrical resistivity of equivalent mortars. *Construction and Building Materials* 199, pp. 50–62. Available at: http://dx.doi.org/10.1016/j.conbuildmat.2018.11.191.

EFNARC. 2005. *The European Guidelines for Self-Compacting Concrete*. UK. Available at: www.efnarc.org.

Eshelby, J.D. 1957. The determination of the elastic field of an ellipsoidal inclusion in an anisotronic medium. *Proceedings of the royal society of London, Series A. Mathematical and physical sciences* 241(1226), pp. 376–396.

Esmaeilkhanian, B., Khayat, K.H. and Wallevik, O.H. 2017. Mix design approach for low-powder self-consolidating concrete: Eco-SCC—content optimization and performance. *Materials and Structures/Materiaux et Constructions* 50(2), pp. 1–18. Available at: http://dx.doi.org/10.1617/s11527-017-0993-y.

Esmaeilkhanian, B., Khayat, K.H., Yahia, A. and Feys, D. 2014. Effects of mix design parameters and rheological properties on dynamic stability of self-consolidating concrete. *Cement and Concrete Composites* 54, pp. 21–28. Available at: http://dx.doi.org/10.1016/j.cemconcomp.2014.03.001.

Eurocode 2. 2004. *Design of Concrete Structures-Part 1–1: General Rules and Rules for Buildings.*

Faifer, M., Ottoboni, R., Toscani, S. and Ferrara, L. 2011. Nondestructive testing of steel-fiber-reinforced concrete using a magnetic approach. *IEEE Transactions on Instrumentation and Measurement* 60(5), pp. 1709–1717. Available at: http://dx.doi.org/10.1109/TIM.2010.2090059.

Ferrara, L., Bamonte, P., Caverzan, A., Musa, A. and Sanal, I. 2012a. A comprehensive methodology to test the performance of Steel Fibre Reinforced Self-Compacting Concrete (SFR-SCC). *Construction and Building Materials* 37, pp. 406–424. Available at: http://dx.doi.org/10.1016/j.conbuildmat.2012.07.057.

Ferrara, L., Cremonesi, M., Tregger, N., Frangi, A. and Shah, S.P. 2012b. On the identification of rheological properties of cement suspensions: Rheometry, Computational Fluid Dynamics modeling and field test measurements. *Cement and Concrete Research* 42(8), pp. 1134–1146. Available at: http://dx.doi.org/10.1016/j.cemconres.2012.05.007.

Ferraris, C.F. 1999. Measurement of the rheological properties of high performance concrete: State of the art report. *Journal of Research of the National Institute of Standards and Technology* 104(5), pp. 461–478. Available at: http://dx.doi.org/10.6028/jres.104.028.

Ferraris, C.F. and Martys, N.S. 2012. *Concrete rheometers*. Woodhead Publishing Limited. Available at: http://dx.doi.org/10.1533/9780857095282.1.63.

Ferraris, C.F., Obla, K.H. and Hill, R. 2001. The influence of mineral admixtures on the rheology of cement paste and concrete. *Cement and Concrete Research* 31(2), pp. 245–255. Available at: http://dx.doi.org/10.1016/S0008-8846(00)00454-3.

Feys, D. et al. 2023. RILEM TC 266-MRP: Round-robin rheological tests on high performance mortar and concrete with adapted rheology—rheometers, mixtures and procedures. *Materials and Structures/Materiaux et Constructions* 56(4), pp. 1–19. Available at: https://doi.org/10.1617/s11527-023-02173-1.

Feys, D., Cepuritis, R., Jacobsen, S., Lesage, K., Secrieru, E. and Yahia, A. 2017. Measuring Rheological Properties of Cement Pastes: Most common Techniques, Procedures and Challenges. *RILEM Technical Letters* 2, pp. 129–135. Available at: http://dx.doi.org/10.21809/rilemtechlett.2017.43.

Feys, D., Heirman, G., de Schutter, G., Verhoeven, R., Vandewalle, L. and van Gemert, D. 2007. Comparison of two concrete rheometers for shear thickening behaviour of SCC. *5th Int. RILEM Symposium on Self-Compacting Concrete* (1), pp. 1–6.

Feys, D. and Khayat, K.H. 2013. Comparing Rheological Properties of SCC Obtained with the ConTec and ICAR Rheometers. *Fifth North American Conference on the Design and Use of Self-Consolidating Concrete, 12-15 May* (July 2017), pp. 1–11.

FIB. 2013. *Fib Model Code for Concrete Structures 2010*. Lausanne, Switzerland.

De Figueiredo, A.D. and Ceccato, M.R. 2015. Workability analysis of steel fiber reinforced concrete using slump and Ve-Be test. *Materials Research* 18(6), pp. 1284–1290. Available at: http://dx.doi.org/10.1590/1516-1439.022915.

Fuglsang Nielsen, L. 2003. *Rheology of some fluid extreme composites Such as fresh self-compacting concrete*.

Gal, E. and Kryvoruk, R. 2011. Meso-scale analysis of FRC using a two-step homogenization approach. *Computers and Structures* 89(11–12), pp. 921–929. Available at: http://dx.doi.org/10.1016/j.compstruc.2011.02.006.

Gao, Y., De Schutter, G., Ye, G., Tan, Z. and Wu, K. 2014. The ITZ microstructure, thickness and porosity in blended cementitious composite: Effects of curing age, water to binder ratio and aggregate content. *Composites Part B: Engineering* 60, pp. 1–13. Available at: http://dx.doi.org/10.1016/j.compositesb.2013.12.021.

Garboczi, E.J. and Berryman, J.G. 2001. Elastic moduli of a material containing composite inclusions: Effective medium theory and finite element computations. *Mechanics of Materials* 33(8), pp. 455–470. Available at: http://dx.doi.org/10.1016/S0167-6636(01)00067-9.

Geiker, M.R., Brandl, M., Thrane, L.N. and Nielsen, L.F. 2002. On the effect of coarse aggregate fraction and shape on the rheological properties of self-compacting concrete. *Cement, Concrete and Aggregates* 24(1), pp. 3–6. Available at: http://dx.doi.org/10.1520/cca10484j.

Gettu, R., Gardner, D.R., Saldívar, H. and Barragán, B.E. 2005. Study of the distribution and orientation of fibers in SFRC specimens. *Materials and Structures* 38(275), pp. 31–37. Available at: http://dx.doi.org/10.1617/14021.

Ghanbari, A. and Karihaloo, B.L. 2009. Prediction of the plastic viscosity of self-compacting steel fibre reinforced concrete. *Cement and Concrete Research* 39(12), pp. 1209–1216. Available at: http://dx.doi.org/10.1016/j.cemconres.2009.08.018.

Ghasemi, M., Ghasemi, M.R. and Mousavi, S.R. 2018. Investigating the effects of maximum aggregate size on self-compacting steel fiber reinforced concrete fracture parameters. *Construction and Building Materials* 162, pp. 674–682. Available at: https://doi.org/10.1016/j.conbuildmat.2017.11.141.

Ghasemi, M., Ghasemi, M.R. and Mousavi, S.R. 2019. Studying the fracture parameters and size effect of steel fiber-reinforced self-compacting concrete. *Construction and Building Materials* 201, pp. 447–460. Available at: https://doi.org/10.1016/j.conbuildmat.2018.12.172.

Gitman, I.M., Askes, H. and Sluys, L.J. 2007. Representative volume: Existence and size determination. *Engineering Fracture Mechanics* 74(16), pp. 2518–2534. Available at: http://dx.doi.org/10.1016/j.engfracmech.2006.12.021.

Goodier, C.I. 2003. Development of self-compacting concrete. Proceedings of the ICE-Structures and Buildings, pp. 405–414.

de Grazia, M.T., Sanchez, L.F.M., Romano, R.C.O. and Pileggi, R.G. 2019. Investigation of the use of continuous particle packing models (PPMs) on the fresh and hardened properties of low-cement concrete (LCC) systems. *Construction and Building Materials* 195, pp. 524–536. Available at: https://doi.org/10.1016/j.conbuildmat.2018.11.051.

Griffin, A. and Myers, J.J. 2016. Shear behavior of high strength self-consolidating concrete in Nebraska University bridge girders. *PCI Journal* 61(3), pp. 31–46. Available at: https://doi.org/10.15554/pcij61.3-01.

Grunewald, S. 2004. *Performance-based design of self-compacting fibre reinforced concrete*. Delft University Press, Delft (The Netherlands).

Grzeszczyk, S. and Podkowa, P. 2009. Effect of microfiller on the properties of self-compacting concrete mixture. *XIX Conference JADWISIN 2004, Concrete and prefabrication* 17, pp. 257–262.

Guo, Z., Zhang, J., Jiang, T., Jiang, T., Chen, C., Bo, R. and Sun, Y. 2020. Development of sustainable self-compacting concrete using recycled concrete aggregate and fly ash, slag, silica fume. *European Journal of Environmental and Civil Engineering*, pp. 1–22. Available at: https://doi.org/10.1080/19648189.2020.1715847.

Gupta, N., Siddique, R. and Belarbi, R. 2021. Sustainable and Greener Self-Compacting Concrete incorporating Industrial By-Products: A Review. *Journal of Cleaner Production* 284. Available at: https://doi.org/10.1016/j.jclepro.2020.124803.

Haido, J.H., Tayeh, B.A., Majeed, S.S. and Karpuzcu, M. 2021. Effect of high temperature on the mechanical properties of basalt fibre self-compacting concrete as an overlay material. *Construction and Building Materials* 268, p. 121725. Available at: https://doi.org/10.1016/j.conbuildmat.2020.121725.

Hanif, A., Kim, Y., Lu, Z. and Park, C. 2017. Early-age behavior of recycled aggregate concrete under steam curing regime. *Journal of Cleaner Production* 152, pp. 103–114. Available at: https://doi.org/10.1016/j.jclepro.2017.03.107.

Hashin, Z. and Shtrikman, S. 1963. A variational approach to the theory of the elastic behaviour of multiphase materials. *Journal of the Mechanics and Physics of Solids* 11(2), pp. 127–140. Available at: https://doi.org/10.1016/0022-5096(63)90060-7.

Hill, R. 1952. The elastic behaviour of a crystalline aggregate. *Proceedings of the Physical Society. Section A* 65(5), pp. 349–354.

Hill, R. 1965. A self-consistent mechanics of composite materials. *Journal of the Mechanics and Physics of Solids* 13(4), pp. 213–222. Available at: https://doi.org/10.1016/0022-5096(65)90010-4.

Hillerborg, A. 1985. The theoretical basis of a method to determine the fracture energy GF of concrete. *Materials and Structures* 18, pp. 291–296.

Hillerborg, A., Modeer, M. and Petersson, P.E. 1976. Analysis of crack formation and crack growth in concrete by means of fracture mechanics and finite elements. *Cement and Concrete Research* 6, pp. 773–782.

Holschmacher, K. and Klug, Y. 2002. A Database for the Evaluation of Hardened Properties of SCC . *Lacer* 7, pp. 123–134.

Hu, J. 2005. *A study of effects of aggregate on concrete rheology*.

Hu, J. and Wang, K. 2007. Effects of size and uncompacted voids of aggregate on mortar flow ability. *Journal of Advanced Concrete Technology* 5(1), pp. 75–85. Available at: https://doi.org/10.3151/jact.5.75.

Huang, H., Gao, X., Li, L. and Wang, H. 2018. Improvement effect of steel fiber orientation control on mechanical performance of UHPC. *Construction and Building Materials* 188, pp. 709–721. Available at: https://doi.org/10.1016/j.conbuildmat.2018.08.146.

Huang, H., Gao, X. and Teng, L. 2021. Fiber alignment and its effect on mechanical properties of UHPC: An overview. *Construction and Building Materials* 296, p. 123741. Available at: https://doi.org/10.1016/j.conbuildmat.2021.123741.

Hussien, A.S. and Mohammed, M.K. 2023. Optimum characteristics of plastic fibres for sustainable self-compacting concrete SCC. *European Journal of Environmental and Civil Engineering* 27(9), pp. 2967–2984. Available at: https://doi.org/10.1080/19648189.2022.2119605.

Jalal, M., Pouladkhan, A., Harandi, O.F. and Jafari, D. 2015. Comparative study on effects of Class F fly ash, nano silica and silica fume on properties of high-performance self-compacting concrete. *Construction and Building Materials* 94, pp. 90–104. Available at: https://doi.org/10.1016/j.conbuildmat.2015.07.001.

Jasiūnienė, E., Cicėnas, V., Grigaliūnas, P., Rudžionis, Ž. and Navickas, A.A. 2018. Influence of the rheological properties on the steel fibre distribution and orientation in self-compacting concrete. *Materials and Structures/Materiaux et Constructions* 51(4). Available at: https://doi.org/10.1617/s11527-018-1231-y.

Jawahar, J.G., Sashidhar, C., Reddy, I.V.R. and Peter, J.A. 2013. Effect of coarse aggregate blending on short-term mechanical properties of self-compacting concrete. *Materials and Design* 43, pp. 185–194. Available at: http://dx.doi.org/10.1016/j.matdes.2012.06.063.

JCI-S-002-2003. 2003. Method of Test for Load-Displacement Curve of Fiber Reinforced Concrete by Use of Notched Beam. *Japan Concrete Institute Standard Method* (L), pp. 1–6.

Jiao, D., Shi, C., Yuan, Q., An, X., Liu, Y. and Li, H. 2017. Effect of constituents on rheological properties of fresh concrete-A review. *Cement and Concrete Composites* 83, pp. 146–159. Available at: https://doi.org/10.1016/j.cemconcomp.2017.07.016.

Jovein, H.B. and Shen, L. 2016. Effects of aggregate properties on rheology of self-consolidating concrete. *Advances in Civil Engineering Materials* 5(1), pp. 235–255 Available at: https://doi.org/10.1520/ACEM20160008.

JSCE Concrete Committee. 2007. *Standard Specifications for Concrete Structures*. Available at: https://doi.org/10.3151/coj1975.46.7_3.

Kadhim, S. 2020. The Effects of Using Steel Fibers on Self-Compacting Concrete Properties: A Review. *Engineering and Technology Journal* 38(11), pp. 1666–1675. Available at: https://doi.org/10.30684/etj.v38i11a.1678.

Kaish, A.B.M.A., Breesem, K.M. and Abood, M.M. 2018a. Influence of pre-treated alum sludge on properties of high-strength self-compacting concrete. *Journal of Cleaner Production* 202, pp. 1085–1096. Available at: https://doi.org/10.1016/j.jclepro.2018.08.156.

Kaish, A.B.M.A., Breesem, K.M. and Abood, M.M. 2018b. Influence of pre-treated alum sludge on properties of high-strength self-compacting concrete. *Journal of Cleaner Production* 202, pp. 1085–1096. Available at: https://doi.org/10.1016/j.jclepro.2018.08.156.

Kang, S.T., Lee, B.Y., Kim, J.K. and Kim, Y.Y. 2011. The effect of fibre distribution characteristics on the flexural strength of steel fibre-reinforced ultra high strength concrete. *Construction and Building Materials* 25(5), pp. 2450–2457. Available at: http://dx.doi.org/10.1016/j.conbuildmat.2010.11.057.

Kanit, T., Forest, S., Galliet, I., Mounoury, V. and Jeulin, D. 2003. Determination of the size of the representative volume element for random composites: Statistical and numerical approach. *International Journal of Solids and Structures* 40(13–14), pp. 3647–3679. Available at: https://doi.org/10.1016/S0020-7683(03)00143-4.

Kanouté, P., Boso, D.P., Chaboche, J.L. and Schrefler, B.A. 2009. Multiscale methods for composites: A review. *Archives of Computational Methods in Engineering* 16(1), pp. 31–75. Available at: https://doi.org/10.1007/s11831-008-9028-8.

Karihaloo, B.L. and Ghanbari, A. 2012. Mix proportioning of self compacting high-and ultrahigh-performance concretes with and without steel fibres. *Magazine of Concrete Research* 64(12), pp. 1089–1100. Available at: https://doi.org/10.1680/macr.11.00190.

Kazemi, M.T., Golsorkhtabar, H., Beygi, M.H.A. and Gholamitabar, M. 2017. Fracture properties of steel fiber reinforced high strength concrete using work of fracture and size effect methods. *Construction and Building Materials* 142, pp. 482–489. Available at: http://dx.doi.org/10.1016/j.conbuildmat.2017.03.089.

Kerkhoff, B., Panarese, W.C. and Kosmatka, S.H. 2002. *Design and Control Design and Control of concrete mixtures*. Fourteenth. Portland Cement Association.

Khaleel, O.R., Al-Mishhadani, S.A. and Abdul Razak, H. 2011. The effect of coarse aggregate on fresh and hardened properties of Self-Compacting Concrete (SCC). *Procedia Engineering* 14, pp. 805–813. Available at: http://dx.doi.org/10.1016/j.proeng.2011.07.102.

Khaloo, A., Raisi, E.M., Hosseini, P. and Tahsiri, H. 2014. Mechanical performance of self-compacting concrete reinforced with steel fibers. *Construction and Building Materials* 51, pp. 179–186. Available at: http://dx.doi.org/10.1016/j.conbuildmat.2013.10.054.

Khayat, K.H. 1999. Workability , Testing , and Performance of Self-Consolidating. *Materials Journal,* 96(3), pp. 346-353.

Khayat, K.H., Ghezal, A. and Hadriche, M.S. 1999a. Factorial design models for proportioning self-consolidating concrete. *Materials and Structures/Materiaux et Constructions* 32(223), pp. 679–686. Available at: https://doi.org/10.1007/bf02481706.

Khayat, K.H., Hu, C. and Monty, H. 1999b. Stability of self-consolidating concrete, Advantages, and Potential Applications. *1st International RILEM Symposium on Self-Compacting Concrete*, pp. 143–152.

Khayat, K.H. and Roussel, Y. 1999. Testing and performance of fiber-reinforced self-consolidating concrete. In: *First International RILEM symposium on self-compacting concrete*. Stockholm, Sweden, pp. 509–520.

Kheder, G.F. and Al Jadiri, R.S. 2010. New method for proportioning self-consolidating concrete based on compressive strength requirements. *ACI Materials Journal* 107(5), pp. 490–497. Available at: https://doi.org/10.14359/51663969.

Kim, K.Y., Yun, T.S., Choo, J., Kang, D.H. and Shin, H.S. 2012. Determination of air-void parameters of hardened cement-based materials using X-ray computed tomography. *Construction and Building Materials* 37, pp. 93–101. Available at: https://doi.org/10.1016/j.conbuildmat.2012.07.012.

Kirthika, S.K., Singh, S.K. and Chourasia, A. 2020. Alternative fine aggregates in production of sustainable concrete- A review. *Journal of Cleaner Production* 268. Available at: https://doi.org/10.1016/j.jclepro.2020.122089.

Koehler, E.P. and Fowler, D.W. 2007. *Aggregates in Self-Consolidating Concrete. The Aggregates Foundation for Technology. Research and Education, Research Report ICAR.* Austin, TX.

Krieger, I.M. and Dougherty, T.J. 1959. A Mechanism for Non-Newtonian Flow in Suspensions of Rigid Spheres. *Transactions of the Society of Rheology* 3(1), pp. 137–152. Available at: https://doi.org/10.1122/1.548848.

de Kruif, C.G., van Iersel, E.M.F., Vrij, A. and Russel, W.B. 1985. Hard sphere colloidal dispersions: Viscosity as a function of shear rate and volume fraction. *The Journal of Chemical Physics* 83(9), pp. 4717–4725. Available at: https://doi.org/10.1063/1.448997.

de la Rosa, Á., Poveda, E., Ruiz, G. and Cifuentes, H. 2018. Proportioning of self-compacting steel-fiber reinforced concrete mixes based on target plastic viscosity and compressive strength: Mix-design procedure & experimental validation. *Construction and Building Materials* 189, pp. 409–419. Available at: https://doi.org/10.1016/j.conbuildmat.2018.09.006.

de la Rosa, Á., Poveda, E., Ruiz, G., Moreno, R., Cifuentes, H. and Garijo, L. 2020. Determination of the plastic viscosity of superplasticized cement pastes through capillary viscometers. *Construction and Building Materials* 260. Available at: https://doi.org/10.1016/j.conbuildmat.2020.119715.

Lachemi, M., Hossain, K.M.A., Lambros, V., Nkinamubanzi, P.C. and Bouzoubaâ, N. 2004. Performance of new viscosity modifying admixtures in enhancing the rheological properties of cement paste. *Cement and Concrete Research* 34(2), pp. 185–193. Available at: https://doi.org/10.1016/S0008-8846(03)00233-3.

Leemann, A., Münch, B., Gasser, P. and Holzer, L. 2006. Influence of compaction on the interfacial transition zone and the permeability of concrete. *Cement and Concrete Research* 36(8), pp. 1425–1433. Available at: https://doi.org/10.1016/j.cemconres.2006.02.010.

Li, P., Ran, J., Nie, D. and Zhang, W. 2021. Improvement of mix design method based on paste rheological threshold theory for self-compacting concrete using different mineral additions in ternary blends of powders. *Construction and Building Materials* 276, p. 122194. Available at: https://doi.org/10.1016/j.conbuildmat.2020.122194.

Li, T., Bai, W., Zhang, K. and Pan, Z. 2019a. A study on image-processing based identification of aspect ratio of coarse aggregate. *MATEC Web of Conferences* 275(201 9), p. 02007. Available at: https://doi.org/10.1051/matecconf/201927502007.

Li, X., Zhang, J., Liu, J. and Cao, W. 2019b. Bond Behavior of Spiral Ribbed Ultra-high Strength Steel Rebar Embedded in Plain and Steel Fiber Reinforced High-Strength Concrete. *KSCE Journal of Civil Engineering* 23(10), pp. 4417–4430. doi: 10.1007/s12205-019-2449-0.

Liang, T., Jin, F., Huang, D. and Wang, G. 2022. On the elastic modulus of rock-filled concrete. *Construction and Building Materials* 340(May), p. 127819. Available at: https://doi.org/10.1016/j.conbuildmat.2022.127819.

Limbachiya, V., Ganjian, E. and Claisse, P. 2016. Strength, durability and leaching properties of concrete paving blocks incorporating GGBS and SF. *Construction and Building Materials* 113, pp. 273–279. Available at: http://dx.doi.org/10.1016/j.conbuildmat.2016.02.152.

Liu, J., Li, C., Liu, J., Cui, G. and Yang, Z. 2013. Study on 3D spatial distribution of steel fibers in fiber reinforced cementitious composites through micro-CT technique. *Construction and Building Materials* 48, pp. 656–661. Available at: http://dx.doi.org/10.1016/j.conbuildmat.2013.07.052.

Long, G., Gao, Y. and Xie, Y. 2015a. Designing more sustainable and greener self-compacting concrete. *Construction and Building Materials* 84, pp. 301–306. Available at: https://doi.org/10.1016/j.conbuildmat.2015.02.072.

Long, G., Gao, Y. and Xie, Y. 2015b. Designing more sustainable and greener self-compacting concrete. *Construction and Building Materials* 84, pp. 301–306. Available at: https://doi.org/10.1016/j.conbuildmat.2015.02.072.

Madandoust, R., Ranjbar, M.M., Ghavidel, R. and Fatemeh Shahabi, S. 2015. Assessment of factors influencing mechanical properties of steel fiber reinforced self-compacting concrete. *Materials and Design* 83, pp. 284–294. Available at: http://dx.doi.org/10.1016/j.matdes.2015.06.024.

Mahmoodzadeh, F. and Chidiac, S.E. 2013. Rheological models for predicting plastic viscosity and yield stress of fresh concrete. *Cement and Concrete Research* 49, pp. 1–9. Available at: https://doi.org/10.1016/j.cemconres.2013.03.004.

Majeed, S.S., Haido, J.H., Atrushi, D.S., Al-Kamaki, Y., Dinkha, Y.Z., Saadullah, S.T. and Tayeh, B.A. 2021. Properties of self-compacted concrete incorporating basalt fibers: Experimental study and Gene Expression Programming (GEP) analysis. *Computers and Concrete* 28(5), pp. 451–463. Available at: https://doi.org/10.12989/cac.2021.28.5.451.

Marks, B., Miletić, M., Lee, B.C.H., Zia, M.H., Barros, J.A.O. and Dias-da-Costa, D. 2021. Monitoring steel fibre orientation in self-compacting cementitious composite slabs during pouring with dynamic X-ray radiography. *Cement and Concrete Research*. Available at: https://doi.org/10.1016/j.cemconres.2021.106390.

Martinie, L. and Roussel, N. 2011. Simple tools for fiber orientation prediction in industrial practice. *Cement and Concrete Research* 41(10), pp. 993–1000. Available at: http://dx.doi.org/10.1016/j.cemconres.2011.05.008.

Matos, P.R. de, Foiato, M. and Prudêncio, L.R. 2019. Ecological, fresh state and long-term mechanical properties of high-volume fly ash high-performance self-compacting concrete. *Construction and Building Materials* 203, pp. 282–293. Available at: https://doi.org/10.1016/j.conbuildmat.2019.01.074.

de Matos, P.R., Sakata, R.D. and Prudêncio, L.R. 2019. Eco-efficient low binder high-performance self-compacting concretes. *Construction and Building Materials* 225, pp. 941–955. Available at: https://doi.org/10.1016/j.conbuildmat.2019.07.254.

Mechtcherine, V., Khayat, K. and Secrieru, E. 2020. *Rheology and Processing of Construction Materials*. Available at: http://link.springer.com/10.1007/978-3-030-22566-7.

Michels, J., Waldmann, D., Maas, S. and Zürbes, A. 2012. Steel fibers as only reinforcement for flat slab construction - Experimental investigation and design. *Construction and Building Materials* 26(1), pp. 145–155. Available at: https://doi.org/10.1016/j.conbuildmat.2011.06.004.

Mikanovic, N. and Jolicoeur, C. 2008. Influence of superplasticizers on the rheology and stability of limestone and cement pastes. *Cement and Concrete Research* 38(7), pp. 907–919. Available at: https://doi.org/10.1016/j.cemconres.2008.01.015.

Miletić, M., Kumar, L.M., Arns, J.Y., Agarwal, A., Foster, S.J., Arns, C. and Perić, D. 2020. Gradient-based fibre detection method on 3D micro-CT tomographic image for defining fibre orientation bias in ultra-high-performance concrete. *Cement and Concrete Research* 129(December 2019), p. 105962. Available at: https://doi.org/10.1016/j.cemconres.2019.105962.

Mineral Products Association. 2015. *Fact Sheet 18: Embodied CO 2 e of UK cement , additions and cementitious material*.

Moravvej, M. and Rashidi, M. 2020. Structural performance of self-compacting concrete *In Self-Compacting Concrete: Materials, Properties and Applications* Elsevier Inc., pp. *371-387*. Available at: http://dx.doi.org/10.1016/B978-0-12-817369-5.00013-1.

Mori, T. and Tanaka, K. 1973. Average stress in matrix and average elastic energy of materials with misfitting inclusions. *Acta Metall* 21(5), pp. 571–574.

Moruza, G.M. and Ozyildirim, H.C. 2017. Self-Consolidating concrete in Virginia Department of Transportation's bridge structures. *ACI Materials Journal* 114(1), pp. 57–64. Available at: https://doi.org/10.14359/51689480.

Mueller, F., Wallevik, O. and Khayat, K. 2016. Robustness of low-binder SCC (Eco-SCC), lean SCC, and binder-rich SCC. *8th International RILEM Symposium on Self-Compacting Concrete—SCC 2016* (Washington DC, USA: RILEM Publications SARL), pp. 25–34.

Naaman, A.E. 2008. High Performance Fiber Reinforced Cement Composites. In: *High-performance Construction Materials: Science and Applications*. pp. 91–153.

Nadeau, J.C. 2003. A multiscale model for effective moduli of concrete incorporating ITZ water-cement ratio gradients, aggregate size distributions, and entrapped voids. *Cement and Concrete Research* 33(1), pp. 103–113. Available at: https://doi.org/10.1016/S0008-8846(02)00931-6.

National Research Council. 2006. *CNR-DT 204: Guide for the Design and Construction of Fiber-Reinforced Concrete Structures*.

Nehdi, M., Pardhan, M. and Koshowski, S. 2004. Durability of self-consolidating concrete incorporating high-volume replacement composite cements. *Cement and Concrete Research* 34(11), pp. 2103–2112. Available at: https://doi.org/10.1016/j.cemconres.2004.03.018.

Nehdi, M. and Rahman, M.A. 2004. Estimating rheological properties of cement pastes using various rheological models for different test geometry, gap and surface friction. *Cement and Concrete Research* 34(11), pp. 1993–2007. Available at: https://doi.org/10.1016/j.cemconres.2004.02.020.

Nemat-Nasser, S. and Hori, H. 1993. *Micromechanics: Overall properties of heterogeneous materials*. Elsevier Science.

Neville, A. and Aïtcin, P.C. 1998. High performance concrete - An overview. *Materials and Structures/Materiaux et Constructions* 31(2), pp. 111–117. Available at: https://doi.org/10.1007/bf02486473.

Nguyen, V.P., Stroeven, M. and Sluys, L.J. 2011. Multiscale Continuous and Discontinuous Modeling of Heterogeneous Materials: A Review on Recent Developments. *Journal of Multiscale Modelling* 03(04), pp. 229–270. Available at: https://doi.org/10.1142/s1756973711000509.

Ogierman, W. and Kokot, G. 2017. Homogenization of inelastic composites with misaligned inclusions by using the optimal pseudo-grain discretization. *International Journal of Solids and Structures* 113–114, pp. 230–240. Available at: http://dx.doi.org/10.1016/j.ijsolstr.2017.03.008.

Okamura, H. and Ouchi, M. 1999. Self-compacting concrete, present use and future. *1st International RILEM Symposium on Self-Compacting Concrete*, pp. 3–14.

Okamura, H. and Ouchi, M. 2003. Self-Compacting Concrete, Journal of Advanced Concrete Technology, Vol.1, No.1, April 2003. 1(1), pp. 5–15.

Okamura, H. and Ozawa, K. 1996. Self-compacting high performance concrete. *Structural Engineering International: Journal of the International Association for Bridge and Structural Engineering (IABSE)* 6(4), pp. 269–270. Available at: http://dx.doi.org/10.2749/101686696780496292.

Öner, M., Erdogdu, K. and Günlü, A. 2003. Effect of components fineness on strength of blast furnace slag cement. *Cement and Concrete Research* 33(4), pp. 463–469. Available at: http://dx.doi.org/10.1016/S0008-8846(02)00713-5.

Pająk, M. and Ponikiewski, T. 2013. Flexural behavior of self-compacting concrete reinforced with different types of steel fibers. *Construction and Building Materials* 47, pp. 397–408. Available at: http://dx.doi.org/10.1016/j.conbuildmat.2013.05.072.

Parra, C., Valcuende, M. and Gómez, F. 2011. Splitting tensile strength and modulus of elasticity of self-compacting concrete. *Construction and Building Materials* 25(1), pp. 201–207. Available at: http://dx.doi.org/10.1016/j.conbuildmat.2010.06.037.

Pavía, S. and Condren, E. 2008. Study of the Durability of OPC versus GGBS Concrete on Exposure to Silage Effluent. *Journal of Materials in Civil Engineering* 20(4), pp. 313–320. Available at: http://dx.doi.org/10.1061/(asce)0899-1561(2008)20:4(313).

Pierard, O., González, C., Segurado, J., LLorca, J. and Doghri, I. 2007. Micromechanics of elasto-plastic materials reinforced with ellipsoidal inclusions. *International Journal of Solids and Structures* 44(21), pp. 6945–6962. Available at: http://dx.doi.org/10.1016/j.ijsolstr.2007.03.019.

du Plessis, A. and Boshoff, W.P. 2019. A review of X-ray computed tomography of concrete and asphalt construction materials. *Construction and Building Materials* 199, pp. 637–651. Available at: https://doi.org/10.1016/j.conbuildmat.2018.12.049.

du Plessis, A., le Roux, S.G. and Guelpa, A. 2016. Comparison of medical and industrial X-ray computed tomography for non-destructive testing. *Case Studies in Non-destructive Testing and Evaluation* 6, pp. 17–25. Available at: http://dx.doi.org/10.1016/j.csndt.2016.07.001.

Ponikiewski, T., Gołaszewski, J., Rudzki, M. and Bugdol, M. 2015a. Determination of steel fibres distribution in self-compacting concrete beams using X-ray computed tomography. *Archives of Civil and Mechanical Engineering* 15(2), pp. 558–568. Available at: http://dx.doi.org/10.1016/j.acme.2014.08.008.

Ponikiewski, T. and Katzer, J. 2016. X-ray computed tomography of fibre reinforced self-compacting concrete as a tool of assessing its flexural behaviour. *Materials and Structures/Materiaux et Constructions* 49(6), pp. 2131–2140. Available at: http://dx.doi.org/10.1617/s11527-015-0638-y.

Ponikiewski, T., Katzer, J., Bugdol, M. and Rudzki, M. 2014. Determination of 3D porosity in steel fibre reinforced SCC beams using X-ray computed tomography. *Construction and Building Materials* 68, pp. 333–340. Available at: http://dx.doi.org/10.1016/j.conbuildmat.2014.06.064.

Ponikiewski, T., Katzer, J., Bugdol, M. and Rudzki, M. 2015b. Steel fibre spacing in self-compacting concrete precast walls by X-ray computed tomography. *Materials and Structures/Materiaux et Constructions* 48(12), pp. 3863–3874. Available at: http://dx.doi.org/10.1617/s11527-014-0444-y.

Qin, X. and Xu, Q. 2016. Statistical analysis of initial defects between concrete layers of dam using X-ray computed tomography. *Construction and Building Materials* 125, pp. 1101–1113. Available at: http://dx.doi.org/10.1016/j.conbuildmat.2016.08.149.

Qsymah, A., Sharma, R., Yang, Z., Margetts, L. and Mummery, P. 2017. Micro X-ray computed tomography image-based two-scale homogenisation of ultra-high-performance fibre reinforced concrete. *Construction and Building Materials* 130, pp. 230–240. Available at: http://dx.doi.org/10.1016/j.conbuildmat.2016.09.020.

Qsymah, A.M. 2016. In-situ X-ray Computed Tomography Tests and Numerical Modelling of UHPFRC. p. 170.

Rahla, K.M., Mateus, R. and Bragança, L. 2019. Comparative sustainability assessment of binary blended concretes using Supplementary Cementitious Materials (SCMs) and Ordinary Portland Cement (OPC). *Journal of Cleaner Production* 220, pp. 445–459. Available at: https://doi.org/10.1016/j.jclepro.2019.02.010.

Rajakarunakaran, S.A. et al. 2022. Prediction of strength and analysis in self-compacting concrete using machine learning based regression techniques. *Advances in Engineering Software* 173(September), p. 103267. Available at: https://doi.org/10.1016/j.advengsoft.2022.103267.

Raju, R.A., Lim, S., Akiyama, M. and Kageyama, T. 2020. Effects of concrete flow on the distribution and orientation of fibers and flexural behavior of steel fiber-reinforced self-compacting concrete beams. *Construction and Building Materials*. Available at: https://doi.org/10.1016/j.conbuildmat.2020.119963.

Rasekh, H., Joshaghani, A., Jahandari, S., Aslani, F. and Ghodrat, M. 2020. *Rheology and workability of SCC*. Elsevier Inc. Available at: http://dx.doi.org/10.1016/B978-0-12-817369-5.00002-7.

Rich, D. 2014. *On-site application of self-compacting concrete (SCC)*.

Rich, D., Glass, J., Gibb, A.G.F. and Goodier, C. 2012. UK contractors' views on self compacting concrete in construction. *Proceedings of Institution of Civil Engineers: Construction Materials* 165(4), pp. 201–210. Available at: http://dx.doi.org/10.1680/coma.10.00036.

RILEM FMC-50. 1985. Determination of the fracture energy of mortar and concrete by means of three-point bend tests on notched beams. *Materials and Structures* 18(106), pp. 285–290.

RILEM TC 89-FMT. 1990. Size-effect method for determining fracture energy and process zone size of concrete. *Materials and Structures* 23(6), pp. 461–465. Available at: http://dx.doi.org/10.1007/BF02472030.

RILEM TC 162-TDF. 2002. Rilem TC 162-TDF: Test and design methods for steel fibre reinforced concrete - Bending test (Final Recommendation). *Materials and Structures/Materiaux et Constructions* 35(253), pp. 579–582. Available at: http://dx.doi.org/10.1617/13884.

Roussel, N., Lemaître, A., Flatt, R.J. and Coussot, P. 2010. Steady state flow of cement suspensions: A micromechanical state of the art. *Cement and Concrete Research* 40(1), pp. 77–84. Available at: http://dx.doi.org/10.1016/j.cemconres.2009.08.026.

Saak, A.W., Jennings, H.M. and Shah, S.P. 2001. New methodology for designing self-compacting concrete. *Materials Journal* 98(6), pp. 429–439.

Şahin, Y. and Köksal, F. 2011. The influences of matrix and steel fibre tensile strengths on the fracture energy of high-strength concrete. *Construction and Building Materials* 25(4), pp. 1801–1806. Available at: http://dx.doi.org/10.1016/j.conbuildmat.2010.11.084.

Salas, A., Delvasto, S., de Gutierrez, R.M. and Lange, D. 2009. Comparison of two processes for treating rice husk ash for use in high performance concrete. *Cement and Concrete Research* 39(9), pp. 773–778. Available at: http://dx.doi.org/10.1016/j.cemconres.2009.05.006.

Santos, A.C.P., Ortiz-Lozano, J.A., Villegas, N. and Aguado, A. 2015. Experimental study about the effects of granular skeleton distribution on the mechanical properties of self-compacting concrete (SCC). *Construction and Building Materials* 78, pp. 40–49. Available at: http://dx.doi.org/10.1016/j.conbuildmat.2015.01.006.

Schlumpf, J. 2004. Self-compacting concrete structures in Switzerland. *Tunnelling and Underground Space Technology* 19(4–5), p. 480. http://dx.doi.org/10.1016/j.tust.2004.02.080.

De Schutter, G., J. M. Bartos, P., Domone, P. and Gibbs, J. 2008. *Self-compacting concrete*. Whittles Pub.

Sharma, R., Mahajan, P. and Mittal, R.K. 2013. Elastic modulus of 3D carbon/carbon composite using image-based finite element simulations and experiments. *Composite Structures* 98, pp. 69–78. Available at: http://dx.doi.org/10.1016/j.compstruct.2012.11.019.

Shi, C., Wu, Z., Lv, K. and Wu, L. 2015. A review on mixture design methods for self-compacting concrete. *Construction and Building Materials* 84, pp. 387–398. Available at: http://dx.doi.org/10.1016/j.conbuildmat.2015.03.079.

Shuguang, L. and Qingbin, L. 2015. Method of meshing ITZ structure in 3D meso-level finite element analysis for concrete. *Finite Elements in Analysis and Design* 93(C), pp. 96–106. http://dx.doi.org/10.1016/j.finel.2014.09.006.

Sivakrishna, A., Adesina, A., Awoyera, P.O. and Kumar, K.R. 2020. Green concrete: A review of recent developments. *Materials Today: Proceedings* 27, pp. 54–58. Available at: https://doi.org/10.1016/j.matpr.2019.08.202.

Sivanantham, P.A., Prabhu, G.G., Vimal Arokiaraj, G.G. and Sunil, K. 2022. Effect of Fibre Aspect-Ratio on the Fresh and Strength Properties of Steel Fibre Reinforced Self-Compacting Concrete. *Advances in Materials Science and Engineering* 2022. Available at: http://dx.doi.org/10.1155/2022/1207273.

Skarendahl, Å. 2000. Environment. In: Petersson, Å. S. and Ö. ed. *Self-Compacting Concrete - State-of-the-Art Report of RILEM TC 174-SCC*. pp. 91–92.

Sonebi, M. and Yahia, A. 2020. Mix design procedure, tests, and standards. In: *Self-Compacting Concrete: Materials, Properties and Applications*. Elsevier Inc., pp. 1–30. Available at: http://dx.doi.org/10.1016/B978-0-12-817369-5.00001-5.

Sorelli, L., Constantinides, G., Ulm, F.J. and Toutlemonde, F. 2008. The nano-mechanical signature of Ultra High Performance Concrete by statistical nanoindentation techniques. *Cement and Concrete Research* 38(12), pp. 1447–1456. Available at: http://dx.doi.org/10.1016/j.cemconres.2008.09.002.

Stefaniuk, D., Niewiadomski, P., Musiał, M. and Łydżba, D. 2019. Elastic properties of self-compacting concrete modified with nanoparticles: Multiscale approach. *Archives of Civil and Mechanical Engineering* 19(4), pp. 1150–1162. http://dx.doi.org/10.1016/j.acme.2019.06.006.

Stock, A.F., Hannant, D.J., Williams, R.I.T. and Hobbs, D.W. 1980. The effect of aggregate concentration upon the strength and modulus of elasticity of concrete. *Magazine of Concrete Research* 32(113), pp. 246–250. http://dx.doi.org/10.1680/macr.1980.32.113.246.

Struble, L. and Sun, G.K. 1995. Viscosity of Portland cement paste as a function of concentration. *Advanced Cement Based Materials* 2(2), pp. 62–69. http://dx.doi.org/10.1016/1065-7355(95)90026-8.

Sun, X., Gao, Z., Cao, P. and Zhou, C. 2019. Mechanical properties tests and multiscale numerical simulations for basalt fiber reinforced concrete. *Construction and Building Materials* 202, pp. 58–72. Available at: https://doi.org/10.1016/j.conbuildmat.2019.01.018.

Tangtermsirkul, S. and Khayat, K. 2000. Fresh concrete: properties and tests. In: *Self-Compacting Concrete - State-of-the-Art Report of RILEM TC 174-SCC*. pp. 17–22.

Thomas, B.S. 2018. Green concrete partially comprised of rice husk ash as a supplementary cementitious material – A comprehensive review. *Renewable and Sustainable Energy Reviews* 82(July 2016), pp. 3913–3923. Available at: https://doi.org/10.1016/j.rser.2017.10.081.

Thomas, B.S. et al. 2021. Sugarcane bagasse ash as supplementary cementitious material in concrete – a review. *Materials Today Sustainability* 15. Available at: https://doi.org/10.1016/j.mtsust.2021.100086.

Trindade, Y.T., Bitencourt, L.A.G., Monte, R., de Figueiredo, A.D. and Manzoli, O.L. 2020. Design of SFRC members aided by a multiscale model: Part I – Predicting the post-cracking parameters. *Composite Structures* 241. http://dx.doi.org/10.1016/j.compstruct.2020.112078.

Vasilić, K. 2015. *A Numerical Model for Self-Compacting Concrete Flow through Reinforced Sections : a Porous Medium Analogy*.

Vilanova, A., Fernandez-Gomez, J. and Landsberger, G.A. 2011. Evaluation of the mechanical properties of self compacting concrete using current estimating models: Estimating the modulus of elasticity, tensile strength, and modulus of rupture of self compacting concrete. *Construction and Building Materials* 25(8), pp. 3417–3426. Available at: http://dx.doi.org/10.1016/j.conbuildmat.2011.03.033.

Vivek, S.S. 2021. Performance of ternary blend SCC with ground granulated blast furnace slag and metakaolin. In: *Materials Today: Proceedings*. Elsevier Ltd, pp. 1337–1344. https://doi.org/10.1016/j.matpr.2021.06.422.

Van Der Vurst, F., Grünewald, S., Feys, D., Lesage, K., Vandewalle, L., Vantomme, J. and De Schutter, G. 2017. Effect of the mix design on the robustness of fresh self-compacting concrete. *Cement and Concrete Composites* 82, pp. 190–201. Available at: http://dx.doi.org/10.1016/j.cemconcomp.2017.06.005.

Wallevik, J.E. 2009. Rheological properties of cement paste: Thixotropic behavior and structural breakdown. *Cement and Concrete Research* 39(1), pp. 14–29. Available at: https://doi.org/10.1016/j.cemconres.2008.10.001.

Wallevik, O.H. and Wallevik, J.E. 2011. Rheology as a tool in concrete science: The use of rheographs and workability boxes. *Cement and Concrete Research* 41(12), pp. 1279–1288. Available at: http://dx.doi.org/10.1016/j.cemconres.2011.01.009.

Wang, J.J., Wang, Y.F., Sun, Y.W., Tingley, D.D. and Zhang, Y.R. 2017. Life cycle sustainability assessment of fly ash concrete structures. *Renewable and Sustainable Energy Reviews* 80(September 2016), pp. 1162–1174. Available at: http://dx.doi.org/10.1016/j.rser.2017.05.232.

Wang, W., Shen, A., Lyu, Z., He, Z. and Nguyen, K.T.Q. 2021. Fresh and rheological characteristics of fiber reinforced concrete——A review. *Construction and Building Materials* 296, p. 123734. Available at: https://doi.org/10.1016/j.conbuildmat.2021.123734.

Wang, X., Wang, K., Taylor, P. and Morcous, G. 2014. Assessing particle packing based self-consolidating concrete mix design method. *Construction and Building Materials* 70, pp. 439–452. Available at: https://doi.org/10.1016/j.conbuildmat.2014.08.002.

Weng, Y., Lu, B., Li, M., Liu, Z., Tan, M.J. and Qian, S. 2018. Empirical models to predict rheological properties of fiber reinforced cementitious composites for 3D printing. *Construction and Building Materials* 189, pp. 676–685. Available at: https://doi.org/10.1016/j.conbuildmat.2018.09.039.

Wong, R.C.K. and Chau, K.T. 2005. Estimation of air void and aggregate spatial distributions in concrete under uniaxial compression using computer tomography scanning. *Cement and Concrete Research* 35(8), pp. 1566–1576. Available at: https://doi.org/10.1016/j.cemconres.2004.08.016.

Wu, Z., Shi, C. and Khayat, K.H. 2019. Investigation of mechanical properties and shrinkage of ultra-high-performance concrete: Influence of steel fiber content and shape. *Composites Part B: Engineering* 174(March), p. 107021. Available at: https://doi.org/10.1016/j.compositesb.2019.107021.

Xu, L., Wu, F., Chi, Y., Cheng, P., Zeng, Y. and Chen, Q. 2019. Effects of coarse aggregate and steel fibre contents on mechanical properties of high-performance concrete. *Construction and Building Materials* 206, pp. 97–110. Available at: https://doi.org/10.1016/j.conbuildmat.2019.01.190.

Yardimci, M.Y., Baradan, B. and Taşdemir, M.A. 2014. Effect of fine to coarse aggregate ratio on the rheology and fracture energy of steel fibre reinforced self-compacting concretes. *Sadhana* 39(6), pp. 1447–1469. Available at: https://doi.org/10.1007/s12046-014-0257-2.

Yen, T., Tang, C.W., Chang, C.S. and Chen, K.H. 1999. Flow behaviour of high strength high-performance concrete. *Cement and Concrete Composites* 21(5–6), pp. 413–424. https://doi.org/10.1016/S0958-9465(99)00026-8

Yoo, D.Y., Banthia, N. and Yoon, Y.S. 2016. Predicting the flexural behavior of ultra-high-performance fiber-reinforced concrete. *Cement and Concrete Composites* 74, pp. 71–87. Available at: http://dx.doi.org/10.1016/j.cemconcomp.2016.09.005.

Yousuf, S., Sanchez, L.F.M. and Shammeh, S.A. 2019. The use of particle packing models (PPMs) to design structural low cement concrete as an alternative for construction industry. *Journal of Building Engineering* 25. https://doi.org/10.1016/j.jobe.2019.100815.

Yu, J., Zhang, B., Chen, W. and He, J. 2020. Experimental and multi-scale numerical investigation of ultra-high performance fiber reinforced concrete (UHPFRC) with different coarse aggregate content and fiber volume fraction. *Construction and Building Materials* 260, p. 120444. Available at: https://doi.org/10.1016/j.conbuildmat.2020.120444.

Yu, R.C., Cifuentes, H., Rivero, I., Ruiz, G. and Zhang, X. 2016. Dynamic fracture behaviour in fibre-reinforced cementitious composites. *Journal of the Mechanics and Physics of Solids* 93, pp. 135–152. Available at: http://dx.doi.org/10.1016/j.jmps.2015.12.025.

Zerbino, R., Tobes, J.M., Bossio, M.E. and Giaccio, G. 2012. On the orientation of fibres in structural members fabricated with self compacting fibre reinforced concrete. *Cement and Concrete Composites* 34(2), pp. 191–200. Available at: http://dx.doi.org/10.1016/j.cemconcomp.2011.09.005.

Zhang, J.L., Liu, X., Yuan, Y. and Mang, H.A. 2015. Multiscale modeling of the effect of the interfacial transition zone on the modulus of elasticity of fiber-reinforced fine concrete. *Computational Mechanics* 55(1), pp. 37–55. Available at: https://doi.org/10.1007/s00466-014-1081-6.

Zhang, P., Wang, C., Gao, Z. and Wang, F. 2023. A review on fracture properties of steel fiber reinforced concrete. *Journal of Building Engineering* 67(January), p. 105975. Available at: https://doi.org/10.1016/j.jobe.2023.105975.

Zhang, S., Liao, L., Song, S. and Zhang, C. 2018. Experimental and analytical study of the fibre distribution in SFRC: A comparison between image processing and the inductive test. *Composite Structures* 188(September 2017), pp. 78–88. Available at: https://doi.org/10.1016/j.compstruct.2018.01.006.

Zhang, S., Zhang, C., Liao, L., Wang, C. and Zhao, R. 2020. Investigation into the effect of fibre distribution on the post-cracking tensile strength of SFRC through physical experimentation and numerical simulation. *Construction and Building Materials* 248, p. 118433. Available at: https://doi.org/10.1016/j.conbuildmat.2020.118433.

Zhao, Y., Bi, J., Huo, L., Wang, Z., Guan, J. and Zhao, Y. 2021a. Development of a coupled numerical framework of steel fiber reinforced self-compacting concrete. *Construction and Building Materials* 303(August), p. 124582. Available at: https://doi.org/10.1016/j.conbuildmat.2021.124582.

Zhao, Y., Bi, J., Wang, Z., Huo, L., Guan, J., Zhao, Y. and Sun, Y. 2021b. Numerical simulation of the casting process of steel fiber reinforced self-compacting concrete: Influence of material and casting parameters on fiber orientation and distribution. *Construction and Building Materials* 312(October), p. 125337. Available at: https://doi.org/10.1016/j.conbuildmat.2021.125337.

Zhou, B. and Uchida, Y. 2017. Relationship between fiber orientation/distribution and post-cracking behaviour in ultra-high-performance fiber-reinforced concrete (UHPFRC). *Cement and Concrete Composites* 83, pp. 66–75. Available at: http://dx.doi.org/10.1016/j.cemconcomp.2017.07.007.

Zhou, F.P., Lydon, F.D. and Barr, B.I.G. 1995. Effect of coarse aggregate on elastic modulus and compressive strength of high-performance concrete. *Cement and Concrete Research* 25(1), pp. 177–186.

Zhu, W. 2020. Permeation properties of self-compaction concrete. In: *Self-Compacting Concrete: Materials, Properties and Applications*. Elsevier Inc., pp. 117–130. Available at: http://dx.doi.org/10.1016/B978-0-12-817369-5.00005-2.

Appendix A MATLAB Programming

```
%*********************************************************************
% % Cardiff University - School of Engineering
% Custom MATLAB Script for Optimizing High-Strength Self-Compacting Concrete Mix Design, 2022
% Developed to achieve specified compressive strength and optimize plastic viscosity based on the method in chapter 3 and the MATLAB code in Abo Dhaheer, M. 2016. Design and properties of self-compacting concrete mixes and their simulation in the J-Ring test.

%*********************************************************************
% Variable Definitions
% Name Description
% ----- ------------
% WCM Ratio of water to binder materials
% PV Calculated paste viscosity, dependent on water/binder ratio and super-plasticizer dosage
% TMV Desired viscosity for the concrete mix
% Z, U, X Variables used in solving the mix design equations
% t1, t2 Coefficients chosen such that their product equals 1, used in formulation calculations
% H Unity factor, defined as the product of t1 and t2
% CM Total weight of SCMs used in the mix
% WTR Total water content in kilograms
% CEM Total cement content in kilograms
% GG Cement replacement materials (kg) e.g. ggbs
% FLA Weight of fly ash used in the mix (kg)
% SP Amount of super-plasticizer added (kg)
% VPS Total volume of paste in the mix per cubic meter
% FS Proportion of fine aggregates in the mix
% FG Proportion of coarse aggregates in the mix
% WS Weight of fine aggregates (kg)
% WG Weight of coarse aggregates (kg)
% VS Volume of fine aggregate per cubic meter
% VG Volume of coarse aggregate per cubic meter
```

```
% TV Overall volume of the concrete mix (cubic meters)
% PSRATIO Ratio of paste to solid materials in the mix
% FFS Adjustment factor for viscosity change due to fine aggregate addition
% FFG Adjustment factor for viscosity change due to coarse aggregate addition
% AMV Calculated actual mix plastic viscosity using a micromechanical approach
% ERR Deviation between the target and actual mix viscosities, expressed as a percentage
% PWDR Total content of powdery materials
% WTPR Water to powder ratio
% FIRSTLINE Normalized content of binder materials
% SECONDLINE Normalized content including binder materials, and fine aggregates
% THIRDLIN Normalized content covering binders, fillers, fine and coarse aggregates
%**********************************************************************
%**********************************************************************
%**********************************************************************
%**********************************************************************
clear
clc
% Input water to binder (cementitious materials) ratio from Eq. 3.1
WCM=0.26;    %C100
% Input the paste viscosity from Table 3.1
PV=0.39;
%**********************************************************************
s=0;
p=0;
for TMV=5:0.05:15
Z=0.63^ (-1.9)*0.74^ (-1.9);
U= (TMV/PV*Z) ^ (-1/1.9);
X=U^ (1/2);
t1=0.63/X ;
t2=0.74/X ;
a=linspace (0, t1, 500) ;
b=linspace (0, t2, 500) ;
```

```
for i= 1:500
for j= 1:500


H=a (i)*b (j);
if (H<=1.0001 && H>=0.9999)
s=s+1;
% Input the cementitious materials contents limits
for CM=380:5:600
WTR(s) =CM*WCM;
CEM(s) =0.6*CM;
GG(s) =0.2*CM;
FLA(s)=0.2*CM;
SP(s) =0.01*CM;  %change the dosage of SP
VPS(s) =CEM(s)/3150+GG(s)/2400+FLA(s)/2400+WTR(s)/1000+SP(s)/1070+0.02;

FS(s) =0.63-a (i)*X;
FG(s) =0.74-b (j)*X;

WS(s) =2550*FS(s)*VPS(s)/(1-FS(s));
WG(s) =2650*FG(s)*(VPS(s) + (WS(s)/2550))/ (1-FG(s));

VS(s) =WS(s)/2550;
VG(s) =WG(s)/2650;
TV(s) =VS(s) +VG(s) +VPS(s)-0.02;

WCEMnew(s) =CEM(s)*0.98/TV(s);
WGGnew(s) =GG(s)*0.98/TV(s);
WFLAnew(s) =FLA(s)*0.98/TV(s);
WWTRnew(s) =WTR(s)*0.98/TV(s);
WSPnew(s) =SP(s)*0.98/TV(s);
```

```
WSnew(s) =WS(s)*0.98/TV(s);
WGnew(s) =WG(s)*0.98/TV(s);

VCEMnew(s) =WCEMnew(s)/3150;
VGGnew(s) =WGGnew(s)/2400;
VFLAnew(s) =WFLAnew(s)/2400;
VWTRnew(s) =WWTRnew(s)/1000;
VSPnew(s) =WSPnew(s)/1070;
VSnew(s) =WSnew(s)/2550;
VGnew(s) =WGnew(s)/2650;

TVnew(s) =VCEMnew(s) +VGGnew(s)+VFLAnew(s) +VWTRnew(s) +VSPnew(s) +VSnew(s)
+VGnew(s) +0.02;
WCMnew(s) =WCEMnew(s) +WGGnew(s)+WFLAnew(s);
STAG(s) =VSnew(s)/ (VSnew(s) +VGnew(s))*100;
GTAG(s) =VGnew(s)/ (VSnew(s) +VGnew(s))*100;
VPSnew(s) =VCEMnew(s) +VGGnew(s) +VFLAnew(s)+VWTRnew(s) +VSPnew(s) +0.02;
PSRATIO(s) = VPSnew(s)/ (VSnew(s) +VGnew(s));
FSnew(s) =VSnew(s)/ (VSnew(s)  +VPSnew(s));
FGnew(s) =VGnew(s)/ (VGnew(s) +VSnew(s)  +VPSnew(s));

FFS(s) = (1-FSnew(s)/0.63) ^ (-1.9);
FFG(s) = (1-FGnew(s)/0.74) ^ (-1.9);
AMV(s) =PV*FFS(s)*FFG(s);

ERR(s) = (AMV(s)-TMV)/TMV*100;
PWDR=WCMnew(s);
WTPR(s) =VWTRnew(s)/ (VCEMnew(s) +VGGnew(s)+VFLAnew(s))*100;
 A=TVnew(s);
 C=WSnew(s);
 D=WGnew(s);
 E=STAG(s);
```

```
F=GTAG(s);
G=PSRATIO(s);
I=AMV(s);
L=ERR(s);
J=WTPR(s);
K=WCMnew(s);
R=WSPnew(s);
WCMRnew(s) =WWTRnew(s)/WCMnew(s);
EEE=WCMRnew(s);
WWTR=WWTRnew(s);

% Check the typical range of SCC mix compositions according to EFNARC

if (WWTR>=150 && WWTR<=210)
if (D>=750 && D<=1000)

if (E>=48 && E<=55)
% Check the percentage difference between (TMV) and (AMV)
if (L>=-5 && L<=5)

p=p+1;
AA (p) =K/I;
CC (p) =(K+C)/I;
DD (p) =(K+C+D)/I;
EE (p) =C/I;
FF (p) =D/I;
TT (p) =(C+D)/I;
StoTOTAL (p) =E/I;
CMplusSAND (p) = (K+C)/I;

AAA=AA (p);
CCC=CC (p);
```

```
DDD=DD (p);
GGG=EE (p);
FFF=FF (p);
TTT=TT (p);
STST=StoTOTAL (p);
CMSAND=CMplusSAND (p);

TotalVolume (p) =A;
Sand (p) =C;
CoarseAGG (p) =D;
StoTAG (p) =E;
GtoTAG (p) =F;
PtoSRATIO (p) =G;
Viscosity (p) =I;
ERROR (p) =L;
SUPER (p) =R;
WATER (p) =WWTR;
CMmaterials (p) =K;
WtoPRatio (p) =J;
FIRSTLINE (p) =AAA;
SECONDLINE (p) =CCC;
THIRDHLINE (p) =DDD;
WATERtoCM (p) =EEE;
SANDtoVISCOSITY (p) =GGG;
GRAVELtoVISCOSITY (p) =FFF;
CAplusFA (p) =TTT;
StoTOTALAGG (p) =STST;
CMandSAND (p) =CMSAND;

 end
 end
 end
```

```
 end
 end
 end
end
end
end

%*********************************************************************
% print the results in order to plot the graphs
GtoTAG = round (GtoTAG);
Sand = round (Sand);
CoarseAGG = round (CoarseAGG);
StoTAG = round (StoTAG);
TotalVolume = round (TotalVolume*1000)/1000;
ERR = round (ERR);
PSRATIO = round (PSRATIO);
%*********************************************************************
%*********************************************************************
%*********************************************************************
% Desired parameters to be printed in the output sheet
myMatrix =
[CMmaterials;Sand;CoarseAGG;WATER;SUPER;TotalVolume;WATERtoCM;WtoPRatio;StoTAG;
GtoTAG;PtoSRATIO;ERROR;Viscosity;FIRSTLINE;SECONDLINE;THIRDLINE]';
HeaderNames='CMmaterials,Sand,CoarseAGG,WATER,SUPER,TotalVolume,WATERtoCM,Wto
PRatio,StoTAG,GtoTAG,PtoSRATIO,ERROR,Viscosity,FIRSTLINE,SECONDLINE,THIRDLINE';
%*********************************************************************
%*********************************************************************
%*********************************************************************
% preferable output sheet name printed here (change the underline text)
fileName ='Proportions for C70.csv';
outid = fopen (fileName, 'w+');
fprintf (outid, '%s', HeaderNames);
```

```
fclose (outid);
dlmwrite(fileName,myMatrix,'roffset',1,'-append', 'precision', 4);
% you may need to increase precision to allow all digits to be saved
disp (strcat ('Generated report ''', fileName,''''))
%*****************************************************************
%*****************************************************************
%*****************************************************************
```

Appendix B Load Deflection Curves

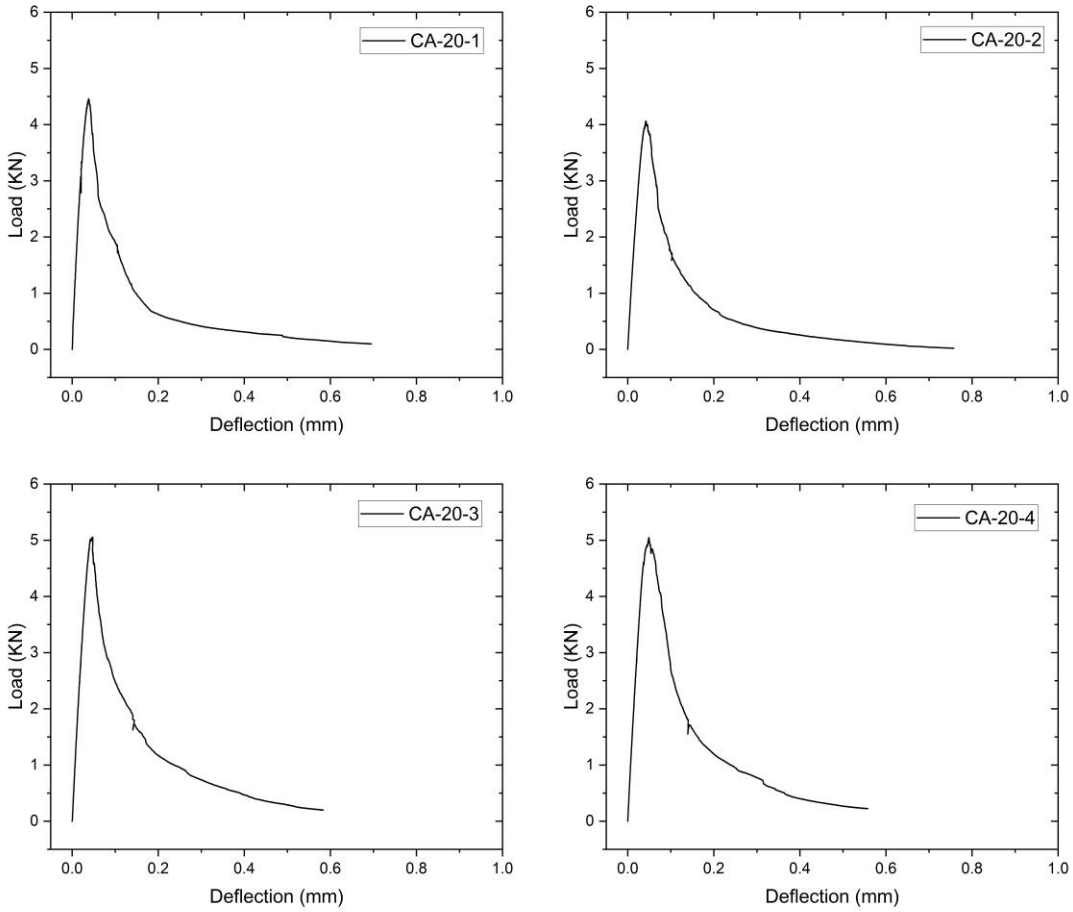

Figure B.1 Load-deflection curves for Mix CA-20 specimens

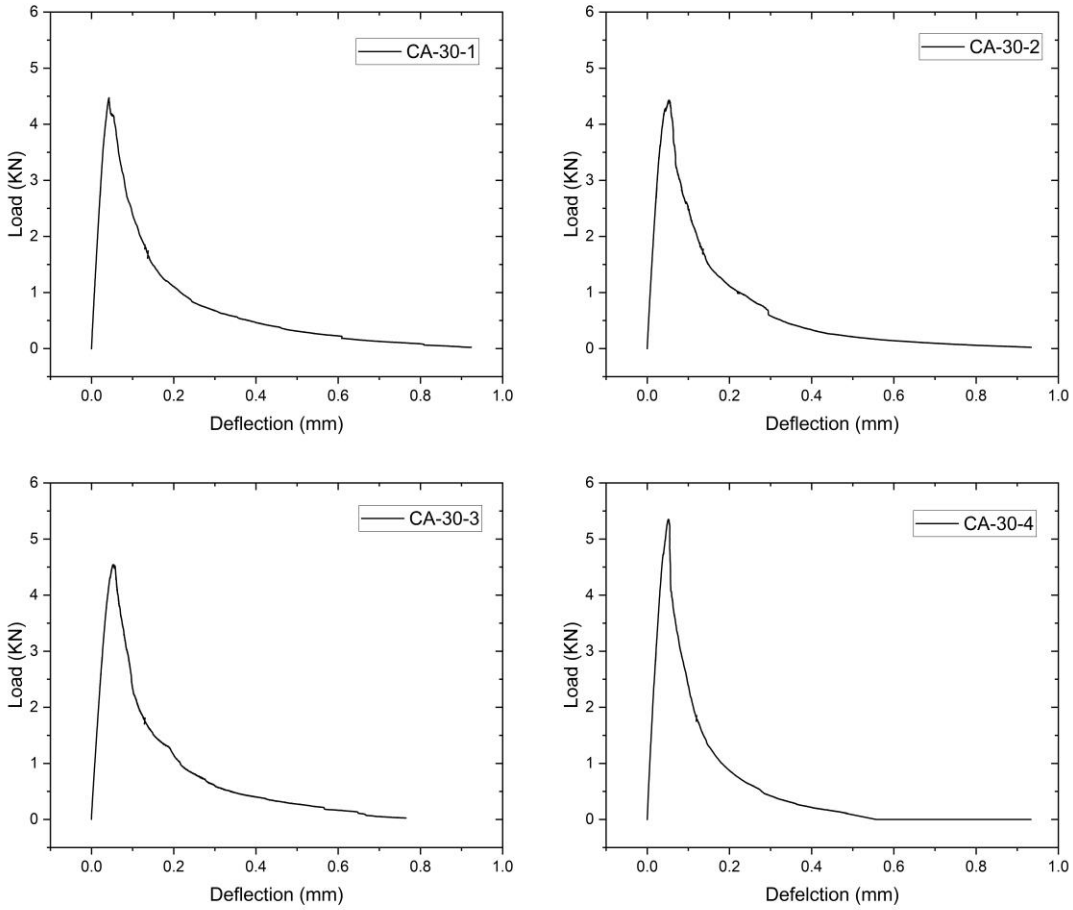

Figure B.2 Load-deflection curves for Mix CA-30 specimens

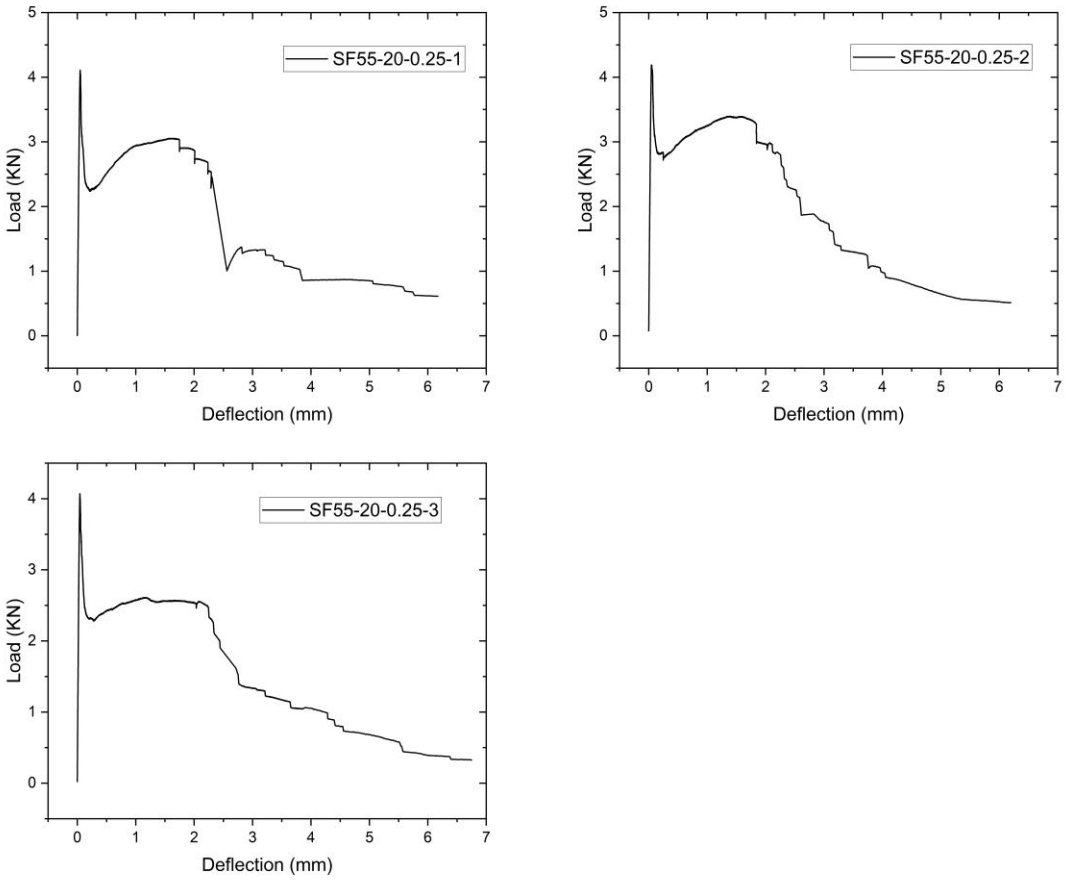

Figure B.3 Load-deflection curves for Mix SF55-20-0.25 specimens

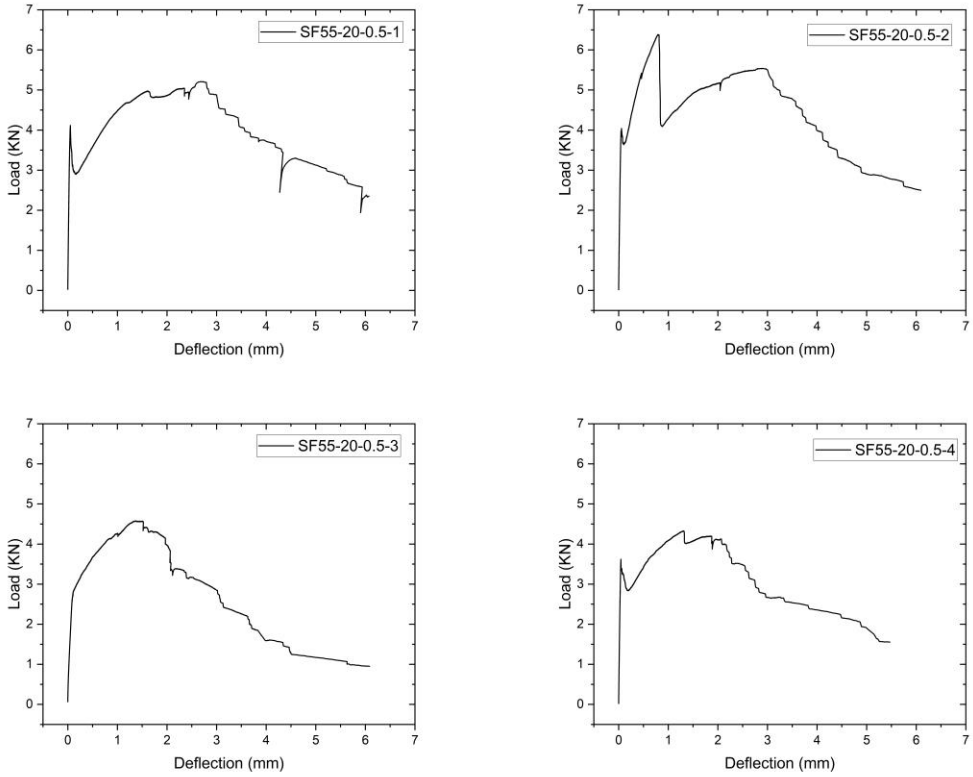

Figure B.4 Load-deflection curves for Mix SF55-20-0.5 specimens

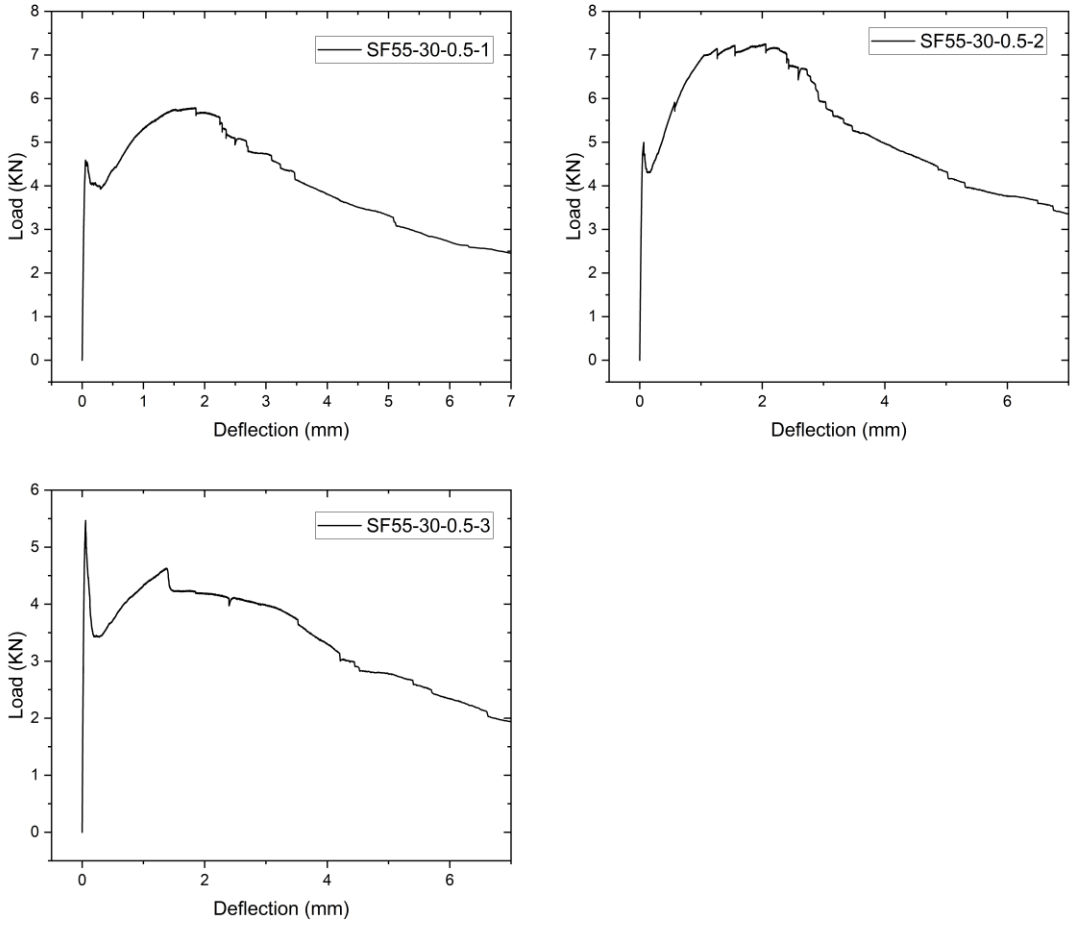

Figure B.5 Load-deflection curves for Mix SF55-30-0.5 specimens

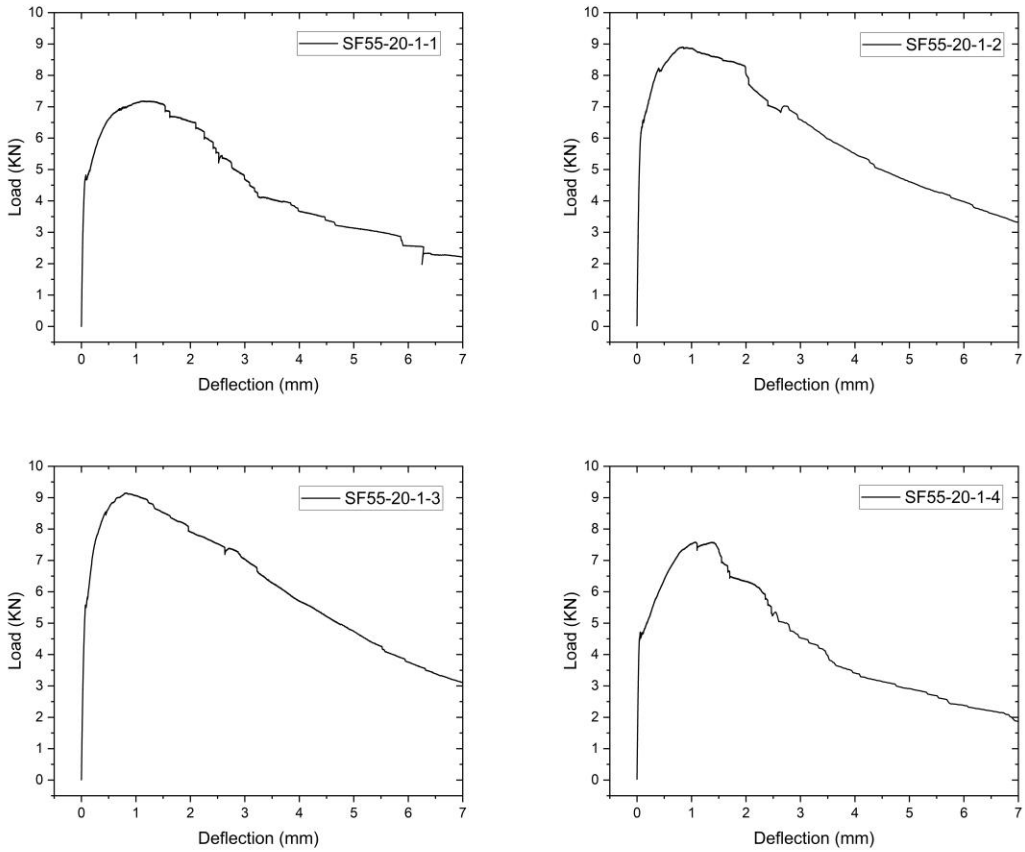

Figure B.6 Load-deflection curves for Mix SF55-20-1 specimens

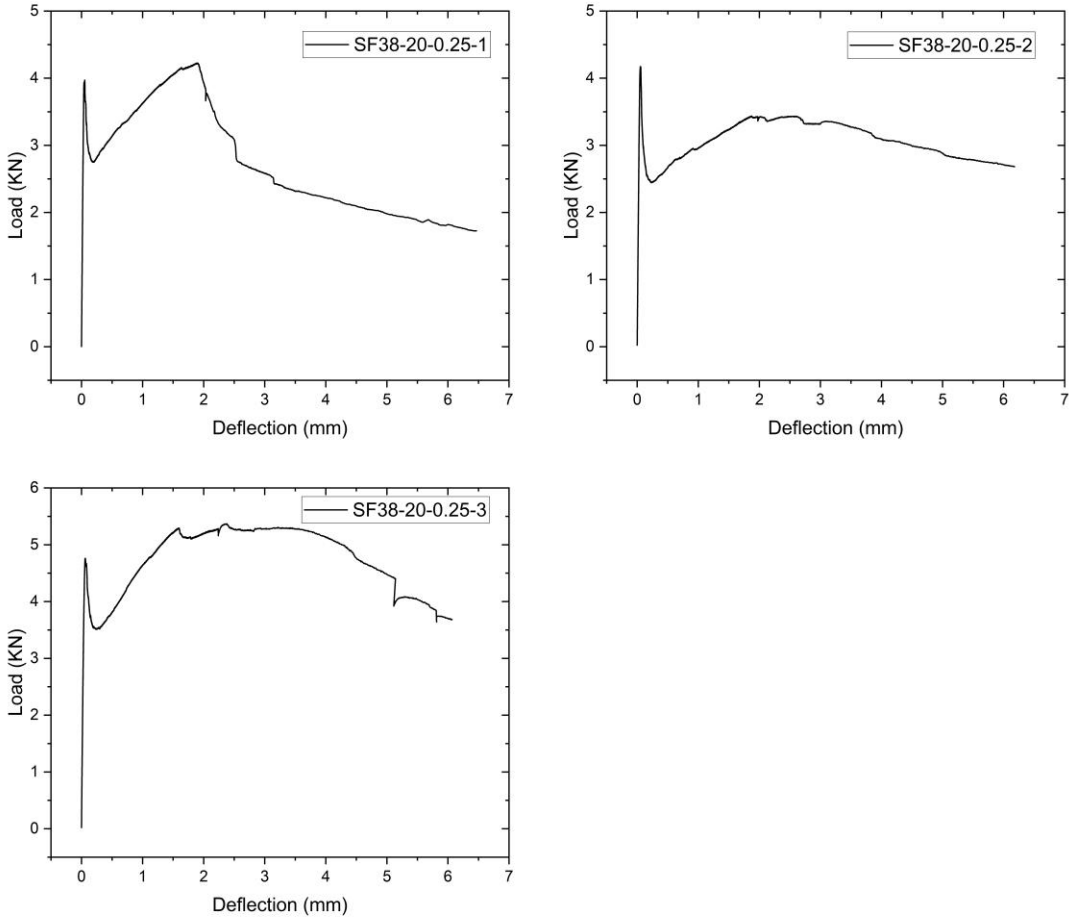

Figure B.7 Load-deflection curves for Mix SF38-20-0.25 specimens

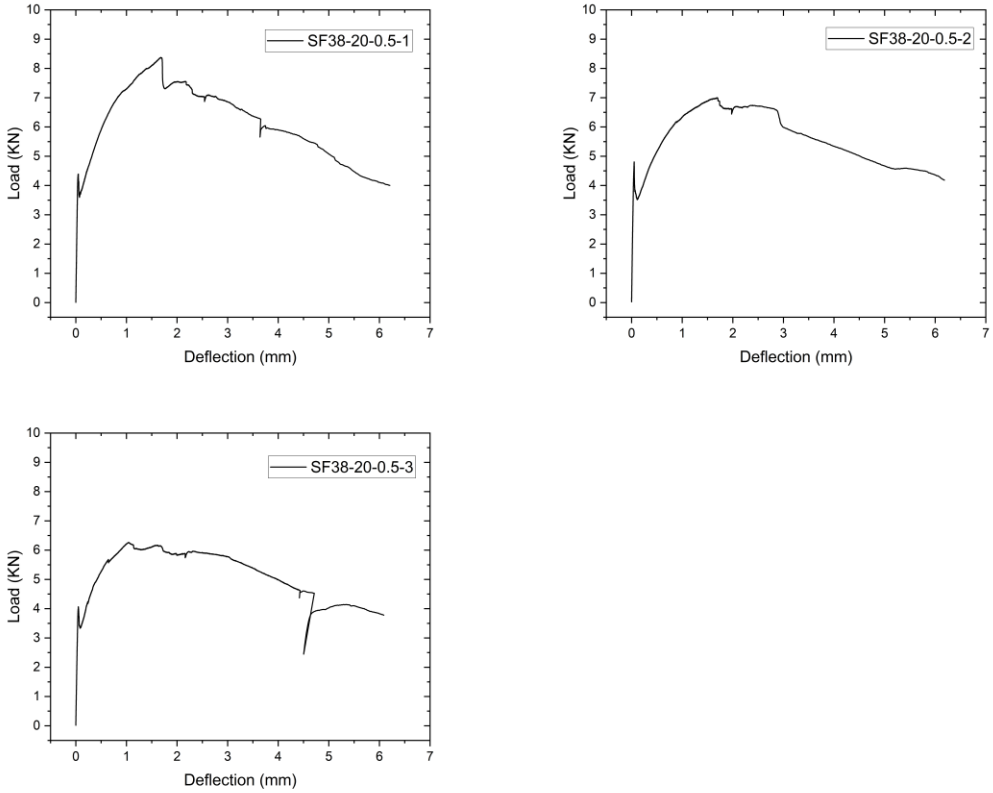

Figure B.8 Load-deflection curves for Mix SF38-20-0.5 specimens

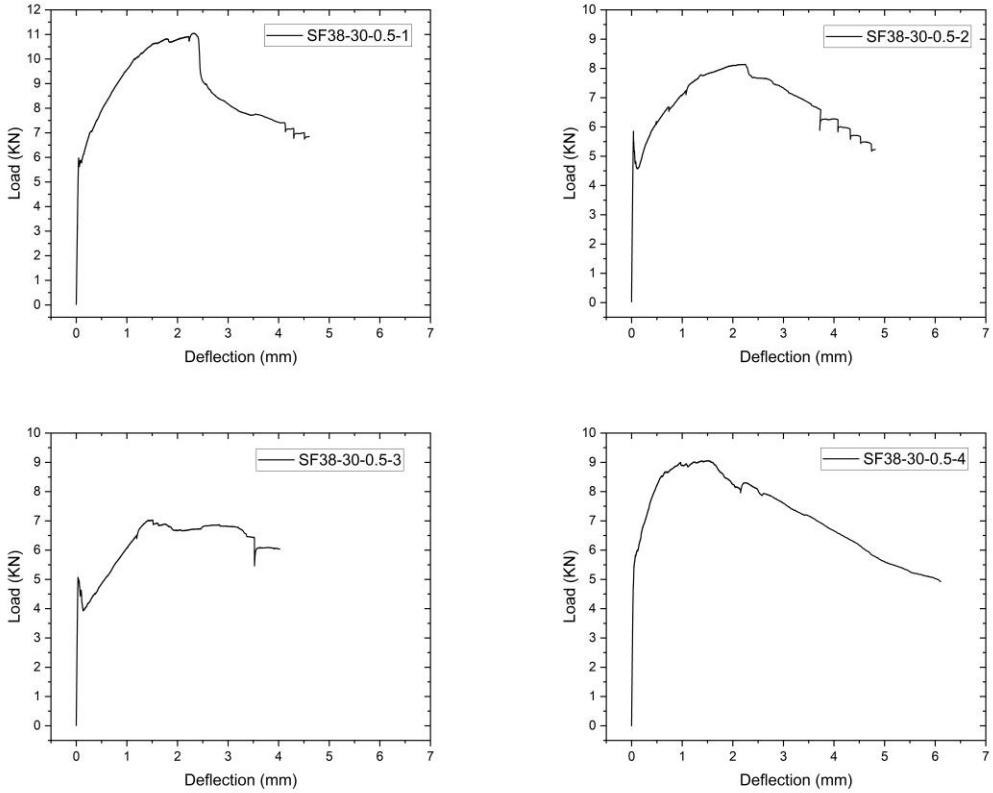

Figure B.9 Load-deflection curves for Mix SF38-30-0.5 specimens

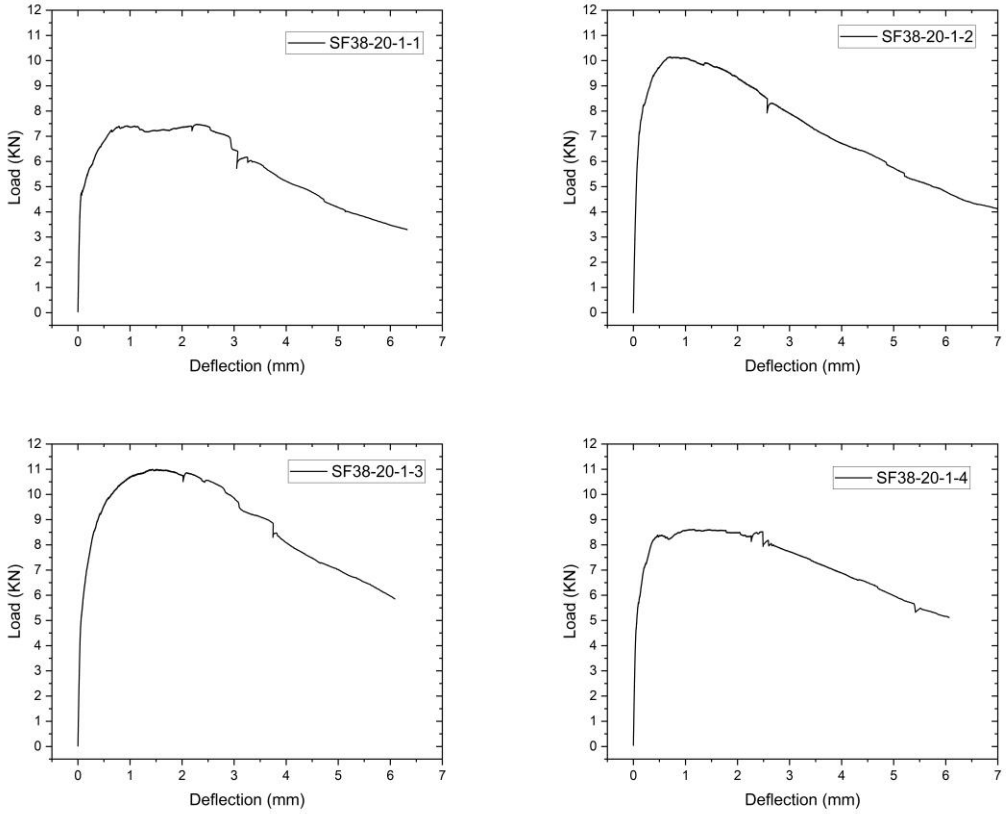

Figure B.10 Load-deflection curves for Mix SF38-20-1 specimens

Appendix C Load-CMOD Curves

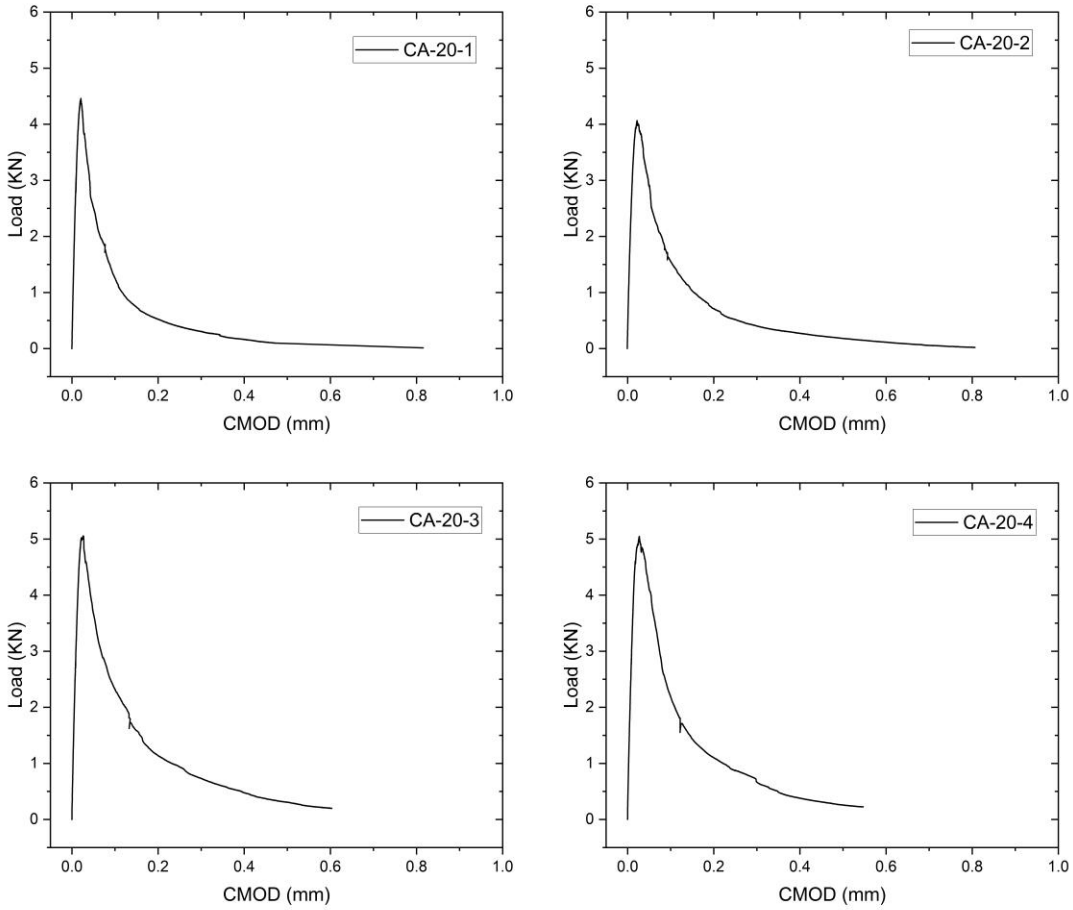

Figure C.1 Load-CMOD curves for Mix CA-20 specimens

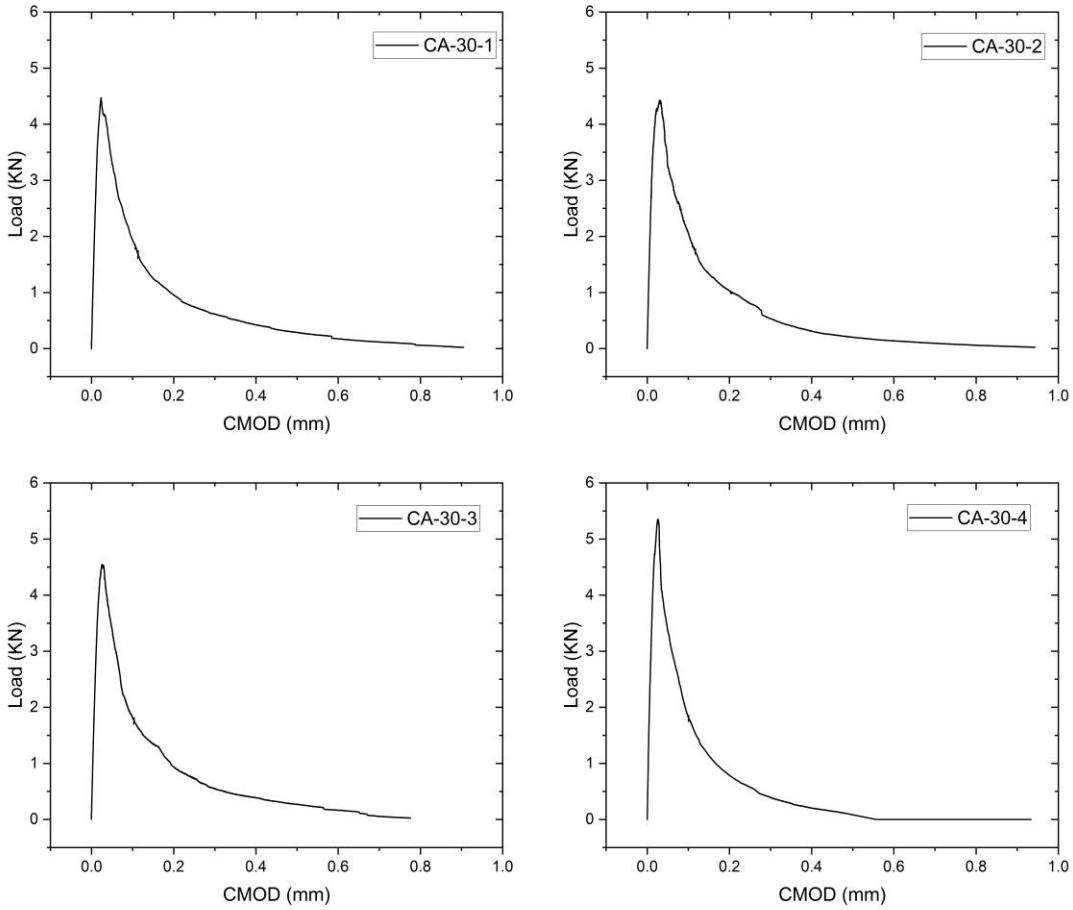

Figure C.2 Load-CMOD curves for Mix CA-30 specimens

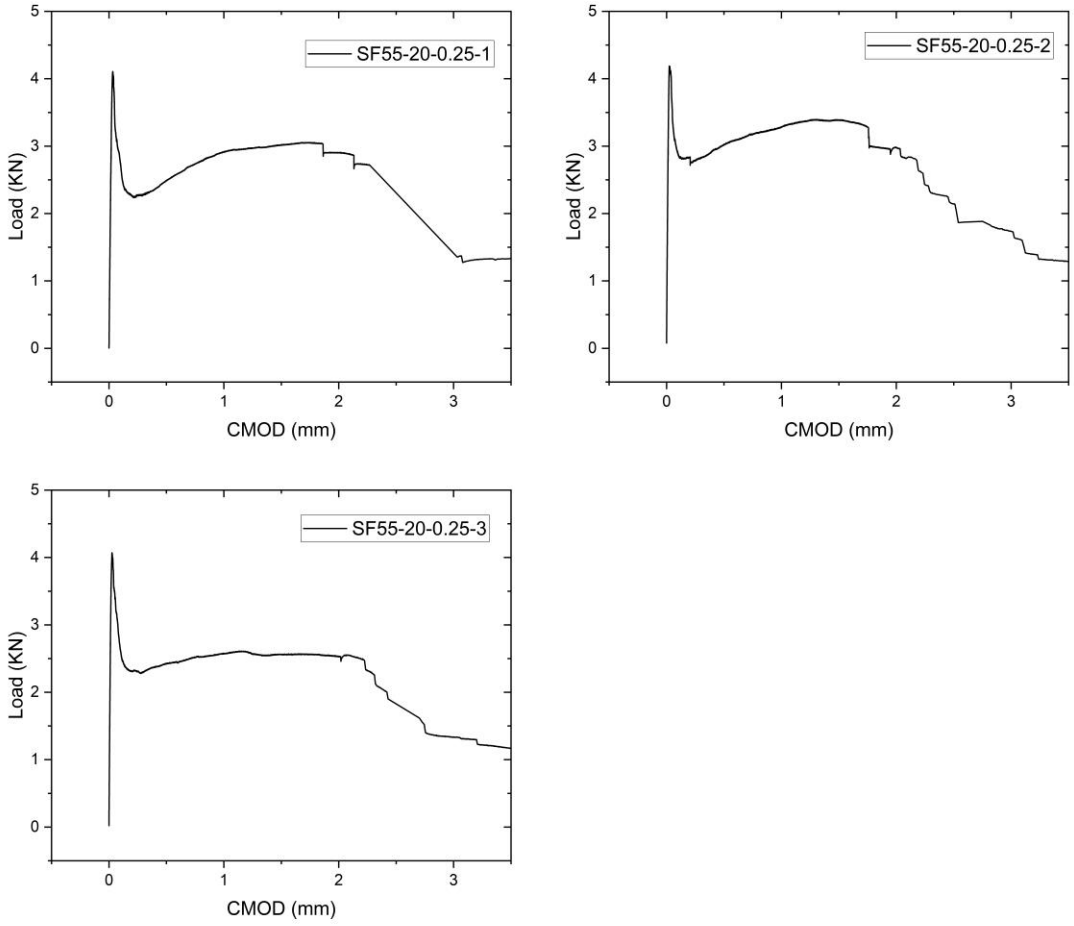

Figure C.3 Load-CMOD curves for Mix SF55-20-0.25 specimens

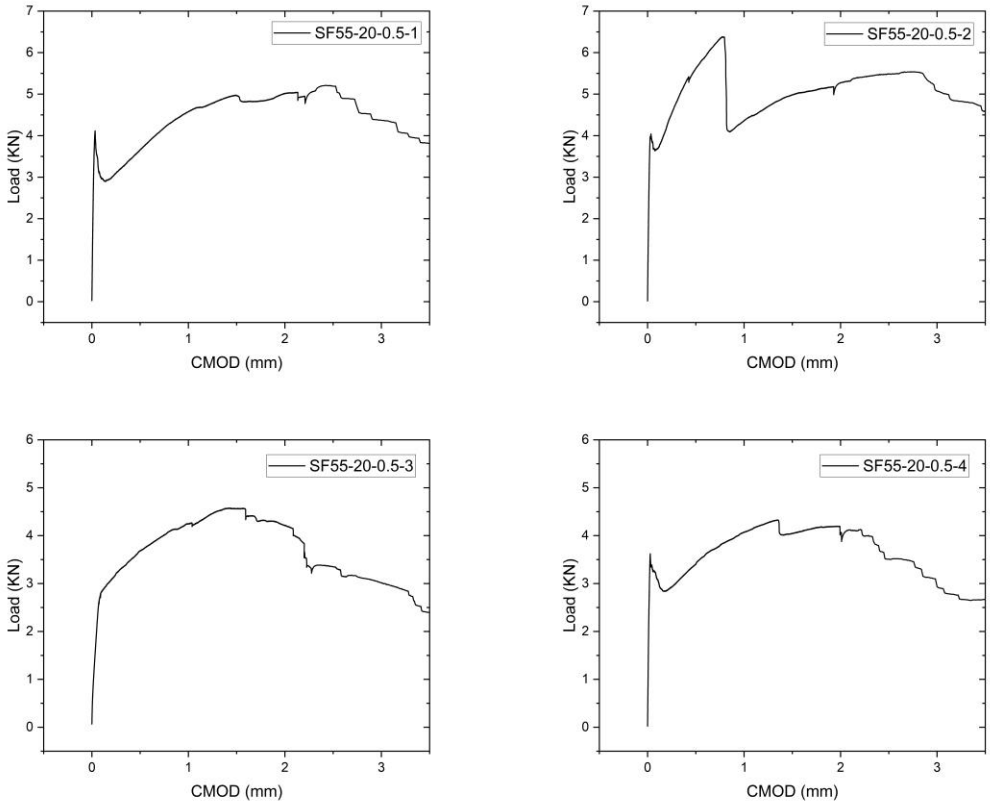

Figure C.4 Load-CMOD curves for Mix SF55-20-0.5 specimens

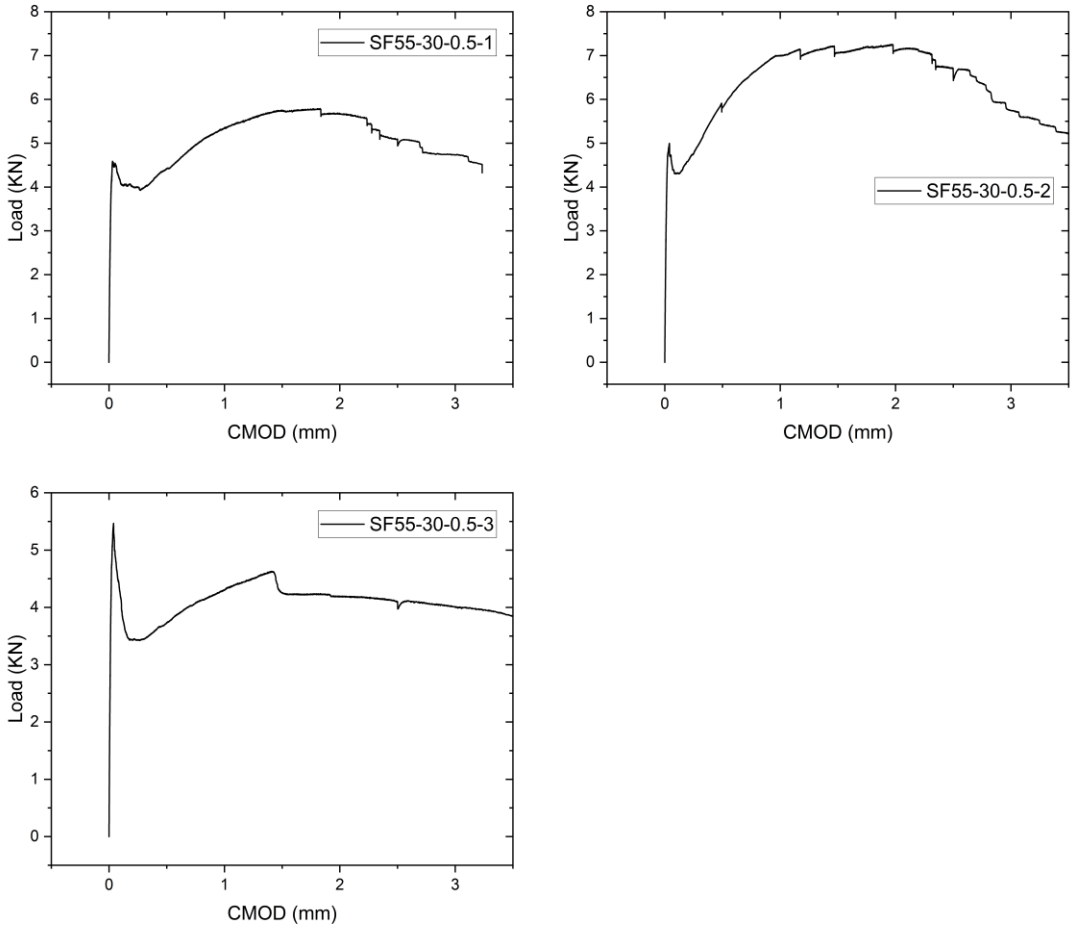

Figure C.5 Load-CMOD curves for Mix SF55-30-0.5 specimens

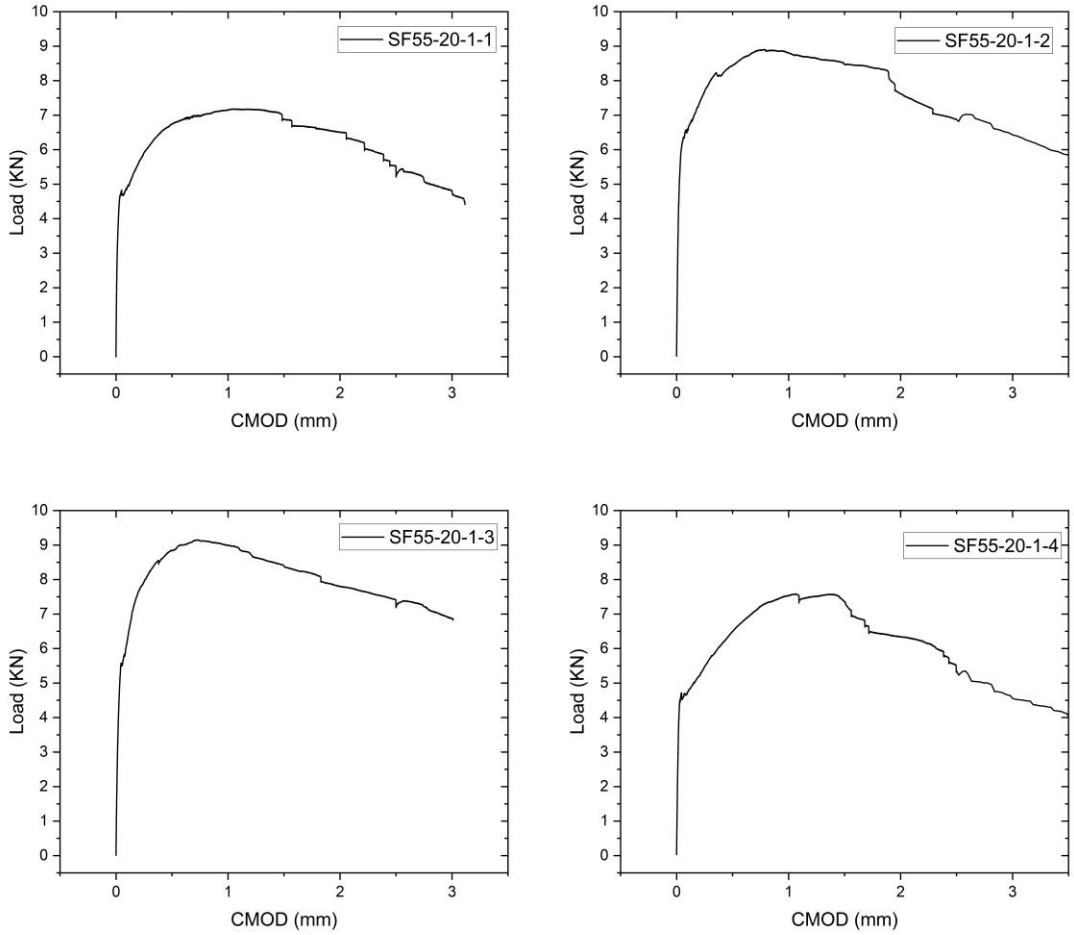

Figure C.6 Load-CMOD curves for Mix SF55-20-1 specimens

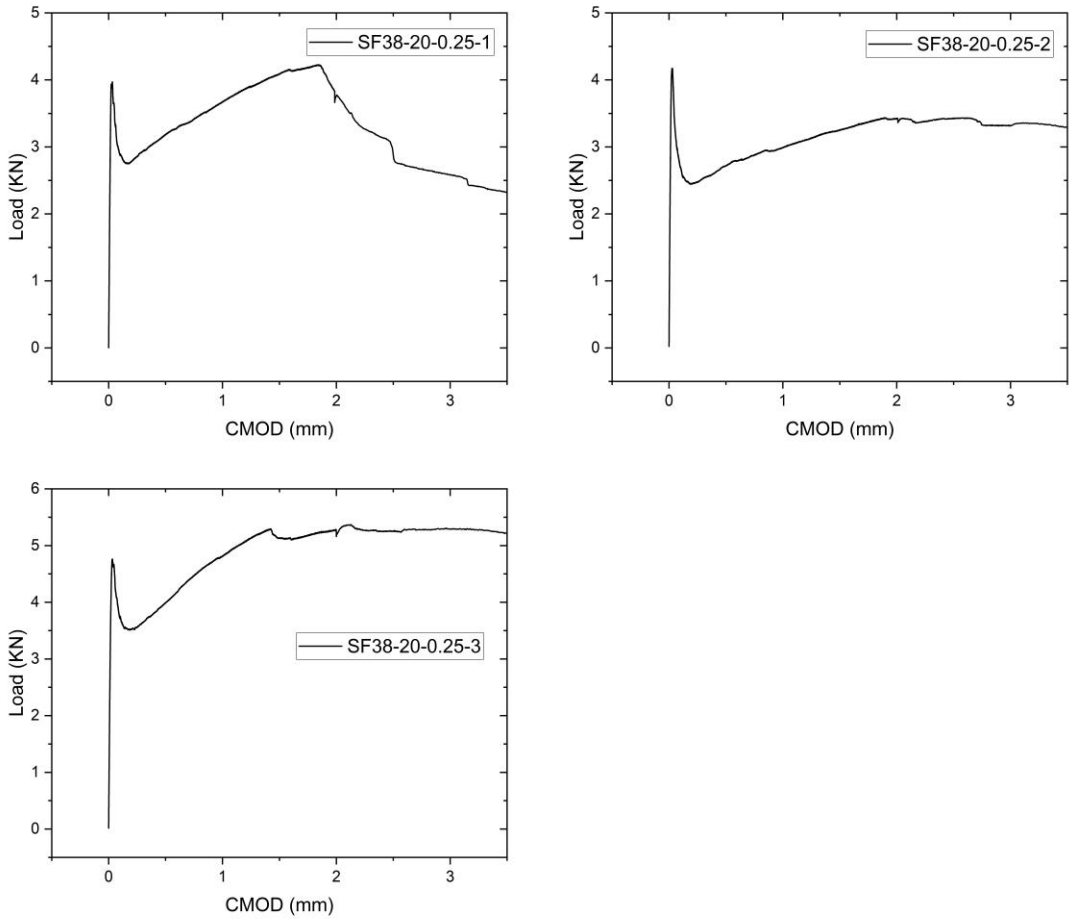

Figure C.7 Load-CMOD curves for Mix SF38-20-0.25 specimens

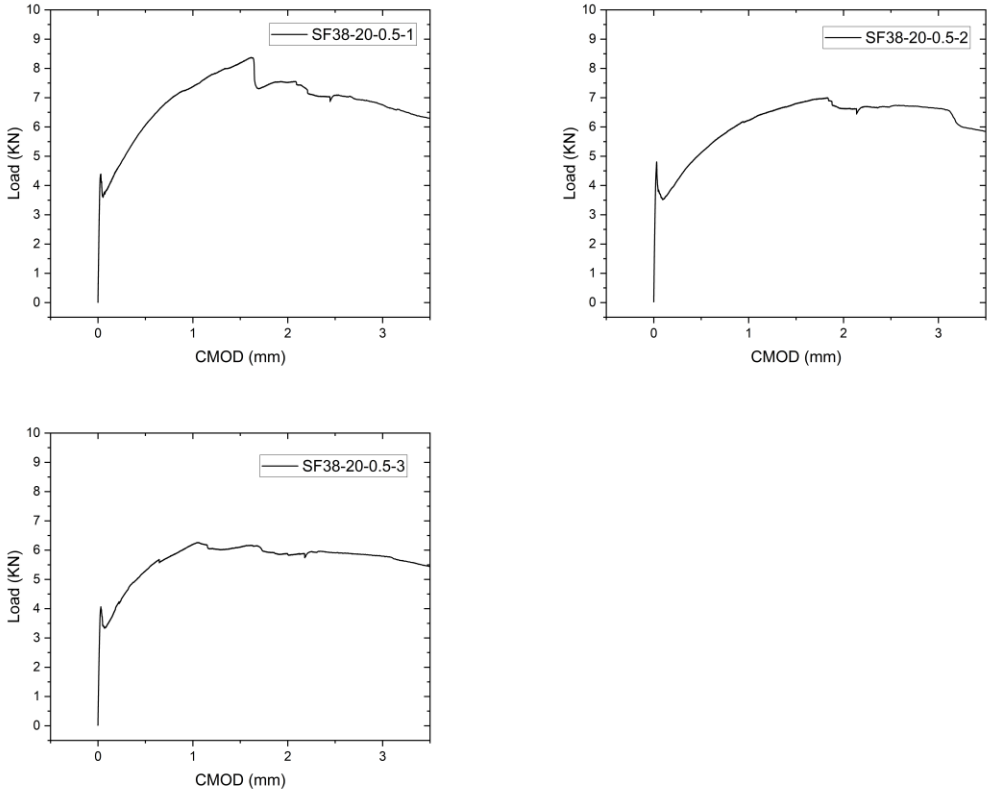

Figure C.8 Load-CMOD curves for Mix SF38-20-0.5 specimens

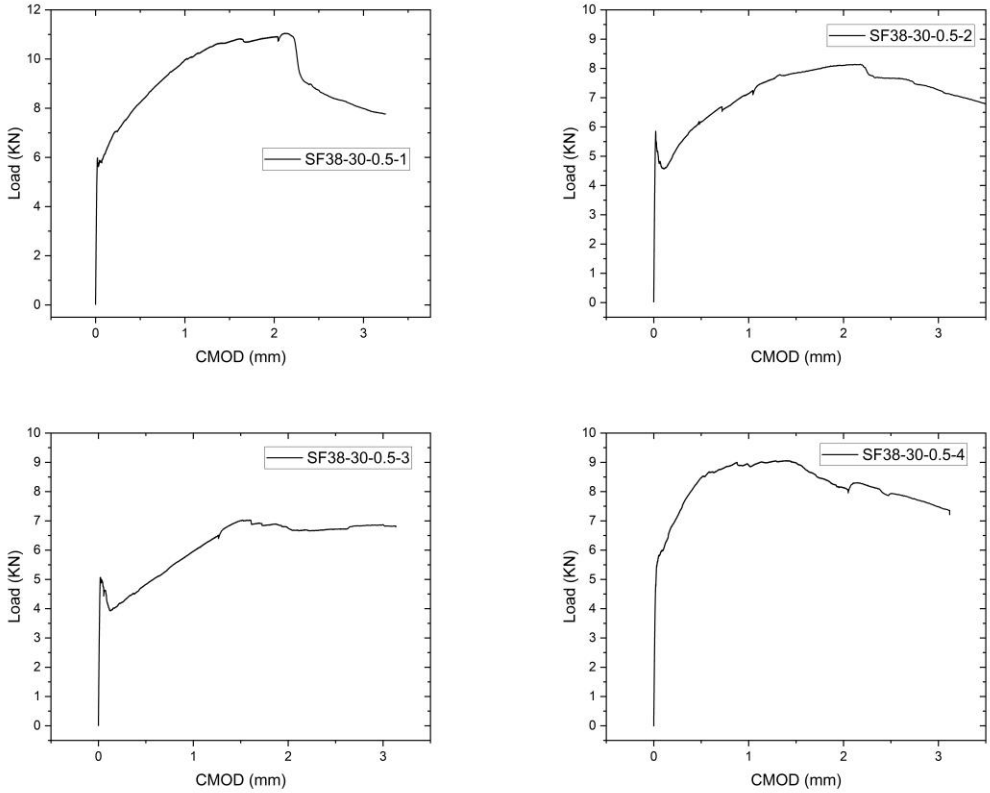

Figure C.9 Load-CMOD curves for Mix SF38-30-0.5 specimens

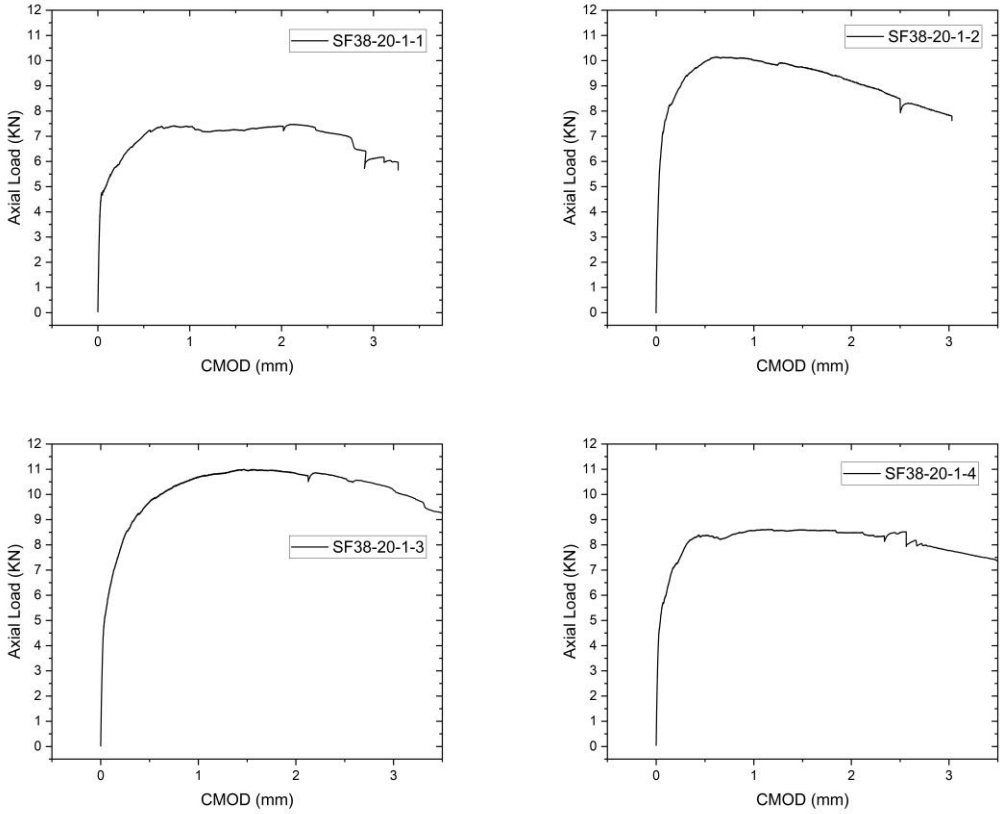

Figure C.10 Load-CMOD curves for Mix SF38-20-1 specimens